The Investigation of Axonal Pathology in the Cerebellum of Patients with Mitochondrial Disease

Jonathan Phillips BSc (Hons), MRes

A thesis submitted for the degree of Doctor of Philosophy

Wellcome Trust Centre for Mitochondrial Research

Institute of Neuroscience

Declaration

This thesis is submitted for the degree of Doctor of Philosophy to Newcastle University. The research was performed within the Wellcome Trust Centre for Mitochondrial Research, Institute of Neuroscience, Newcastle University, and is my own work. The research was carried out under the supervision of Professor D. M. Turnbull, Professor R. N. Lightowlers and Dr N. Z. Lax between October 2012 and September 2015.

I certify that none of the material offered in this thesis has been previously submitted by me for a degree or any other qualification at this or any other university.

Abstract

Cerebellar ataxia affects 68% of adult patients with mitochondrial disease and is associated with progressive loss of co-ordination, impaired balance, and speech difficulties. In these patients, the cerebellum shows numerous neuropathological changes, and a prominent feature is the appearance of axonal torpedoes which represent swollen axons from Purkinje cells. Axonal torpedoes occur in the proximal portion of the Purkinje cell axon projecting into the granular cell layer and are mainly comprised of hyper phosphorylated neurofilament H. Although they have been reported in mitochondrial disease, their significance and contribution to disease is not known.

Immunohistochemistry and immunofluorescence was used to characterise and quantify axonal torpedoes in the cerebellums of ten patients with mitochondrial disease and fourteen controls. A triple immunofluorescent assay was developed to reliably quantify the level of respiratory chain protein expression in axonal torpedoes compared to Purkinje cell bodies and their axons.

A major limitation of current immunofluorescent techniques is the ability to use very thin brain sections (5µm) due to the intrinsic properties of the tissue causing scattering of light emitted from the fluorophores reducing the resolution of the image. To overcome this limitation, I have optimised the novel clearing technique known as CLARITY (Clear, Lipid-exchanged, Acrylamide-hybridized Rigid, Imaging/immunostaining compatible, Tissue hYdrogel) to use on both mouse and human cerebellar sections from both control individuals and patients. The optimisation of CLARITY has allowed for the use of 250µm thick cerebellar sections to further characterise the morphology of axonal torpedoes in 3D volume as well as determining the degree of axonal changes between patients and controls on a global scale.

This study provides a detailed characterisation of axonal pathology that occurs in the cerebellum of patients with mitochondrial disease. The success in optimising the clearing method that produces quality staining of neuronal structures in thick (250µm) cerebellar tissue from both mouse and human tissue will allow for further investigation of changes in the vascular, dendritic or axonal networks in 3D volume on a global scale.

Acknowledgements

I would like to start by thanking both Doug and Bob for providing me with the opportunity to start my career in the MRG and for their continued guidance and support throughout the project. Thank you very much to Nic, for being both an amazing supervisor and also a friend that I can rely on. You've made my whole PhD run smoothly and have always been there to keep me calm when I'm having one of those moments.

I would also like to thank Peter Straker and Elspeth Straker for their charitable work that has funded my PhD. If it were not for your good work, I would not have had this incredible chance to begin my scientific career at the MRG.

Thank you Dr Alex Laude and Dr Trevor Booth for their technical help and expertise on microscopy and helping me produce quality images for my thesis. I would also like thank Dr John Grady for all his stats help and being patient with me when I struggled to keep up with it all.

A big thank you to everyone in the MRG who has helped me over the last three years. It is a lot easier to deal with the bad science days when you are amongst friends. Thank you Amy, Alexia, Nic and Lyndsey for proof reading my chapters, I hope it was not too much of a tedious task.

Katherine, you may be on the other side of the world at the moment (good timing, you missed all the fun!) but that hasn't stopped you from supporting me through the bad moments and it has given me something to strive towards, a holiday in New Zealand, woop! Throughout the PhD, you have always been there for me, and ensured I stayed sane by doing fun things at the weekend as well as showing me the delights of Scotland along with Belle.

Lastly, thank you Mum and Dad, your weekend visits have always been most enjoyable and have kept me stress free, who knew the north east was so beautiful! Most importantly though thank you for all your support throughout the years, without it I wouldn't have made it this far.

Publications and Presentations

Publications

Phillips, J., Laude, A., Lightowlers, R., Morris, C., Turnbull, D., Lax, N., "Development of passive CLARITY and immunofluorescent labelling of multiple proteins in human cerebellum: understanding mechanisms of neurodegeneration in mitochondrial disease" Scientific reports.

Phillips J, Hayhurst H, Lax N.Z. "Neurodegeneration in Mitochondrial Disorders". Invited contribution to "Mitochondrial Dysfunction in Neurodegenerative disorders" – 2nd Edition. Springer, November 2015

Presentations

"Providing CLARITY To Ataxia In Patients With Mitochondrial Disease." Wellcome trust Molecular Neurodegneneration workshop, Cambridge, UK (2016)

"Providing CLARITY To Ataxia In Patients With Mitochondrial Disease." BNA 2015 Festival of neuroscience. Edinburgh, UK (2015)

"Investigating the Contribution of Axonal Torpedo Formation to Purkinje Cell Vulnerability in with Mitochondrial Disease" at Euromit 2014 Tampere, Finland (June 2014)

"Investigation of Axonal Pathology in the Cerebellum of Individuals with Mitochondrial Disease" at Joint meeting of the European society for Neurochemistry and biochemical society. Bath, UK (June 2013)

Shortlisted for the SET for Britain award

Table of Contents

List of Figures

List of Tables

Abbreviations

3D	Three dimensions
Aβ	Amyloid Beta
AD	Alzheimer's disease
ADP	Adenosine diphosphate
AIF	Apoptosis inducing factor
AIS	Axon initial segment
ALS	Amyotrophic lateral sclerosis
APAF	Apoptosis protease-activating factor
AP	Abasic site
APP	Amyloid Precursor Protein
ATP	Adenosine Triphosphate
BBB	Blood brain barrier
BER	Base excision repair
BC	Basket cells
bp	Base pair
Ca2+	Calcium ion
CCD	Charge-coupled device
CCCP	Carbonyl cyanide m-chlorophenylhydrazone
CF	Climbing fibre
CLARITY	Clear Lipid-exchanged Acrylamide-hybridized Rigid Imaging compatible Tissue hYdrogel
CNS	Central nervous system
COX1	Mitochondrially encoded cytochrome c oxidase I
COX4	Cytochrome c oxidase subunit IV
CSF	Cerebral spinal fluid
CT	X-ray computed tomography
dH2O	Distilled water
D-loop	Displacement loop
DCN	Deep cerebellar nuclei
DNA	Deoxyribonucleic acid
DWI	Diffusion weighted imaging

EAE	Experimental autoimmune encephalomyelitis
EDTA	Ethylenediaminetetraacetic acid
EM	Electron Microscopy
ER	Endoplasmic reticulum
ERRα	Oestrogen related receptor α
FAD	Flavin adenine dinucleotide
FADD	Fas-associated death domain
FADH2	Reduced flavin adenine dinucleotide
FFPE	Formalin-fixed, paraffin-embedded
FMNH	Flavin mononucleotide
FAT	Fast axonal transport
Fe-S	Iron-sulphur cluster
Fis1	Mitochondrial fission protein 1
F(ab)	Fragment antigen-binding
FRDA	Friedreich's Ataxia
GAD	Glutamic acid decarboxylase
GCL	Granular cell layer
GoC	Golgi cell
GrC	Granule cell
GTPase	Guanosine triphosphatase
H+	Proton
H2O	Water
H2O2	Hydrogen peroxide
H-strand	Heavy strand
H+-MRS	Proton magnetic resonance spectroscopy
HR2	Heptad repeats
HRP	Horse radish peroxidase
HSP	Heavy strand promoter
IMM	Inner mitochondrial membrane
IMS	Inter-membrane space
kDa	Kilo Dalton
KO	Knock out

KSP	Lysine-Serine-Proline
KSS	Kearns Sayre syndrome
LHON	Leber hereditary optic neuropathy
LSP	Light strand promoter
L-strand	Light strand
MAG	Myelin associated glycoprotein
MBP	Myelin basic protein
MCU1	Mitochondrial calcium uniporter 1
MCUR	Mitochondrial calcium uniporter regulator 1
MCL	Molecular cell layer
MELAS	Mitochondrial encephalomyopathy and stroke-like symptoms
MERRF	Myoclonic epilepsy with ragged-red fibres
MF	Mossy fibre
Mff	Mitochondrial fission factor
Mfn1	Mitofusin 1
Mfn2	Mitofusin 2
MiD49	Mitochondrial dynamics proteins of 49 kDa
MiD51	Mitochondrial dynamics proteins of 51 kDa
MIDD	maternally inherited deafness and diabetes (MIDD)
MILS	Maternally inherited Leigh's syndrome
MIRAS	Mitochondrial inherited recessive ataxia syndrome without ophthalmoplegia
MLI	Molecular layer interneurons
MNGIE	Mitochondrial neurogastrointestinal encephalopathy syndrome
MPP	Mitochondrial processing peptidase
mRNA	Messenger ribonucleic acid
MRI	Magnetic resonance imaging
MRS	Magnetic resonance spectroscopy
MT	Microtubules
mtDNA	mitochondrial DNA
mt-KR	A genetically encoded photosensitizer targeted to mitochondria
mtRF1a	mitochondrial release factor 1a
mtSSB	mitochondrial single stranded binding proteins

MTS	Mitochondrial targeting sequence
NARP	Neuropathy, ataxia, and retinitis pigmentosa
Nav1.6	Type VI Sodium Channels
NBTR	Newcastle Brain Tissue Resource
NCX	Sodium calcium exchanger
NDUFA9	NADH dehydrogenase (ubiquinone) 1 alpha subcomplex 9
NDUFA13	NADH dehydrogenase (ubiquinone) 1 alpha subcomplex 13
NDUFB8	NADH dehydrogenase (ubiquinone) 1 beta subcomplex 8
NDUFS1	NADH dehydrogenase (ubiquinone) Fe-S protein 1
NDUFS3	NADH dehydrogenase (ubiquinone) Fe-S protein 3, 30kDa (NADH-coenzyme Q reductase)
NFL	Neurofilament L
NFM	Neurofilament M
NFH	Neurofilament H
npNFH	Non-phosphorylated neurofilament H
NRF1	Nuclear respiratory factor 1
NRF2	Nuclear respiratory factor 2
O2-	Superoxide anion
OH	Origin of heavy strand synthesis
OL	Origin of light strand synthesis
OMM	Outer mitochondrial membrane
OXPHOS	Oxidative phosphorylation
PARL	Presenilin-associated rhomboid like protein
PB	Phosphate buffer solution
PBS	Phosphate buffered saline
PD	Parkinson’s Disease
PCL	Purkinje cell layer
PGC-1α	Peroxisome proliferator activated receptor γ coactivator 1α
PEO	Progressive external ophthalmoplegia
Pi	Inorganic phosphate
PMI	Post mortem interval
pNFH	Phosphorylated neurofilament H

Polγ	Polymerase gamma
POLRMT	mitochondrial RNA polymerase
Q	Ubiquinone
QH2	Ubiquinol
RNA	Ribonucleic acid
RIMS	Refractive index matching solution
rPEO	recessive Progressive external ophthalmoplegia
ROS	Reactive oxygen species
SANDO	Sensory ataxia, neuropathy dysarthria and ophthalmoplegia
SC	Stellate cell
SBB	Sodium Borate buffer
SDHA	Succinate dehydrogenase complex subunit A
SDS	Sodium dodecyl sulphate
SOD	Superoxide dismutase
tBid	Truncated Bid
TBS	Tris buffered saline
TCA cycle	Tricarboxylic acid cycle
TFAM	Mitochondrial transcription factor A
TFBM2	Mitochondrial transcription factor B2
TIM	Translocase of the Inner mitochondrial membrane
TOM	Translocase of the outer mitochondrial Membrane
TOMM	MOM translocase complex
UV	Ultra violet
VDAC	Voltage dependent anion channel

Chapter 1. Introduction

The central nervous system (CNS) contributes to only 2% of the total body mass, however it consumes 20% of total oxygen of which 95% is utilised by mitochondria to produce adenosine triphosphate (ATP) via oxidative phosphorylation (OXPHOS) (Mink et al., 1981). The dependence of the CNS on mitochondria for the production of cellular energy makes it vulnerable to impaired ATP production.

1.1. Mitochondria

Originally mitochondria and eukaryotic cells existed as independent organisms until environmental pressures lead to the formation of a favourable endosymbiotic relationship. This relationship was able evolve due to mitochondria's capacity to readily generate ATP by OXPHOS. Eventually the two organisms became reliant on one another for survival as a result all eukaryotic cells are dependent on mitochondria for energy, while the majority of mitochondrial proteins have become nuclear encoded (Margulies et al., 1976).

Mitochondria are intracellular double membrane organelles 1-4μm in length and 0.3-0.7μm in diameter (Palade, 1953). In the outer mitochondrial membrane (OMM), voltage dependent anion channels (VDAC) form hydrophilic pores that regulate the movement of ions and molecules (<10kDa) between the cytoplasm and the inter-membrane space (IMS) (Shoshan-Barmatz et al., 2010). Unlike the OMM, the inner mitochondrial membrane (IMM) is highly impermeable, restricting passive ion movement into the matrix, allowing for the creation of proton gradients, a step pivotal to the OXPHOS process. As both membranes are impermeable to large proteins, polypeptides and proteins that have mitochondrial targeting sequences are transported across the membranes by the protein complexes; translocase of the outer mitochondrial membrane (TOM) and translocase of the Inner mitochondrial Membrane (TIM) (Wagner et al., 2009).

The mitochondrial cristae are invaginations of distinct membrane that are connected to the intermembrane space through cristae junctions creating a large surface area within the mitochondrial matrix (Frey and Mannella, 2000). The large surface area of the cristae membrane makes it suitable for the site of OXPHOS as well as iron-sulphur cluster biogenesis and the synthesis of mitochondrial DNA(mtDNA)-encoded and transport proteins (Vogel et al., 2006). The mitochondrial matrix contains the mitochondrial genome as well as a large number of enzymes required for β-oxidation and the tricarboxylic acid cycle. The mitochondrial genome (mtDNA) encodes for a number of subunits that constitute a series of protein complexes that are pivotal to OXPHOS, the electron transport chain.

1.2. Functions of Mitochondria

As well as their essential role in the production of ATP, mitochondria are also involved in the production of reactive oxygen species (ROS) and iron-sulphur clusters, and are crucial for the modulation of calcium dynamics and apoptosis.

1.2.1. Oxidative Phosphorylation

The multi-subunit polypeptide complexes (I-IV) that form the respiratory chain are located in the IMM and are vital to the efficient biochemistry of OXPHOS. ATP is produced by the condensation of inorganic phosphate (Pi) and adenosine diphosphate (ADP) through a series of oxido-reduction reactions along the respiratory chain and is assisted by a number of molecules such as copper ions, cytochromes, nicotinamides, flavins and iron-sulphur centres. The oxido-reduction reactions result in the transport of protons across the inner membrane by NADH oxidoreductase (complex I), ubiquinol cytochrome c reductase (complex III) and cytochrome c oxidase (complex IV) and the transverse movement of electrons through the respiratory chain. The movement of protons and elections creates an electrochemical gradient that facilitates the generation of ATP through the hypothesised chemiosmosis process (Mitchell, 1961), where the electrochemical gradient drives the protons through complex V (ATP synthase) converting kinetic energy to stored chemical energy (Figure 1.1).

Approximately 45 genes encode subunits for Complex I (NADH oxidoreductase), 7 of which are mtDNA encoded (Ugalde et al., 2004). The subunits form three modules (N, Q and P), which have distinct functions. In module N, the donation of two electrons from NADH to complex I, reduces the attached prosthetic group flavin mononucleotide (FMNH) to FMNH2, to begin the process of ATP production. The electrons produced from this reaction are passed via iron sulphur (Fe-S) clusters to ubiquinone (Q), resulting in its reduction to ubiquinol (QH2). The transfer of electrons, causes a conformational change in module P, opening a pore and allowing for four protons to be pumped across the IMM into the IMS

The next step is the reduction of succinate to fumarate occurring at complex II (succinate dehydrogenase). Complex II is also involved in the tricarboxylic acid (TCA) cycle. Complex II is composed of 4 subunits which are completely nuclear encoded. The catalytic subunit SDHB is located in the matrix, while SDHC and SDHD anchor complex II to the IMM (Hagerhall, 1997). Subunit SDHA is involved in catalysing the deprotonation of succinate to fumarate. The generation of fumarate, produces reduced flavin adenine dinucleotide (FADH2) which when oxidised to flavin adenine dinucleotide (FAD) releases electrons that are passed through Fe-S clusters to converge at Complex III with electrons produced from Complex I (Cecchini, 2003).

Of the 11 subunits that make up complex III (ubiquinol cytochrome c reductase), it is the cytochrome b subunit that is encoded by the mitochondrial genome. Electrons are transferred through the two step Q cycle, which is coupled with the oxidation and reduction of ubiquinol-ubiquinone resulting in two protons being pumped across for every electron that is transferred (Trumpower, 1990). The electrons are transferred from complex III to the CuA site of complex IV via the Rieske heme group of cytochrome c (Mathews, 1985).

Complex IV (cytochrome c oxidase) is comprised of 13 subunits of which the mtDNA encodes for subunits I-III. Once complex IV receives the electrons at the CuA site, they are moved on to the catalytic site haema3 and CuB (Faxen et al., 2005). At complex IV, H2O is formed through the reduction of O2 by four electrons from cytochrome c. The transfer of the first two electrons from cytochrome b results in the reduction of haema3 and CuB forming a peroxide bridge once a molecular oxygen is added. The next round of electron transfer results in two protons being bound to the metal groups and releasing the peroxide bridge. The further addition of two proton ions results in the formation of two molecules of water (H2O) and the transfer of four protons into the intermembrane space. (Yoshikawa et al., 2006).

All the protons that have been pumped into the intermembrane space generates an electrochemical gradient which Complex V (ATP synthase) utilises to convert ADP and Pi into ATP. There are two distinct structural domains of complex V; FO and F1. FO forms a c-ring in the membrane through 8 hydrophobic subunits which allows the protons to pass through. While F1 extends into the matrix and is composed of 5 subunits forming a stationary ring and a central rotatory stalk (Wittig and Schagger, 2008). As protons are moved through the c-ring of the FO domain, glutamate residues are protonated and deprotonated causing the rotation of subunits ε and γ of the stationary ring. The continued rotation generates energy that is used to convert ADP and Pi into ATP (Yoshida et al., 2001). It takes eight protons to cause 360˚ of rotation producing three ATP molecules.

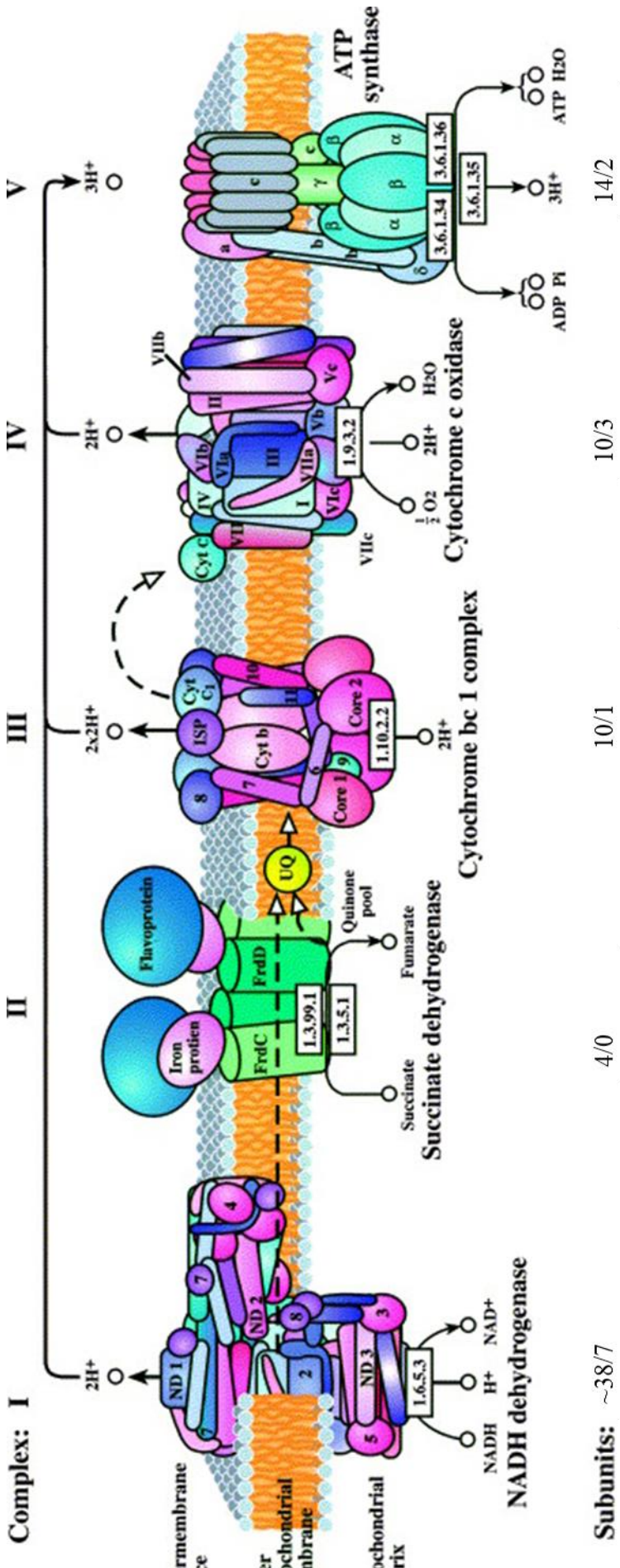

Figure 1.1: Graphical depiction of the respiratory chain and the genetic origins of the subunits. The five protein complexes involved in oxidative phosphorylation (OXPHOS) are located in the inner mitochondrial membrane. The movement of electrons from complex I and II via complex III and cytochrome c to complex IV creates energy that extrudes protons into the intermembrane space generating an electrochemical gradient. The kinetic energy of protons moving back down this gradient into the matrix is utilised by complex V to convert ADP and inorganic phosphate into ATP. At the bottom of the figure, the number of subunits encoded by the nuclear/mitochondrial genomes are shown. *Image modified and taken from Mandavilli et al. (2002)*

1.2.2. Reactive Oxygen Species

Reactive oxygen species (ROS) are reactive molecules that have an oxygen atom with a 'free radical' pair of electrons attached to it. In the cell, mitochondria along with the endoplasmic reticulum and peroxisomes are a major source of ROS (Brown and Borutaite, 2012). In mitochondria, it is complexes I and III that are the main producers of ROS such as superoxide (O2-). Both complexes release ROS into the mitochondrial matrix, but Complex III also releases ROS into the intermembrane space (Muller et al., 2004).

ROS has been shown to be involved in a number of cellular processes such as cell differentiation, autophagy and signalling cascades through reversible post translational protein modifications (Rhee et al., 2000; Sena and Chandel, 2012). However an overabundance of ROS can lead to cellular damage, apoptosis, and de novo mtDNA mutations, therefore the tight regulation of ROS is imperative. There a number of mechanisms present to detoxify ROS, for example within mitochondria O2- detoxification occurs through the reduction of O2- to H2O2 by the different isoforms of superoxide dismutase (SOD).

1.2.3. Iron-Sulphur clusters

Mitochondria play an important role in the biogenesis of iron-sulphur (Fe-S) clusters and iron regulation in the cell. Fe-S clusters are essential for OXPHOS as they are present within complexes I, II and III where they function to facilitate electron transfer by repeatedly changing the redox status of iron from Fe2+ to Fe3+. In addition to their role in OXPHOS, Fe-S clusters are important cofactors in a number of cellular process such as DNA repair and maintenance, enzyme catalysis and gene expression (Lill et al., 1999). Therefore the efficient formation of Fe-S clusters in the mitochondria is paramount to survival.

1.2.4. Calcium Dynamics

The internal concentration of calcium has to be tightly controlled as it is involved in numerous processes essential to cellular viability ranging from roles in excitatory neurotransmission to the activation of enzymes involved in both cell signalling and apoptosis. Mitochondria are vital to the regulation of intracellular Ca2+ concentration, so when cytosolic concentration exceeds 10μM, there is massive influx of calcium down a steep electrochemical gradient through the voltage-dependent anion channel (VDAC) in the outer membrane, and the Mitochondrial Calcium Uniporter (MCU) (Baughman et al., 2011) and MCUR1 (mitochondrial calcium uniporter regulator 1) (Mallilankaraman et al., 2012) in the inner membrane(Bernardi, 1999). The subsequent increase in matrix calcium concentration causes an increase in ATP production by increasing respiratory rate and the rate of proton extrusion (McCormack and Denton, 1989).

The regulation of Ca2+ in neurons is more imperative than other cell types, as Ca2+ plays an integral role in a number of neuronal processes such as synaptic plasticity and neurotransmitter release as well as determining the location of mitochondria along the axon of a neuron (MacAskill et al., 2009). Ca2+ is involved in the regulation of mitochondrial mobility, where there is a increase in Ca2+ mitochondria become concentrated. This allows for an increased density of mitochondria at sites where calcium influx is dynamic such as presynaptic terminals and postsynaptic dendritic spines (Yi et al., 2004). Mutations of mtDNA not only disrupt the mitochondrion's ability to produce ATP but also its ability to handle Ca2+, for example mature neurons derived from embryonic stem cells harbouring mtDNA mutations have been shown to exhibit progressive deficits in Ca2+ transients when a repeated glutamate stimuli was applied (Trevelyan et al., 2010).

1.2.5. Apoptosis

Not only do mitochondria produce the molecule that is essential for life but they also play a crucial role in programmed cell death through the release of cytochrome c during apoptosis. Apoptosis is a form of cell death, whereby death is caused by a general process of blebbing of the cell membrane, cell shrinkage, condensation of chromosomes and nuclear fragmentation. Apoptosis can be initiated either intrinsically through a cell damage mediated pathway or extrinsically by a cell receptor mediated pathway.

A mitochondrion's role in apoptosis is initiated when a ligand specific to a death receptor such as (FAS) binds to it, resulting in procaspase 8 being cleaved into the active caspase 8 through the Fas-associated death domain (FADD). Caspase 8 initiates the mitochondrial pathway of apoptosis by cleaving the BH-3 protein Bid into truncated Bid (tBID). It is disputed whether tBid activates the pro-apoptotic proteins Bax (Wang et al., 1996) and Bak or prevents these proteins from forming heterodimers (Willis et al., 2007), either way tBid allows for the monomers of Bax or Bak to homo-oligomerise into proteolipid pores in the outer mitochondrial membrane resulting in the permeabilisation of the outer mitochondrial membrane (Renault et al., 2013). The permeabilisation of the membrane results in the release of cytochrome c and pro-apoptotic proteins such as SMAC/Diablo and apoptosis inducing factor (AIF). The permeabilisation of the mitochondrial outer membrane does not affect the structural integrity of mitochondria (von Ahsen et al., 2000). Cytochrome c binds to apoptosis- protease-activating factor 1 (APAF-1) forming the apoptosome, which cleaves procaspase 9 into caspase 9 which activates downstream effector caspases that leads to chromogen condensation and DNA fragmentation. While nuclear DNA undergoes

fragmentation during apoptosis, mtDNA has been observed to remain intact (Murgia et al., 1992).

Mitochondrial dynamics as explained in section 1.3 have also been shown to regulate apoptosis, for example an overexpression of mitochondrial fission proteins like hFis1, leads to an increase in apoptosis (James et al., 2003). This is negated when those mitochondrial fission proteins are inhibited or fusion proteins like OPA1 are over expressed (Lee et al., 2004; Frezza et al., 2006).

1.3. Mitochondrial Dynamics

Mitochondria are highly mobile and do not always exist as single organelles. Through the process of fission and fusion they form dynamic networks facilitating the appropriate distribution of mitochondria within the cell and as a method of mitochondrial quality control (Campello and Scorrano, 2010).

Mitochondrial fission is a way of isolating damaged portions of mitochondria preventing further oxidative damage to the network therefore preserving the integrity of mtDNA and the functioning capabilities of the remaining mitochondria (Parone et al., 2008). While mitochondrial fusion allows nuclear encoded mitochondrial proteins to be exchanged between two individual mitochondria as well as functional complementation (Gilkerson et al., 2008; Kowald and Kirkwood, 2011). Functional complementation occurs when mitochondria carrying a mtDNA mutation fuse, allowing for the mixing of mtDNA transcripts keeping the levels of mtDNA mutations low and tolerable and subsequently maintaining a higher quality of mitochondria throughout the mitochondrial population (Nakada et al., 2001).

1.3.1. Fission

The process of mitochondrial fission is mediated by the large guanosine triphosphatase (GTPase) DRP-1, a dynamin-related protein (Smirnova et al., 2001). DRP-1 is a cytosolic protein that is recruited to the mitochondrial membrane through receptors anchored on the outer mitochondrial membrane (Loson et al., 2013). There are four receptors known to be involved in the recruitment of DRP-1; mitochondrial fission protein 1 (Fis1) (Yoon et al., 2003), mitochondrial fission factor (Mff) (Gandre-Babbe and van der Bliek, 2008), and mitochondrial dynamics proteins of 49 and 51 kDa (MiD49 and MiD51) (Palmer et al., 2011; Zhao et al., 2011). Recently it has been shown that the role of Fis1 in fission is only a minor role and that it has a more significant role in the degradation of mitochondria through mitophagy (Otera et al., 2010; Shen et al., 2014). Mff is seen as the main recruiter of DRP-1 as an overexpression of mff results in the fragmentation of the mitochondrial network due to an increase in fission rates while a knockdown or knockout of mff reduces the recruitment of

DRP-1 as shown by a reduction in the numbers of mitochondrial DRP-1 puncta (Otera et al., 2010; Loson et al., 2013). As with Mff, both MiD49 and MiD51 have been shown to recruit DRP-1 to the mitochondria independently of Mff (Palmer et al., 2013). However when MiD49 and MiD51 are overexpressed there is an inhibition of fission, this has been attributed to MiD49 and MiD51 binding to DRP-1 dimers that are inactive (Palmer et al., 2013; Liu and Chan, 2015).

DRP-1 molecules oligomerise to form active helices that have the same dimensions as the mitochondrial constriction sites and wrap around the mitochondrion (Ingerman et al., 2005). As the constriction point at which DRP-1 wraps around the mitochondria has a dimension of 129nm (Ingerman et al., 2005) and the normal diameter of mitochondria is 500-1000nm, DRP-1 relies on the endoplasmic reticulum (ER) to wrap tightly around the mitochondrial network causing it to constrict and allowing for the DRP-1 helices to wrap round (Friedman et al., 2011). The recruitment proteins Mff, MiD49 and MiD51 have been observed at the ER-mitochondria contact sites, indicating that these are the primary sites of mitochondrial fission (Elgass et al., 2015). Hydrolysis of GTP by DRP-1 is thought to provide the force to scission the outer and inner membranes (Ingerman et al., 2005).

Disruption of fission can have devastating effects, as exemplified by a neonate case where a dominant-negative mutation to the DRP-1 gene caused abnormal brain development, optic atrophy and persistent lactic acidemia (Waterham et al., 2007). In mice, knocking out DRP-1 has been shown to be embryonic lethal (Wakabayashi et al., 2009). While in adult mouse forebrain neurons, inducible DRP-1 ablation was shown to cause deficits in synaptic transmission and memory function with hippocampal atrophy (Oettinghaus et al., 2016). Using a Drp1flox/flox::L7-Cre mouse model, Kageyama and colleagues knocked out DRP-1 in mouse post mitotic Purkinje cells which resulted in the mitochondria becoming elongated due to the inhibition of fission. There was also an increase in oxidative stress leading to a loss of respiratory function, an accumulation of ubiquitin and mitophagy markers ultimately leading to Purkinje cell degeneration (Kageyama et al., 2012).This phenotype was rescued when the DRP1 KO Purkinje cells were treated with anti-oxidants. These findings indicate that mitochondrial fission is critical for the functioning of mitochondria and the survival of neurons.

1.3.2. Fusion

Unlike mitochondrial fission, mitochondrial fusion involves the co-ordinated fusion of both the OMM and IMM. The OMM is fused together through the activity of mitofusin 1 (Mfn 1) and mitofusin 2 (Mfn2), two large GTPases (Chen et al., 2003). Both proteins contain two 4,3 hydrophobic heptad repeats (HR2) and through the interaction of HR2 repeats the mitofusins form stable complexes (Koshiba et al., 2004). Two transmembrane regions within the mitofusin proteins anchor the proteins to the OMM leaving the C and N terminal projecting into the cytosol and their interaction promotes mitochondrial fusion (Rojo et al., 2002). Mutations within Mfn2 are known to be the primary cause of Charcot-Marie-Tooth neuropathy type 2A, a disease characterised by axonopathy resulting in weakness and atrophy of distal muscles and mild sensory loss (Zuchner et al., 2004; Grandis and Shy, 2005). Knockout of Mfn1 and Mfn2 in murine dopaminergic neurons results in motor deficits (Pham et al., 2012), in addition Mfn2 KO mice showed reduced mitochondrial mass and transport within dopaminergic terminals in the striatum.

OPA1, a GTPase located in the intermembrane space is essential for the fusion of the IMM (Chen et al., 2005). OPA1 requires the presence of Mfn 1 to regulate fusion (Cipolat et al., 2004). Mutations within OPA1 result in Optic atrophy type 1, a dominantly inherited optic neuropathy that occurs in 1 in 50,000 individuals (Delettre et al., 2000). A downregulation of OPA1 in Hela cells caused the fragmentation of the mitochondrial network along with the loss of the mitochondrial membrane potential, disorganization of the cristae and the release of cytochrome c (Olichon et al., 2003). As shown, when there is a disruption to mitochondrial dynamics there can be serve consequences for the cell and the correct functioning of the proteins involved is required for the neurons survival.

1.3.3. Mitochondrial Motility

Biogenesis of mitochondria takes place in the soma of the neuron and with neurons being polar cells with extensive axons (Hirokawa, 1993), the efficient transport of mitochondria to areas of high energy demand such as the synapses and Nodes of Ranvier is imperative (Grafstein and Forman, 1980). This is shown by mitochondria being highly motile organelles with one third being mobile at any given point and 70% of those are undergoing anterograde transport at a rate of rate of 0.1-2μM Sec-1 (Ligon and Steward, 2000). Through the rapid transition from anterograde motor proteins to retrograde motor proteins, mitochondria achieve bidirectional movement (Figure 1.2A).

The kinesin motor protein superfamily are the main motor proteins to provide the kinetic energy for anterograde transportation, with the isoform KIF5β being the main motor protein for the transport of mitochondria (Tanaka et al., 1998). KIF5β binds to mitochondria through the recruitment of a protein complex composed of Miro and Milton. Milton was shown to be important for this interaction as overexpressed kinesin would only bind to mitochondria when Milton was co-expressed in rat cultured hippocampal neurones (Wang and Schwarz, 2009). Miro provides the link between Milton and kinesin, and also is pivotal to in the role of stopping the anterograde transport of mitochondria.

Miro contains a calcium binding EF hand motif composed of 29 residues (Fransson et al., 2003), when calcium binds to the helix-loop-helix structure formed from the EF motif (Nelson and Chazin, 1998), it promotes an interaction between the heavy chain of kinesin and Miro subsequently arresting anterograde transport (Figure 1.2B (Cai and Sheng, 2009). The cessation of transport by calcium would enable an increase in mitochondrial density in areas with a high cytosolic calcium concentration such as the synaptic terminals especially following an action potential and increasing the availability of ATP for processes such as neurotransmitter uptake and rebalancing of ionic gradient and calcium handling (MacAskill et al., 2009).

Retrograde transport is minus-end microtubule directed and the kinetic energy for this is provided by the multi-subunit complex Dynein. The interaction between mitochondria and Dynein is dependent on the accessory factor Dynactin. Prevention of Dynactin binding through antibodies and pharmacological agents caused a termination in retrograde transport (Hafezparast et al., 2003). Retrograde transport becomes important when mitochondria become dysfunctional are transported to the soma to be selectively degraded in a process known as mitophagy.

Correct functioning of the mitochondria and the respiratory chain has been shown to have important effects on the rate and direction of mitochondrial transport. When 100μM antimycin, a complex III inhibitor is applied, an increase in retrograde transport of mitochondria was observed (Miller and Sheetz, 2004). When the mitochondrial uncoupler carbonyl cyanide m-chlorophenylhydrazone (CCCP) was applied, there was a complete termination of all mitochondrial transport with transport recovering once the CCCP had been washed from the cells (Miller and Sheetz, 2004). The application of Annonacin, a lipohillic inhibitor of complex I, to striatal neurons derived from embryos of Wistar rats resulted in an expected decrease in ATP but also an increase in retrograde transport of mitochondria (Escobar-Khondiker

et al., 2007). The application of pharmacological agents show that the correct functioning of mitochondria is required for the efficient transport of these organelles and that a disruption to the respiratory chain arising from mtDNA mutation is likely to impair axonal transport (Brini et al., 1999).

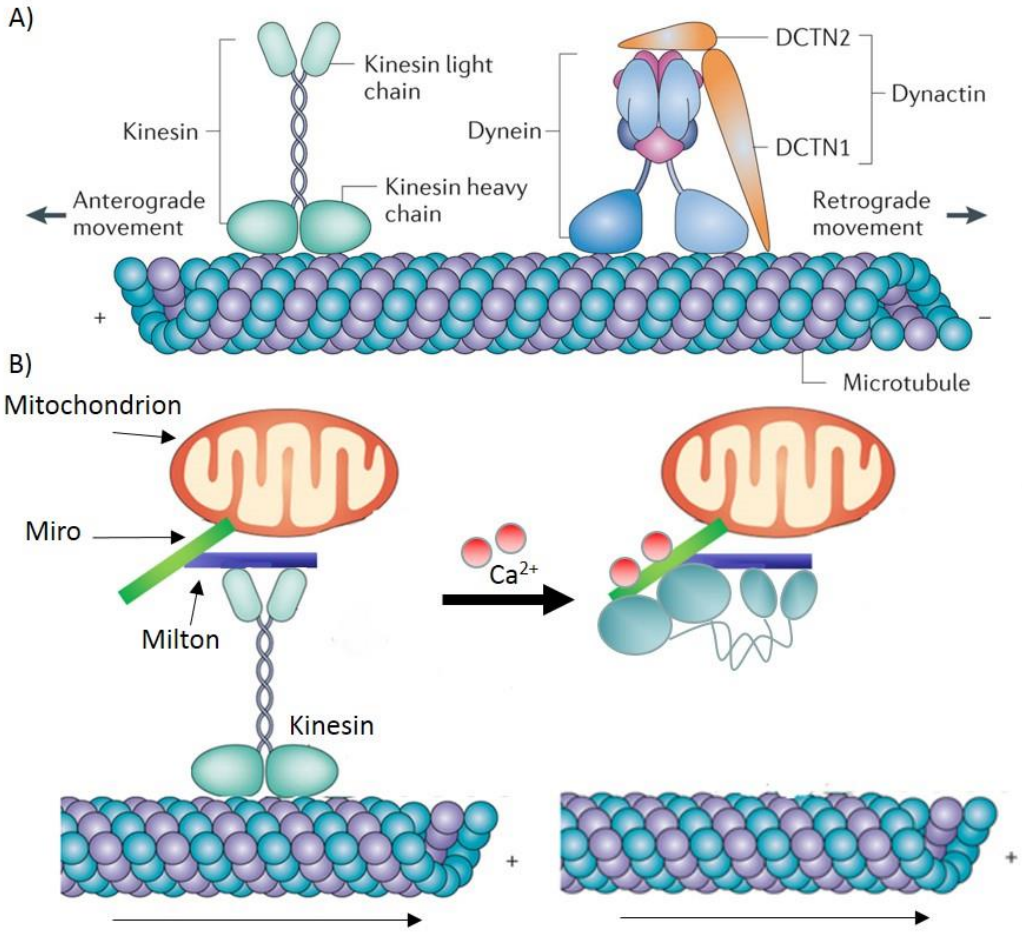

Figure 1.2: Axonal transport of mitochondria.

A) Anterograde transport of mitochondria in the axons (towards plus end of microtubules in the axon tips) is facilitated by Kinesin, a motor protein composed of two heavy chains and two light chains. Retrograde transport is completed by the dynein complex, which is composed of the dynein heavy, intermediate, intermediate light and light chains and several dynactin subunits (such as DCTN1 and DCTN2). B) The proteins Miro and Milton mediates the connection of kinesin to the mitochondria and is involved in the cessation of anterograde transport. When there is an increase in cytosolic Ca2+, Ca2+ binds to the EF hand motif in Miro causing a conformational change resulting in an interaction between the

heavy chain of kinesin and Miro subsequently arresting anterograde transport. Figure was adapted from Millecamps and Julien (2013)

1.4. Mitochondrial Biogenesis

A cell's requirement for ATP can fluctuate in response to environmental and metabolic stimuli such as exercise. Biogenesis of mitochondria is initiated to increase mitochondrial number and activity to ensure the ATP demands are met (Kelly and Scarpulla, 2004). The main protein involved in the regulation of biogenesis is the peroxisome proliferator activated receptor γ coactivator 1α (PGC-1α) (Puigserver and Spiegelman, 2003). Through its interactions with transcription factors such as Nuclear respiratory factor 1 (NRF1), nuclear respiratory factor 2 (NRF2) and oestrogen related receptor α (ERRα) (Wu et al., 1999; Scarpulla, 2002), PGC-1α can regulate the expression of genes involved in the function of mitochondria. For example, the activation of NRF1 and NRF2 by PGC-1α results in downstream activation of other factors and proteins which include mitochondrial transcription factor A (TFAM), mitochondrial transcription factor B2 (TFBM2) and a number of nuclear encoded respiratory chain proteins such as cytochrome c (Evans and Scarpulla, 1989; Gleyzer et al., 2005). Additionally TFAM is involved in the transcription of mtDNA, resulting in a further increase in respiratory chain protein production. The increase in production of proteins through the activity of PGC-1α results in an increase in mitochondrial activity and production of ATP.

It was originally believed that all synthesis of proteins and organelles was completed in the soma of the neuron before being transported to the distal regions. However recent evidence has shown a repertoire of mRNA's in both the axons and growth cones of neurons (Gumy et al., 2011; Deglincerti and Jaffrey, 2012). mRNAs that encode nuclear transcribed mitochondrial proteins have been located in the axons and presynaptic terminal (Gioio et al., 2001; Hillefors et al., 2007; Taylor et al., 2009). When translation of the mRNA or mitochondrial protein import was inhibited in the axons of cultured sympathetic neurons, there was a decrease in mitochondrial membrane potential in cultured sympathetic neurons (Hillefors et al., 2007). These findings and the observation of mRNA in axons suggests that nuclear-encoded mitochondrial proteins are synthesised and imported into the mitochondria locally at the axon, allowing axonal mitochondria to respond quickly to a change in local energy demands.

1.5. Mitochondrial Mitophagy

Mitophagy is the process of selective destruction of mitochondria via autophagosomes to either control the number of mitochondria or to remove damaged mitochondria from the cell. One comprehensively characterised pathway for the clearance of dysfunctional or depolarised mitochondria via mitophagy is the ubiquitin-dependent PINK1/Parkin pathway (Figure 1.3). This pathway first gained major interest following the discovery that mutations to the Parkin gene (PARK2) accounted for almost 50% of all familial autosomal recessive juvenile Parkinson's Disease (PD) (Lucking et al., 2000). Pink1 mutations have also be attributed to be the cause of a rare familial form of PD (Valente et al., 2004).

PINK1 is a Ser/Thr kinase that is found partially inserted into the OMM that has its C-terminal kinase domain exposed to the cytosol (Zhou et al., 2008). When a mitochondrion is healthy (Figure 1.3A), PINK1 is imported across the OMM and IMM via a N-terminal mitochondrial targeting sequence (MTS) which is immediately cleaved by a mitochondrial processing peptidase (MPP) in the matrix and then the remaining PINK1 protein is further cleaved by the IMM protease, Presenilin-associated rhomboid like protein (PARL) (Deas et al., 2011; Greene et al., 2012). When mitochondria become damaged or depolarised (Figure1.3B), PINK1 is no longer imported or cleaved by MPP or PARL, resulting in an accumulation of PINK1 on the OMM (Jin et al., 2010). The accumulation of PINK1 on the OMM results in its interaction with MOM translocase (TOMM) complex, then homodimerisation and self-phosphorylation, causing PINK1 to become a highly active kinase which subsequently recruits Parkin, an E3 ubiquitin ligase from the cytosol to the mitochondria (Narendra et al., 2008; Okatsu et al., 2013; Aerts et al., 2015). PINK1 then phosphorylates Parkin and ubiquitin, resulting in phosphor-Parkin which undergoes a conformational change allowing for phosphor-ubiquitin to bind to it creating a maximally activated phosphor-Parkin (Shiba-Fukushima et al., 2012; Koyano et al., 2014). The activated Parkin then ubiquitinates a number of proteins on the OMM such as mfn1(Glauser et al., 2011). These ubiquitin chains are further phosphorylated by PINK1, promoting the recruitment of more Parkin to the mitochondria and accelerating the process of Parkin recruitment, activation and ubiquitination of mitochondria (Shiba-Fukushima et al., 2014; Okatsu et al., 2015). The formation of a ubiquitin chain causes the recruitment of p62 and HDAC6 (Lee et al., 2010b). Both are key regulatory components of the autophagy machinery, with p62 binding to the key autophagosome component LC3, while cortactin-dependent actin-

remodelling machinery that promotes the recruitment of autophagosome and lysosomes is activated by HDAC6 (Lee et al., 2010a; Lee et al., 2010b). Once mitochondria have been recruited into the autophagosome/lysosome they then undergo enzymatic degradation. In addition to its role in activating Parkin, PINK1 also phosphorylates MIRO, causing its degradation in a Parkin dependent manner with the loss of MIRO causing a dissociation of mitochondria from kinesin and a cessation of movement (Wang et al., 2011). It has been postulated that the reason MIRO is targeted by PINK1 is so that the arrest of mitochondrial motility prevents further fusion, helping to quarantine depolarised or damaged mitochondria within a defined location and before promoting engulfment by an autophagosome (Wang et al., 2011).

The majority of the work characterising the PINK1/Parkin pathway of mitophagy was completed on immortalized and non-neuronal cell lines with results being controversial as the levels of mitochondrial damage induced to initiate the PINK1/Parkin pathway of mitophagy is viewed as non-physiological (Grenier et al., 2013). It is important to understand the physiological role of mitophagy in neurons especially axons as most neuronal mitochondria reside in distal dendritic and axonal processes while axonal degeneration is known to precede the loss of soma in PD (Burke and O'Malley, 2013). Lysosomes have been observed in the axons of primary dorsal root ganglion neurons (Maday et al., 2012). In a recent study, a genetically encoded photosensitizer targeted to mitochondria (mt-KR), was expressed in rat hippocampal neurons which when induced by light caused local ROS-mediated damage to mitochondria (Ashrafi et al., 2014). When distal axonal mitochondria were selectively damaged, the study showed that mt-KR created fragmented or rounded mitochondria and there was an accumulation of both Parkin and LC3 on those mitochondria, indicating that the autophagosomes had formed around the mitochondria. This accumulation of Parkin and LC3 was also observed when antimycin A was applied to distal axonal mitochondria to cause depolarisation, and the colocalization of Parkin and LC3 at the mitochondria was inhibited when completed in either Parkin-/- or PINK1 -/- axons (Ashrafi et al., 2014). This study along with earlier experiments by Cai et al. (2012), which showed in mature cortical neurons that a dissipation of the mitochondrial membrane potential induced Parkin-mediated mitophagy in somatodendritic regions, highlighted that in neurons the PINK1/Parkin pathway of mitophagy is a used method to remove damaged mitochondria.

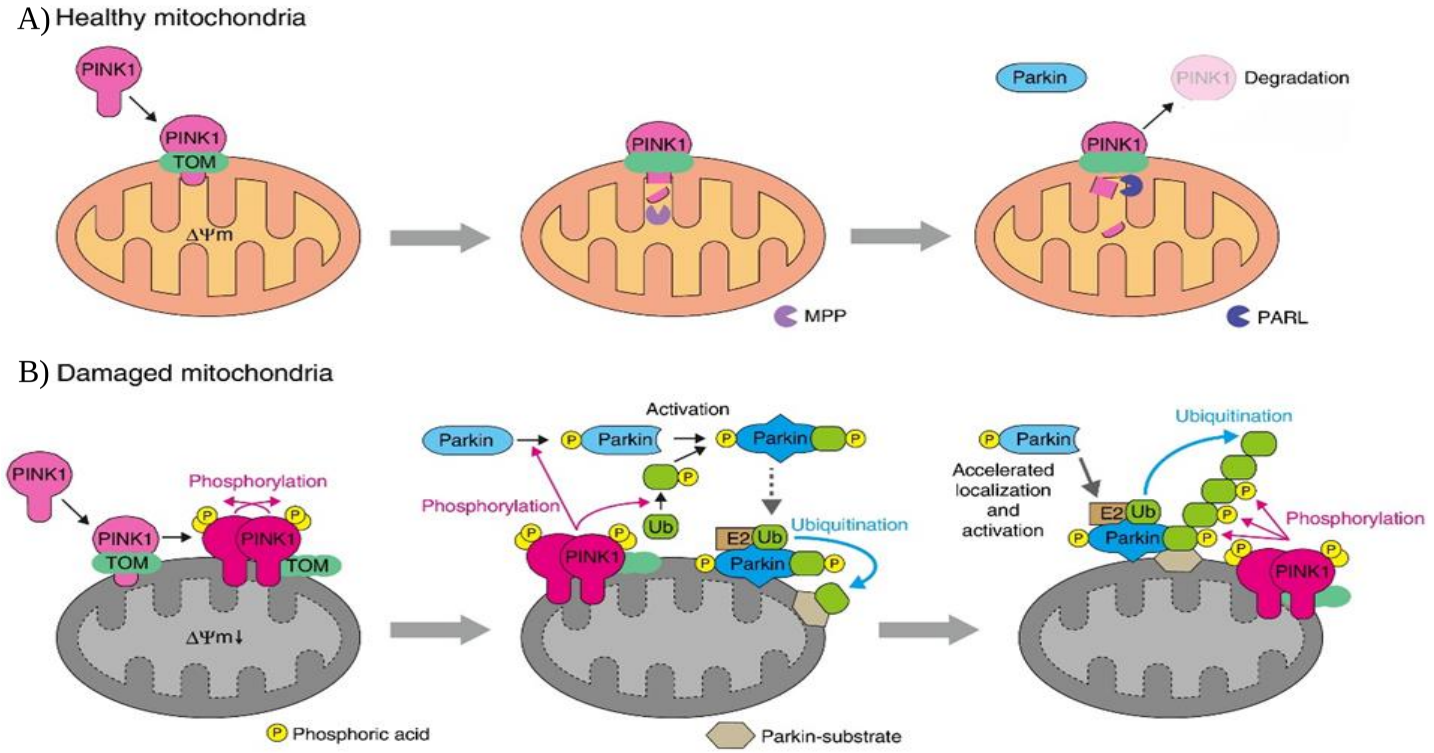

Figure 1.3: PINK1/Parkin pathway of mitochondrial mitophagy.

A) In healthy mitochondria, PINK1 is targeted to the mitochondrial matrix by an N-terminal mitochondrial targeting sequence (MTS) by passing through the translocase of the outer membrane TOM. As PINK1 is entering the matrix, the MTS is removed by the mitochondria processing peptidase (MPP), resulting in PINK1 entry into the matrix stalling. The stalled PINK1 is then further cleaved by the IMM protease, Presenilin-associated rhomboid like protein (PARL). B) When mitochondria are damaged, there is a loss of mitochondrial potential preventing PINK1 from entering the matrix. Instead PINK1 forms a heterooligomeric complex with TOM, allowing for two molecules of PINK1 to dimerise and cross-phosphorylate each other becoming highly active. The highly active PINK1 then phosphorylates Parkin and ubiquitin. The phosphorylated Parkin undergoes a conformational change, allowing for the phospho-Parkin to bind to phoso-ubiquitin which results in phosphor-Parkin becoming fully active. The activated Parkin then ubiquitinates a number of proteins on the OMM, which are then subsequently phosphorylated by PINK1. This process increases the recruitment of Parkin to the mitochondria and accelerating the process of Parkin recruitment, activation and ubiquitination of mitochondria and their recruitment into autophagosomes and lysosomes. *This modified image is taken from Eiyama and Okamoto (2015)*

1.6. Mitochondrial Genome

Mitochondria are semi-autonomous organelles that uniquely contain their own DNA in the matrix. Mitochondrial DNA (mtDNA) exists in multiple copies of a circular, double stranded genome. mtDNA is observed as discrete nucleoids, composed of 1-2 mtDNA molecules (Wang and Bogenhagen, 2006; Kukat et al., 2011). The mtDNA genome is 16,569 base pairs (bp) long, encoding 37 genes for 22 tRNA's, 13 proteins for subunits of respiratory chain complexes, 12S and 16S rRNA (Figure 1.4 (Nass et al., 1965)). There is very little non-coding capacity in the mitochondrial genome, with only the strand-displacement loop (D-loop), which contains elements necessary for mtDNA transcription, the only known non-coding region in the mtDNA (Arnberg et al., 1971; Kasamatsu et al., 1971) . This lack of introns makes mtDNA a very compact and concise molecule (Anderson et al., 1981).

MtDNA has a guanine-rich heavy chain that encodes two rRNAs, 12 mRNAs and 14 tRNAs while the cytosine-rich light chain encodes 1 mRNA and 8 tRNAs (Figure 1.4 (Bestwick and Shadel, 2013)). As mentioned in section 1.2.1, genes within mtDNA encode for subunits within complex I, complex III, complex IV and complex V while complex II is entirely nuclear encoded (Grossman, 1990).

It is widely accepted that mtDNA is solely inherited through the maternal lineage as mitochondria within the sperm are destroyed by a ubiquitin-dependent mechanism (Sutovsky and Schatten, 2000). However there is one case of paternal mitochondrial inheritance, where paternal mtDNA was identified in the skeletal muscle of an individual (Schwartz and Vissing, 2002).

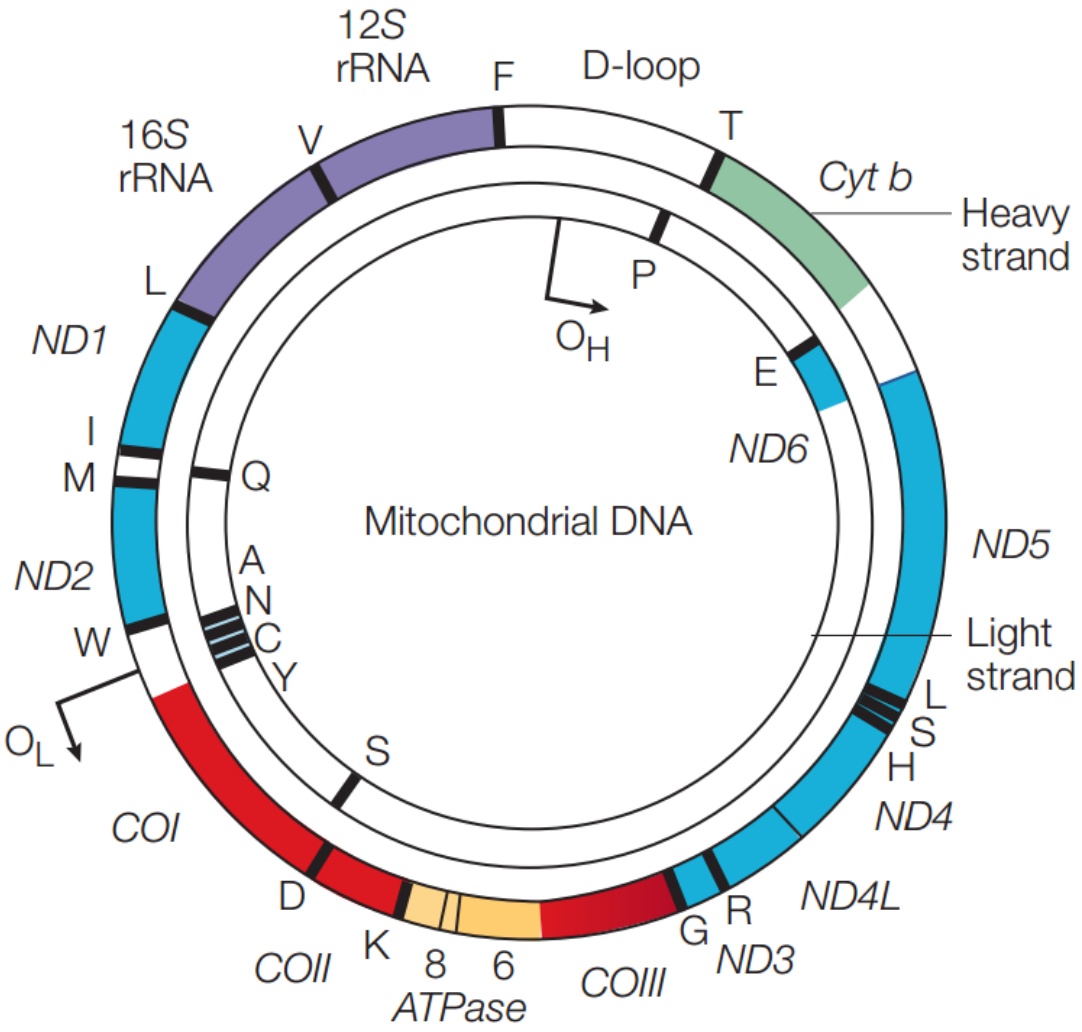

Figure 1.4: The mitochondrial DNA genome.

The mitochondrial genome is found as discreet circular pieces of DNA within the matrix of mitochondria. The mtDNA genome is 16,569 bp long and encodes 37 genes; 22 tRNAs, 13 subunits of complexes, 12S and 16S rRNA. The majority of genes are located on the guanine rich heavy strand rather than the cytosine-rich light chain. The 22 tRNA's are depicted by black lines with each letter representing the amino acid that it encodes for. The 13 subunits are colour coded for each complex; complex I (blue), Complex III (green), complex IV (red) and complex V (yellow). MtDNA replication begins on the heavy chain at OH before being initiated at OL site. Image taken from Taylor and Turnbull (2005).

1.6.1.Heteroplasmy, Homoplasmy and Threshold

As mentioned, there are multiple copies of mtDNA in each mitochondrion, ranging from 100 of copies in sperm to hundreds of thousands of mitochondria in the unfertilized oocyte (Stewart and Chinnery, 2015). As each copy of mtDNA replicates independently and the mtDNA repair mechanism is less efficient compared to nuclear DNA, mutated or wild type mtDNA can coexist within the same mitochondria. When all copies of mtDNA have the same sequence (whether mutated or wild type), the cell is deemed to be homoplasmic. However when there is small genetic variation within a number of the mtDNA molecules the cell is deemed to be heteroplasmic.

If the cell contains a pathogenic mutation, depending on the cell type, it can normally tolerate a high percentage of mutated mtDNA and must pass a threshold before a biochemical defect is observed (Figure 1.5). For a point mutation involving tRNA genes a typical threshold level is around ~90% , while the threshold for a mtDNA deletion is ~70-80% (Sciacco et al., 1994; Wallace et al., 1995; Yoneda et al., 1995; Durham et al., 2007). The threshold frequency is dependent on the tissue and mutation type, for example neuronal mitochondria were more vulnerable to complex I deficiencies when compared to isolated mitochondria from the heart, kidney, liver or muscle (Rossignol et al., 1999).

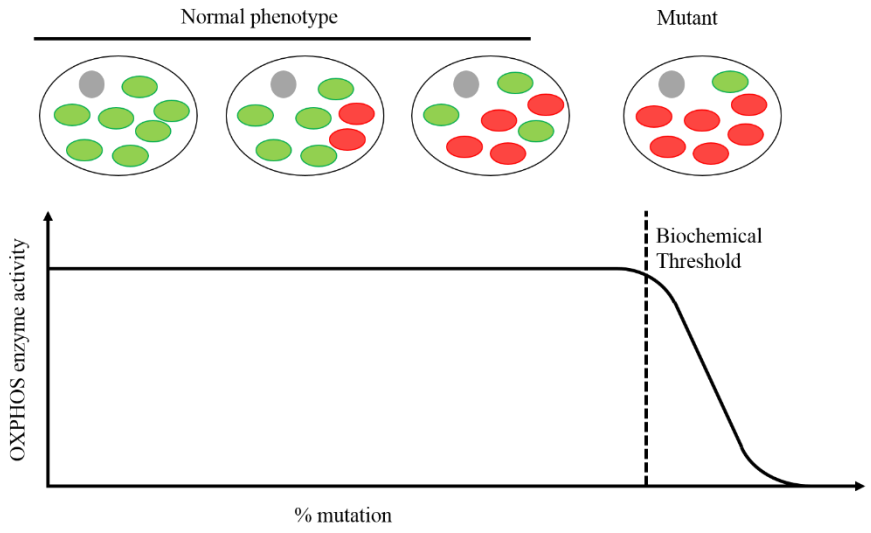

Figure 1.5: Mitochondrial DNA heteroplasmy and Biochemical threshold effect.
As there are multiple copies of mtDNA in a single mitochondria, both wild type (green) and mutated (red) mtDNA can co-exist in the same mitochondria resulting in heteroplasmy. The cell can tolerate high levels of a pathogenic mutations, typically the threshold is ~90% for a point mutation involving a tRNA gene or for a mtDNA deletion it is ~70-80% and needs to be exceeded before a biochemical defect is observed.

1.6.2. Replication of mtDNA

MtDNA replication is continually occurring and is independent of nuclear DNA replication ('relaxed replication'). However expression of both nuclear and mitochondrial DNA must be closely co-ordinated as all the proteins involved in mtDNA replication are nuclear encoded and imported into the mitochondria. The machinery involved in the replication of mtDNA is composed of DNA polymerase γ (POLG), a DNA helicase (Twinkle), mitochondrial single stranded binding (mtSSB) proteins and a mitochondrial RNA polymerase (POLRMT) (Spelbrink et al., 2001; Fuste et al., 2010).

POLG is a nuclear encoded protein that is translated from 23 exons on chromosome 15q25 (Walker et al., 1997). It is a heterodimer, composed of the 140kDa catalytic subunit POLG-A, and two copies of the accessory protein POLG-B. POLG-A is the catalytic component that contains the DNA polymerase site and a 3'-5' exonuclease for proof reading, while POLG-B improves the rate of DNA synthesis by improving the ground state nucleotide binding and increasing the rate of reaction (Johnson et al., 2000; Lee et al., 2009). While Twinkle, separates the two strands of DNA in a 5′–3′ direction, allowing for the mtDNA to be replicated (Spelbrink et al., 2001).

The first method of mtDNA replication proposed was the strand displacement model (Clayton, 1982). In this model, replication begins unidirectionally on the heavy (H) strand at the origin of heavy strand synthesis (OH), the progression of replication displaces the heavy strand. The H strand is progressively replicated, leading to the eventual exposure of the origin of light-strand synthesis (OL) on the light strand. Exposure of the OL, results in the formation of a stem loop structure which initiates the replication of the light strand (Wong and Clayton, 1985). For the first 25 nucleotides, human mitochondrial RNA polymerase (POLRMT) is bound to the light strand before being displaced by POLG commencing the replication of the light strand in the opposite direction (Fuste et al., 2010). Replication will continue until both strands have been replicated creating a daughter mtDNA molecule (Brown et al., 2005).

650 nucleotides away from the OH is a series of DNA sequence motifs know as termination associated sequences (TAS) that result in the termination of 95% of replication initiated at OH (Doda et al., 1981). Premature termination at these sites, results in a strand of DNA being formed known as 7S DNA which remains bound to the parental L strand creating a triple-stranded displacement loop (D-loop). It is thought that the 3' end of the D loop, can initiate termination, allowing for a regulatory mechanism of mtDNA replication and the subsequent control over copy number (Jemt et al., 2015).

However an alternative method has been proposed, a synchronous model of replication where by replication of both the leading and lagging strands are coupled together (Holt et al., 2000). Further investigation into this model has established the incorporation of ribonucleotides along the displaced lagging strand (Yasukawa et al., 2006). The ribonucleotides role in initiating the lagging strand replication was confirmed when it was shown, in vitro, that OL-dependent initiation of replication was achieved using only POLRMT and DNA replication factors (Fuste et al., 2010). POLRMT and ribonucleotides are likely to generate RNA primers, which initiates lagging strand replication by POLG (Holt, 2009). The benefit of this model over the strand displacement model is that it prevents long repeats of DNA being exposed, as this exposure in bacteriophages is associated with increased frequency of DNA damage (Bron et al., 1991). The models of mtDNA replication are depicted in Figure 1.6.

1.6.3. Transcription of mtDNA

The three promoter sites for the initiation of transcription of mtDNA are Heavy strand promoter 1 (HSP1) and 2 (HSP2) and light strand promoter (LSP) on the light strand (Bestwick and Shadel, 2013). Transcription from the initiation sites LSP and HSP2 results in a full genome length polycistronic copy of the mtDNA (Bonawitz et al., 2006). Bi-directional transcription is completed by POLRMT, human mitochondrial transcription factor B2 (TFB2M) and the mitochondrial transcription factor A (TFAM) (Rebelo et al., 2011). TFAM preferentially activates transcription at LSP and HSP1 by binding downstream of the promoter and causing a 90˚ bend in the DNA, opening the promoter up and allowing enhanced interaction of the c-terminal of TFAM with TFB2M (Ngo et al., 2011).

When transcription is initiated at HSP1, it is prematurely terminated due to the termination factor, MTERF, binding to a 22bp termination site in the sequence of tRNA Leu (UUR) producing a transcript containing two rRNA genes and two tRNA genes (Yakubovskaya et al., 2010).

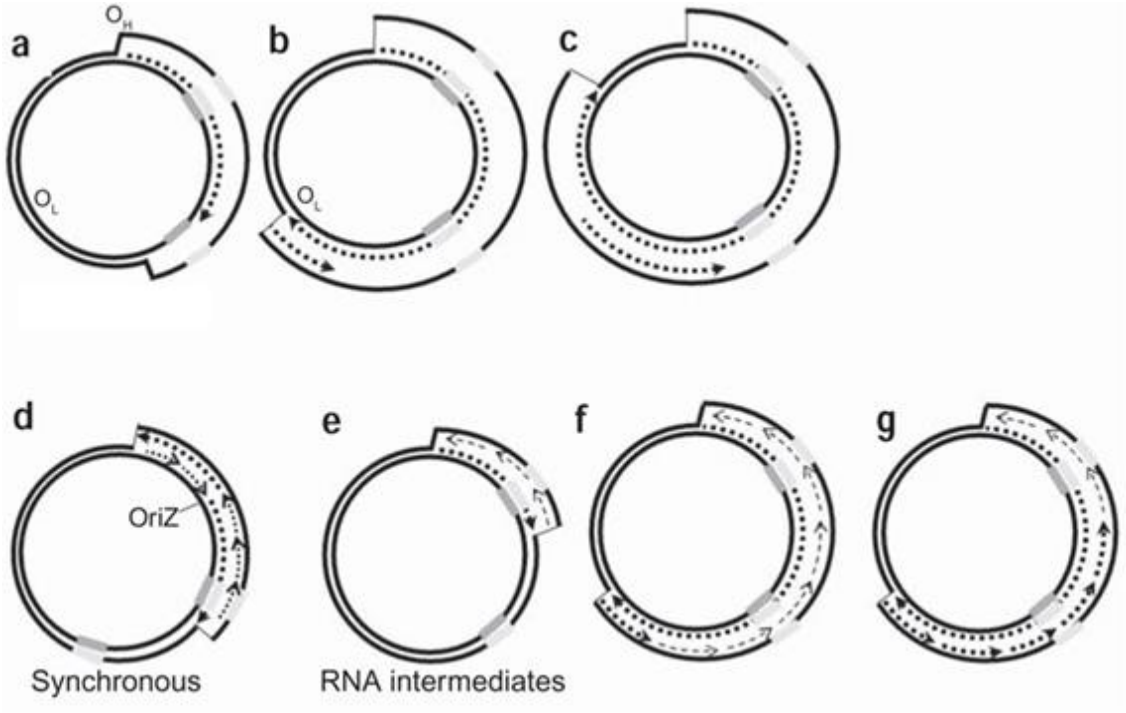

Figure 1.6: Models of mtDNA replication.

In the strand displacement model (a-c), replication begins unidirectional at the OH within the D-loop displacing the heavy strand from the light strand (a). Replication of the H strand progresses until, it eventually expose the origin of light-strand synthesis (OL) on the light strand (b). Following exposure of the OL, replication of the light strand begins in the opposite direction, replication continues in both directions until both strands have been fully replication. In the synchronous model (d), mtDNA replication begins at a zone of replication (OriZ), where replication occurs bi-directionally. The ribonucleotide incorporation throughout the lagging strand (RITOLS) model (e-g) is similar to the strand displacement model, in that replication begins at OH. However as the heavy strand is displaced, RNA intermediates are produced (dashed lines) on the light strand before being converted to DNA. The inclusion of RNA intermediates prevents long repeats of DNA being exposed, reducing the chance of DNA damage (Krishnan et al., 2008). Image taken from Krishnan et al. (2008)

1.6.4. Translation of mtDNA

The mRNA produced from the mtDNA has a number of unusual features which includes that they have a poly(A) tail that may form a part of the stop codon (Ojala et al., 1981), are uncapped (Grohmann et al., 1978) and they contain very few 5' untranslated nucleotides (Montoya et al., 1981).

The translation of mtDNA is completed by the mitoribosome which is comprised of two subcomplexes; the small and the large complexes which contain 81 nuclear encoded proteins and two mitochondrially-encoded rRNAs (12S RNA and 16S RNA). The 16S RNA and 48 proteins make up the larger 39S subunit while the smaller 28S subunit is assembled of 12S RNA and 33 proteins (Anderson et al., 1981; O'Brien, 2003).

There are three phases of mtDNA translation; initiation, elongation and termination. AUG is the main codon for the initiation of translation but AUA and AUU have been shown to initiate protein synthesis (Anderson et al., 1981). These codons are recognised by two initiation factors: mtIF1 and mtIF3, and recruit the mitoribosome (Koc and Spremulli, 2002). As the mitoribosome proceeds along the mRNA, three elongation factors: mtEF-Tu, mtEF-Ts and mtEF-G1, support and regulate translation (Ling et al., 1997).

Termination of translation is driven by the typical stop codons of UAA and UAG and is facilitated by the mitochondrial release factor 1a (mtRF1a) (Soleimanpour-Lichaei et al., 2007). In addition to the typical stop codons, it is postulated that the codons AGA and AGG, could represent stop codons since there are no tRNAs are encoded by these codons in the mtDNA. However, it was shown that the codons are not stop codons but initiate translation termination through the induction of a -1 frameshift due to mitorobosome stalling. The consequence of the frameshift, is for the mitoribosome to read a UAA or UAG codon, initiating the termination of translation (Temperley et al., 2010).

1.6.5. Mutations to mtDNA

The mutation rate in mtDNA is 10-20 fold higher than that of nuclear DNA (Brown et al., 1979). This susceptibility arises due to a number of factors. Firstly, nucleoids in mitochondria do not contain protective histones therefore making mtDNA vulnerable to damage by ROS. This was confirmed in human fibroblasts where mtDNA damage by H2O2 and ROS was 3x and 16x higher compared to nuclear DNA (Corral-Debrinski et al., 1992). Another factor is that ROS production is a by-product of OXPHOS and the location of mtDNA in the matrix increases its exposure to ROS therefore increasing the chance of oxidative damage to mtDNA. Oxidative damage to the mtDNA includes oxidised bases, abasic (AP) sites and DNA strand cleavage due to oxidation products from the AP sites (Sung and Demple, 2006). Additionally as mtDNA is relatively compact with no introns or non-coding regions, any base change will potentially lead to a pathological mutation.

It was originally believed that the DNA repair mechanisms in mitochondria were limited in comparison to those in the nucleus, as pyrimidine dimers that were induced by UV radiation had not been removed from mtDNA (Clayton et al., 1974). However it was shown that although mitochondria lack the machinery to repair mtDNA as a result of UV damage, they do contain isoforms of enzymes that are utilised in the base excision repair (BER) pathway, providing an efficient mechanism for the repair of oxidative damage (Bogenhagen et al., 2001). BER is initiated by a DNA glycosylase like uracil glycosylase (Slupphaug et al., 1996), 8oxoG-glycosylase (Nishioka et al., 1999), or thymine glycosylase (Miller et al., 2004) completing a base excision that removes the damaged base leaving an apurinic/apyrimidine site. An AP endonuclease then cleaves the DNA strand at the AP site creating a break in the strand allowing polymerase-γ, to repair the break. Taken with the observation that oxidative damage to mtDNA in both rats (Driggers et al., 1993) and Chinese hamster ovarian cells (Taffe et al., 1996) had undergone some repair, it shows that base excision repair is the favoured DNA repair mechanism for the mitochondrial genome. It is likely that the BER mechanism is sufficient to remove oxidative damage from mtDNA when the level of ROS production is normal, however if the equilibrium moves towards an increase in ROS production, for whatever reason then the BER would not be able to keep up and mutations would accumulate.

1.6.6. Types of mutations

The mitochondrial genome can undergo a number changes that include point mutations, and deletions while the total copy number can become depleted in the cell. As mentioned these mutations can either occur sporadically or be inherited through the maternal germ cell resulting in impaired oxidative phosphorylation and manifest as a clinical disorder that are grouped under the name mitochondrial disease.

1.6.6.1. Point Mutations

Point mutations are single nucleotide changes within the mtDNA sequence. The mutations can be within a region that encodes for a tRNA. For example one of the most common point mutations is the m.3243A>G mutation, which is the primary cause of ~80% of mitochondrial encephalomyopathy with lactic acidosis and stroke like episodes (MELAS) cases (Goto et al., 1990). The m.3243A>G mutation reduces the rate of translation by preventing 5-taurinomethyluridine modification of the uridine wobble-position in tRNALeu(UUR) (Kirino et al., 2004). As explained by the "wobble hypothesis", a wobble position is the site where the third base in mRNA forms a non-Watson-Crick base pairing with the first base of a tRNA anticodon (Crick, 1965; Barrell et al., 1980) .

Other point mutations may affect a gene that encodes an OXPHOS protein, for example the point mutation m.8993T>G in ATPase subunit 6. This point mutation causes an amino acid change from leucine to arginine. This amino acid change causes a loss of function by limiting the ability of the c- ring of complex V to rotate therefore no rotational torque is produced and the F1 subunit of complex V is unable to generate ATP (Sgarbi et al., 2006). The m.8993T>G mutation is known to cause neuropathy, ataxia, retinitis pigmentosa (NARP) disease (Holt et al., 1990) as well as maternally inherited Leigh's syndrome (MILS) (Tatuch et al., 1992).

1.6.6.2. Rearrangements of mtDNA

In addition to point mutations, the mitochondrial genome can also undergo sporadic rearrangements that include duplication, micro-deletions and large-scale deletions.

Normal mtDNA becomes duplicated when a section is duplicated in tandem creating a genome larger than the normal 16,569-bp genome. The first observation of mtDNA duplication was observed in a patient with Kearns–Sayre syndrome (KSS) (Zeviani et al., 1988). Duplication has also been implicated in other diseases such as a patient with myopathy where a 21.1 kbp duplication was observed (Manfredi et al., 1997) or a patient with diabetes mellitus that had a tandem duplication of approximately 6 kbp (Dunbar et al., 1993). It is not certain how duplications of mtDNA become pathogenic but it has been suggested that the duplications results in aberrant translation products by the fusion of genes at the duplication breakpoint or cause an imbalance of mitochondrial tRNAs or proteins (Poulton et al., 1989; Poulton, 1992).

There are two forms of mtDNA deletions; microdeletions (<5bp) or large-scale deletions. Large-scale deletions are mainly sporadic (Chinnery et al., 2004) and found in the major arc between the OH and OL, flanked by short direct repeats (Samuels et al., 2004; Bua et al., 2006). Large scale deletions are thought to arise either during mtDNA replication or during repair of damaged mtDNA. Single large scale deletions are most commonly associated with KSS (Zeviani et al., 1988). While multiple mtDNA deletions can arise due to mutations in nuclear encoded proteins such as Polγ which can result in Polymerase γ encephalopathies.

1.6.6.3. mtDNA depletions.

In addition to point mutations, duplications and deletions, the total mtDNA copy number can become depleted within a cell. mtDNA depletion is the consequence of mutations in genes that are involved in either the replication of mtDNA, its maintenance or production of nucleotides. A mutation to the gene that encodes POLG has been shown to cause a depletion of mtDNA in Alpers' syndrome (Naviaux et al., 1999). While a mutation to TYMP which encodes for a Thymidine Phosphorylase, results in a depletion of copy number through impaired thymidine metabolism, leading to impaired mtDNA replication or maintenance resulting in mitochondrial neurogastrointestinal encephalomyopathy (MNGIE) (Nishino et al., 1999).

1.7. Mitochondrial diseases and their neurological manifestations

Mitochondrial disease is defined as a genetic human disorder which leads to a defect in the mitochondrial OXPHOS. Originally believed to be a rare disorder, mitochondrial disease has recently been shown to be a common human genetic disorder. Gorman et al. (2015) have shown that mitochondrial disease affects up to 1 in 4,300 adults in the United Kingdom. Mitochondrial diseases are very heterogeneous disorders as they can manifest at birth or in old age, they affect multiple organs and the severity can vary widely (DiMauro et al., 2013).

The CNS is particularly vulnerable to mitochondrial disorders, as exemplified by the prominent neurological disorders observed in patients with mitochondrial disease (Figure 1.7 (McFarland et al., 2010)). The vulnerability of the CNS arises due to its high metabolic demand, reduced antioxidant abilities and finally as neurons are post-mitotic they are generally unable to divide, with the exception of neurons in the subventricular zone, hippocampus and olfactory epithelium. In addition to the neurological symptoms associated with mitochondrial disease, the susceptibility of the CNS to mitochondrial disease is exemplified by a common feature of brain atrophy. In eighteen post-mortem brains from patients with genetically and clinically diverse mitochondrial disease, it was shown that all but two had a reduced brain weight compared to age matched controls. The average reduction in weight was ~16% (Lax and Jaros, 2012).

As mentioned, neurological features are very prominent in mitochondrial disorders and include cerebellar ataxia, seizures, stroke-like episodes and neuronal deafness (DiMauro et al., 2013). Patients can manifest with a multitude of symptoms and are not typically restricted to those required for a clinical definition of a specific syndrome.

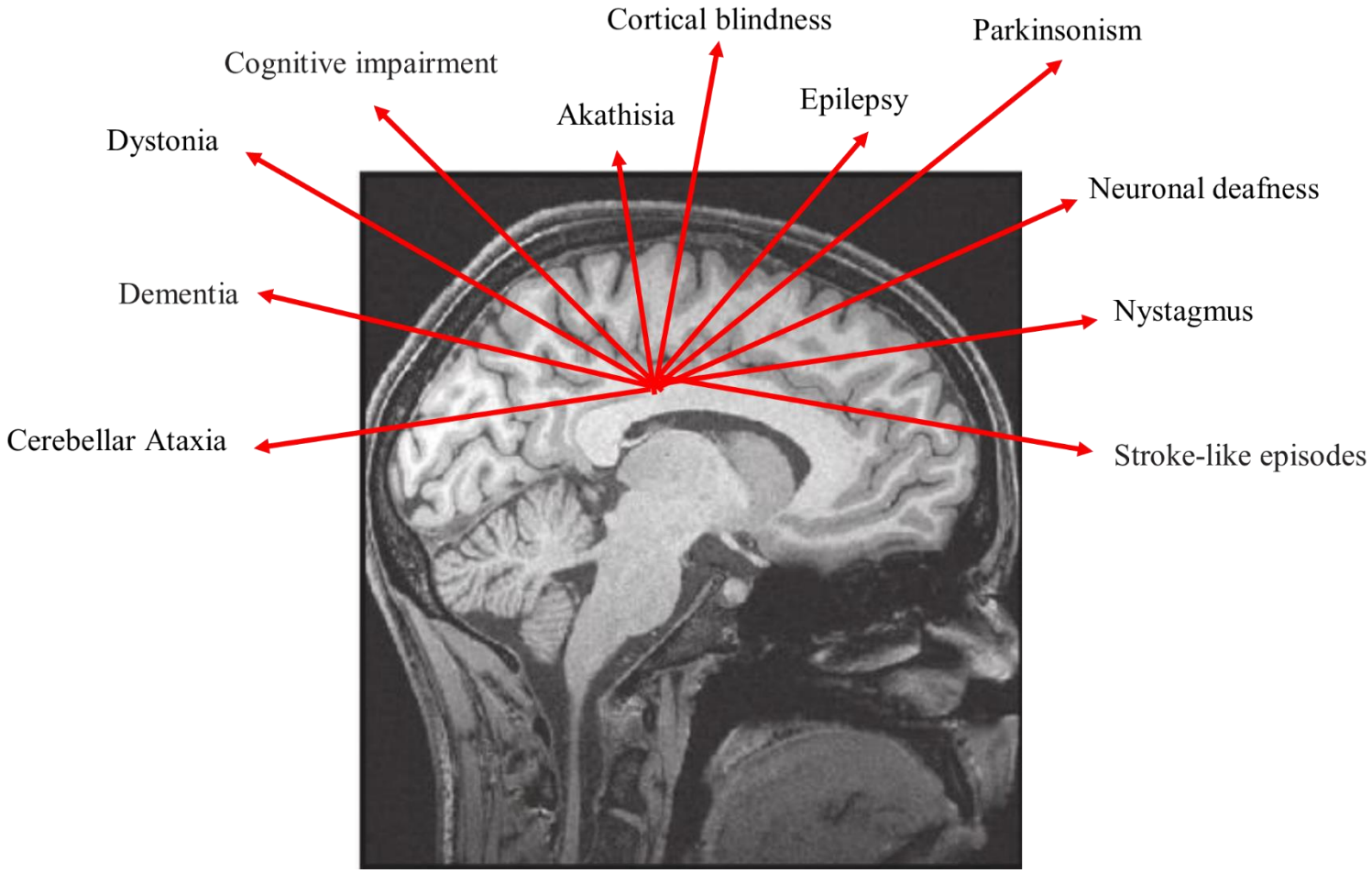

Figure 1.7: Examples of neurological symptoms associated with mitochondrial disease.
Due to the high energy demand of CNS, any perturbation to the supply of ATP can result in the CNS being severely affected. This is exemplified by the prominent neurological symptoms observed in patients with mitochondrial disease.

1.7.1. Kearns Sayre Syndrome

Kearns Sayre Syndrome (KSS) is a mitochondrial disorder caused by a single sporadic large-scale deletion or complex rearrangement of the mtDNA. Two thirds of KSS patients harbour a deletion of 4,977 bp but the deletions can range from 2.0 to 7.0 kbp in size (Zeviani et al., 1988).The deletions are most commonly found between the two proposed origins of replication (OH and OL) in the major arc.

KSS typically manifests before the age of 20 years with retinitis pigmentosa and progressive external opthalmoplegia (Kearns and Sayre, 1958). Other neurological symptoms associated with KSS are subclinical neuropathy, cerebellar ataxia, cognitive impairments in visuospatial attention and executive function, deafness and raised cerebrospinal fluid (CSF) protein levels. As with other mitochondrial diseases, KSS is a multi-system disorder and symptoms that are also observed are proximal myopathy, dysphagia, complete heart block and endocrinopathies.

1.7.2. Leber Hereditary Optic Neuropathy

First described by Theodore Leber in 1871 (Leber, 1871), Leber hereditary optic neuropathy (LHON) is one of most common mitochondrial diseases affecting 1 in 25,000 individuals in the north of east of England (Chinnery et al., 2000). 95% of LHON cases are caused by either of three point mutations to subunits of complex I; m.3460G>A (MT-ND1), m.11778G>A (MT-ND4) and m.14484T>C (MT-ND6) (Mackey et al., 1996). It has been demonstrated that the mutations involved in LHON cause a decrease in the rate of complex I driven ATP synthesis while the production of ROS is chronically increased (Vergani et al., 1995; Ghelli et al., 2003; Floreani et al., 2005).

The age of onset in LHON is typically 20-40 years of age, with males being more afflicted than females. The disorder is clinically characterised by a centrocecal scotoma due to the degeneration of cells in the retinal ganglion cell layer and optic nerve (Man, 2002).

1.7.3. Mitochondrial encephalomyopathy with lactic acidosis and stroke like episodes (MELAS)

As mentioned in section 1.6.6.1, the m.3243A>G mutation, found in the MT-TL1 gene encoding for tRNALeu, is the most common cause of MELAS. A number of other point mutations within the MT-TL1gene have been identified as a cause of MELAS phenotype and this includes the point mutations; m.3251A>G (Morten et al., 1993), m.3271T>C (Goto et al., 1992), and m.3291T>C (Hess et al., 1991). Point mutations at m.1642G>A (tRNAVal) and m.9957T>C (subunit III of cytochrome oxidase c) have also been shown to cause a MELAS phenotype (Manfredi et al., 1995; Taylor et al., 1996).

The MELAS phenotype associated with the m.3243A>G mutation is characterised by a triad of symptoms; seizures, lactic acidosis and stoke-like episodes. Patients with the m.3243A>G mutation can also present with cerebellar ataxia, cognitive decline, deafness, hemianopia, hemiparesis, migraine and peripheral neuropathy (Nesbitt et al., 2013; Mancuso et al., 2014). In addition to causing the MELAS syndrome, the m.3243A>G mutation is also responsible for other clinical syndromes that include maternally inherited deafness and diabetes (MIDD) and progressive external ophthalmoplegia (PEO) (Nesbitt et al., 2013). The variability of the symptoms exemplifies how heterogeneous the phenotypes associated with the m.3243A>G mutation can be.

1.7.4. m.8344A>G

The m.8344A>G mutation is found in the TψC loop of mitochondrial tRNALys (Yasukawa et al., 2000) and the most common clinical disorder associated with the mutation is myoclonic epilepsy ragged red fibres (MERRF). MERRF can also be caused by a less common mutation in the same gene (m.8356T>C) (Silvestri et al., 1992). Patients harbouring the m.8344A>G mutation clinically present in childhood and adolescence, and their symptoms include deafness cerebellar ataxia, myoclonic epilepsy, myoclonus and myopathy but may also present with cognitive impairment, migraine, neuropathy and optic neuropathy (Mancuso et al., 2013; Whittaker et al., 2015).

1.7.5. POLG encephalopathies

Polymerase γ (POLG) encephalopathies are caused by mutations to the POLG gene, POLG, resulting in depletion, multiple deletions and multiple point mutations of mtDNA (Hudson and Chinnery, 2006). To date there are over 200 mutations reported in POLG, with 90 mutations confirmed to cause a disease phenotype. POLG mutations may lead to a number of clinical entities including Alpers' syndrome, autosomal dominant and recessive progressive external ophthalmoplegia (rPEO), mitochondrial inherited recessive ataxia syndrome without ophthalmoplegia (MIRAS) (Hakonen et al., 2008), Parkinsonism (Davidzon et al., 2006) and sensory ataxia, neuropathy dysarthria and ophthalmoplegia (SANDO) (Van Goethem et al., 2003).

POLG encephalopathies have variable age of onset, clinical picture, genotype and severity but there are common features to all the syndromes in that the nervous system and liver are selectively involved. For example, Alpers' syndrome is an early onset neurodegenerative disorder that is caused by an autosomal recessive mutation to Polγ gene, POLG. The mutations p.Ala467Thr, p.Trp748Ser, and p.Gly848Ser are commonly thought to be the primary cause of Alpers' syndrome (Naviaux et al., 1999). The mutations result in impaired

mtDNA replication and repair, which typically leads to mtDNA depletion and subsequently impaired OXPHOS in patients with Alpers' syndrome (Wong et al., 2008). Alpers' syndrome is typically defined by a tetrad of clinical symptoms; 1) Refractory seizures, 2) Episodic psychomotor regression, 3) cortical blindness, 4) Liver disease with micronodular cirrhosis (Naviaux and Nguyen, 2004). Additionally, individuals may also present with ataxia, dementia, hypotonia and spasticity eventually leading to death from status epilepticus or hepatic failure (Harding, 1990).

The progression of POLG encephalopathies typically follows episodes of progressive decline that includes loss of consciousness, severe epilepsy and the development of acute cerebral lesions which are predominately found in the posterior parts of the brain (Tzoulis et al., 2010).

1.8. Neurodegeneration in Mitochondrial Disease

The advent of neuro-radiological imaging technologies such as computed tomography (CT) scans and Magnetic Resonance Imaging (MRI), has been very beneficial in improving the clinical diagnosis of primary mitochondrial disease. The diagnosis of MELAS through the observation of non-vascular distributed focal stroke-like lesions that are located predominantly in the occipital lobe with MRI imaging, exemplifies the benefit of these technologies (Allard et al., 1988). A recent study looked at 33 patients with genetically and clinically defined mitochondrial disease and found that the major findings on the MRI images were cerebellar atrophy, cerebral atrophy, basal ganglia lesions, brainstem signal changes, stroke like lesions and white matter lesions (Bindu et al., 2015).

In patients with MELAS, the typical MRI findings are signal changes that mimic infarcts (stroke-like lesions) in the grey and white matter predominantly in the occipital and parietal lobes. However, these lesions do not follow vascular territories. Imaging studies using MRI, diffusion-weighted imaging (DWI) on MRI, perfusion imaging on MRI, and 1H magnetic resonance spectroscopy (1H-MRS) provide evidence that the stroke-like episodes are related to vasogenic edema, hyperperfusion, and neuronal damage (Yoneda et al., 1999; Ito et al., 2008a). MRI imaging has also shown that calcification of the basal ganglia is a common observation in m.3243A>G patients (Sue et al., 1998). Atrophy to the cerebral cortex, cerebellum, pallidal and superior cerebellar peduncles were observed in patients with the m.8344A>G point mutation (Ito et al., 2008b). In addition to the atrophy, T2 hyperintensities were observed in the striatum and cerebral white matter. Demyelination in the thalamus has also been observed in one individual with the m.8344A>G mutation but they did not have the classical phenotype of MERRF (Erol et al., 2009).

Typical findings in patients with KSS were high-signal lesions on T2-weighted images in the subcortical white matter with cerebral and cerebellar atrophy (Chu et al., 1999). Occasionally hyperintensities in the basal ganglia, midbrain, peripheral white matter and thalami (Haas and Dietrich, 2004). Proton Magnetic Resonance Spectroscopy (MRS) showed that resting pyruvate levels were increased in KSS patients compared to controls (Kuwabara et al., 1994). MRS imaging one month after the treatment of Co-enzyme Q (CoQ) in a patient returned the lactate baseline to normal levels, however sequential imaging at 10 months and 16 months showed the lactate levels had once again become elevated (Choi et al., 2000).

MRI imaging of 26 patients with a combined mitochondrial spinocerebellar ataxia and Alpers phenotype due to mutations in POLG (homozygous or compound heterozygotes for A467T and W748S) found lesions in the basal ganglia, deep cerebellar nuclei, occipital lobe and thalamus (Tzoulis et al., 2006). One patient received sequential imaging, and the evolution of lesions in the left occipital lobe, right motor and prefrontal cortex could be observed. Another study completed cerebral MR imaging of two patients with compound heterozygous POLG mutations and observed bilateral signal abnormalities and hyperatrophy of the inferior olives (Kinghorn et al., 2013). Imaging of the cerebellum in thirteen patients with POLG-associated ataxia found that the majority of patients (85%) had no or only mild atrophy visible in the cerebellum (Synofzik et al., 2012). In patients with Mitochondrial Neurogastrointestinal Encephalopathy (MNGIE), diffuse white matter lesions are observed along with demyelination of sensory neurons ((Hirano et al., 1994; Nishino et al., 1999; Labauge et al., 2002)

A common observation reported in all of the mentioned syndromes is intracerebral calcification, predominantly calcification of the basal ganglia (Chu et al., 1999; Ito et al., 2008b). Calcification appears as a common feature, 54% of patients with the m.3243A>G mutation were shown to have calcification in the caudate, globus pallidus, putamen and thalamus in a study in 1998 (Sue et al., 1998). The calcification of the basal ganglia is not associated with atrophy and there appears to be no correlation between clinical symptoms and degree of basal ganglia calcification (Brannan et al., 1980; Wider et al., 2009).

A multitude of changes can occur in the different brain regions that are undetectable through neuro-radiological imaging technologies. Therefore, microscopic investigations are required to help understand the course of degeneration in patients with mitochondrial disease.

1.9. Neuropathological studies.

The microscopic analysis of post-mortem tissue from patients with mitochondrial disease has allowed for a deeper understanding of which regions and more specifically the type of neurons that are more susceptible to perturbed energy supply. The results from those studies have shown that deficits in the expression of complex I and complex IV are the most prominent, while neuronal loss, astrogliosis, and microgliosis are a typical feature in observed lesions.

1.9.1. Kearns Sayre Syndrome

The neuropathological hallmark of KSS is spongiform encephalopathy in the white matter tracts of the basal ganglia, cerebellum, cerebrum, spinal cord and thalamus (Oldfors et al., 1990; Sparaco et al., 1993; Tanji et al., 1999). The main site of pathology in KSS is the white matter, where there is a preferential loss of myelin associated glycoprotein (MAG) (Figure 1.8A) and a reduction in oligodendrocyte lineage cells (Lax et al., 2012a). Investigation into respiratory chain deficiency, found a marked reduction in cytochrome c oxidase subunit I in astrocytes and oligodendrocytes while axonal mitochondria remained intact (Lax et al., 2012a) . In addition to white matter pathology, the cerebellum is shown to have a moderate loss of Purkinje cells and formation of axonal torpedoes in the granular cell layer, while spongiform degeneration and capillary proliferation was observed in the dentate nucleus (Tanji et al., 1999). Remaining Purkinje cells and neurons of the dentate nucleus (Figure 1.8B and 1.8C) was observed to have a decrease in complex I and IV protein expression deficiencies (Lax et al., 2012b). In a KSS patient, there was a loss of GABAergic interneurons in the temporal cortex, while the remaining neurons displayed a severe reduction in the expression of complex I and IV protein expression (Lax et al., 2016). Accompanying the respiratory chain deficient interneurons were COX deficient blood vessels. Changes to the blood brain barrier and vascular network have been observed with vascular proliferation, fibronectin extravasation in the cerebral cortex and capillary and arterial walls were observed to have iron and calcium deposits in and around them (Oldfors et al., 1990; Sparaco et al., 1993; Tanji et al., 1999)

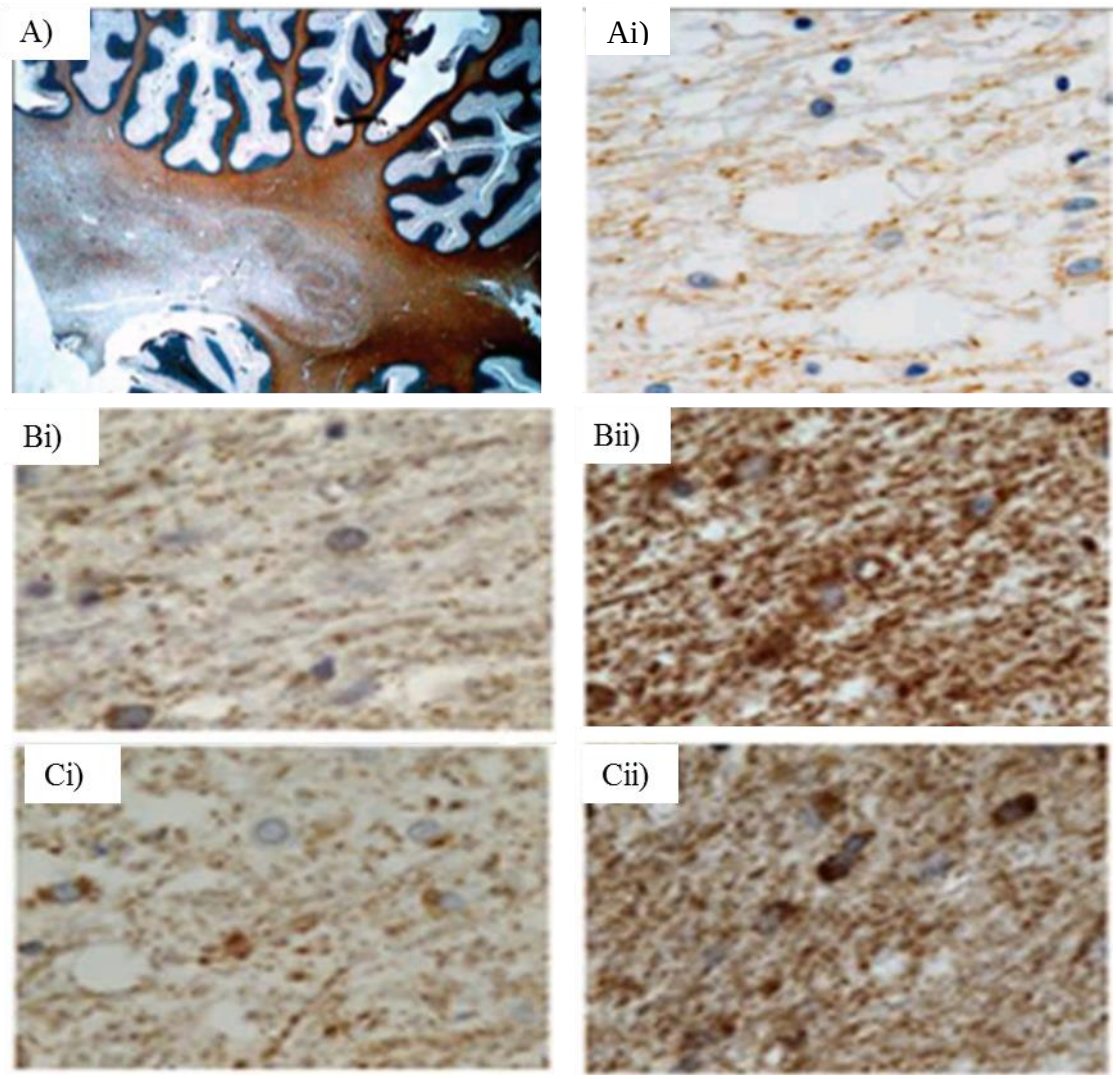

Figure 1.8: Examples of neuropathology in the cerebellum of patients with Kearns Sayre syndrome (KSS).

There is a loss of myelin-associated glycoprotein (A and Ai) in the cerebellum of a KSS patient. Immunohistochemical analysis shows there is a loss of porin (B) and complex II (C) in the dentate nucleus white matter of KSS patients (Bi and Ci) compared to controls (Bii and Cii). Image modified from Lax et al. (2012a).

1.9.2. Leber Hereditary Optic Neuropathy

The primary neuropathological feature of LHON, is the degeneration of retinal ganglion cells and axonal loss in the optic nerve (Milesi et al., 2012). During the initial stages of the disease, it is the small calibre axon fibres of the papillomacular bundle that are selectively lost resulting in optic nerve atrophy during advanced stages of the disease (Sadun et al., 2000). Surviving retinal ganglion cells, were observed to have calcium deposits and the mitochondria within those cells appeared enlarged and swollen (Kerrison et al., 1995). The spinal cord has been observed to be involved in a number of LHON cases, with axonal loss observed in the cuneate fasciculus, posterior spinal cord roots and gracile fasciculus. Alongside axonal loss, neuropil vacuolation and disintegration, neuron loss, capillary proliferation and macrophage accumulation has been observed in the gracile fasciculus (Jaros et al., 2007). Small intra-cytoplasmic hematoxylinophilic bodies were observed in the remaining neurons in the gracile fasciculus, indicating the cells are undergoing apoptosis (Jaros et al., 2007).

1.9.3. m.3243A>G

The classical neuropathological features of MELAS, are the presence of micro-infarcts or "stroke-like" lesions in the cerebellar cortex, occipital, parietal and temporal lobes (Figure1.9A) (Tanji et al., 2001; Lax et al., 2012b). The microvasculature in the cerebellum of patients with the m.3234A>G mutation has been shown to undergo a number of changes; with the mineralisation of arterioles in deep cerebellar white matter, an increase in collagen IV deposition, thinning of the smooth muscle cell layer and with COX deficiency (Figure 1.9B) observed in the vascular smooth muscle and endothelial cell layers (Lax et al., 2012c). The study by Lax et al. (2012c) also found evidence of a breakdown to the blood-brain barrier, with thinning and fragmentation of the tight junction proteins ZO-1 and occludin in m.3243A>G patients compared to controls (Lax et al., 2012c). Blood vessels walls in the basal ganglia, globus pallidus and thalamus have been shown to be undergoing calcification even though these regions are spared of neuronal degeneration (Sue et al., 1998). Electron microscopy has shown that in the smooth muscle and endothelial cell layers of cerebral and cerebellar arterioles and small arteries there is an aggregation of enlarged mitochondria (Ohama et al., 1988; Mizukami et al., 1992; Tanahashi et al., 2000). The presence of stroke like lesions and vascular pathology in the brains of m.3243A>G is likely to be associated but it is unclear if the mitochondrial impairment observed in the blood vessels is sufficient to cause lesions.

In the cerebellum, atrophy of the molecular layer and granular cells results in the increased inter-folia spacing. Additionally, there was a decrease in neuronal cell densities in the dentate

nucleus, inferior olive and Purkinje cell layer with the remaining neurons displaying a deficiency in complex I expression (Lax et al., 2012b). When the heteroplasmy of the remaining neurons in the Purkinje cell layer, inferior olive and dentate nucleus was investigated, it was shown that the percentage of the m.3243A>G mutation was typically greater than 73%, however there was no correlation between cell loss and mutation load (Lax et al., 2012b). The morphology of surviving Purkinje cells has been observed to undergo a number of changes with an increase in dendritic arborisation, mitochondria becoming trapped in thickened axons, and the formation of axonal torpedoes (Figure 1.9C) (Tanahashi et al., 2000; Lax et al., 2012b). In the dentate nucleus there are signs of a change to the synaptic input with the observations of decreased synaptophysin immunoreactivity and grumose degeneration in the close vicinity of dentate nucleus neurons (Tanahashi et al., 2000; Lax et al., 2012b). Moreover, Chrysostomou et al. (2016) has observed a loss on inhibitory synaptic contact on the dentate nucleus and the remaining GABAergic presynaptic terminals were deficient for complex I deficiency (Figure 19.D). GABAergic interneuron densities in the frontal, occipital and temporal lobes were reduced while the remaining interneurons were shown to be deficient for complex I (Lax et al., 2016).

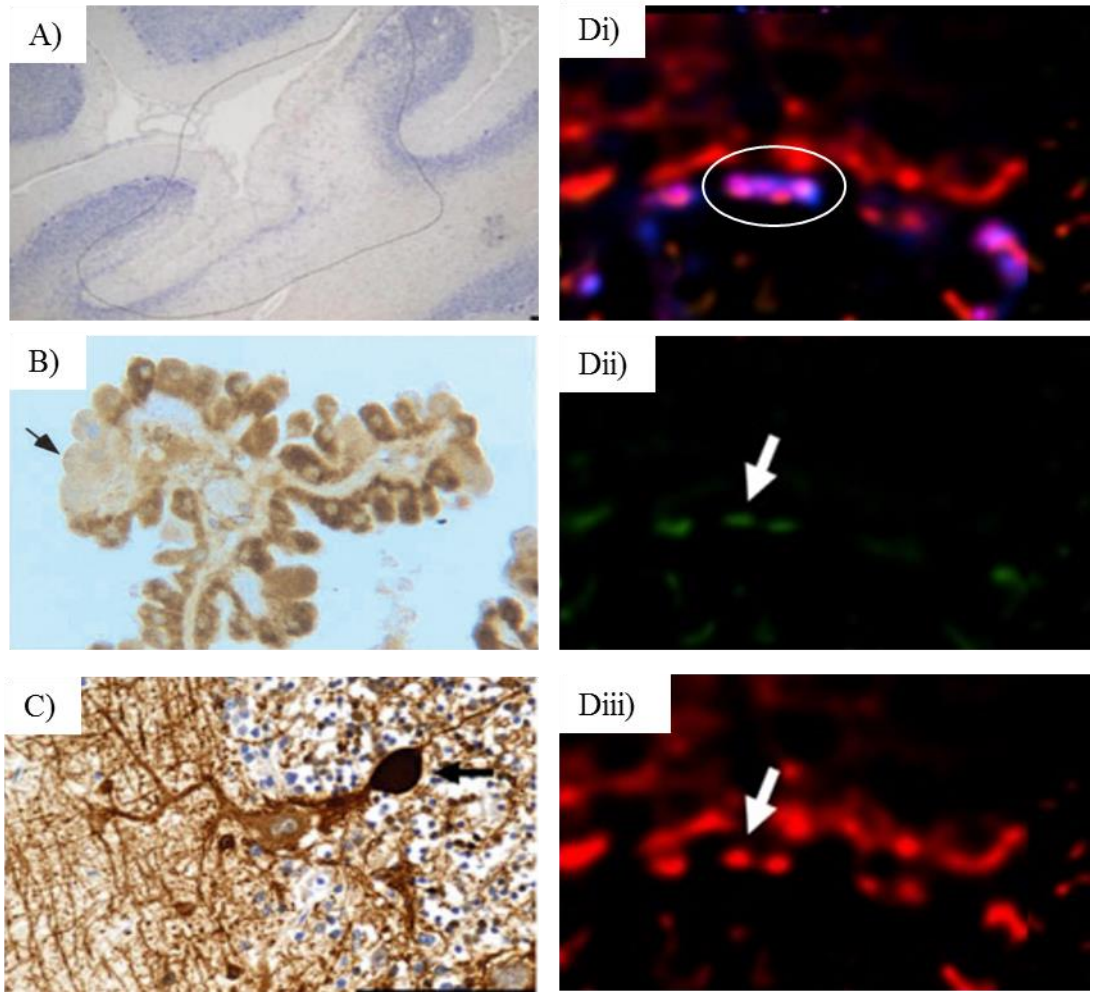

Figure 1.9: Cerebellar neuropathology in patients harbouring the m.3243A>G mutation. A) The degeneration of the white matter, granular cell layer, Purkinje cell layer and molecular layer can be observed in the stroke-like lesion (Outlined). B) COX II immunodeficiency is clearly observable in the epithelial cells (arrow) of the choroid plexus. C) A axonal torpedo has formed in the granule cell layer. D) In the inhibitory presynaptic terminals (Ci, white circle) there is a decrease in the expression of complex I expression (Cii, white arrow) compared to the mitochondrial marker (Ciii, white arrow) indicating mitochondrial dysfunction. Images modified from; A and C) Lax and Jaros (2012) B) Tanji et al. (2001) D) Chrysostomou et al. (2016)

1.9.4. m.8344A>G

The neuropathological changes observed in patients harbouring the m.8344A>G mutation are astrocytosis, demyelination and neuronal loss, found prominently in the cerebellum, spinal cord and inferior olive, red nuclei and substantia nigra of the brain stem (Takeda et al., 1988; Fukuhara, 1991). In the cerebellum, the dentate nucleus (Figure 1.10A) and inferior olive have severe neuronal loss, while there is a mild loss of Purkinje cell numbers (Tanji et al., 2001; Lax et al., 2012b). In the spinal cord, there is a mild loss of neurons to the anterior and posterior horns while in the Clark's nucleus there is a significant reduction in neuronal numbers (Sparaco et al., 1993). Investigations into respiratory chain deficiency have shown that dopaminergic neurons in the substantia nigra in a MERRF patient had a 22% and 16.3% reduction in NDUFB8 and NDUFA13 respectively (Reeve et al., 2013). This observation was confirmed by Grunewald et al. (2014), who observed a 32% reduction in NDUFB8 compared to VDAC1 in substantia nigra neurons of a patient harbouring the m.8344A>G mutation when compared to control substantia nigra neurons. A immunofluorescent study has shown that surviving GABAergic interneurons in the frontal, temporal and occipital cortices from patients harbouring the m.8344A>G mutation were deficient for NDUFA13 and COX I (Figure 1.10C) (Lax et al., 2016). It was also shown that the level of NDUFA13 was decreased in the Purkinje cell soma when compared to COX4, additionally there was a loss of GABAergic presynaptic terminals innervating dentate nucleus neurons in one of the patients harbouring the m.8344A>G mutation which correlated with the observed reduction in Purkinje cell density (Chrysostomou et al., 2016).

Abnormalities are not restricted to the neurons, cerebellar blood vessels were shown to have a high level of high heteroplasmy (≥86%), and the smooth muscle and endothelial cell layers of the arterioles were COX-deficient (Figure 1.10C) (Lax et al., 2012c). The presence of immunoreactivity against plasma proteins in Purkinje cell and dentate nucleus neurons indicates a breakdown of the blood brain barrier (BBB), this observation is further supported by the decrease in expression of tight junction proteins (Lax et al., 2012c).

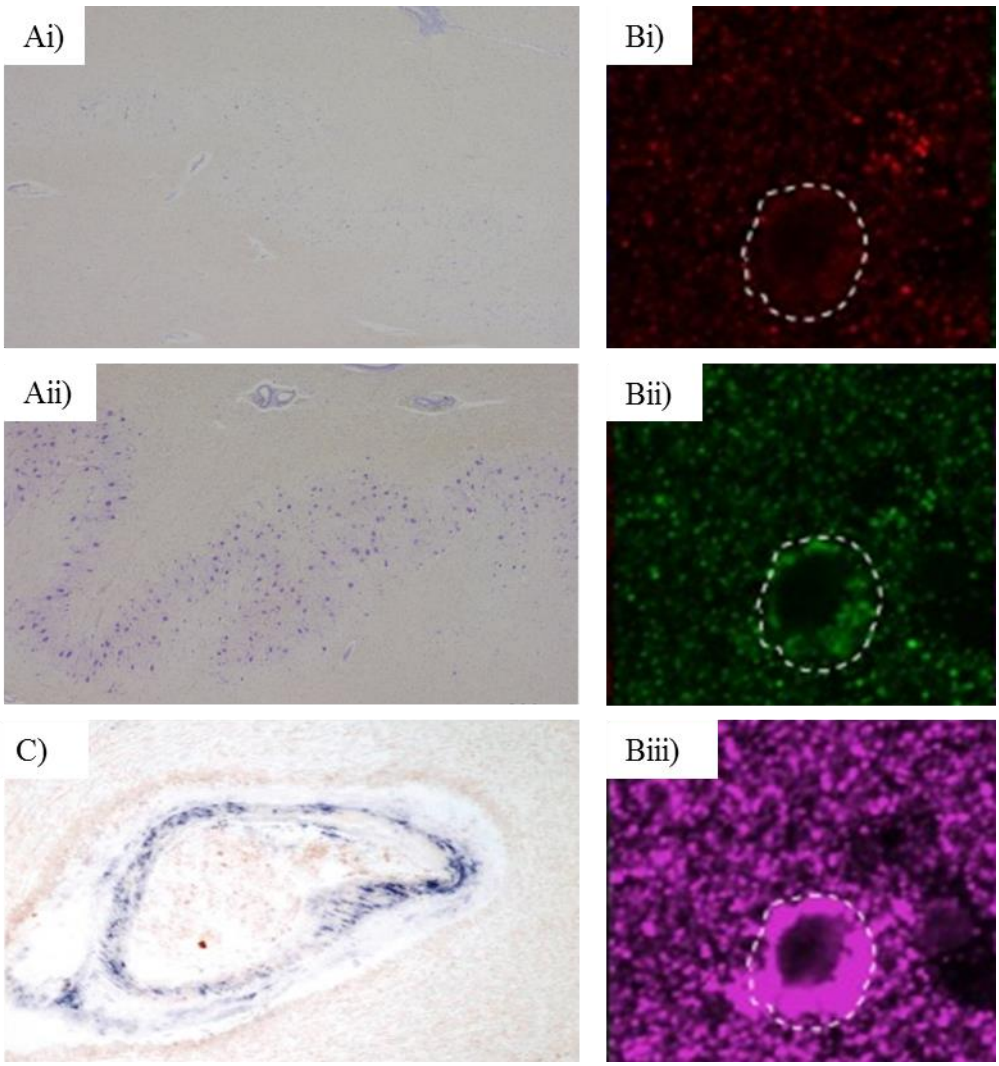

Figure 1.10: Neuropathology in patients harbouring the m.8344A>G mutation.
There is a clear loss of neurons in the dentate nucleus of a patient harbouring the m.8344A>G mutation (Ai) when compared to the dentate nucleus of a control individual (Aii). In GABAergic interneurons from the inferior temporal lobe (highlighted by dashed line), there is a reduction in the expression of complex I (NDUFB8, Bi) and complex IV (COX1, Bii) when compared to the expression of a mitochondrial protein (porin, Biii). The smooth muscle and endothelial cell layers of cerebellar arterioles are COX-deficient. Images used are modified from; A) Turnbull et al. (2010) B) Lax et al. (2016) C) Lax et al. (2012c).

1.9.5. POLG-related encephalopathy

Pathology in POLG patients can be varied with either acute focal lesions or diffuse progressive changes with intraregional distributions. Focal demarcated lesions have been observed in the neocortex, hippocampus, cerebellum (Figure 1.11A) and thalamus and the lesions are characterised by neuronal loss, eosinophilic neuronal necrosis, vacuolation of the neuropil, astrocytosis (Figure 1.11B) and diffuse microglia activation (Figure 1.11C) (Tzoulis et al., 2014).

In patients with Alpers syndrome, neuropathological examination showed that predominantly the occipital and temporal lobe of the cerebral cortex, but also the cerebellum, hippocampus and olfactory lobe, had symmetrical but multifocal ischaemic encephalopathy with laminar necrosis and neuronal degeneration (Khan et al., 2012). Other pathology has also been observed with gliosis reported in the basal ganglia, brainstem and most prominently the occipital lobe (Wiltshire et al., 2008). In a recent study by Tzoulis et al. (2014), showed that 8 patients with POLG-related encephalopathy, all had focal lesions in the cerebellar cortex, where there was severe loss of Purkinje cells and granule cells with Bergman gliosis. In the dentate nucleus there was severe neuronal loss and the surviving neurons had a pronounced accumulation of lipofuscin. In those patients, neuronal loss and gliosis was also observed in the thalamus and locus coeruleus and inferior olivary nucleus of the brainstem. While focal lesions in the neocortex, hippocampus, thalamus and cerebellum showed astrocytosis, diffuse microglial activation, eosinophilic neuronal necrosis, neuronal loss and vacuolation of the neuropil (Tzoulis et al., 2014). When expression levels of components of the ETC were investigated, the remaining neurons in the regions with chronic changes and higher neuronal density had the greatest level of deficiency when compared to sites of focal degeneration. The substantia nigra, red, olivary and pontine nucleus were shown to have the greatest reduction in expression of ETC proteins (Tzoulis et al., 2014).

The midbrain has also been shown to be susceptible in POLG encephalopathies, with the observation of significant loss of the dopaminergic neurons (Figure 1.11D), astrogliosis and microglia activation in the red nucleus and the substantia nigra pars compacta. The remaining neurons in these regions were shown to have complex I deficiency and had 50-60% less mtDNA than control neurons (Tzoulis et al., 2013).

Microinfarcts with astrogliosis were observed in the cerebellums of patients with heterozygous POLG mutations, (Lax et al., 2012b). The study also observed neuronal loss and demyelination in the dentate nucleus which was surprising as the heteroplasmic levels of deleted mtDNA deletion were low in those regions. In a more recent study by the same

colleagues, the occipital, temporal and frontal cortices were shown to have a significant reduction in inhibitory interneurons while a quadruple immunofluorescent assay showed the remaining inhibitory interneurons to be complex I deficient (Lax et al., 2016).

A study by Lax et al. (2012d), investigating pathology in the spinal cord of 11 patients with compound heterozygous mutations in POLG, found evidence of myelin and axonal loss in the posterior spina funiculus. While in the dorsal root ganglion, posterior and anterior horn there was a reduction in neuronal density. The surviving neurons in the posterior horn were deficient for NDUFB8, NDUFS3 and NDUFA9. A similar observation in the dorsal root ganglion was also observed, with a 33% and 34% reduction in the presence of NDUFS1and NDUFB8, respectively. In addition to the complex I deficiency, there was abnormal distribution of mitochondria in the cytoplasm in the dorsal root ganglion (Figure 1.11E). When investigating the mtDNA copy number in the remaining neurons of the dorsal root ganglion it was shown that MT-ND1 was markedly reduced compared to control neurons, inferring that in addition to the mtDNA deletions associated with the POLG mutation, the neurons also have a reduction in wild type copy number.

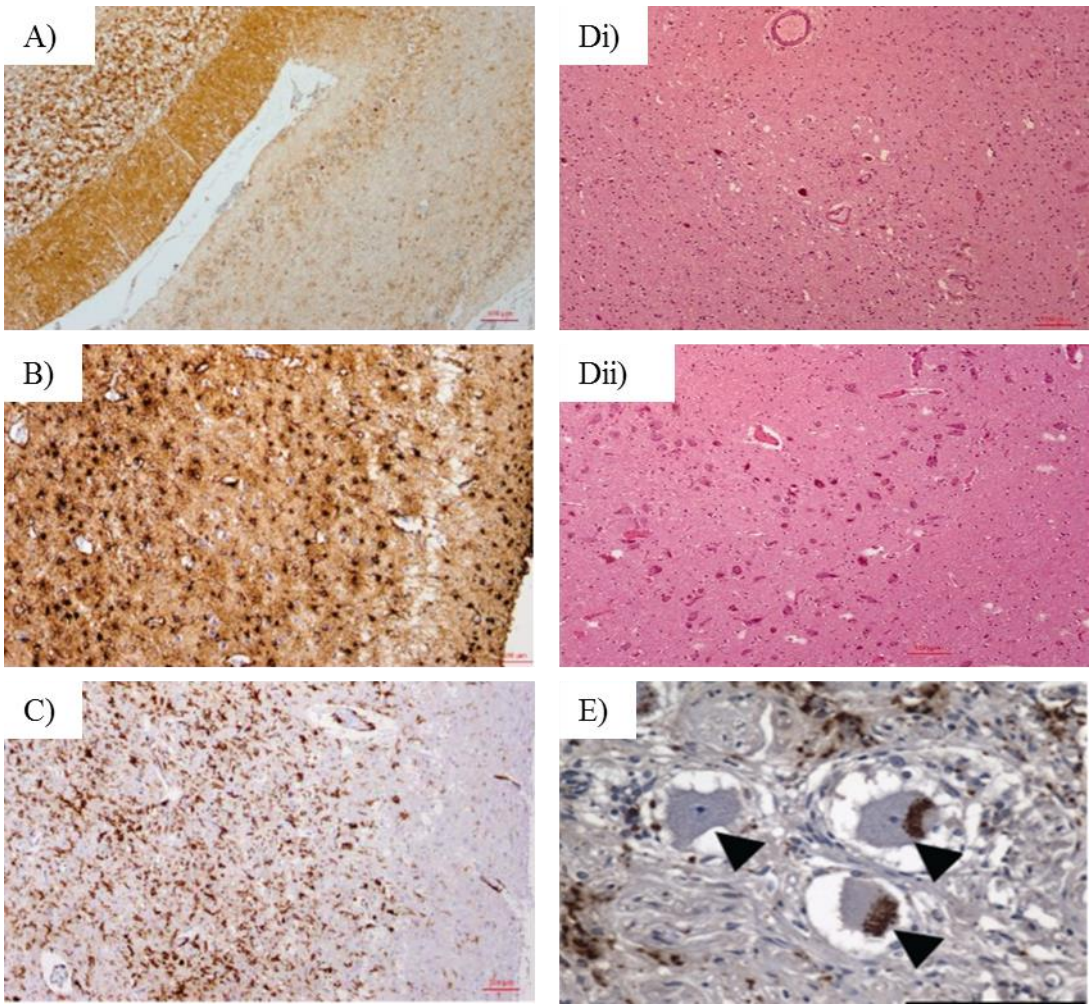

Figure 1.11: Neuropathology in POLG-related encephalopathy.

A) Microscopic focal, sharply demarcated lesions can be observed in the cerebellum. B) Increased immunohistochemical reactivity to glial fibrillary acidic protein shows the presence of astrocytosis C) Diffuse microglial activation can be observed in cortical acute lesions. D) The profound loss of dopaminergic neurons in ventrolateral tier of the substantia nigra in POLG encephalopathy (Di) is made evident when compared to the substantia nigra in a control individual (Dii). E) In dorsal root ganglions there was abnormal clustering of mitochondria (arrow heads). Images modified from; A, B and C)Tzoulis et al. (2014) D) Lax et al. (2012d)

1.10. Mitochondrial dysfunction and axonal pathology

In mitochondrial disease, it is predominantly the grey matter that is observed to be degenerating, however the white matter is also susceptible to degeneration or changes. Typically white matter involvement in primary mitochondrial disease is not a prominent feature but in the case of individuals with KSS, demyelination along with spongiform degeneration predominantly in the cerebral white matter and basal ganglia and to a lesser degree in the cerebellar white matter and spinal cord is characteristic of the disease mechanism (Sparaco et al., 1993; Lax et al., 2012a). In individuals with MELAS and MERRF necrotic lesions of cerebral and cerebellar white matter show a decrease in myelin and axon number (Sparaco et al., 1993; Terauchi et al., 1996). MRI studies on patients with MELAS have observed bilateral deep white matter changes in the frontal and occipital lobes (Fujii et al., 1990), changes to the parieto-occipital white matter (Barkovich et al., 1993), both diffuse and focal changes to the periventricular white matter (Castillo et al., 1995) and cerebral and cerebellar white matter lesions in located the border zones between two major cerebral arteries (Apostolova et al., 2005). Diffuse axonal loss was observed in the medulla oblongata and cerebral white matter while in the deep white matter there were multiple necrotic lesions in a MELAS case (Yokoyama et al., 2010). Severe demyelination and axonal degeneration was observed in the spinal cord and to a lesser degree in the cerebellar white matter and thalamus of a patient with the m.8344A>G mutation (Sparaco et al., 1993; Erol et al., 2009). In LHON, electron microscopy (EM) studies found degenerating optic nerve axons with varying levels of myelination and some axons were completely demyelinated (Sadun et al., 1994; Carelli et al., 1999). In the myelinated post-laminar portion of the optic nerve, accumulated swollen mitochondria were observed while cytoskeletal molecules accumulated in the axons (Sadun et al., 1994; Carelli et al., 1999).

An additional observation in the cerebellum of individuals with mitochondrial disease is the presence of large swellings in the Purkinje cell axons, known as axonal torpedoes (Mori et al., 2000b; Lax et al., 2012b), which will be further described in chapter 3. In addition to causing white matter disturbances in mitochondrial diseases, mitochondrial dysfunction has been involved in the pathogenesis of axonal injury in other neurological disorders such as Multiple Sclerosis (MS) (Trapp and Stys, 2009). In a study by Mahad et al. (2009), mitochondrial changes were observed in chronic active lesions, where there was a decrease in COXIV activity in demyelinated axons. While in demyelinated axons from inactive areas of chronic lesions mitochondrial respiratory chain complex IV activity and mitochondrial mass were increased. Additionally, the activity of complex I and III were observed to be decreased in

mitochondria-enriched fractions from the motor cortex of tissue isolated from post-mortem MS motor cortex (Dutta et al., 2006).

With the demonstration of axonal loss preceding neuronal death in MS, where axonal degeneration is associated with the progressive neurological decline (Bjartmar et al., 2000) and PD (Burke and O'Malley, 2013) as well as the observation of mitochondrial dysfunction in association with white matter disturbances and demyelination. The investigation of respiratory chain deficiency on axons and the subsequent changes in axonal morphology, like the formation of axonal torpedoes in the cerebellum of patients, may allude to the mechanisms leading to cerebellar ataxia.

1.11. The Cerebellum

As described above the cerebellum is commonly afflicted in mitochondrial disease with both paediatric and adult's patients commonly presenting clinically with cerebellar ataxia which is defined by a lack of balance, coordination and motor control. Additionally, neuropathological abnormalities, including cerebellar atrophy and those described throughout section 1.10 are frequently detected (Lebre et al., 2011). The prominent involvement of the cerebellum indicates that the cerebellar neurons are particularly vulnerable to disrupted OXPHOS.

1.11.1. Cerebellar structure

The cerebellum is located in the posterior region of the brain and is a part of the hind brain along with the medulla and pons. The main role of the cerebellum is to process the ascending sensory and descending motor signals which are crucial for muscle tone and motor movement coordination. In addition to its role in motor coordination recent evidence has shown the cerebellum plays a role in cognition and emotion (Ito, 2008; Stoodley, 2012; Buckner, 2013).

The architecture of the cerebellum is one of the most elaborate in the whole CNS and contains over half the mature neurons in the adult CNS. The cerebellum has a three longitudinal regions either side of the midline that run along the rostral to caudal plane. These regions are then further folded into 10 lobules (I-X) and then further divided in to folia (figure 1.12A (Apps and Hawkes, 2009). In addition to the longitudinal organization, the cerebellum can also be divided into traverse zones based on gene expression. The four traverse zones are; anterior, posterior, central and nodular zones. Each traverse zone can be further divided into a series of stripes or bands that are positioned along the rostrocaudal axis (Apps and Hawkes, 2009). The stripes are defined by the expression of molecular markers, with the metabolic enzyme aldolase C (zebrin II) being the most extensively studied (Brochu et al., 1990; Hawkes and Herrup, 1995).

The cerebellar cortex has a rather basic histological structure composed of three stratums, the Purkinje cell layer (PCL), the granular cell layer (GCL) and the molecular layer (ML) (Figure 1.12B). The main excitatory neuron in the cerebellum, are the granule cells and are found abundantly in the GCL along with the inhibitory Golgi cells. Purkinje cells are inhibitory neurons which are the major output neuron of the cerebellum and form a distinct "neuronal ribbon" between the GCL and the ML (Martin, 2002). The inhibitory interneurons, Basket and stellate cells, reside in the molecular cell layer. Along with the cerebellar cortex there is the medullary core of white matter and three deep cerebellar nuclei (DCN); the dentate, the fastigial and the interposed nucleus.

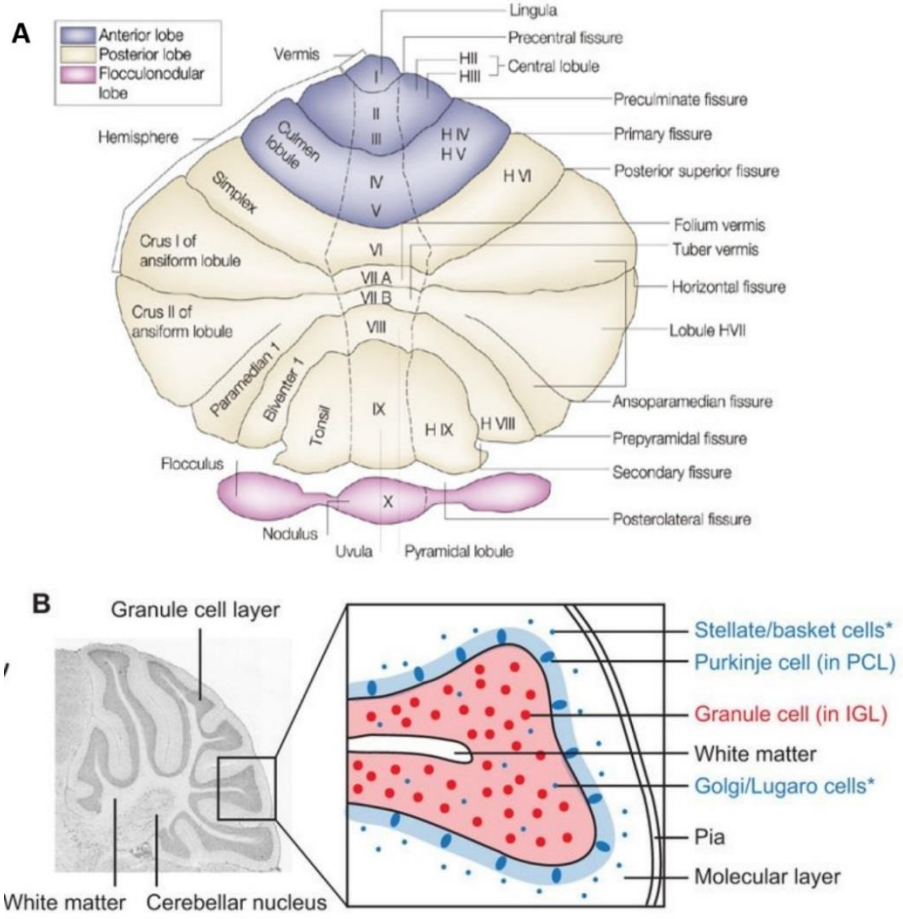

Figure 1.12: The structure of the cerebellum.

A) A graphical representation of the lobes, lobules and main fissures in the unfolded cerebellar cortex. B) The three stratums of the cerebellum. Inhibitory interneurons are annotated in blue text, while excitatory neurons are annotated in red text. Figure 1.9A is modified from Manni and Petrosini (2004) and 1.9B is modified from Butts et al. (2014)

1.11.2. Cerebellar circuitry

The cerebellum receives input from the inferior olive (IO), the brainstem and spinal cord. The main input neurons are the climbing fibres and mossy fibres which act upon the main output neuron, the Purkinje cell.

The climbing fibres originate from the inferior olive in the caudal brain stem and project their thick ramifications through the GCL and PCL to act directly on the Purkinje cell by forming excitatory synapses on the smooth lower branches of the dendritic tree in the ML. Only one climbing fibre innervates a single Purkinje cell, but that single climbing fibres makes multiple synaptic contact generating the largest depolarising event seen in any neuron (Eccles et al., 1966).

Unlike the climbing fibers, Mossy fibers indirectly innervate the Purkinjec cells. Mossy fibers originate from the cuneocerebellar, dorsal spinocerebellar, pontocerebellar, and vestibulocerebellar tracts and finish in the GCL where glutamatergic synapses innervate granule cells and occasionally Golgi cells. Granule cells are excitatory neurons whose extending axons bifurcate in a T-fashion in the ML forming parallel fibres that extend horizontally along the long axis of the folia and parallel to the PCL (Voogd and Glickstein, 1998). The parallel fibres intersect the expansive dendrites of the Purkinje cells in the ML, where they form excitatory synapse on either the spiny branches of Purkinje cell dendrites or the interneurons; stellate and basket cells. A single parallel fibre will innervate several hundred Purkinje cells as it traverses along the ML (Napper and Harvey, 1988). An inhibitory feed-back loop is formed by the Golgi cells as they receive excitatory input from the mossy fibres and granule cells but they also innervate the granule cells and parallel fibres.

Purkinje cells are large GABAergic inhibitory neurons, whose axons are the sole output of the cerebellum and extend through the GCL and white matter tract to the deep cerebellar nuclei where the axons terminates with inhibitory synapses. As Purkinje cells are the main output neurons they must integrate both excitatory input from climbing and mossy fibres with inhibitory input from basket and stellate cells. Occasionally climbing fibres and mossy fibres also innervate the deep cerebellar nuclei. The circuit between the Purkinje cells and the dentate nucleus is the main intra-cerebellar circuit. The microcircuit of the cerebellum is depicted in Figure 1.13.

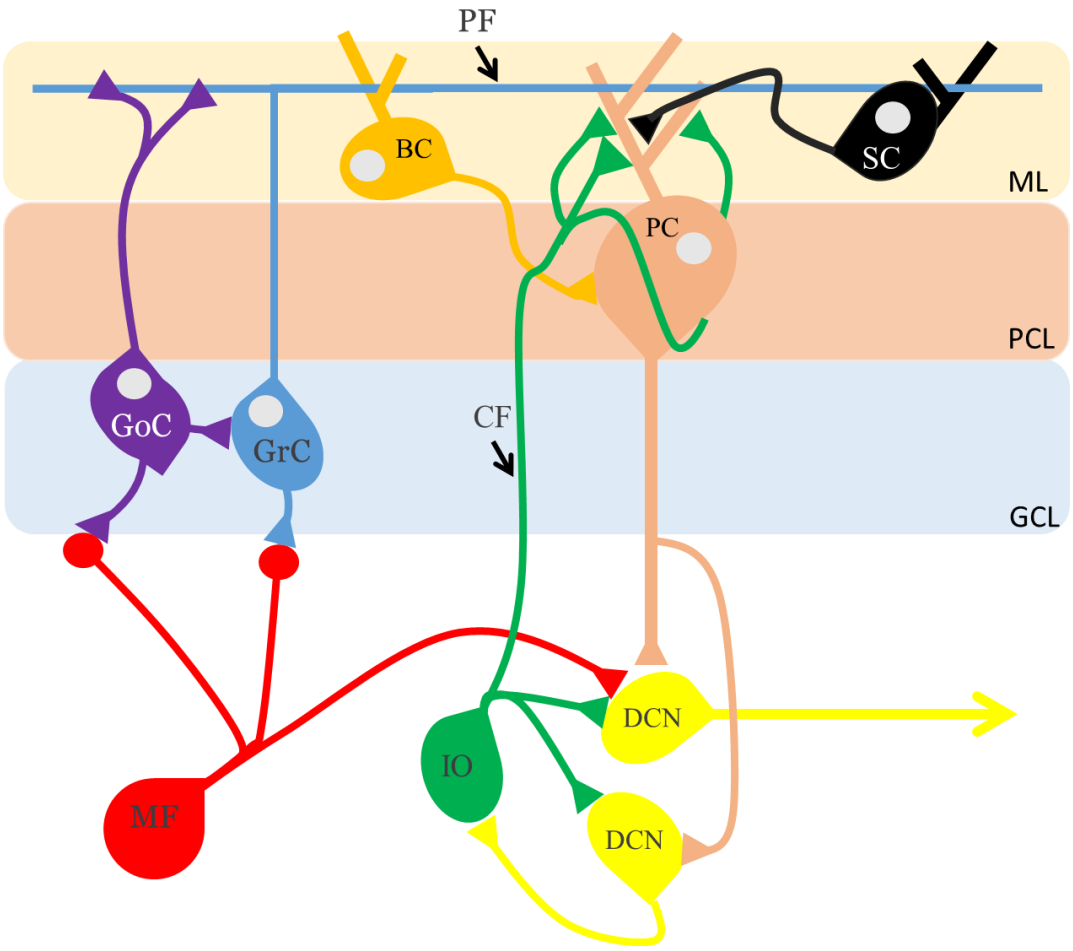

Figure 1.13: The circuitry of the olivo-cerebellar pathways.

The two main afferent neurons in the cerebellum are the mossy fibres (MF) and the thick ramifications known as climbing fibres (CF). Originating from numerous brain stem and spinal cord nuclei, the MF's make excitatory synaptic contacts with granule cells (GrC) and with Golgi cells (GoC) in the Granular cell Layer (GCL) as well as neurons in the deep cerebellar nuclei (DCN). Bifurication of the GrC ascending axons forms Parallel fibres (PF) in the molecular layer. The PF's form excitatory synapses with Purkinje cells (PC) and with interneurons (stellate (SC) and basket cells (BC)) in the molecular layer (ML) as well as GoC's. The second main afferent the CF's ascend from the Inferior Olive (IO) to the PC where it forms a powerful 'climbing' multi-synaptic contact. The PC forms a distinct "neuronal ribbon" known as the Purkinje cell layer (PCL) and are the main output neurons of the cerebellum which inhibits DCN. It is only the GrC that make excitatory synapses the rest of the cerebellar cortical neurons, make inhibitory synaptic connections with their target neurons with the end goal being controlling the signal output from the DCN.

1.13. Aims

As described above, the cerebellum is commonly affected in patients with mitochondrial disease. A common observation in the cerebellum is the presence of axonal torpedoes which are explained in detail in chapter 3. As these structures have not been thoroughly characterised in mitochondrial disease, the aims of my thesis are to characterise axonal torpedoes as well as morphological changes to the Purkinje cell axons in patients with mitochondrial disease. This work will aim to provide an insight into how respiratory chain deficiency relates to axonal torpedo formation and changes in the Purkinje cell connectivity which may provide an insight into the genesis of cerebellar ataxia. The aim of characterising the axonal torpedoes further will help understand how the axonal torpedoes are detrimental and degenerative to the Purkinje cell and may present a therapeutic target. I aim to answer the following questions:

1. Are axonal torpedoes more prevalent in patients with mitochondrial disease and is there evidence that the axonal torpedoes are involved in a degenerative process?
2. What are the structural abnormalities or changes associated with the presence and formation of axonal torpedoes?
3. Is there any evidence for respiratory chain deficiency in axonal torpedoes, Purkinje cell bodies and Purkinje cell axons?
4. Is there any evidence that respiratory chain deficiency causes a change to the morphology of Purkinje cell axons?

Chapter 2. Materials and Method

2.1. Materials

2.1.1. Equipment

Equipment	Manufacturer
65˚C Oven	Genlab MIN016
2100 Antigen Retriever	Aptum Biologics Ltd
2511 Dry Vacuum Pump	Welch
Balance	Adventurer Ohaus
Desiccator chamber	Scienceware
Laminar Flow hood	Jencons-PLS
Magnetic Stirrer	IKA RCT Basic
Microwave	Sharp R95ST
Nanopure Water	Elga
Nikon A1R Single photon Confocal	Nikon
pH meter	Jenway 3510
Rotatest Shaker	Luckham R100
See-Saw Rocker SSL4	Stuart
Software	
ImageJ	National Institute of Health
Imaris v8	Berkin
SAS	SAS Institute Inc.
Volocity 3D Image Analysis	PerkinElmer
Stereology BX51 Light Microscope	Olympus
Water bath	Grant Subaqua pro
Hyrax V50 Vibratome	Zeiss

2.1.2.

Consumables

Coverslips (22 x 22mm, 22 x 40mm, 22 x 50mm)	VWR

Eppendorf tubes (1.5mL, 2mL)	Biogene
Falcon Tubes (15mL, 50mL)	BD biosciences
Glass Pasteur pipettes 230mm	Volac
Pipette Tips	Star Lab
Pasteur Pipettes	VWR
Pipettes	
p10	Eppendorf
p20, p200	Ergone
p1000, p5000	Gilson
Six well plates	Greiner Bio-one
Whatman grade I filter paper	Merk

2.1.3. Solutions

Unless stated otherwise, all solutions made using nanopure 18 mega Ω activity water.

Solution	Components
10 % Normal goat serum (NGS) blocking solution	100µl Normal goat serum 1 ml dH2O
Clearing Solution	12.366 g Boric acid 40 g Sodium dodecyl sulphate 1 l dH2O pH 8.5
3,3′-Diaminobenzidine	2 3,3′-Diaminobenzidine tablet 5 ml dH2O
EDTA	0.416 g EDTA 1 l dH2O pH8
Fructose (20%,60%,80%, 100% weight/volume)	Xg Fructose 50 ml dH2O
Glycine	1.5 g glycine 100 ml dH2O pH 7.4
Hydrogel solution	20 ml Acrylamide 10 ml bis-acrylamide 1 g VA-044 Initiator 40 ml PBS 310 ml dH2O
3% Hydrogen Peroxide Solution	12 ml Hydrogen Peroxide 388 ml dH2O

1X Phosphate buffered saline (PBS)	8 g Sodium Chloride 0.2 g Potassium Chloride 1.42 g Sodium hydrogen phosphate 0.245 g Potassium dihydrogen phosphate 1 l dH2O pH 7.4
10X Phosphate buffered saline (PBS)	80 g Sodium Chloride 20 g Potassium Chloride 14.2 g Sodium hydrogen phosphate 2.45 g Potassium dihydrogen phosphate 1 l dH2O pH 7.4
Phosphate buffer solution (PB)	0.62 g Sodium dihydrogen phosphate 2.18 g Sodium hydrogen phosphate 1 l dH2O pH 7.4
Refractive Index Matching Solution (RIMS)	40 g Histodenze 30 ml PB 0.1% tween-20
Scotts tap water	20 g Magnesium sulphate 2 g Sodium bicarbonate few crystals of thymol 1 l dH2O
SeeDB	20.25 g fructose 5 ml dH2O 100 µl α-thioglycerol
Sodium Borate Buffer	61.83 g boric acid 10 g Sodium Hydroxide 1 l dH2O
Sudan Black	0.5 g Sudan Black 100 ml 70% Ethanol

Tris Buffer Saline	1.2 g Trizma Base 17 g Sodium Chloride 2 l dH2O pH 7.4
Tri-sodium citrate	2.94g tri-sodium citrate 1 l dH20 pH 6

2.1.4. Chemicals

Chemical	Manufacturer
α-thioglycerol	Sigma
Acrylamide	BioRad
Bis-acrylamide	BioRad
Boric Acid	Sigma
3,3′-Diaminobenzidine tablets	Sigma
DPX Mountant	Sigma
EDTA	Affymetrix USB Products
Ethanol	Fisher Chemicals
Fructose	Sigma
Glycine	Sigma
Haemotoxylin	TCS Biosciences Ltd
Histoclear	National Diagnostics
Histodenze	Sigma
Horse-radish peroxidase (HRP)-polymer	CellPath Ltd
Hydrogen Peroxide	Sigma
Magnesium sulphate	Sigma
Normal Goat serum	Sigma
4% Paraformaldehyde	Santa Cruz
Potassium dihydrogen phosphate	AnalR
Potassium Chloride	Sigma
Prolong Gold Antifade	Life Technologies
Sodium Bicarbonate	Sigma
Sodium Chloride	Sigma
Sodium dihydrogen phosphate	AnalR

Sodium Dodecyl sulphate	Sigma
Sodium hydrogen phosphate	AnalR
Sodium Hydroxide	AnalR
Sudan black	Reactifs Ral
Trizma Base	Sigma
Tween 20	Sigma
VA-044 Initiator	Alpha Laboratories
Universal probe	CellPath Ltd

2.1.5. Tissue Details

2.1.5.1. Human

Human cerebellum brain tissue was obtained from the Newcastle Brain Tissue Resource (NBTR) and Edinburgh Sudden Death Brain Bank and included tissues from 13 patients with clinically and genetically well characterised mitochondrial disease (Table2.1) and 16 non-neurologically affected control individuals (Table 2.2). All patients and their families provided informed consent to donate their tissue for research purposes and ethical approval for this study was gained from Newcastle and North Tyneside Local Research Ethics Committee (LREC 2002/205).

2.1.5.2. Mice

For the optimisation of the Clear Lipid-exchanged Acrylamide-hybridized Rigid Imaging/Microscopy (CLARITY) method, 12 month old wild type C57BL/6 mice were used. These mice were cared for and housed at the Comparative Biology Centre, Newcastle University under conditions and regulations in compliance with the Animals (Scientific Procedures) Act 1986 and its associated Codes of Practice.

	Gender	Age (Years)	PMI (Hours)	Genetic defect	Cause of Death
Patient 1	F	40	58	m.3243A>G	Respiratory Failure
Patient 2	F	20	187	m.3243A>G	Aspiration pneumonia with MELAS
Patient 3	F	36	9	m.3243A>G	Myocardial infarction
Patient 4	M	45	43	m.3243A>G	Complications associated with mitochondrial disease
Patient 5	M	59	67	POLG (p.Gly848Ser and p.Ser1104Cys)	Unknown
Patient 6	M	30	21	m.3243A>G	Unknown
Patient 8	F	60	10	m.3243A>G	Multi-organ failure
Patient 7	F	42	59	m.8344A>G	Respiratory failure
Patient 9	M	58	66	m.8344A>G	Unknown
Patient 10	M	79	85	POLG (p.Thr251Ile/p.Pro 587Leu; p.Ala467Thr)	Pneumonia due to mitochondrial disease
Patient 11	M	55	112	POLG (p.Trp748Ser and p.Arg1096Cys)	Complications associated with mitochondrial disease
Patient 12	F	60	39	Unconfirmed Multiple mtDNA deletions due a nDNA defect	Pulmonary embolus
Patient 13	M	47	76	m.3243A>G	Myocardial infarction

Table 2.1: Summary of patients with mitochondrial disease that were used in this project.

The details of patients include age, gender, post mortem interval (PMI) and cause of death from tissue that was supplied by NBTR.

	Gender	Age (Years)	PMI (Hours)	Cause of Death
Control 1	F	69	16	Gastric Cancer
Control 2	F	74	53	Heart Failure
Control 3	M	55	51	Liver Cancer
Control 4	F	74	67	Lung Cancer
Control 5	M	70	72	Metastatic Ovarian Cancer
Control 6	F	77	83	Myocardial Infarction
Control 7	M	48	46	Coronary Artery Atherosclerosis
Control 8	M	44	83	Coronary Artery Atherosclerosis
Control 9	M	45	44	Complications of Bronchopneumia and Coronary Artery Atherosclerosis
Control 10	M	25	53	Hanging
Control 11	M	61	61	Hanging
Control 12	M	48	43	Coronary Artery Thrombosis
Control 13	M	72	17	Oesophageal adenocarcinoma
Control 14	F	78	34	Metastatic Ovarian Cancer
Control 15	F	72	27	Pulmonary oedema
Control 16	F	58	39	Cushings Disease

Table 2.2: Summary of control individuals that were used in this project.

The details of controls include age, gender, post mortem interval (PMI) and cause of death from tissue that was supplied by NBTR and Edinburgh Sudden Death Brain Bank.

2.2. Methods

All the primary and secondary antibodies used in this project are summarised in table 2.3 and 2.4 respectively. The appropriate dilution and antigen retrieval method will be explained in chapter when specifically used.

2.2.1. Immunohistochemistry

5µm formalin-fixed, paraffin-embedded (FFPE) cerebellar sections cut on the sagittal plane were deparaffinised using Histoclear then rehydrated through a graded ethanol series. The next step was to complete the appropriate method of antigen retrieval followed by incubation of the sections in a 3% hydrogen peroxide solution for 30 minutes to block endogenous peroxidase activity. The sections were washed 3x 5 minutes with tris buffered saline (TBS) and then the primary antibodies were applied at the optimal dilution for 1 hour. Post primary antibody incubation the sections underwent 3x 5minute TBS washes followed by a 30 minute incubation with a universal probe. Another 3x 5 minutes TBS washes were applied before a 30 minute incubation with horse-radish peroxidase (HRP)-polymer. The sections were then washed thoroughly with distilled water followed by a 5 minute incubation with 3, 3'-diaminobenzadine (DAB). A further 5 minute wash with distilled water was applied before being counterstained with Mayer's haematoxylin and using Scott's tap water. Finally the sections were dehydrated and mounted in DPX.

2.2.2. Immunofluoresence

Immunofluorescence was performed on 5µM FFPE sagittal cerebellar sections. The sections were deparaffinised and rehydrated before performing antigen retrieval specific to the primary antibodies used (table 2.3). Sections were washed well in distilled water before incubation in 10% (v/v) normal goat serum for 60 minutes to minimise non-specific binding of the secondary antibodies and to give the highest signal to noise ratio. The sections were incubated in primary antibodies diluted in PBS at 4˚C overnight. The following day, sections were washed with PBS before being incubated with fluorescent secondary antibodies for 120 minutes at 4˚C. Sections were incubated in Sudan black solution (0.3% w/v in 70% v/v ethanol) 10 minutes and washed well in distilled water. The sections were then mounted in prolong gold anti-fade solution and cover slipped before being stored at -20˚C.

Primary antibody	Target	Host and isotype	Supplier
Anti-GAD65/67	Glutamic acid decarboxylase 65–67	Rabbit IgG	Sigma
Anti-SMI-31R	Phosphorylated heavy subunit of neurofilaments	Mouse IgG1	Biolegend
Anti-SMI-32	Non-phosphorylated heavy subunit of neurofilaments	Mouse IgG1	Biolegend
Anti-amyloid precursor protein	Amyloid Precursor Protein	Rabbit IgG	Thermo Fisher Scientific
Anti-synaptophysin	Synaptophysin	Mouse IgG1	Dako
Anti-beta III Tubulin [TUJ-1]	β-tubulin (TuJ-1)	Mouse IgG2a	Abcam
Anti-Acetylated alpha Tubulin	Acetylated alpha Tubulin	Mouse IgG2b	Abcam
Anti-complex I 19 kDa	NDUFA13	Mouse IgG2b	Abcam
Anti-neurofilament H 200kDa	neurofilament H (200 kDa)	Rabbit IgG	Millipore
Anti-SMI-94	Myelin Basic Protein	Mouse IgG1	Biolegend
Anti-SMI-99	Myelin Basic Protein	Mouse IgG2b	Abcam
Anti-Porin	porin	Mouse IgG2b	Abcam
Anti-MTCO1	Cytochrome C Oxidase subunit I (COX1)	Mouse IgG2a	Abcam
Anti-COX4 + COX4L2	cytochrome C oxidase subunit IV (COX4)	Mouse IgG2a	Abcam
Anti-glut-1	Glut-1 (endothelial)	Rabbit IgG	Sigma
Anti-SDHA	Succinate Dehydrogenase Complex, Subunit A (SDHA)	Mouse IgG1	Abcam
Anti-myelin basic protein	Myelin Basic Protein	Chicken IgY	Aves Lab
Anti-neurofilament H 200kDa	Neurofilament H (200 kDa)	Chicken IgY	Aves Lab
Anti-α smooth muscle actin	α smooth muscle actin	Mouse IgG2a	Dako
Anti-parvalbumin	Parvalbumin	Mouse IgG1	Swant
Anti-calbindin D-28k	Calbindin D-28k	Mouse IgG1	Swant
Anti-NaV1.6	Type VI Sodium Channel	Rabbit IgG	Alamone Labs

Table 2.3: Summary of primary antibodies used.
Properties of the primary antibodies used throughout the project.

Antibody	Target	Manufacturer
Alexa Fluor 633 anti-mouse IgG1	Mouse IgG1	Thermo Fisher Scientific
Alexa Fluor 633 anti-mouse IgG2a	Mouse IgG2a	
Alexa Fluor 633 anti-mouse IgG2b	Mouse IgG2b	
Alexa Fluor 647nm anti-mouse IgG1	Mouse IgG1	
Alexa Fluor 405nm anti-rabbit IgG	Rabbit IgG	
Alexa Fluor 405nm anti-mouse IgG2a	mouse IgG2a	
Alexa Fluor 405nm Streptavidin Conjugate	Biotin	
Alexa Fluor 488nm anti-mouse IgG1	Mouse IgG1	
Alexa Fluor 488nm anti-mouse IgG2b	Mouse IgG2b	
Alexa Fluor 488nm anti-mouse IgG2a	Mouse IgG2a	
Alexa Fluor 488nm anti-Rabbit IgG	Rabbit IgG	
Fluorescein Goat Anti-Chicken IgY	Chicken IgY	
Alexa Fluor 546nm anti-mouse IgG1	Mouse IgG1	
Alexa Fluor 546nm anti-rabbit IgG	Rabbit IgG	
Alexa Flour 546nm anti-mouse IgG2a	mouse IgG2a	
Alexa Flour 546nm anti-mouse IgG2b	mouse IgG2b	
Biotinylated anti-Rabbit IgG	anti-Rabbit IgG	Jackson Laboratories

Table 2.4: Summary of secondary antibodies used.
Details about all the secondary antibodies that were used throughout the project. The host species of each secondary antibody was goat and the dilution used was 1:100.

2.2.3. SeeDB

The SeeDB method is based on the technique described in the study by Ke et al. (2013). 12 month old wild type C57BL/6 mice were killed humanely and their brains were removed. The brains were incubated in 4% paraformaldehyde at 4ºC overnight and then washed with PBS. The brains were then sectioned to 250µm using a Hyrax V50 vibratome (Frequency 70Hz, Amplitude 0.7m, Zeiss). The sections were then blocked in 10% Normal Goat Serum (NGS) in PBS for one hour before having the primary antibodies (anti-SMI-31R, Anti-neurofilament H 200kDa and Anti-MTCO1)in PBS applied for 4 days at 4ºC. The sections were then washed the sample in PBS three times for an hour each. The secondary antibodies (Alexa Fluor 488nm anti-mouse IgG1, Alexa Fluor 546nm anti-rabbit IgG and Alexa Fluor 633 anti-mouse IgG2a) were then applied in PBS for 3 days at 4˚C. The sections are then washed again with 3x1hour PBS washes.

The sections then undergo the SeeDB clearing method. Sections are incubated ~20 ml of 20% (w/v) fructose solution for 8 hrs at 37 °C. The sections are then incubated in 40% (w/v) fructose for 8 hrs at 37 °C. The next step is to incubate the section in 60% (w/v) fructose for 8 hrs at 37 °C. The sections are then incubated in 80% (w/v) fructose for 12 hrs at 37ºC before being incubated in 100% (w/v) fructose for 12 hrs at 37ºC. The sections are finally incubated in the SeeDB solution for 24hrs at 37ºC. The sections should be continuously rotated or rocked during the incubation steps. The sections are then placed between coverslips imaged on the Nikon A1R Single photon Confocal Microscope as described in chapter 2.3.2

2.2.4. Clear Lipid-exchanged Acrylamide-hybridized Rigid Imaging/Microscopy (CLARITY)

The CLARITY technique is adapted from the method first described in the original study by Chung et al. (2013).

2.2.4.1. Tissue Preparation

For the optimisation of CLARITY, 12 month old wild type C57BL/6 mice were sacrificed using cervical dislocation before the brains were excised and incubated in 4% paraformaldehyde at 4ºC overnight. While for the human sections, smaller sub-sections, approximately 3cm x 3cm x 1cm (WxLxD) were excised from formalin fixed sagittal cerebellar brain sections that contained both cerebellar folia and dentate nucleus were collected from the NBTR, where they had been stored in formalin. The cases selected for use in the CLARITY chapters all had a fixation time less than six years. The human sections were washed in PBS over night before undergoing the CLARITY technique.

2.2.4.2. Hydrogel Preparation

The hydrogel solution was prepared by combining 20mL acrylamide (40%), 10mL bis-acrylamide (2%), 1 g VA-044 initiator (10% wt) , 40mL 10X PBS and 310mL dH2O. This was completed on ice and then stored at -20˚C until needed.

2.2.4.3. Tissue embedding

The tissue was placed in 50mL of hydrogel solution and incubated for 3 days (mice) or 7 days (human) at 4˚C. Once the incubation was completed, the falcon tubes were opened and placed in a desiccator chamber where it was filled with nitrogen for 10mins. A vacuum pump then removed all gas from desiccator chamber for 10 minutes before being refilled with nitrogen from a tank for another 10 minutes. The falcon tubes were then sealed, ensuring exposure to the oxygen is minimal and the falcon tubes were transferred to a 37ºC water bath for 3 hours to initiate the polymerisation of the hydrogel.

2.2.4.4. Passive Clearing of Tissue

The tissue was removed from the polymerised hydrogel in a fume hood. The tissue was washed in PBS overnight and then sectioned to 250µm on a Hyrax V50 vibratome (Frequency 70Hz, Amplitude 0.7m, Zeiss). The clearing solution was prepared by combining 24.722 g boric acid, 80 g sodium dodecyl sulphate, and 2L dH2O and then pH to 8.5 by adding NaOH. The 250 µm sections were placed in a 50mL falcon tube and filled with 40ml clearing solution before being placed in a 37ºC water bath. The clearing solution was changed every other day.

The length of time for passive clearing was assessed visually but for mouse 250µm thick cerebellar sections it was typically 7 days while in human 250 µm thick cerebellar sections it was > 4weeks likely due to length of time spent in formalin.

2.2.4.5. Immunofluorescent staining.

Once clearing was completed, the sections are washed with PBS 5 times for 30 minutes. The sections are then incubated in 10% (v/v) normal goat serum for 1hr 30mins. Once completed, the sections were then incubated in 1mL PBS 0.1% tween with the appropriate antibody dilution. The sections were incubated in the primary antibody at 4C for 6 days and then followed by a round of 5x 30mins PBS wash. The secondary antibodies were diluted in 1mL PBS 0.1% Tween and applied to the sections for 4 days at 4˚C. The sections then underwent 5x 30mins PBS washes before a 30mins incubation in 0.2M glycine and an overnight incubation in Refractive Index Matching Solution (RIMS).

2.2.4.6. Imaging

The cleared and stained sections were placed between two coverslips and then imaged on the Nikon A1R Single photon Confocal Microscope as described in chapter 2.3.2

2.3. Microscopy

2.3.1. Light Microscope

A light microscope uses visible light in conjunction with a series of lenses to magnify the section. The image can then be projected to a charge-coupled device (CCD) camera allowing the user to capture a digital image of the magnified section. A modified light microscope (Olympus BX51), with a motorised stage and CCD colour video camera were used in conjunction with stereological software (Stereo investigator, MBF Bioscience, USA) to quantify axonal torpedo and Purkinje cell density.

2.3.2. Laser scanning confocal microscope

Confocal microscopy differs from wide-field fluorescence microscopes, in that confocal microscopes only excite a very small focal plane, building up an image rather than exciting the entire field of interest. By only scanning a small focal point and the use of a spatial pinhole which eliminates out of focus emitted light, a laser scanning confocal microscope greatly improves the signal-to-noise ratio, therefore, increasing the optical resolution of the image.

In a confocal microscope, the excitatory light source is a laser which is reflected by a beam splitter and focused onto the specimen by the objective. The laser excites the fluorophores in that focal region, resulting in emitted fluorescence. The emitted light is captured by the objective, passes through the beam splitter and pin hole to the photomultiplier (PMT) detector. Emitted light from regions that are out of focus are unable to pass through the pin hole and are therefore not detected by the PMT detector reducing the amount of noise detected. The principles of confocal microscopy is summarised in Figure 2.1. The ability of a confocal microscope to carry out optical sectioning, the process of detecting signal at different focal depths to create a 3D image makes confocal microscopy well suited for imaging thick tissue sections.

Imaging of immunofluorescence staining was completed on the Nikon A1R microscope (Nikon Corporation, Japan). The Nikon A1R is a point scanning confocal microscope that is mounted on a fully automated Nikon inverted microscope with a motorized nosepiece and stage and contains a hybrid-scanner (galvano/resonant) and a 4 channel detection (excitation wavelengths 405nm, 491, 515, 561 and 640nm). The Nikon A1R microscope was also

equipped with six different objectives (air or oil) and a Step-by-step Nikon A1 Piezo Z scanner and Nikon TI-S-EJOY (Nikon) which allowed for Z stack images of the regions of interest to be imaged.

Before images were capture, for quantification, the laser settings needed to be set. To achieve this, the photomultiplier tube gain (HV), laser power and offset functions were adjusted when imaging a neurologically normal control section to ensure that there was no avoiding under or over exposure of each channel. For the 5µm thick sections, imaging was completed using the x60 oil immersion objective in conjunction with an electronic zoom of x3 using the resonant scanning method with a line average of 8 and 1.2AU pin hole. While the passively cleared sections were imaged using an x20 objective and a 2.56 zoom on the axonal torpedoes. In the instances of the CLARITY cleared sections, galvano was the preferred scanning method with a line average of two and 1.2AU pin hole. Images were captured using the intuitive NIS:Elements operating software (Nikon corporation, Japan) that is attached with the Nikon A1R.

2.4. Image Analysis

Analysis of respiratory chain deficiency was achieved using the velocity software (Volocity v6.3, Perkin Elvin). While 3D rendering of images was complete using the Imaris software (Imaris v8, Bitplane).

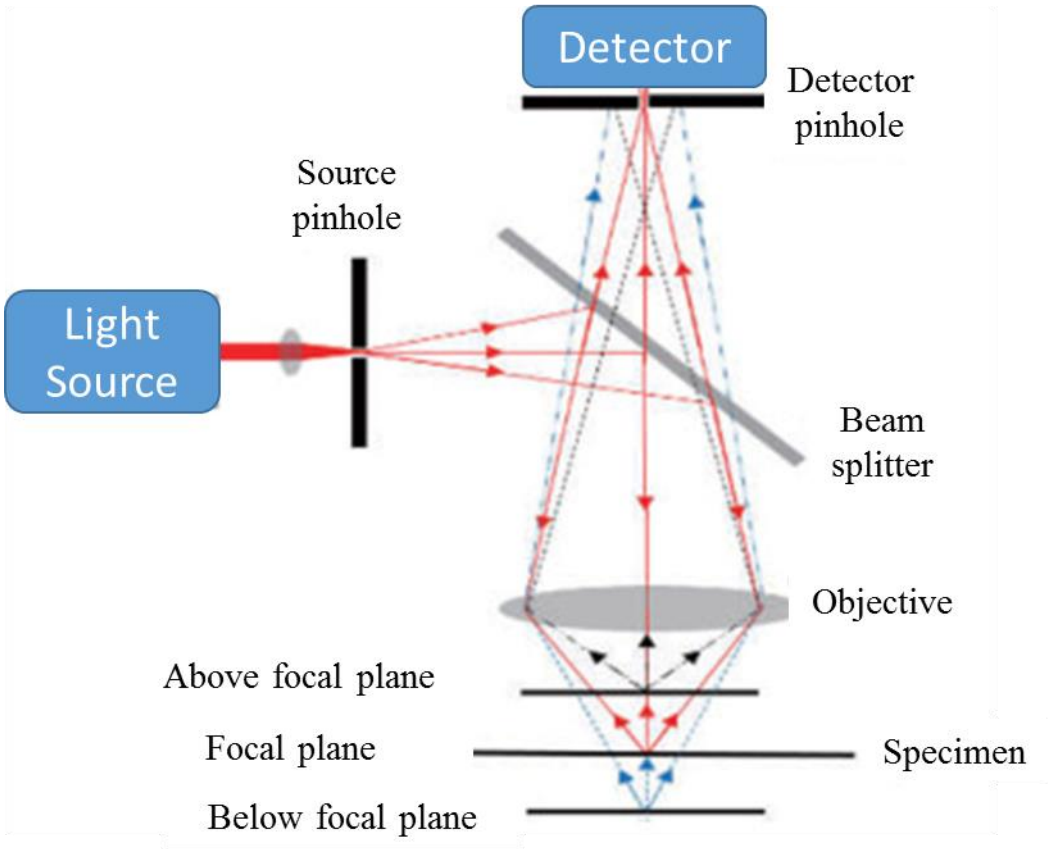

Figure 2.1: Schematic diagram detailing the principles of confocal microscopy. The light source (red line) passes through the source pinhole and is reflected by the beam splitter through the objective, which focuses the light on to the focal plane. The emitted excited light is collected by the objective lens and where it passes through the beam splitter and detector pinhole to the photomultiplier (PMT) detector. The detector pinhole prevents out of focus light from above (black line) and below (blue line) from being detected by the P<T detector. The image was taken from Wang et al. (2015a)

Chapter 3. Characterisation of Axonal Torpedoes in the Cerebellum of Patients with Mitochondrial Disease

3.1. Introduction

The cerebellum only occupies 10% of the brain volume but contains 50% of the brain's total neuronal population resulting in a dense network of neurons (Knierim, 1997). This high density of neurons results in the cerebellum consuming a vast quantity of energy, with computational modelling predicting that Purkinje cells alone require 10 11 molecules of ATP per second to maintain neuronal function (Howarth et al., 2010). The cerebellum is therefore vulnerable to mitochondrial dysfunction due to its high energy requirements. A common clinical manifestation of this in mitochondrial disease is cerebellar ataxia, defined as a lack of balance, coordination and motor control. This is present in approximately 70% of the patients within the UK MRC Mitochondrial Disease Patient cohort (Lax et al., 2012b; Nesbitt et al., 2013).

When investigating the cerebellum in patients with mitochondrial disease, abnormal neuroradiological and neuropathological findings are frequently observed (Lax and Jaros, 2012). In patients with the m.8344A>G point mutation, pronounced cerebellar lesions were observed (Fukuhara, 1991) while severe neuronal loss in the dentate nucleus and inferior olive and mild loss of Purkinje cell numbers have also been observed (Tanji et al., 2001; Lax et al., 2012b). In the cerebellum of patients with the m.3243A>G point mutation, there is an increase in inter folia spacing due to atrophy of the molecular and granular cell layer and neuronal densities were reduced in the dentate nucleus, inferior olive and Purkinje cell layer (Lax et al., 2012b). Abnormal Purkinje cell morphology has also been found, including a loss of presynaptic terminals, increase in dendritic arborisation and an increase in the number of thickened axons causing trapping of mitochondria (Tanahashi et al., 2000; Lax et al., 2012b). Patients with secondary mitochondrial disease due to a mutation in mtDNA maintenance genes can also develop cerebellar ataxia, with abnormalities in the cerebellum observed in neuroimaging (Tzoulis et al., 2006). A patient that had multiple mtDNA deletions due to a recessive POLG mutation was shown to have moderate focal loss of Purkinje cells and mild neuronal loss in the dentate nucleus (Betts-Henderson et al., 2009).

3.1.1. Axonal Torpedoes in the Cerebellum

A prominent form of axonal pathology known as axonal torpedoes are commonly observed in the cerebellum of patients with mitochondrial disease (Mori et al., 2000a; Tanahashi et al., 2000; Lax et al., 2012b). Axonal torpedoes are fusiform swellings of the proximal portion of the Purkinje cell axon in the Granular cell layer (GCL) (Figure 3.1 (Lax et al., 2012b)).

Immunofluorescent labelling confirms that the axonal torpedoes belong to the Purkinje cell body through the positive staining with calbindin and the highly phosphorylated neurofilaments found within the axonal torpedoes (Louis et al., 2009b; Redondo et al., 2015)

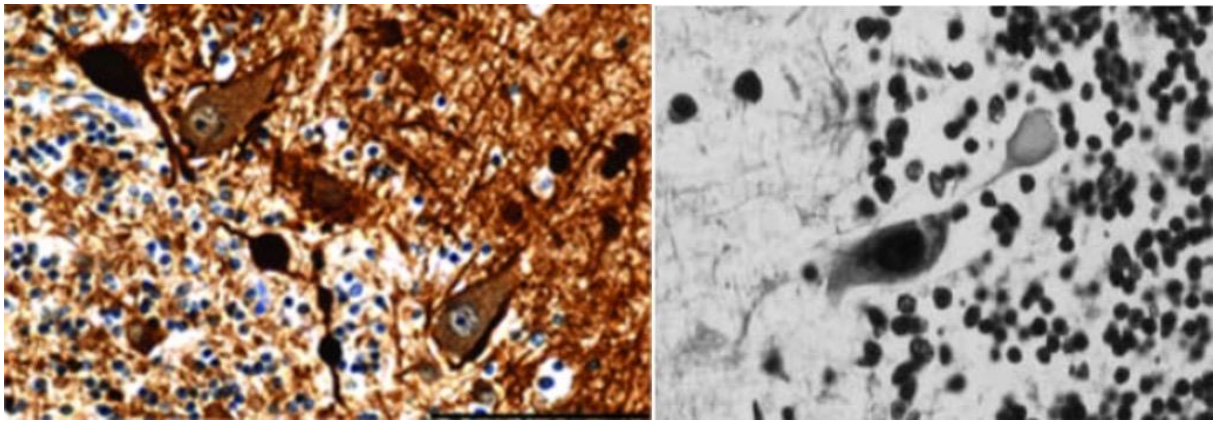

Figure 3.1: Axonal Torpedoes in the Cerebellum of Patients with Mitochondrial Disease. A prominent feature observed in the cerebellum of individuals with mitochondrial disease are the observation of axonal torpedoes in the granular cell layer. These structures are found proximal to Purkinje cell bodies and are found to be highly concentrated with disorganised phosphorylated neurofilaments. Images taken from A) (Lax et al., 2012b) (SMI-31) and B) (Mori et al., 2000b) (Bodain stain).

Axonal torpedoes have also been observed in a number of other neurological disorders such as Friedreich's ataxia (Jitpimolmard et al., 1993) and multiple sclerosis (Redondo et al., 2015). In common neurodegenerative disorders like Alzheimer's and Parkinson's disease, axonal torpedoes have also been observed, with one study detailing 5 times more axonal torpedoes in both diseases compared to controls (Louis et al., 2009a). Axonal torpedoes have been shown to be highly prevalent in the cerebellum of patients with essential tremor, observed in two studies to be 12 times (Louis et al., 2009a) and 6 times (Louis et al., 2007) more prevalent than compared to control tissue. The observation of axonal torpedoes in neurological disorders and the lack of correlation between axonal torpedoes and age (Louis et al., 2007), indicates that the formation of these structures occurs in injured Purkinje cell neurons.

Along with quantifying the number and level of axonal torpedoes in the cerebellum of individuals, a number of early studies have investigated the main constituents that form the torpedoes. A study using electron microscopy (EM) found that the axonal torpedoes in a patient with Essential tremor are mainly comprised of densely accumulated and disorganised neurofilaments which force mitochondria and endoplasmic reticulum to peripheries of the

axonal torpedoes (Louis et al., 2009c). As well as the accumulation of neurofilaments, the EM images show a lack of myelin sheath around the torpedoes. This lack of myelin was also observed with axonal torpedoes in the cerebellum of patients with Friedrich's ataxia (Kemp et al., 2016).

It has been proposed that following a focal insult, there is a block in anterograde and retrograde fast axonal transport resulting in the dis-organisation and accumulation of neurofilaments and other proteins in the axon which subsequently over time produces an axonal torpedo (Figure 3.2). This block in axonal transport would "starve" the distal regions of the neuron and lead to Wallerian degeneration of the distal axon and inevitably cell death.

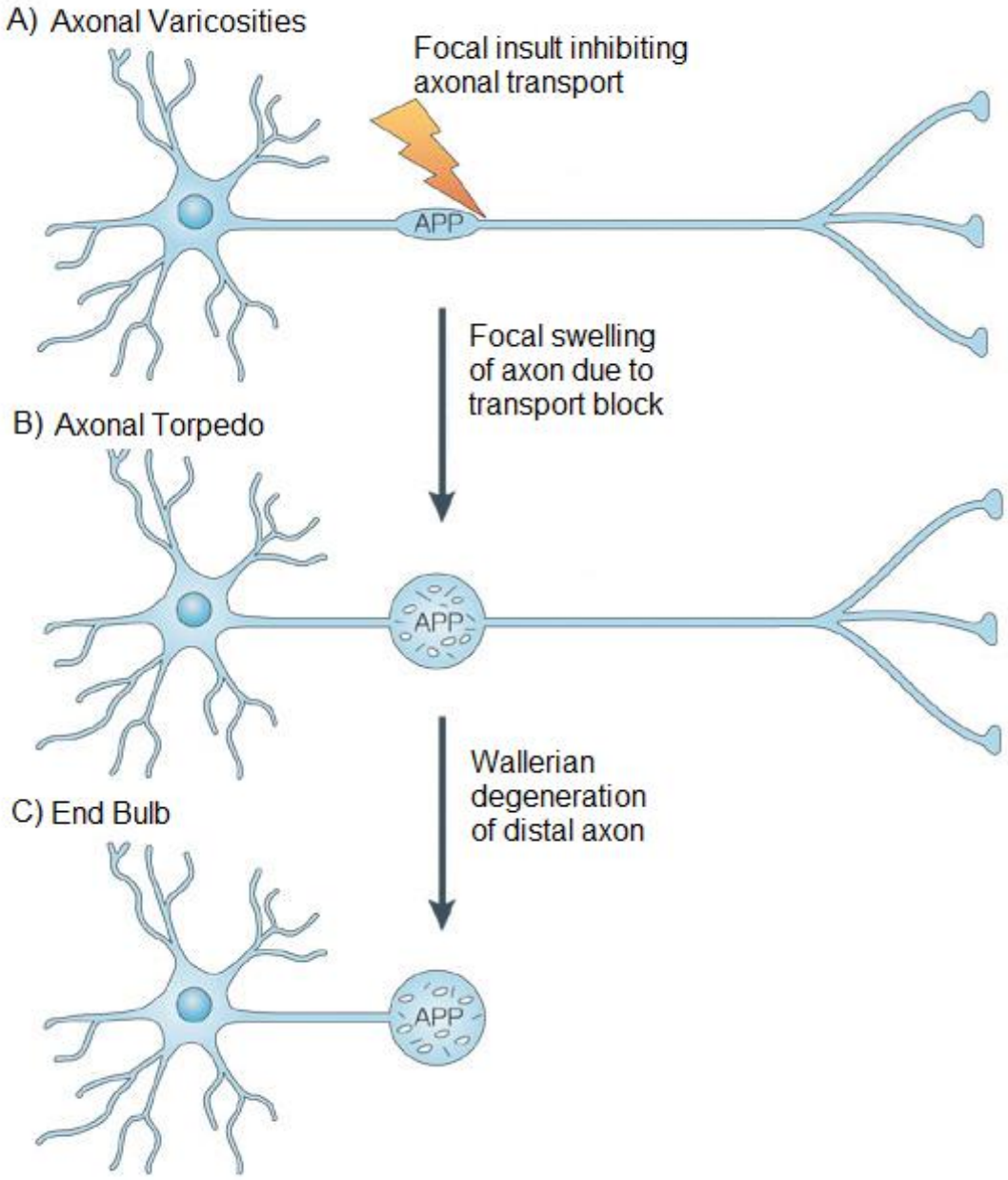

Figure 3.2: Hypothesised sequence of events that lead to the formation of axonal torpedoes.

A focal insult to the axon results in the inhibition of fast axonal transport (A). Proteins involved in axonal transport, like amyloid precursor protein, start to accumulate causing a focal swelling of the axon further inhibiting axonal transport eventually forming an axonal torpedo (B). Ultimately the block in transport becomes too significant and initiates Wallerian degeneration of the distal axon creating an end bulb (C). This image was modified from Coleman (2005).

3.1.1.1.Neurofilaments

Neurofilaments are one of the most abundant intermediate filaments found in the CNS (Lee et al., 1993). There are three isomers of the neurofilament protein; Neurofilament L (70 kDa, NFL), Neurofilament M (150 kDa, NFM) and Neurofilament H (200 kDa, NFH) (Yuan et al., 2012). Each isomer is composed of a globular head domain, a α-helical rod domain and a tail c-domain that differs in length and amino acid composition, determining the weight of the isomer (Figure 3.3A (Yuan et al., 2012)). The globular head domain contains a microtubule (MT) polymerisation inhibitory domain that is involved in the regulation of MT polymerisation and numbers (Bocquet et al., 2009). The α-helical domain is a highly conserved sequence of 310 amino acids that is vital for the co-assembly with other subunits to form filaments and also contains the binding site myosin Va motor protein (Rao et al., 2011). In Neurofilament M and Neurofilament H, the c-terminal domains have fine lateral extensions that can increase the spacing between the neurofilaments, key for the radial growth of axons (Figure 3.3B (Rao et al., 2003)). The three isomers and α- internexin come together to form heteropolymers that have an exceptionally long half-life (Millecamps et al., 2007) and are extremely elastic allowing for them to maintain the asymmetrical shape of neurons (Wagner et al., 2007). These properties allow neurofilaments to regulate axonal calibre and subsequently influence the conduction velocities of the axon. Targeted disruption of the neurofilament network has shown both a reduction in both axon calibre and conduction velocities (Kriz et al., 2000).

Neurofilaments can be phosphorylated at multiple sites depending on the location of the subunits. In the cell body, the globular head domain is non phosphorylated to prevent the formation of filaments (Hisanaga et al., 1990). In the c-terminal domain of NFM and NFH, there are multiple lysine-serine-proline (KSP) sites that can be phosphorylated (Jaffe et al., 1998; Veeranna et al., 2011). The level of c-terminal phosphorylation depends on the location of the neurofilaments. In the cell body or dendrites the neurofilaments are non-phosphorylated while in axons they are highly phosphorylated (Sternberger and Sternberger, 1983). The phosphorylation of the c-terminal regulates the transportation of neurofilaments (Ackerley et al., 2003), modulates the interaction of neurofilaments with microtubules (Hisanaga and Hirokawa, 1989; Hisanaga et al., 1991; Yabe et al., 2000) and also leads to resistance to proteolysis (Goldstein et al., 1987; Pant, 1988).

Aberrant phosphorylation and accumulation of neurofilaments has been associated with a number of neurodegenerative disorders. In disorders such as Alzheimer's disease (AD), amyotrophic lateral sclerosis (ALS), giant axonal neuropathy and Parkinson's disease (PD)

phosphorylated neurofilaments have been observed in neuronal cell bodies (Shea et al., 2009; Liu et al., 2011). In AD, the phosphorylation of KSP repeats on NFH and NFM was observed to be four to eight fold higher in AD patients compared to controls (Rudrabhatla et al., 2011). In ALS, the release of phosphorylated NFH into blood serum is seen as a sign of axonal injury and as a potential biomarker (Shaw et al., 2005; McCombe et al., 2015). In a mice model, where the human variant of NFH was overexpressed, the mice were shown to develop neurological defects at the age 3-4 months and abnormal neurofilamentous swellings, similar to those observed in ALS (Cote et al., 1993). A study showed that 87% of large axonal swellings of the motor neurons which are characteristic of ALS stained heavily for the Kinesin, the motor protein essential for anterograde axonal transport (Carpenter, 1968; Toyoshima et al., 1998). The entrapment of motor proteins will likely lead to an inhibition of axonal transport and a "starvation" of the neuron.

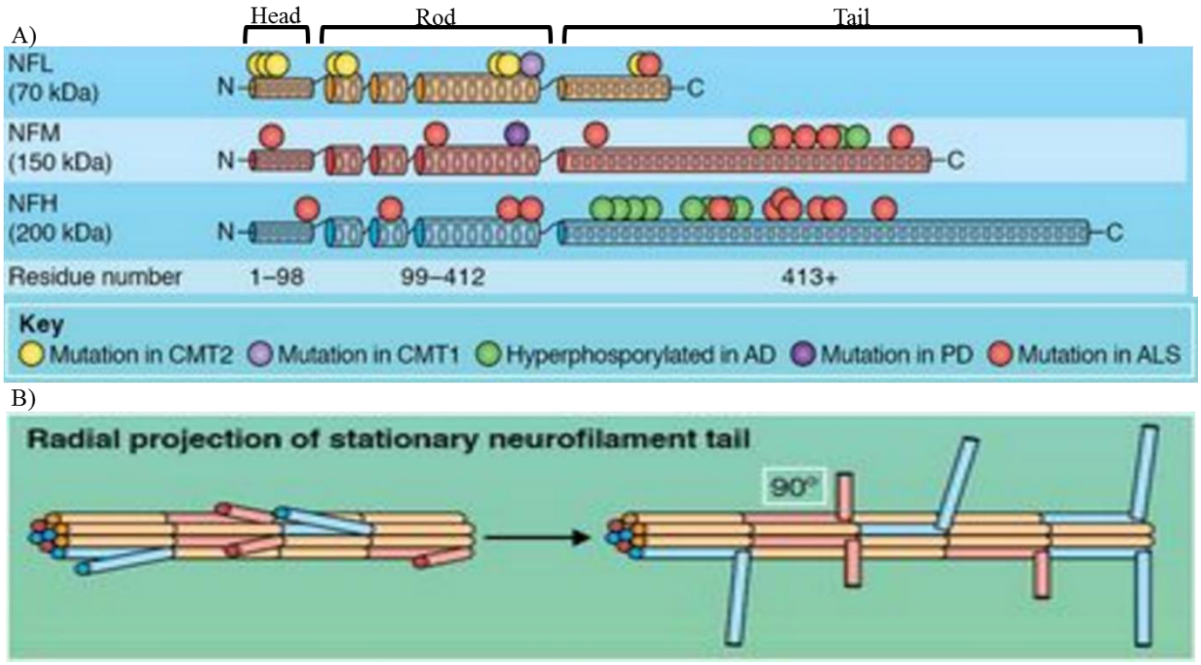

Figure 3.3: Neurofilaments of the central nervous system.

Neurofilaments are intermediate filaments that are found abundantly in the axons. There are three isoforms of neurofilaments; neurofilament heavy (NFH), medium (NFM) and light (NFL) polypeptides. Mutations and aberrant phosphorylation of neurofilaments is associated with a number of neurodegenerative disorders (A). Neurofilaments play an important role in determining the radial growth of axons. This is achieved through the projection of a side arm in the c-terminal domain of the neurofilaments (B). The image was modified from (Yuan et al., 2012).

3.1.1.2. Fast Axonal Transport

Neurons are highly polarised cells, and as organelles, proteins, lipids, and RNA are synthesised in the soma, they rely on axonal transport to direct those molecules to the growth cones and synapses. Additionally, damaged molecules undergo retrograde transport from the distal regions to the soma to be degraded and recycled.

Fast axonal transport (FAT) can reach speeds of 0.5-3 mm/s and is utilised to transport vesicles, organelles, and RNA to the extremities of the neuron (Maday et al., 2014). FAT employs two motor protein families known as kinesin and dynein, and they are capable of hydrolysing one ATP molecule for every 8nm they transport proteins along the axons (Gennerich and Vale, 2009). The motor proteins use microtubules as the tracks to move along the axon. Microtubules (MT) are polymers composed of α and β tubulin forming a highly dynamic component of the cytoskeleton (Salinas et al., 2008). Microtubules are polarised with a fast-growing plus ends directed to the synapse in the axon and a stable minus end directed towards the soma (Stepanova et al., 2003). The polarity of the microtubules helps direct the motor proteins and the directions of FAT.

Kinesins are the main motor protein involved in the anterograde movement of cargo from the soma to the synapse. Kinesins are a part of a superfamily and have many isoforms but Kinesin-1 motors are responsible for the trafficking of the majority of vesicles, organelles, proteins, and RNA particles. They are heterotetramers composed of two heavy chains (KIF5A–C) and two light chains (KLC1/2). The heavy chains (KIFs) contain the motor domain and binding motifs for ATP and microtubule while the light chains (KLC) regulates the motor activity and binding of cargo (Wang et al., 2015b).. In addition to Kinesin-1, Kinesin-3 has been shown to be involved in the transport of synaptic vesicle precursors and dense core vesicles (Lo et al., 2011).

The transport of molecules from the plus end of microtubules to the negative end is known as retrograde transport. Retrograde transport is completed by Dynein, a motor protein consisting of two heavy chains, an intermediate, light intermediate and light chain (Hirokawa et al., 2010). As with Kinesin, the heavy chains of Dynein contains the ATP and microtubule binding motifs. The activity of Dynein is dependent on Dynactin, a multi-subunit cofactor, which among other cofactors such as lissencephaly-1 and huntingtin, Dynein binds to forming a complex (Vale, 2003; Maday et al., 2014).

Two proteins that undergo fast axonal transport are Amyloid Precursor Protein (APP) and synaptophysin and for the purpose of this chapter I will briefly describe them as their presence in axonal torpedoes will be investigated.

Amyloid Precursor Protein (APP) is a type I orientated membrane protein that it is synthesised in the endoplasmic reticulum (ER) and processed in the Golgi network (Haass et al., 2012). Once APP had been processed, it travels unidirectionally and constantly in tubular vesicles via FAT to the presynaptic terminals reaching speeds up to 10 mm/s with an average speed of 4.5 mm/s (Kaether et al., 2000). Once the vesicles reach the pre-synaptic terminal, they fuse with the plasma membrane before forming synaptic vesicle. APP has been shown to accumulate in the axons (Figure 3.3) in a number of neurological disorders from Alzheimer's disease (Stokin et al., 2005), traumatic brain injury (Gentleman et al., 1993) to multiple sclerosis (MS) (Ferguson et al., 1997). The build-up of APP in an end bulb create structures that are highly reminiscent of the axonal torpedoes of the Purkinje cells. If APP is present in the axonal torpedoes then it would also indicate that axonal transport is blocked and that axonal torpedoes may share a similar degenerative mechanism as the one involved in the degenerative process observed in axonal transection or demyelination of the axon (Trapp et al., 1998).

Synaptophysin, a calcium binding membrane glycoprotein, is the second-most abundant protein at the pre-synaptic terminal accounting for 10% of total vesicle protein (Rehm et al., 1986; Takamori et al., 2006) . It is found in the membrane of the small presynaptic vesicles and plays a role in synaptic vesicle biogenesis, exocytosis and endocytosis (Valtorta et al., 2004). In patients with Alzheimer's disease an increase in synaptophysin reactivity was observed in diffuse amyloid deposits and dystrophic plaque neurites (Brion et al., 1991). In the corticospinal tract of a patient with ALS, numerous axonal spheroids were documented to be positive for synaptophysin as well as phosphorylated neurofilaments, ubiquitin and lipid-laden macrophages (Takahashi et al., 1997). Synaptophysin has been observed to increase in concentration distally to the site of injury when an rat optic nerve had been crushed indicating a block in axonal transport (Li and Dahlstrom, 1997). The change in expression or distribution of these proteins is likely to be indicative of disrupted axonal transport and may be an early marker of axonal degeneration.

3.2. Aims

In previous studies that characterised the neuropathology in the cerebellum of patients with mitochondrial disease, axonal torpedoes were phenomenon's that were only observed and never quantified or characterised. The formation of axonal torpedoes may be involved in the degenerative process caused by respiratory chain deficiency in the cerebellum of patients with mitochondrial disease. The aim of this chapter is to further quantify and characterise axonal torpedoes in patients with mitochondrial disease to determine if there is a relationship between respiratory chain deficiency in Purkinje cells and the presence of axonal torpedoes Additionally, the aim of this chapter is to investigate if the formation of axonal torpedoes are a by-product of a cessation or block in axonal transport. Therefore, I aim to:

1. Confirm that axonal torpedoes are more prevalent in patients with mitochondrial disease and age-matched controls
2. Determine if a disruption of fast axonal transport is the cause of axonal torpedo formation.
3. Determine if mitochondria are present within axonal torpedoes and quantify the level of respiratory chain deficiency to determine if axonal torpedoes form in Purkinje cells that have a high level of respiratory chain deficiency.

To achieve these aims I will use a combination of immunohistochemistry and immunofluorescent assays on formalin fixed paraffin embedded cerebellar sections from patients with mitochondrial disease and age matched controls.

3.3. Materials and Methods

3.3.1. Subjects and tissue details

For this chapter formalin-fixed paraffin-embedded (FFPE) cerebellar brain tissue from ten patients (age range: 20-79 years) that were genetically and clinically confirmed to have mitochondrial disease and ataxia were used. While for comparison, fourteen age-matched control individuals (age range: 25-79 years) with no clinical or pathological evidence of neurological disease were used in this study. The age (t-test, p=0.069) and PMI delay (t-test, p= 0.564) of patients and controls showed no statistical difference. Table 3.1 summarises details about the individuals used in this chapter.

3.3.2. Immunohistochemistry and immunofluorescence.

The immunohistochemistry method described in section 2.2.1 was utilised to quantify the number of axonal torpedoes in the cerebellum of patients with mitochondrial disease compared to controls as well as further characterising the components of the axonal torpedoes.

To determine the presence of microtubules in the axonal torpedoes, a triple immunofluorescent will be used with the following antibodies; anti-SMI-31 ((1:1000) 488nm), anti-β-tubulin ((1:500 (546nm)) and anti-acetylated α-tubulin (1:100 (647nm)).

The quantification of respiratory chain deficiency in axonal torpedoes, Purkinje cell bodies and their axons was achieved through the development of a triple immunofluorescent assay. The immunofluorescent protocol is described in section 2.2.2. The assay allowed for the detection of;

i. Axonal torpedoes, Purkinje cells, and proximal axons by using anti-neurofilament H 200 kDa (1:500 (biotinylated 405nm)),
ii. Mitochondrial mass using anti- cytochrome c oxidase subunit 4 (COX4 (1:100) (546nm))
iii. Complex I marker anti-NADH dehydrogenase [ubiquinone] 1 alpha subcomplex subunit 13 (NDUFA13 ((1:100) 488nm)).

The primary antibodies used in this chapter are summarised in table 3.2 while table 3.3 summarises the secondary antibodies used.

	Gender	Age (Years)	PMI (Hours)	Genetic defect	Cause of Death
Patient 1	F	40	58	m.3243A>G	Respiratory Failure
Patient 2	F	20	187	m.3243A>G	Aspiration pneumonia with MELAS
Patient 3	F	36	9	m.3243A>G	Myocardial infarction
Patient 4	M	45	43	m.3243A>G	Complications associated with MELAS
Patient 5	M	59	67	POLG (p.Gly848Ser and p.Ser1104Cys)	Unknown
Patient 6	M	30	21	m.3243A>G	Unknown
Patient 7	F	42	59	m.8344A>G	Respiratory failure
Patient 8	F	60	10	m.3243A>G	Multi-organ failure
Patient 9	M	58	66	m.8344A>G	Unknown
Patient 10	M	79	85	POLG (p.Thr251Ile/p.Pro587Leu; p.Ala467Thr)	Pneumonia due to mitochondrial disease
Control 1	F	69	16	N/A	Gastric Cancer
Control 2	F	74	53		Heart Failure
Control 3	M	55	51		Liver Cancer
Control 4	F	74	67		Lung Cancer
Control 5	M	70	72		Metastatic Ovarian Cancer
Control 6	F	77	83		Myocardial Infarction
Control 7	M	48	46		Coronary Artery Atherosclerosis
Control 8	M	44	83		Coronary Artery Atherosclerosis
Control 9	M	45	44		Complications of Bronchopneumia and Coronary Artery Atherosclerosis
Control 10	M	25	53		Hanging
Control 11	M	61	61		Hanging
Control 12	M	48	43		Coronary Artery Thrombosis
Control 13	M	72	17		Oesophageal adenocarcinoma
Control 14	F	78	34		Metastatic Ovarian Cancer

Table 3.1: Tissue details of individuals that were used in Chapter 3.
Tissue details which include age, gender, Post mortem interval (PMI) and cause of death about the individuals that were used in this chapter.

Primary antibody	Target	Host and isotype	Dilution	Antigen Retrieval
Anti-GAD65/67	Glutamic acid decarboxylase 65–67	Rabbit IgG	1:1000	1mmol EDTA pH 8, pressure cooking
Anti-SMI-31R	Phosphorylated heavy subunit of neurofilaments	Mouse IgG1	1:12,000	No Antigen Retrieval
Anti-SMI-32	Non-phosphorylated heavy subunit of neurofilaments	Mouse IgG1	1:6,000	1mmol EDTA pH 8, pressure cooking
Anti-amyloid precursor protein	Amyloid Precursor Protein	Rabbit IgG	1:2500	10mmol tri-sodium citrate, pH 6, 10 minutes microwave
Anti-synaptophysin	Synaptophysin	Mouse IgG1	1:150	10mmol tri-sodium citrate, pH 6, 10 minutes microwave
Anti-beta III Tubulin [TUJ-1]	β-tubulin (TUJ-1)	Mouse IgG2a	1:100	No Antigen Retrieval
Anti-Acetylated alpha Tubulin	Acetylated alpha Tubulin	Mouse IgG2b	1:100	No Antigen Retrieval
Anti-complex I 19 kDa	NDUFA13	Mouse IgG2b	1:100	1mmol EDTA pH 8, pressure cooking
Anti-complex IV subunit IV	COX4	Mouse IgG2a	1:100	1mmol EDTA pH 8, pressure cooking

Table 3.2: Properties of the Primary antibodies used in Chapter 3.
The properties of primary antibodies used include; target, host, isotype, dilution and method of antigen retrieval.

Secondary	Epitope	Host	Dilution
Alexa Flour 488nm	anti-mouse IgG2b	Goat	1:100
	anti-mouse IgG1		
Alexa Flour 546nm	anti-mouse IgG2a		
Alexa Flour 647nm	anti-mouse IgG2b		
Alexa Flour 405nm	Streptavidin Conjugate		
Biotinylated	anti-Rabbit IgG		

Table 3.3: Properties of the secondary antibodies used in Chapter 3.
The properties of secondary antibodies used include; epitope, host, and dilution.

3.3.3. Quantification of Axonal Torpedo and Purkinje Cell Density

5μM FFPE sagittal cerebellum sections were stained with anti-p-NF-H to quantify the densities of both axonal torpedoes and Purkinje cells. Axonal torpedoes were identified as large spherical structures with high immuno-reactivity to p-NF-H with no visible nucleolus and located in the Purkinje cell layer or granular cell layer. Purkinje cells were defined as having a clearly defined nucleolus and cell body. Using a stereological workstation with a light microscope (Olympus BX51), motorised stage and CCD colour video with Stereology software (StereoInvestigator, MBF Bioscience, USA), the length of the Purkinje cell layer was outlined at 2X magnification. Once completed, magnification was increased to 20X and the total number of axonal torpedoes and Purkinje cells were counted along the length of two superior and two inferior folia. The Axonal torpedo and Purkinje cell counts were then divided by the folia length to calculate densities.

3.3.4. Quantification of Respiratory Chain Deficiency

The quantification of respiratory chain deficiency using the triple immunofluorescent assay was completed using the Nikon A1R confocal microscope with the NIS Elements software. Purkinje cells, axonal torpedoes and axons in the granular cell layer as identified by NFH200 were captured at 60X magnification with 4X electronic zoom under constant gain, offset and laser power. Volocity 3D Image Analysis Software (PerkinElmer, UK) was used to deconvolve images and then analysed by using Neurofilament 200kDa to identify either the cell or axonal torpedo. The pixel intensities for both NDUFA13 labelled with 488nm and COX4 labelled with 546nm were quantified.

Using the statistical software SAS (SAS Institute Inc.) NDUFA13 intensity values were corrected to the mitochondrial marker (COX4) intensity values and then the z scores were calculated for the NDUFA13 intensity values. The normal range of NDUFA13 expression was defined as range of -2 standard deviations (SD) < z < 2 (SD), while high NDUFA13 expression was defined as z >2 SD, low NDUFA13 expression was z < -2 SD and deficient if z < -3 SD. Therefore any z-score below -3 will be defined as deficient for NDUFA13 expression. To determine the difference in NDUFA13 expression between neuronal structures or patients with different genetic defects, two-sample t-test (for parametric data) and Mann-Whitney U tests (for nonparametric data) were performed. While looking at paired data, the Wilcoxon Signed-Rank test was implemented.

Graphical representation of the data was generated using GraphPad prism (GraphPad prism, Inc.).

3.4. Results

3.4.1. Characterisation of Axonal Torpedoes

As previous reports have shown that the main constituents of the axonal torpedoes were disorganised phosphorylated neurofilaments, I aimed to determine if other proteins are found to be accumulated in the axonal torpedoes from controls and patients with mitochondrial disease and whether the presence of these proteins can provide information regarding the origins of the axonal torpedoes.

Immunoreactivity of GAD65-67 in axonal torpedoes confirmed that axonal torpedoes are formed in the axons of control Purkinje cells (arrow, Figure 3.4a). Immunohistochemistry confirmed that phosphorylated neurofilament H (pNFH) was the main constituent of axonal torpedoes (figure 3.4Bi). Axonal torpedoes were shown to be negative for non-phosphorylated NFH (npNFH) whereas the cell bodies were clearly positive for npNFH (arrowhead, Figure 3.4Bii).

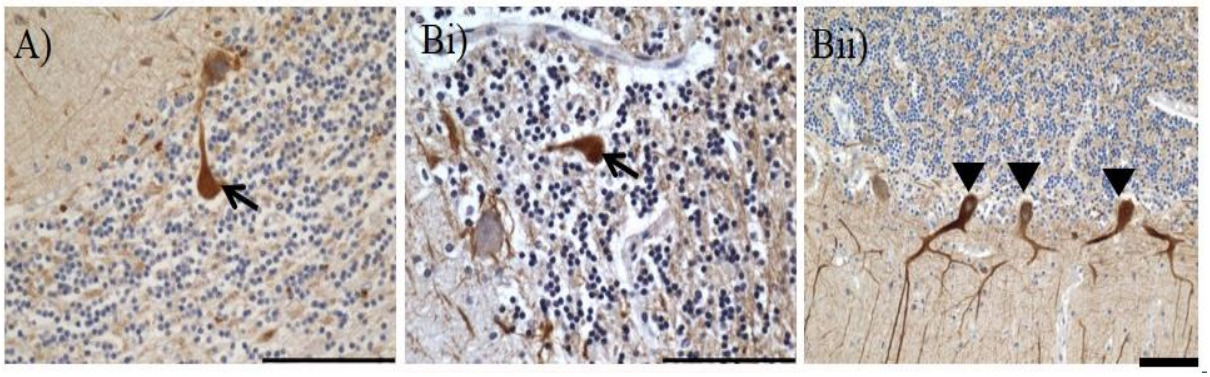

Figure 3.4: Characterisation of axonal torpedoes.

The presence of GAD65/67 in axonal torpedoes (black arrow) confirms that axonal torpedoes originate in Purkinje cell axons (A). Phosphorylated neurofilament H (pNFH) was shown to be the main component in the Axonal Torpedoes (Bi) while non phosphorylated neurofilament H (npNFH) was not observed in axonal torpedoes but was present in Purkinje cell bodies (arrow heads, Bii). scale bar= 100µm

Using phosphorylated neurofilament H (smi-31R, green, Figure 3.5Ai) as a marker for axonal torpedoes (white arrow, Figure 3.5Ai-iv) it was shown that both β-tubulin (tuj1, red, Figure 3.5Aii) and acetylated α tubulin (acetylated α tubulin, cyan, Figure 3.5Aiii) co-localised with phosphorylated neurofilaments in an axonal torpedo, confirming the presence of microtubules in axonal torpedoes (Figure 3.45iv, white arrow).

The next question was to determine if the large accumulation of pNFH in axonal torpedoes resulted in a block in axonal transport. Using immunohistochemistry it was determined that APP was not present in axonal torpedoes since no APP positive axonal torpedoes were observed. However positive staining was observed in the deep white matter, confirming that the protocol had worked and accumulations of APP were present in swellings in distal axons (red arrow, Figure 3.5B). As with APP, there was no immunoreactivity for synaptophysin in axonal torpedoes (black arrow, Figure 3.5Ci) while in the deep cerebellar white matter but there was an accumulation of synaptophysin in axonal swellings (red arrow, Figure 3.5Cii). This observation in conjunction with APP in the axonal swellings, shows that axonal swellings and axonal torpedoes are distinct structures.

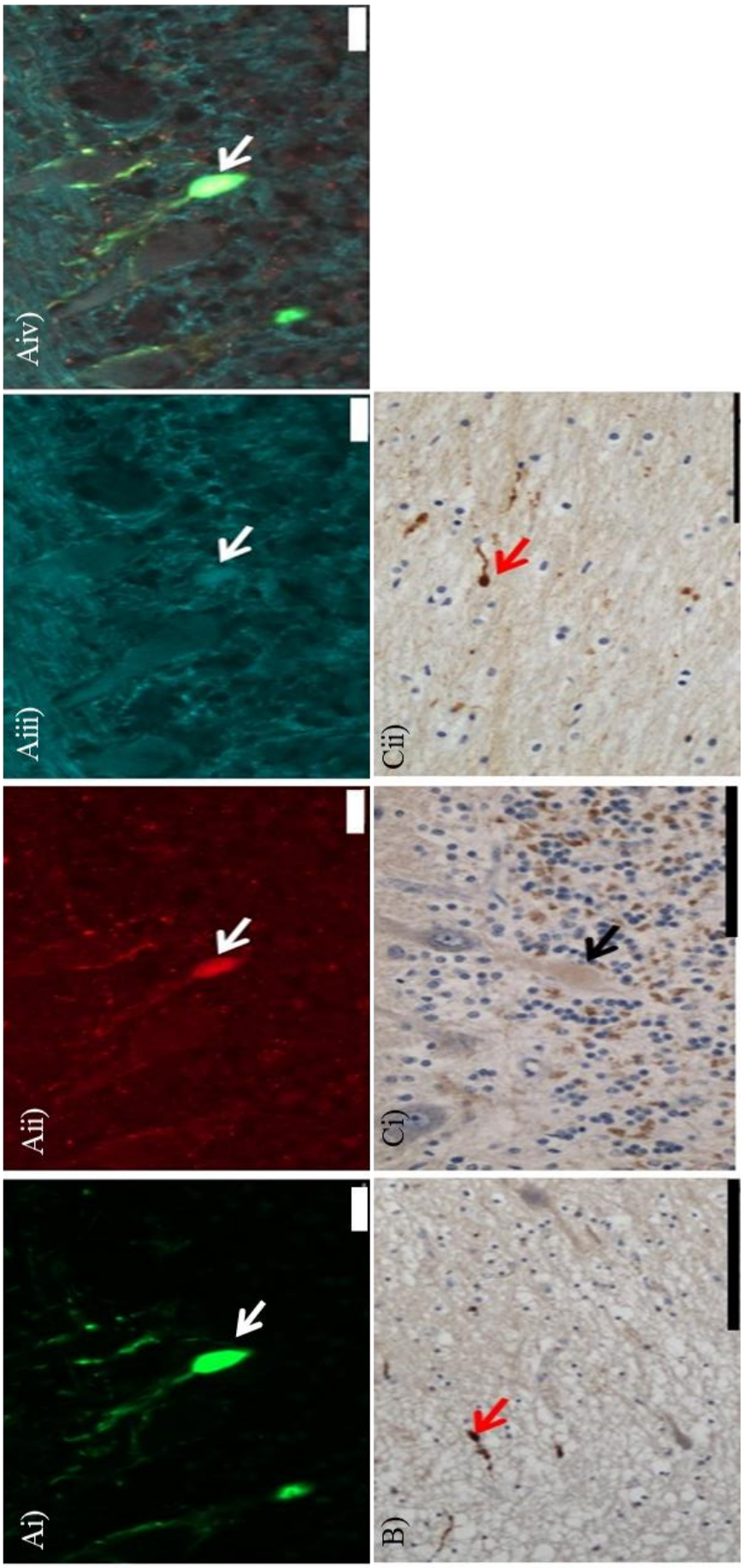

Figure 3.5: Investigating components of axonal transport in axonal torpedoes.
Axonal torpedoes (white arrows) were identified using pNFH (green, Ai) and the co-localisation of both β-tubulin (red, Aii.) and acetylated α-tubulin (cyan, Aiii) can be seen in the axonal torpedoes (Aiv). Amyloid precursor protein was not present in axonal torpedoes but was present in axonal swellings in the deep cerebellar white matter (red arrow, B). Low level immunoreactivity of synaptophysin is observed in axonal torpedoes (arrow, Ci) while strong reactivity is observed in axonal swellings in the deep cerebellar white matter (red arrow, Cii). Black scale bar= 100µm, white scale bar=20µm

3.4.2. Quantification of Axonal Torpedoes and Purkinje Cell Density

As axonal torpedoes have been observed in both control individuals as well as patients with mitochondrial disease, I aimed to determine if axonal torpedoes were found at a higher density in patients compared to controls. Axonal torpedo and Purkinje cell numbers were quantified in the same 4 randomly selected cerebellar regions for each individual. The counts were then divided by the length of the Purkinje cell layer to calculate a density of axonal torpedoes and Purkinje cells. Quantification of axonal torpedo density showed that patients with mitochondrial disease had a significantly higher density of axonal torpedoes compared to controls (unpaired t test, $p=0.0007$) however, patients had a significant decrease in Purkinje cell density compared to control subjects (unpaired t test, $p<0.001$).

To account for Purkinje cell loss, the density of axonal torpedoes was adjusted to Purkinje cell density and it was shown that 7/10 patients had a higher level of axonal torpedoes per Purkinje cells compared to controls (Figure 3.6a) The correlation between axonal torpedo density and Purkinje cell density was investigated (Figure 3.6b) and it was shown in patients there was a non-significant negative relationship (Pearson's correlation coefficient; $R2=0.035$, $p=0.605$). In controls there was a statistically significant relationship ($R2=0.283$, $p=0.04$), indicating that the presence of axonal torpedoes is associated with the loss of Purkinje cells. The relationship between age of individuals and axonal torpedoes was assessed (Figure 3.6c), where it was shown that was a significant positive correlation in controls, with the number of axonal torpedoes increasing with age ($R2=0.431$, $p=0.0147$) but no relationship was observed in patients ($R2=0.027$, $p=0.648$).

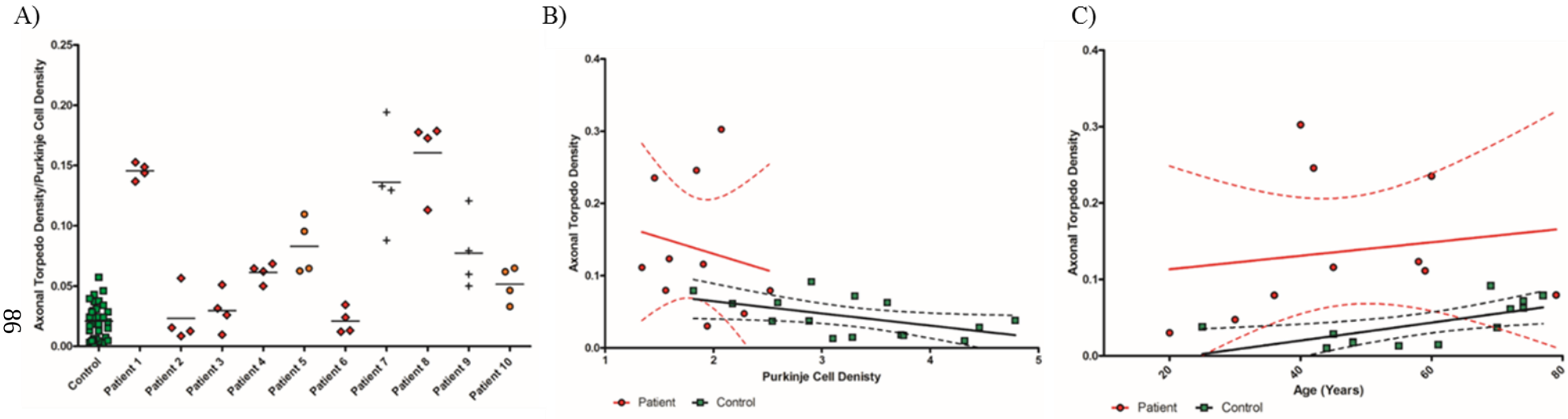

Figure 3.6: Quantification of Axonal torpedoes and Purkinje cells in the cerebellum.

A) Axonal torpedo to Purkinje cell density ratios were elevated in all patients (n=10) with the exception of patients 2, 6 and 10, relative to control individuals (n=13). B**)** In patients there was no correlation between Purkinje cell density and axonal torpedo density (Red line; Pearsons correlation coefficient; R^2= 0.035, p=0.605)**.** While in controls a negative correlation was observed between axonal torpedo density and Purkinje cell density (Green line, R^2= 0.28, p=0.041). C) In patients, axonal torpedoes had no correlation with age (Red line, Pearson's correlation coefficient, R^2= 0.027, p=0.648) while in control tissue, there is a positive correlation between axonal torpedo density and age (Green line, Pearsons's correlation coefficient, R^2=0.432, p= 0.015). A= Each dot represents a single data point, with 4 data points per case. B-C: Each dot represents the mean data from each case.

3.4.3. Quantification of Complex I Deficiency in Purkinje Cells, Axonal Torpedoes and Axons

A Triple immunofluorescent assay was utilised to determine if mitochondria are present in axonal torpedoes and if they are respiratory chain deficient. To achieve this both the expression of the complex I subunit NDUFA13 and a mitochondrial mass marker, COX4, was measured. I chose to look at complex I as a marker of respiratory chain deficiency as previous studies in mitochondrial disease have reported a decrease in subunits of complex I (Reeve et al., 2013; Grunewald et al., 2014; Chrysostomou et al., 2016; Lax et al., 2016). When compared to the expression level in controls, the COX4 expression levels in the axonal torpedoes (unpaired t-test $p = 0.1058$) and Purkinje cells (unpaired t-test $p = 0.1871$) of patients was preserved which is in agreement with previous studies (Lax et al., 2012b; Chrysostomou et al., 2016), confirming that COX4 is a suitable protein to be used as a mitochondrial mass marker.

Immunofluorescence reveals that mitochondria (COX4) are found diffusely throughout the axonal torpedoes (Figure 3.7-9). The data from control axonal torpedoes show NDUFA13 co-localising with COX4 confirming that the expression of NDUFA13 remains intact. In patient axonal torpedoes, there is a reduction in NDUFA13 expression in the patients with either the m.3243A>G point mutation (Figure 3.7) or the mutation in POLG (Figure 3.8). The axonal torpedoes in patients with the m.8344A>G point mutation (Figure 3.9) had NDUFA13 expression that was comparable to the NDUFA13 expression in control axonal torpedoes. In Purkinje cells the expression of NDUFA13 and COX4 is equal in control Purkinje cells (Figure 3.10). In patients, more specifically those with the m.3243A>G (Figure 3.10) and POLG mutations (Figure 3.11), there is a clear reduction in the expression of NDUFA13. However, in the patients with m.8344A>G point mutation there was no discernible difference in NDUFA13 expression when compared to the controls (Figure 3.12). This pattern of deficiency is also observed in Purkinje cell axons that were imaged from a close proximity to the Purkinje cell bodies, with Purkinje cell axons from patients with the m.3243A>G (Figure 3.13) and POLG mutations (Figure 3.14) displaying a reduction in NDUFA13 expression while there the NDUFA13 expression is comparable to controls in the patients with m.8344A>G mutation (Figure 3.15).

The intensities of NDUFA13 and COX4 were quantified in all 3 regions and from this data z scores were derived in order to provide an accurate measure of the difference between patient and control subcellular domains. From the z scores, the different domains could be defined by the standard deviations (SD) and these are as follows; high NDUFA13 expression (z >2 SD), normal NDUFA13 expression (-2SD < z < 2SD), low NDUFA13 expression (z < -2 SD) and deficient (z < -3 SD).

Quantification of z scores revealed that complex I deficiency in the axonal torpedoes was most severe in patients 1 and 2, carrying the m.3243A>G mutation. Respectively, 60% and 66. 667% of the axonal torpedoes, in those patients, displayed a level of NDUFA13 expression that was deemed as deficient while the remainder of patients displayed a minimal level of NDUFA13 deficiency with the majority of axonal torpedoes having normal level of NDUFA13 (Figure 3.16A). The Purkinje cell bodies displayed a greater level of NDUFA13 deficiency in patients, with patient 3 (m.3243A>G) and 6 (m.3243A>G) respectively having 90% and 80% of the Purkinje cells being deficient in NDUFA13 (Figure 3.16B). Interestingly, the majority of the Purkinje cells from the five patients harbouring the m.3243A>G mutation (Patient 1, 2, 3, 4, and 6) all displayed a level of NDUFA13 expression that was below the normal level. Axons displayed a similar pattern of deficiency with patients (Patient 1, 2, 4, and 6) harbouring the m.3243A>G mutation having the greatest reduction in NDUFA13 expression (Figure 3.16C). More specifically Patients 1 and 2 had the highest level of NDUFA13 deficiency, respectively with 71.429% and 75% of axons having deficient NDUFA13 expression and no axons at all displaying a normal range of NDUFA13 expression.

The patients with m.3243A>G mutation appeared to demonstrate the greatest level of complex I deficiency and this was statistically confirmed, with significant differences observed in the Z scores of all of the m.3243A>G structures when compared to controls (paired t test, $p<0.00001$). There was a similar level of complex I deficiency in all the neuronal compartments of patient's harbouring autosomal recessive POLG mutations. However there was no evidence of complex I deficiency in in any of the neuronal compartments of the patients harbouring m.8344A>G mutations.

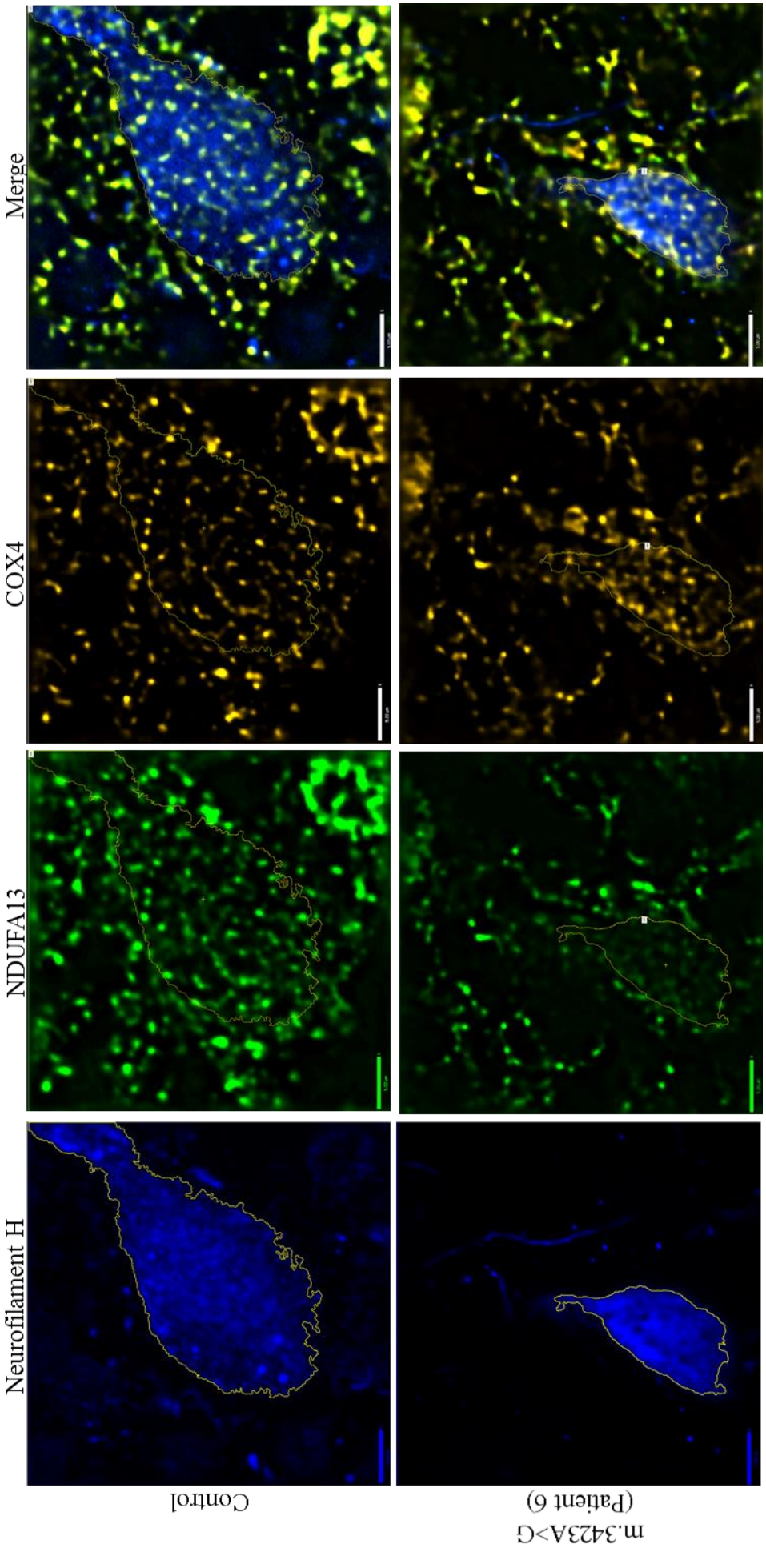

Figure 3.7: Visualisation of mitochondrial respiratory chain proteins in axonal torpedoes from control and m.3243A>G individuals. Representative images of axonal torpedoes (labelled with neurofilament H (blue), outlined by yellow dashed line) from control and m.3243A>G individuals were captured. Control individuals show equal expression of complex I (NDUFA13, green) and mitochondria (COX4, yellow) and which colocalise in the merged image confirming specific labelling. In m.3243A>G, there is a reduction in NDUFA13 while COX4 expression remains comparable to the level in the control axonal torpedo. Scale bar= 5µm.

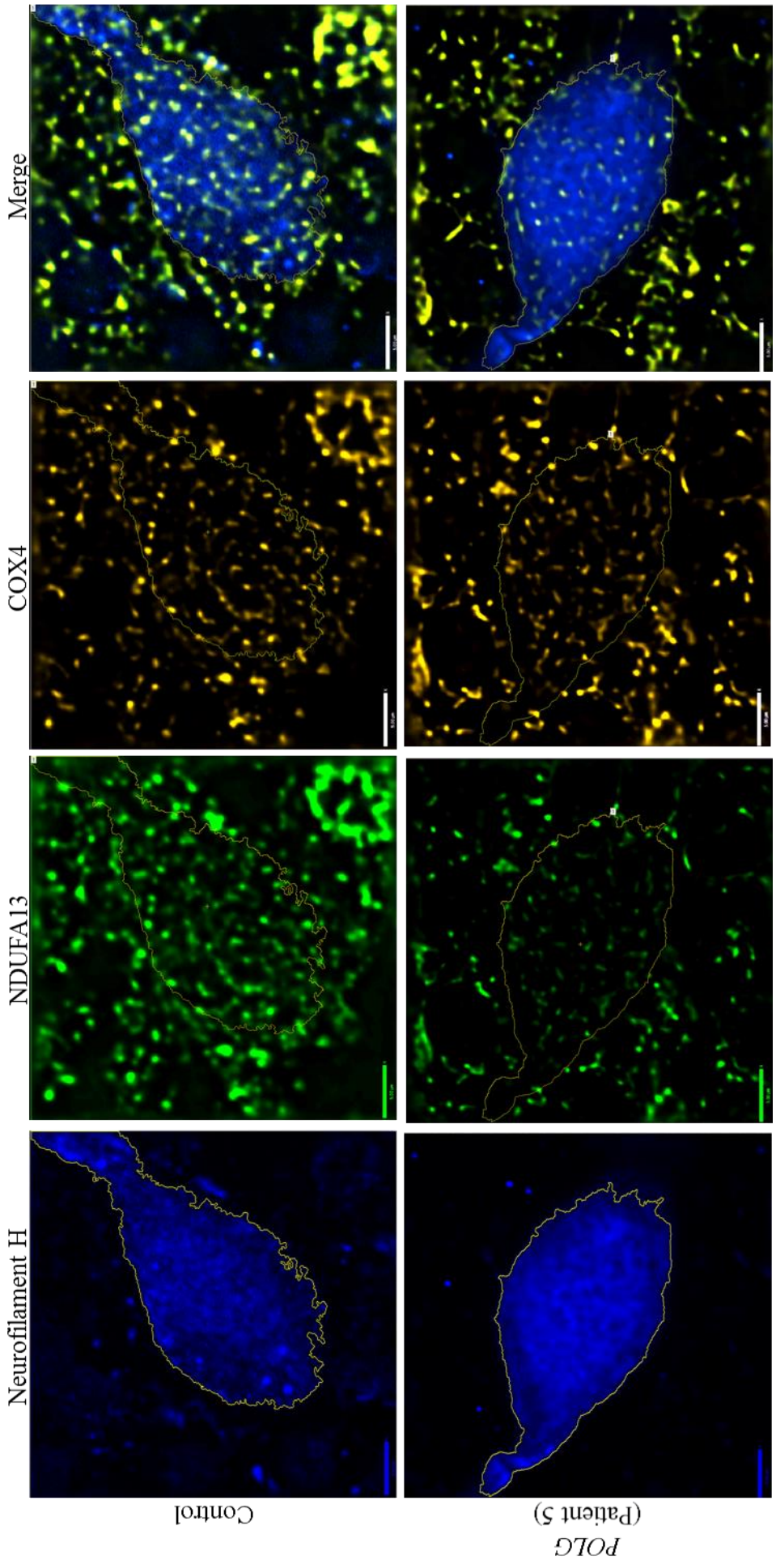

Figure 3.8: Visualisation of mitochondrial respiratory chain proteins in axonal torpedoes from control and POLG individuals.
As before representative images of axonal torpedoes (labelled with neurofilament H (blue), outlined by yellow dashed line) from a *POLG* individual were captured. In axonal torpedo from the POLG individual there is a reduction in NDUFA13 (green) while COX4 (yellow) expression remains comparable to the level in the control axonal torpedo. The same control axonal torpedo as Figure 3.6 is shown as reference for comparable NDUFA13 and COX4 expression. Scale bar= 5µm.

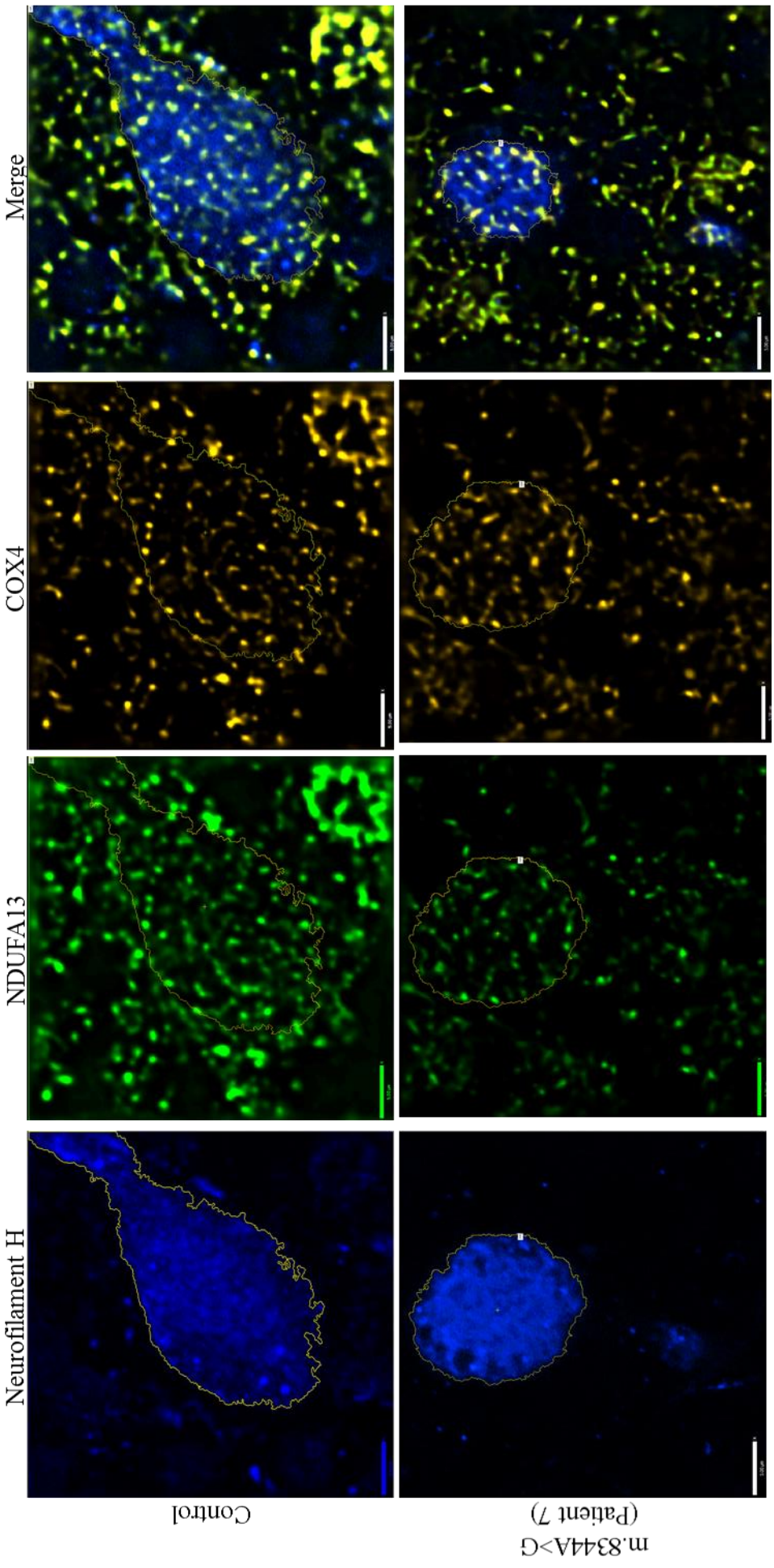

Figure 3.9: Visualisation of mitochondrial respiratory chain proteins in axonal torpedoes from control and POLG individuals.
As before representative images of axonal torpedoes (labelled with neurofilament H (blue), outlined by yellow dashed line) from a m.8344A>G individual were captured. The axonal torpedoes from control and m.8344A>G individuals have comparable levels of NDUFA13 (green) and COX4 (yellow) indicating that there is no complex one deficiency in the axonal torpedoes from m.8344A>G axonal individuals. Scale bar= 5µm.

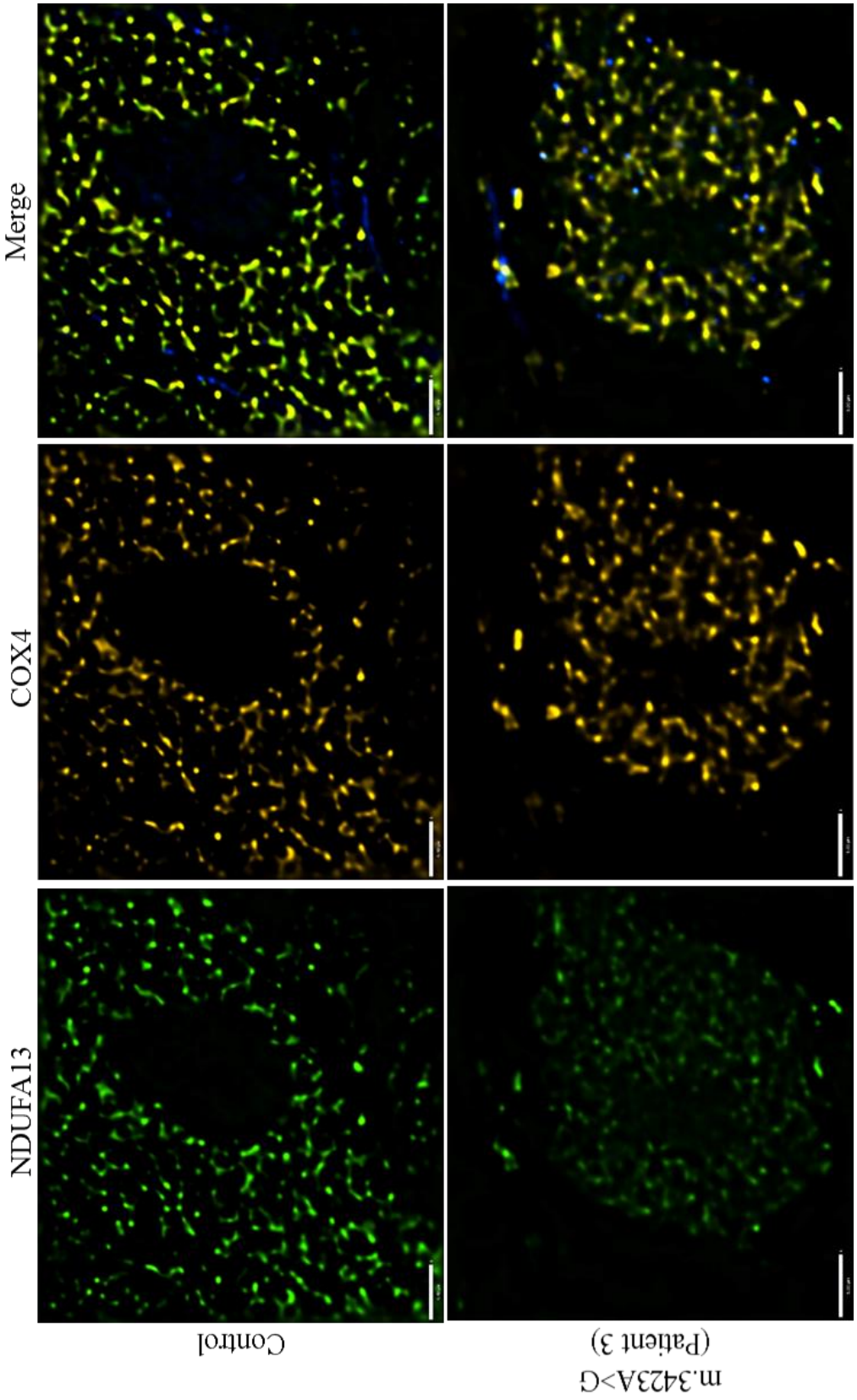

Figure 3.10: Visualisation of mitochondrial respiratory chain proteins in Purkinje cell bodies from control and m.3243A>G individuals. Representative images of Purkinje cell bodies were captured and an equal expression of complex I (NDUFA13, green) and mitochondria (COX4, yellow) can be observed in the control. In m.3243A>G, there is a significant reduction in NDUFA13 while COX4 expression remains comparable to the level in the control Purkinje cell body. Scale bar= 5µm.

Figure 3.11: Visualisation of mitochondrial respiratory chain proteins in Purkinje cell bodies from control and POLG individuals. Representative images of Purkinje cell bodies were captured in control and POLG individuals. An equal expression of complex I (NDUFA13, green) and mitochondria (COX4, yellow) can be observed in the control, with the two proteins colocalising in the merged image. In the *POLG* individual, there is a significant reduction in NDUFA13 while COX4 expression remains comparable to the level in the control Purkinje cell body, showing that this cell body is respiratory chain deficient. Scale bar= 5µm.

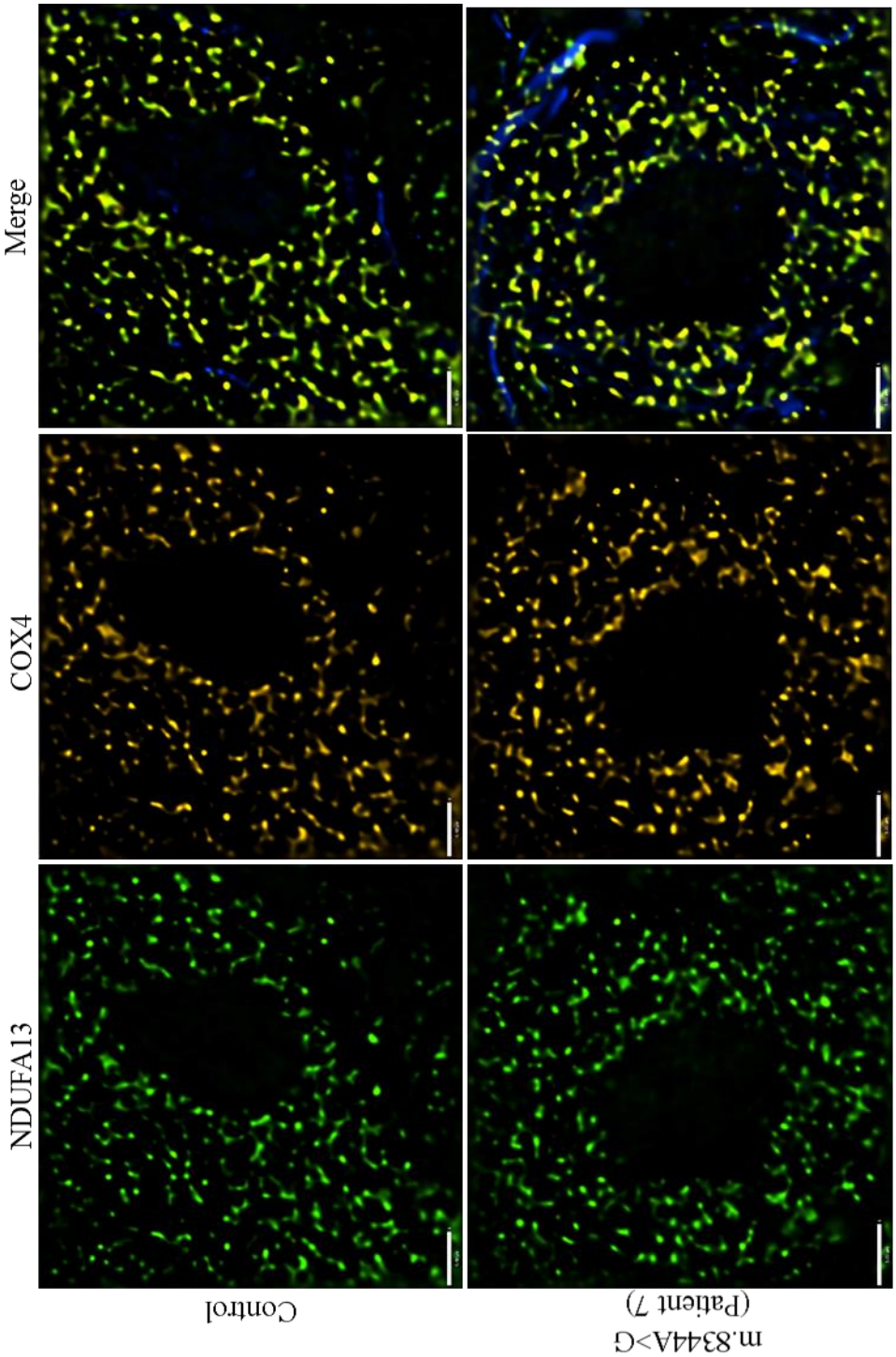

Figure 3.12: Visualisation of mitochondrial respiratory chain proteins in Purkinje cell bodies from control and m.8344A>G individuals. Representative images of Purkinje cell bodies were captured in control and m.8344A>G individuals. An equal expression of complex I (NDUFA13, green) and mitochondria (COX4, yellow) can be observed in both the control and m.8344A>G individuals. Scale bar= 5µm.

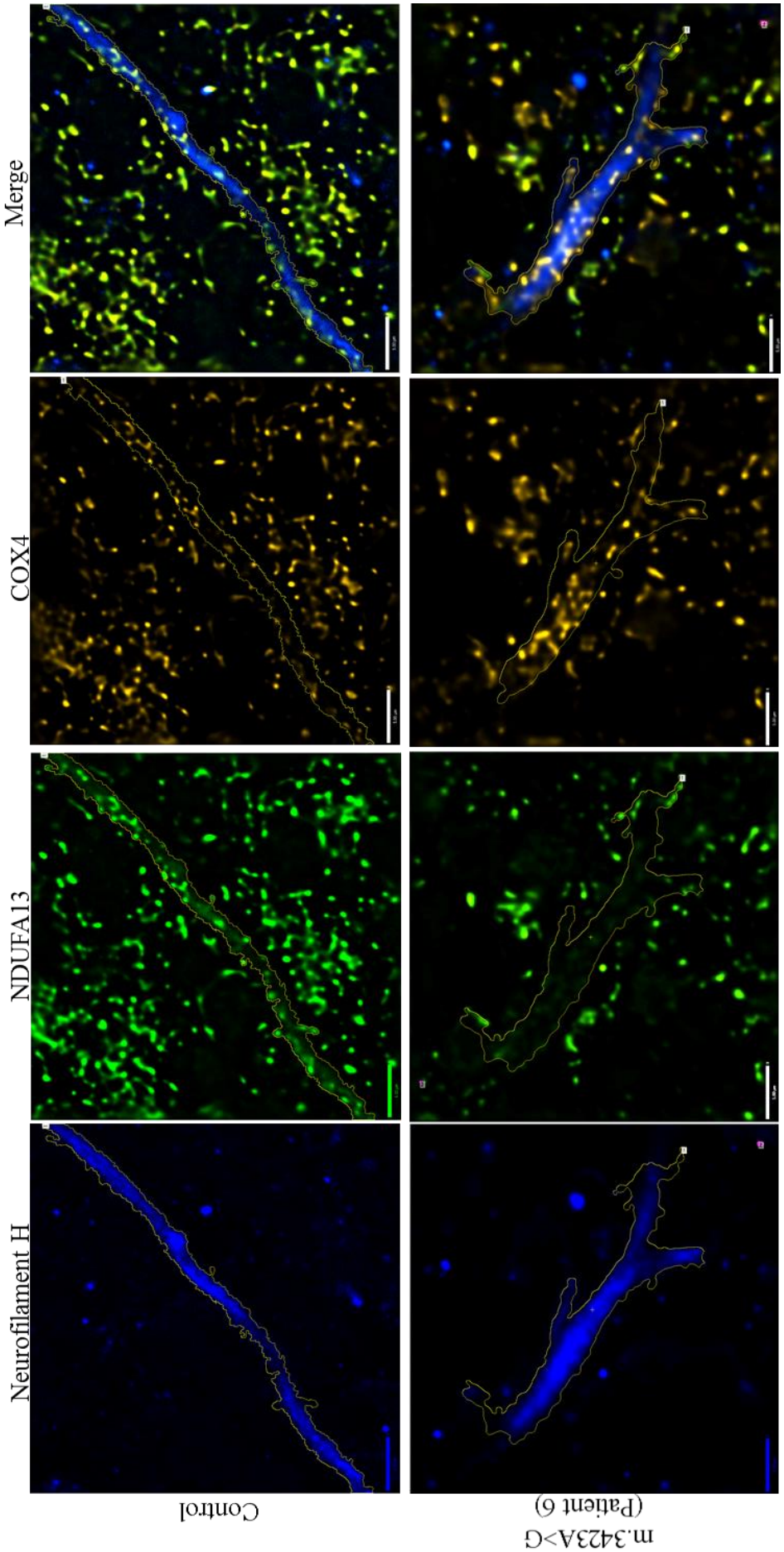

Figure 3.13: Visualisation of mitochondrial respiratory chain proteins in Purkinje cell axons from control and m.3243A>G individuals. Representative images of Purkinje cell axons (neurofilament h, blue) were captured in control and m.m3243A>G individuals. The axons are outlined by the yellow line. In the control axons there is an equal expression of complex I (NDUFA13, green) and mitochondria (COX4, yellow). In the axon from the m.3243A>G, there is no change in mitochondria (COX4, yellow) but there is a decrease in complex I (NDUFA13, green) expression indicating the mitochondria in the axons of the m.3243A>G individuals are respiratory chain deficient. Scale bar= 5um.

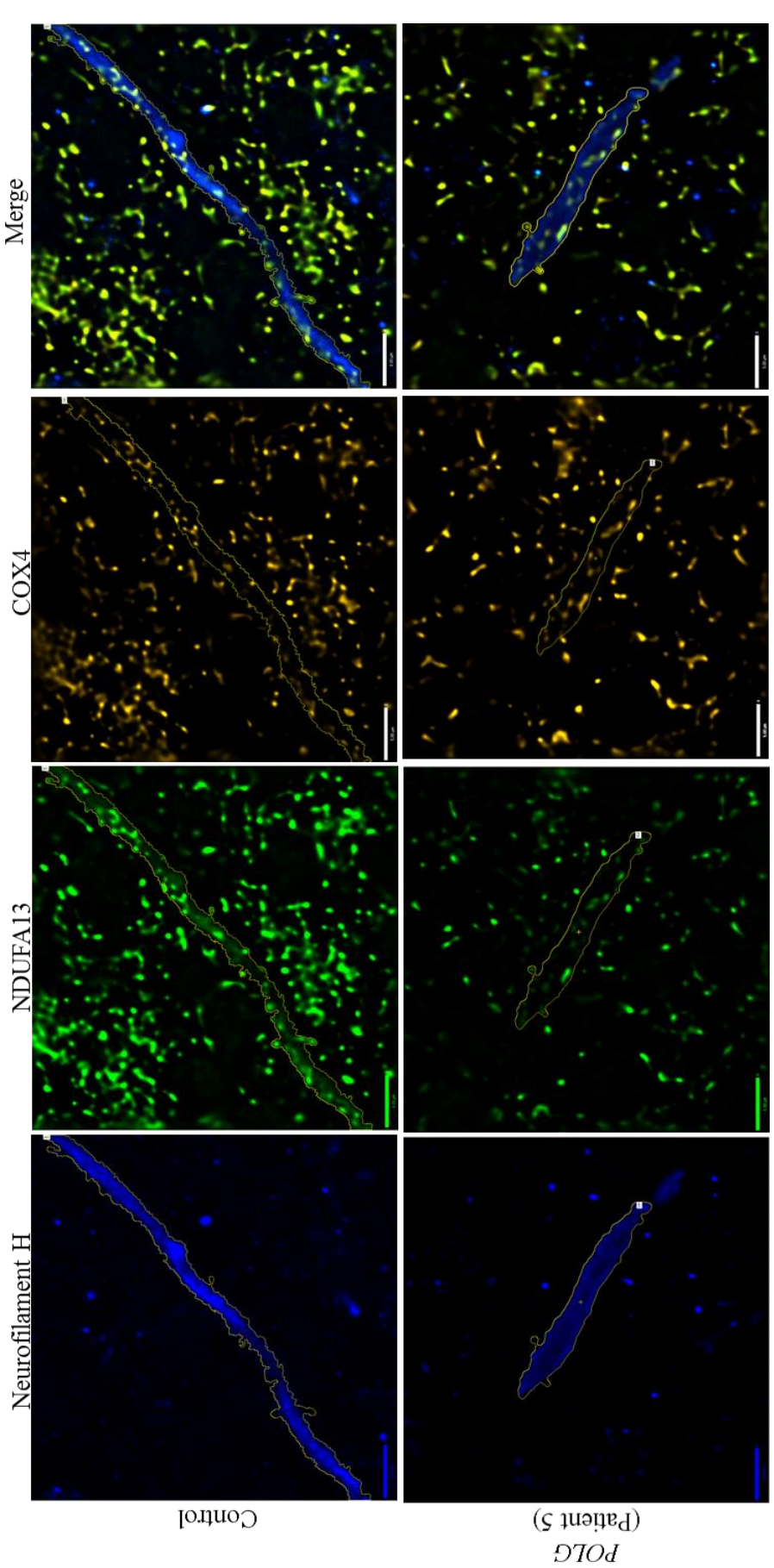

Figure 3.14: Visualisation of mitochondrial respiratory chain proteins in Purkinje cell axons from control and POLG individuals. Representative images of Purkinje cell axons were captured in control and POLG individuals. Using neurofilament H (blue) as the axonal marker expression of complex I (NDUFA13, green) and mitochondria (COX4, yellow) in the axons (axons are outlined by the yellow line), can be visualised. When compared to the control NDUFA13 expression, there is reduction the expression of NDUFA13 in the *POLG* individual. There is no difference in COX4 expression levels show that there mitochondrial density is the same between controls and *POLG* individuals but there is complex I deficiency in the *POLG* individual. Scale bar= 5µm.

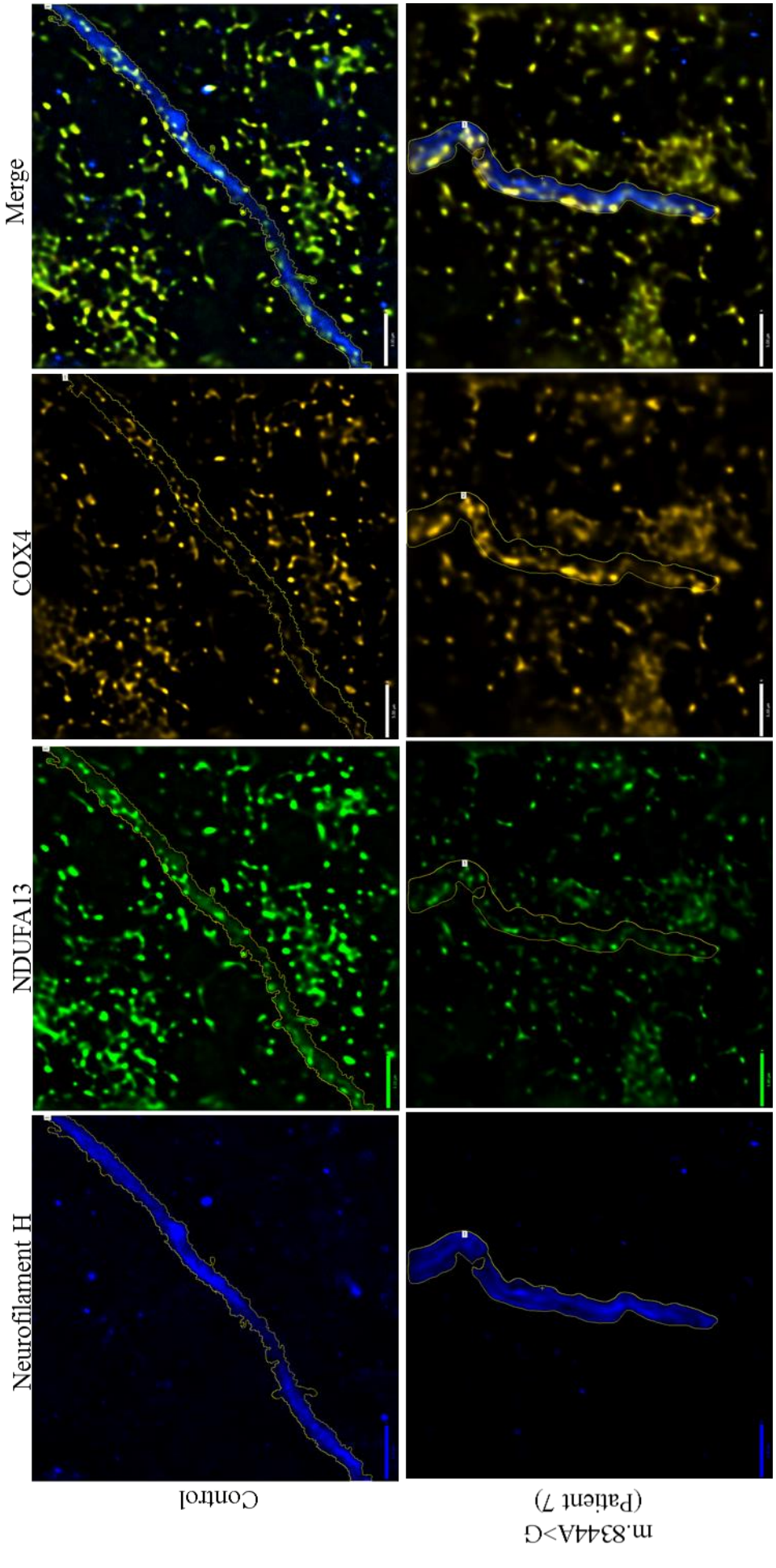

Figure 3.15: Visualisation of mitochondrial respiratory chain proteins in Purkinje cell axons from control and m.8344A>G individuals. Representative images of Purkinje cell axons were captured in control and m.8344A>G individuals. Using neurofilament H (blue) as the axonal marker expression of complex I (NDUFA13, green) and mitochondria (COX4, yellow) in the axons (axons are outlined by the yellow line), can be visualised. There is no difference in COX4 and NDUFA13 expression levels between controls and m.8344A>G individuals indicating that there is no complex I deficiency in the m.8344A>G individual. Scale bar= 5µm.

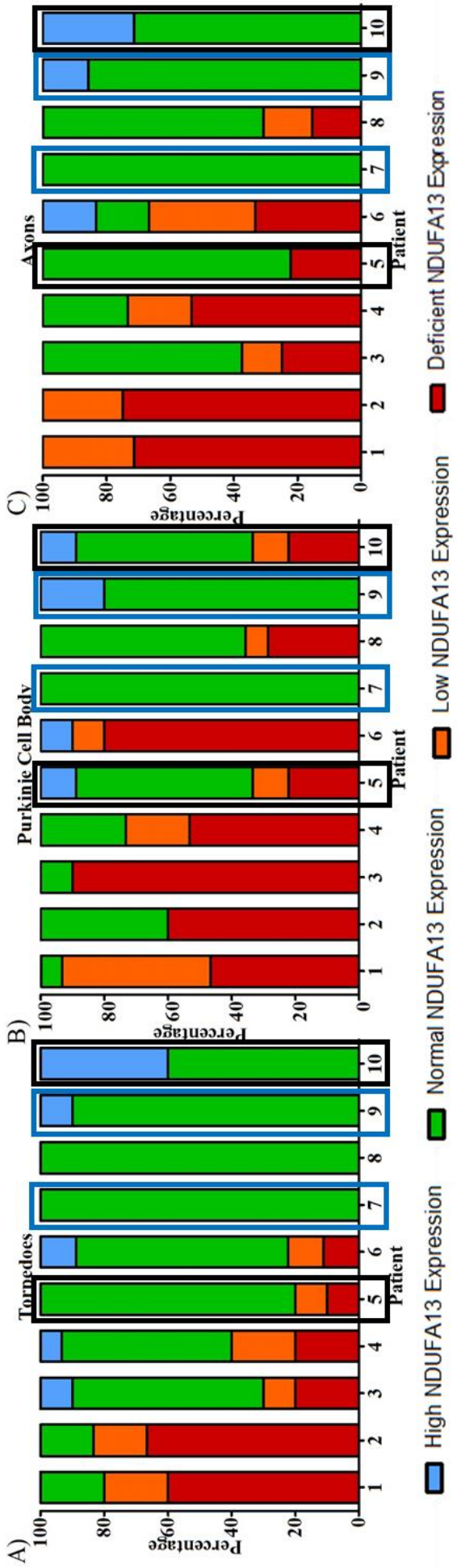

Figure 3.16: Quantification of NDUFA13 deficiency in neuronal structural domains of patients with mitochondrial disease.
Level of NDUFA13 expression was calculated through Z scores and graded on the following scale; High NDUFA13 expression (z > 2SD), Normal NDUFA13 expression (-2SD < z < 2SD), low NDUFA13 expression (z < -2 (SD) and deficient (z < -3 SD). Patients harbouring the m.3243A>G mutation, displayed the greatest level of deficiency in all 3 of the structural domains. Patient 1 (m.3243A>G) and 2 (m.3243A>G) was shown to have the greatest level of deficiency in both the axonal torpedoes and axons. As a whole, Purkinje cell bodies displayed the greatest pattern of NDUFA13 deficiency. Patients 5 and 10 have mutations in *POLG* (black box), patients 7 and 9 have the m.8344A>G mutation (blue box), while the remaining patients have the m.3243A>G mutation.

3.5. Discussion

Patients with mitochondrial disease are commonly affected by neurological deficits which are characterised by progressive decline and have limited treatment options. The poor regenerative capacity and complex architecture of neurons combined with dependence on mitochondria for oxidative phosphorylation explains the vulnerability of the CNS to mitochondrial defects (Attwell and Laughlin, 2001). A common feature in patients with mitochondrial disease is cerebellar ataxia, with recent estimations calculating that 68% of adult patients are suffering with this problem (Lax et al., 2012b; Nesbitt et al., 2013). Despite neuropathological studies confirming the susceptibility of the cerebellum with atrophy, Purkinje cell loss and dentate nucleus neuron loss with complex I deficiency in remaining cells, the mechanisms which result in the degeneration at this early phase are not known (Lax et al., 2012b).

A common and striking pathological phenomenon observed in the cerebellum of patients with mitochondrial disease are axonal torpedoes (Mori et al., 2000b; Lax et al., 2012b). These structures are fusiform swellings of Purkinje cell axons proximal to the cell body. This chapter aimed to confirm that axonal torpedoes are more prevalent in patients with mitochondrial disease than controls, characterise the composition of axonal torpedoes, determine the relationship of axonal torpedoes and respiratory chain deficiency in different neuronal domains and finally determine if axonal torpedoes formed due to a block in axonal transport. I wanted to gain an insight into how they might form, the potential consequence of their formation and how this influences degeneration and therefore progression of disease.

Axonal torpedoes have previously been observed in other disorders with neurological involvement such as Friedreich's ataxia (Jitpimolmard et al., 1993), Creutzfeldt-Jakob disease (Ferrer, 2002) and Huntington's disease (Rub et al., 2013). Where axonal torpedoes have been quantified it was shown that there was 5 times more axonal torpedoes in patients with Alzheimer's and Parkinson's disease compared to controls (Louis et al., 2009a), and patients with essential tremor had on average 7 times more axonal torpedoes than control individuals (Louis et al., 2006; Louis et al., 2007; Louis et al., 2009a). When quantifying the level of axonal torpedoes, the densities of axonal torpedoes were adjusted to Purkinje cell densities and 7/10 patients with mitochondrial disease were observed to have higher axonal torpedo densities than compared to controls. This is therefore in agreement with those previous studies that axonal torpedoes are more prevalent in diseases with neurological involvement. Additionally, Purkinje cell density was also quantified and shown to be markedly decreased in patients which agrees with previous observations in the cerebellum of patients with mitochondrial disease (Lax et al., 2012b). There was no statistically significant relationship

between Purkinje cell density and axonal torpedo density in patients with mitochondrial disease but there was a trend towards an increase in axonal torpedo density when Purkinje cell density was decreased. This observation is similar to results achieved by Louis et al. (2014), where a significant negative correlation was observed between axonal torpedo counts and Purkinje cell counts in the cerebellum of patients with essential tremor. However Louis et al. (2014) also found a positive relationship between axonal torpedo counts and Purkinje cell counts in the cerebellum of patients with multiple system atrophy. These differing observations suggests it may not be possible to conclude a simple linear relationship between Purkinje cell densities and axonal torpedo densities as the cerebellum is likely undergoing torpedo formation and loss, Purkinje cell remodelling and Purkinje cell loss simultaneously making it difficult to conclude relationships in thin post-mortem cerebellar sections. There was no significant relationship between age and axonal torpedo density in patients however in controls a significant relationship was observed with axonal torpedo density increasing with age. My data does contradict published results by Louis et al. (2009a), however our analysis differed as we examined axonal torpedo density whereas the previous study reported absolute torpedo counts, therefore this alternative approach may explain our different results.

Glutamic acid decarboxylase (GAD) 65kDa and 67kDa are isoforms of an enzyme that catalyses the decarboxylation of glutamate to GABA and is only found in inhibitory neurons as GABA is an inhibitory neurotransmitter. Therefore, the immunoreactivity of GAD65/67 in the axonal torpedoes confirms that axonal torpedoes are formed in the axons of Purkinje cells. Electron microscopy studies have shown that disorganised pNFH's were a main component of axonal torpedoes (Mann et al., 1980; Louis et al., 2009c) and through immunohistochemistry, I can confirm that pNFH are the main constituents of axonal torpedoes in patients with mitochondrial disease. The degree at which neurofilaments are phosphorylated is associated with their location, as neurofilament in the axons are phosphorylated while npNFH's are located in the cell body (Sternberger and Sternberger, 1983). The observation of npNFH accumulation in axons is associated with axonal damage and degeneration as seen in axonal end bulbs in the brains of patients with multiple sclerosis (Werner et al., 2001; Trapp and Stys, 2009). In the axonal torpedoes, immunohistochemistical analysis showed that there was no accumulation of npNFHs but there was positive staining of npNHF in the Purkinje cell bodies therefore showing the correct distribution of npNFH in the Purkinje cells and indicating that there is no axonal damage.

The accumulation of neurofilaments have been observed in other neurological disorders (Quan, 2011), and the accumulation of neurofilament in the perikaryon and axon of motor

neurons is a pathological hallmark ALS (Hirano et al., 1984; Robertson et al., 2002). In mice that over express the human form of NFH, neurofilament accumulations occur in the perikaryon causing atrophy of motor axons and altered axonal conductance's (Côté et al., 1993; Križ et al., 2000). This accumulation of pNFH has been hypothesised to cause a "strangulation" of the neuron by causing a physical block to anterograde transport and the disruption of microtubule tracks resulting in the "starvation" of the neurons distal regions causing death (Cleveland, 1999; Louis et al., 2009b). Neurons have highly polarised structures and as all proteins in the neuron are produced in the cell body, they have be transported quickly and efficiently via fast axonal transport (FAT) to the distal regions of the cell which can be up to 1m away. Microtubules which are polymers of α and β tubulin, forms a highly dynamic component of the cytoskeleton and are fundamental for FAT as they are the tracks along which the molecular motor proteins move their cargo up and down axons (Salinas et al., 2008). Anterograde transport utilise the motor protein Kinesin while retrograde transport is achieved through Dynein and both motor proteins hydrolyse one ATP molecule for every 8nm they transport proteins along the axons (Gennerich and Vale, 2009). As an accumulation of pNFH is thought to disrupt the microtubule network, I investigated the presence of microtubules in axonal torpedoes. I was able to show that both β-tubulin and acetylated α tubulin, which are monomers in the microtubules, were present in the axonal torpedoes indicating that the microtubules are still present in the axonal torpedoes. Two proteins that utilise FAT are APP and synaptophysin as they are both located in the presynaptic terminal. The accumulation of APP in axons is associated with axonal damage in diseases like MS (Ferguson et al., 1997) and an accumulation of synaptophysin was observed when the optic nerve had been crushed confirming that these proteins accumulate when FAT is inhibited (Li and Dahlström, 1997). Immunohistochemistry showed a lack of APP and synaptophysin accumulation in the axonal torpedoes. Additionally, when neurofilaments are transported they are in the non-phosphorylated state, as npNFH have a higher affinity for kinesin (Yabe et al., 2000), therefore, if there was a block in axonal transport you would also expect to see an accumulation of npNF's , which was not seen in axonal torpedoes. The lack of positive staining of APP, npNFH and synaptophysin and the positive staining of microtubules in axonal torpedoes infers that fast axonal transport is not inhibited and that the strangulation theory might not be relevant to axonal torpedoes.

In a previous study it had been observed that mitochondria were present in axonal torpedoes but had been forced to the periphery (Louis et al., 2009c). However, I have shown using immunofluorescent labelling of COX4 in axonal torpedoes that mitochondria are found abundantly throughout the axonal torpedoes. Respiratory chain deficiency was then

investigated in the mitochondria found in the axonal torpedoes, as well as those in the Purkinje cell bodies and proximal Purkinje cells axons, to determine if respiratory chain deficiency was a main cause in axonal torpedo formation. A triple immunofluorescent assay was used to measure complex I expression relative to a mitochondrial mass marker. Previous studies have shown that expression of complex I subunits (19kDa 20kDa) were reduced in patients with mitochondrial disease (Lax et al., 2012b; Reeve et al., 2013; Grunewald et al., 2014), therefore a complex I subunit would be a good marker for determining respiratory chain deficiency. Complex IV was used as a mitochondrial mass marker as previous studies have not documented any reduction in complex IV expression in Purkinje cell bodies (Lax et al., 2012b; Chrysostomou et al., 2016). The triple immunofluorescent assay has provided quantified evidence that there is a decrease in NDUFA13 expression in axonal torpedoes, Purkinje cell bodies and axons in the majority of patients with mitochondrial diseases. In line with previous studies by Chrysostomou et al. (2016) and Lax et al. (2016), this study has shown that patients harbouring the m.3243A>G mutation displayed the greatest reduction in complex I deficiency. In the same group of patients, the Purkinje cell body is observed to have the greatest reduction in NDUFA13 expression compared to the other structural domains. This observation differs to data from patients harbouring autosomal recessive POLG mutations which suggests that the complex I deficiency is comparable throughout all structural domains of the neuron. In stark contrast, patients harbouring the m.8344A>G mutations displayed no evidence of complex I deficiency in any of the structural compartments. This is somewhat surprising as both patients were observed to have axonal torpedo densities higher than controls and Purkinje cell density in both patient 7 (m.8344A>G) and patient 9 (m.8344A>G) was reduced compared to controls. The observation that the level of complex I deficiency is greater in Purkinje cell bodies than axonal torpedoes, indicates that axonal torpedoes do not form in the most impaired and affected neurons.

Originally the formation of axonal torpedoes were hypothesised to be a pathological phenomenon that represented the axon dying through a “strangulation” mechanism. However, the characterisation of the axonal torpedoes in this chapter has shown that axonal transport does not appear to be impaired and that axonal torpedoes are more likely to form in “healthy” neurons than sick neurons that harbour a high level of deficiency. If axonal torpedoes were to be involved in a degenerative process, than it would be expected that they would show the greatest level of complex I deficiency but this was not the case. These observations in addition to the high density of axonal torpedoes observed in essential tremor (Louis et al., 2009c), which is not viewed as a neurodegenerative disease (Rajput et al., 2012), suggests

that a variety of stressors can induce the formation of axonal torpedoes but axonal torpedoes are not involved in a degenerative process. The formation of axonal torpedoes in "healthier" neurons suggests that they may be involved in a process of remodelling of the cerebellar circuitry following Purkinje cell loss, explaining the observed trend of increased axonal torpedo density when there is a decrease in Purkinje cell density, in an attempt to maintain efficient functioning of the cerebellum. Understanding the remodelling of Purkinje cell axons following Purkinje cell loss remains an important area of research for understanding and treating patients with ataxia. However, to achieve this utilising thin sections is impossible. Therefore, in the next chapter I will optimise a recently published technique that will enable the use of thicker tissue sections and allow for 3 dimensional visualisation of axonal torpedoes to help determine the level of Purkinje cell axon remodelling in patients with mitochondrial disease compared to controls.

Chapter 4. Three-Dimensional Reconstruction of the Cerebellum: Development of CLARITY technique

4.1. Introduction

Typically, histological studies have relied upon imaging of thin sections in order to investigate the cytoarchitecture and cellular compositions of tissues. This approach has numerous limitations as they only convey fragmented information about structures, spatial arrangements and the relationship between neurons (Figure 4.1). Therefore, to be able to investigate the 3 dimensional (3D) structure of complex cells such as neurons, several groups have depended on the use of serial thin sections for 3D reconstructions. Although very useful, the process of cutting the tissue is extremely laborious and can result in artefacts from tissue distortion, tears, folds or compression leading to a substandard reconstruction of the tissue or organ. An alternative approach is now to use thicker volumes of tissue and image at higher spatial resolutions, but due to several constrains, for a long time, this was not possible.

The first issue related with imaging large volumes of tissue with a traditional epifluorescent microscope was the distortion of the plane of imaging due to the fluorescence emitted by the structures above and below the plane of focus - effect known as out-of-focus. However, the advent of confocal microscopy and the further development of laser scanning microscopes has permitted the filtering and removal of the out of focus light and enabled optical sectioning of the volume to produce a stacked 3D reconstruction of the volume. With advances in microscopy now allowing thicker sections to be imaged at faster rates with higher resolutions, the only limitation restricting the use of thicker sections, was the intrinsic properties of tissues which causes light scattering. A main cause of light scattering in tissue is due to the variable refraction indexes (RI) of components within the tissue, and as RIs across the tissue are not uniformly distributed, the light scattering properties are amplified. In addition to the heterogeneity of RIs within the tissue, the hydrophobicity of the tightly packed lipid bi-layer of the plasma membrane prevents both the chemical penetration of molecular probes and prevention of photon emittance, resulting in further scattering and disruption of the lights pathway.

Recently, a number of methods have been developed aiming at reducing the level of light scattering by either matching the RI throughout the tissue or by removing the molecules that cause the light scattering. This method of tissue clearing was first described by Spatleholtz, where by using organic solvents, the tissue underwent dehydration, tissue bleaching and clearing (Spalteholz, 1914; Richardson and Lichtman, 2015a). Even though this produced unprecedented images in its time, it was found that this original method caused damage to the first few centimetres of tissue ultimately leaving it only useful for large or full organs (Steinke and Wolff, 2001). Since then, clearing methods have evolved and became more refined; some

keep true to the original Spalteholtz method and utilise tissue dehydration and solvent-based clearing while methods that are more recent are aqueous-based.

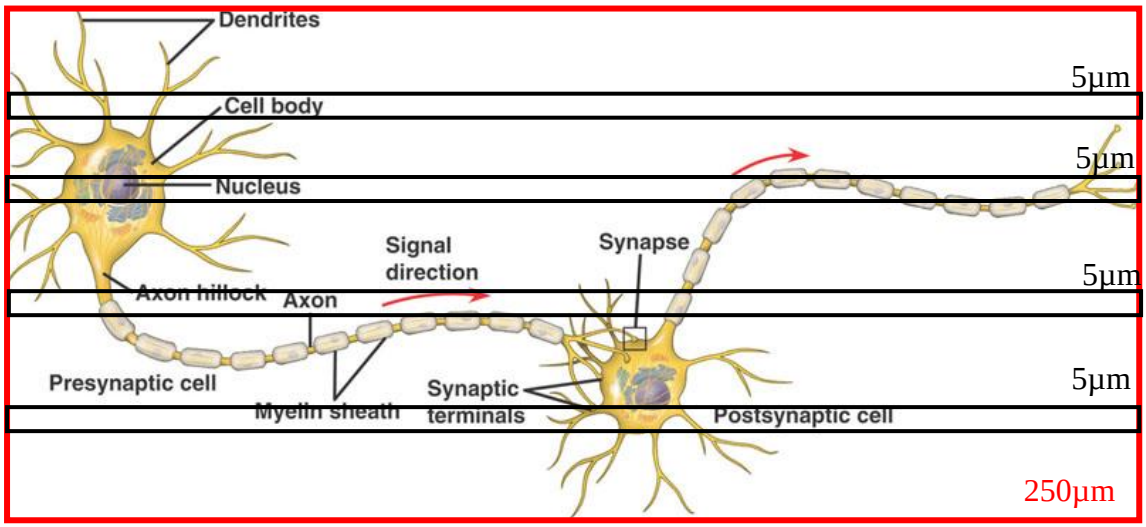

Figure 4.1: The limitations of using 5µm thick sections.

The use of 5µm thick sections (black boxes) limits the amount of information captured. For example, one 5µm thick section might present a neuronal cell body and a axon, however, due to the small thickness of the section it is not possible to control if both cell body and axons belong to the same neuron. Therefore, if thicker volumes are used (red box) then the complete 3D architecture of the neurons and their connections can be visualised.

4.1.1. Solvent Based Clearing Methods

Solvent-based clearing of tissue is typically composed of two steps; the first step involves tissue dehydration using methanol, which sometimes can be mixed with hexane or tetrahydrofurane to remove all the water and some lipids. The second step is to incubate in a clearing solvent to further remove lipids and homogenise RIs across the tissue (Becker et al., 2012). However, one of the major limitation of this technique is the total removal of water molecules which results in fluorescence quenching, as commonly-used fluorescent proteins require water molecules to maintain photon emission (Richardson and Lichtman, 2015b). In addition to fluorophore quenching, the use of solvents in tissue clearance can also cause up to 50% tissue shrinkage, as previously been observed by Becker et al. (2012). The combination of tissue shrinkage, toxic nature of some of the solvents used and fluorophore quenching limits the ease and usefulness of the technique.

4.1.2. Aqueous Based Clearing Methods

To overcome the problems associated with solvent-based techniques, a number of clearing techniques use an aqueous-based method to either increase the RI of the tissue or combine the removal of lipids together with RI increment. In simple immersion techniques, the tissue is placed in a solution that has a higher RI, therefore displacing water and clearing the section. As these sections still contain lipids, the clearing solution requires a RI higher than 1.45 which can be achieved by using molecules such as sucrose (Tsai et al., 2009), fructose (Ke et al., 2013), glycerol (Meglinski et al., 2004)and 2,2'-thiodiethanol (TDE) (Aoyagi et al., 2015). The benefits of using this method is that it takes relatively short incubation periods, the molecules are inexpensive and they are compatible with lipophilic dyes (Ke et al., 2013). However, as these solutions are needed at high concentrations resulting in a very viscous solution and an increased risk of precipitation, it is difficult to clear large pieces of tissue. Additionally, as antibodies are applied before the clearing process, the fluorophores are more likely to become quenched at the high temperatures (37˚C) that are used to help with the clearing method in the SeeDB technique (Ke et al., 2013).

4.1.3. Immersion Clearing Methods

While simple immersion techniques aim to average the RI across the section, a method first described by Hama et al. (2011), by removing the lipids then reducing the RI through incubation in a clearing solution. The Scale method, combines a detergent (triton x) to remove the lipids with both urea and glycerol for hydration and lowering of the RI (Hama et al., 2011). As the urea is able to penetrate and hydrate the most hydrophobic regions of proteins, this can result in the expansion of protein complexes (Hua et al., 2008), as shown by the overall expansion of the tissue section. Therefore, stereological measurements from the sections are not accurate when using this approach.

4.1.4. Clear Lipid-exchanged Acrylamide-hybridized Rigid Imaging compatible Tissue hYdrogel (CLARITY)

The number of limitations associated with the simple immersion method: use of only small sections, hyperhydration is slow and can cause tissue expansion, and the use of solvents and detergents can lower protein content, led to the development of a novel protocol first described by Chung et al. (2013). This technique known as Clear Lipid-exchanged Acrylamide-hybridized Rigid Imaging compatible Tissue hYdrogel (CLARITY) overcomes these limitations by embedding the tissue within a nanoporous hydrogel matrix, through the covalent binding of acrylamide monomers to primary amine groups of molecules in the tissue. The lipids from the tissue are then removed actively by electrophoresis or passively through incubation in a detergent (8% SDS). The principles of the method is summarised in figure 4.2. Following the clearing step, the tissues are then incubated in either FocusClear (Chung et al., 2013) or a Refractive Index Matching Solution (RIMS) (Yang et al., 2014). The benefit of using an acrylamide based hydrogel is that it crosslinks with biological molecules within the sections and reduces protein loss, with only 0.05 mg per mg gross weight protein loss (Yang et al., 2014). Due to the high level of protein retention, the compatibility with normal immunolabelling techniques and its versatility, CLARITY can be applied to a number of different organs from brain to liver and kidney (Lee et al., 2014), and therefore has become very popular for clearing tissue.

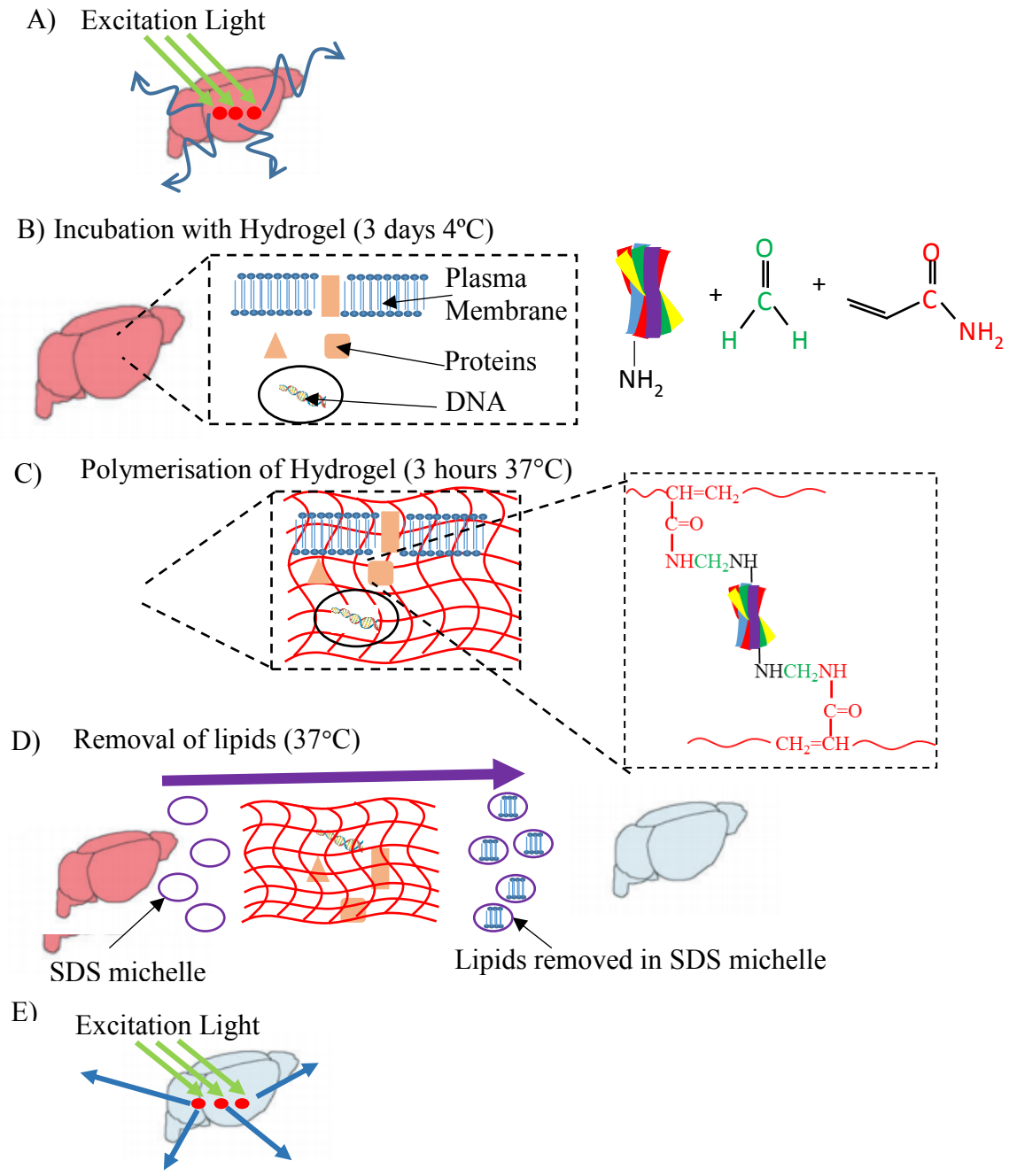

Figure 4.2: The principles of the Clear Lipid-exchanged Acrylamide-hybridized Rigid Imaging compatible Tissue hYdrogel (CLARITY) technique. The heterogeneous nature of the CNS and its high lipid content results in the scattering of emitted light, limiting the thickness of tissue that can be used (A). Sections are incubated with the monomers of the hydrogel (Formaldehyde and acrylamide) at 4ºC for 3 days (B). When the monomers are polymerised in addition to forming a rigid hydrogel they covalently bond to amine groups to the native molecules incorporating those molecules into the hydrogel (C). The removal of lipids can be achieved by passive of active clearing but in both cases the lipids in the section are removed via SDS michelles present in the clearing solution (D).

With the removal of lipids there is reduced light scattering increasing the thickness of tissue that can be used (E).

A number of different groups have utilised the technique to understanding neuron vulnerability in neurodegenerative disorders. For instance, by assessing 500µm thick sections of formalin-fixed frontal cortex from two controls and five patients with Alzheimer's disease, Ando et al. (2014) were the first group to 3D image Amyloid β (Aβ) and tau plaques in human sections. They observed a large axon deflected by a Aβ plaque and, interestingly, a neuron containing a neurofibrillary tangle was shown to have no axonal projections (Ando et al., 2014). Also, the original paper showed that the technique is also suitable for sections that have been fixed in formalin for long periods of time. The investigation of a 500µm thick section from the frontal cortex (fixed in formalin for 6 years) of an infant with autism demonstrated parvalbumin-labelling of interneurons in the deep cellular layers with evidence of isoneuronal and heteroneuronal dendritic bridges, which was not observed in age-matched controls (Chung et al., 2013). Along with human studies documenting changes in neuronal connectivity, CLARITY has been applied to Thy1-YFP mice that have undergone experimental autoimmune encephalomyelitis (EAE). In this study by Spence et al. (2014), they followed axons in the spinal cord that traversed over 5mm in length, and found that 61% of axons in the dorsal corticospinal tract of EAE mice displayed ovoids whereas virtually none were observed in the control mice. While in the cerebral cortex they were able to accurately count the number of layer V pyramidal neurons, something that before could only be achieved as an estimate through serial sections, as well as determining the length of apical dendrites, of which both were shown to be reduced compared to control animals (Spence et al., 2014). These studies highlight that CLARITY permits the visualisation and quantification of axonal pathology associated with neurons in 3D volume in mouse and human post-mortem brain tissues. This methodology provides a wealth of information which is hugely advantageous for elucidating the mechanisms of neuronal vulnerability and connectivity in the human brain associated with different neurodegenerative disorders, and particularly in mitochondrial disease. Therefore, in this chapter, I will describe how I developed CLARITY techniques to allow imaging of large-volumes of cerebellar tissue from patients with mitochondrial disease.

4.2. Aims

The CLARITY method described by Chung et al. (2013) has been successfully completed on human tissue and has the novel property of allowing the sections to undergo multiple staining cycles. The aim of this study is to develop and optimise this technique for use on both human and mouse cerebellar sections. The successful completion of this study would allow for the more comprehensive investigation of changes to Purkinje cell axon morphology in patients with mitochondrial disease compared to controls than was previously achievable in the 5µm thick FFPE sections. Therefore, the aims of this work are:

1. To achieve transparent mouse and human cerebellar sections through the use of the CLARITY method.
2. To optimise a reliable immunolabelling method on the cleared sections that consistently labels Purkinje cell axons, mitochondrial proteins and for the first time attempt a quadruple immunofluorescent assay on cleared sections.
3. To replicate previous findings that it is possible to stain a cleared section, image, remove the previous staining and restain and image the sections with no presence of the original stain.
4. To optimise the imaging of the labelled cleared sections to produce 3D images of the connectivity in the cerebellum.

I will complete the optimisation of mouse cerebellar sections first before completing the protocol on human cerebellar sections.

4.3. Methods

4.3.1. Mice

Five wild type 12 month old C57-BL6 mice were used for this chapter. The mice were sacrificed using cervical dislocation before the brain was excised. Following excision the brains were incubated in 4% Paraformaldehyde at 4ºC overnight and then washed in PBS. All animal experimental procedures were conducted in accordance with the guidelines of the UK home office guidelines.

4.3.2. Human tissue

Formalin-fixed cerebellar brain tissue was obtained from six deceased patients (age range: 55-79years) with genetically and clinically confirmed mitochondrial disease and two control individuals (age: 72 years and 77 years) with no clinical or pathological evidence of neurological disease were used in this study (Table 4.1). The tissue was obtained through the Newcastle Brain Tissue Resource (NBTR) and was approved by the Newcastle and North Tyneside Local Research Ethics Committee.

	Gender	Age (Years)	Fixation (years)	PMI (Hours)	Genetic defect
Control 15	F	72	7	27	N/A
Control 16	F	58	8	39	N/A
Patient 6	M	30	6	21	m.3243A>G
Patient 9	M	58	3	66	m.8344A>G
Patient 10	M	79	4	85	POLG (p.Thr251Ile/p.Pro587Leu; p.Ala467Thr)
Patient 11	M	55	3	112	POLG (p.Trp748Ser and p.Arg1096Cys)
Patient 12	F	60	4	39	Unconfirmed multiple mtDNA deletions due to a nDNA defect
Patient 13	M	47	2	76	m.3243A>G

Table 4.1: Tissue details of individuals that were used in the optimisation of the CLARITY technique.
The details which include age, gender, post mortem interval (PMI) and cause of death from tissue that was supplied by NBTR. N/A – Not applicable

4.3.3. SeeDB

The SeeDB method is fully described in chapter 2.2.3 and is based on the method detailed in the study by Ke et al. (2013). Cerebellar sections from wild type 12 month old C57BL/6 mice were used. Sections were stained with anti-Neurofilament H 200kDa (Neurofilament H, 1:200) and anti-SMI-94 (Myelin Basic Protein, 1:1000).

4.3.4. CLARITY Protocol

Once the tissue had been acquired and processed, the tissue underwent the CLARITY protocol which is described in detail in chapter 2.2.4. The basis of the protocol is depicted in figure 4.3 and a number of factors were adjusted and optimised throughout the chapter and they are explained further in the results section.

Once the tissue had been incubated in the hydrogel solution, both mouse and human cerebellum sections were sectioned to 250µm using a vibratome (Frequency:70Hz, Amplitude:0.7m).

A number of negative consequences have been associated with the active clearing process which include blackening and expansion of the sections as well as the formation of destructive bubbles within the sections (http://forum.CLARITYtechniques.org/). A number of recent publications have concentrated on the optimisation of the conditions used for the active clearing step, to attempt to prevent the destructive consequences (Lee et al., 2014; Poguzhelskaya et al., 2014), However due to those negative consequences and the apparent success of other authors using passive clearing (Spence et al., 2014; Tomer et al., 2014; Yang et al., 2014) the passive clearing method was chosen as the preferred method of clearing to be completed on both mouse and human cerebellar sections.

The primary antibodies and secondary antibodies used in this chapter are summarised in table 4.2 and 4.3. The Refractive Index Matching Solution (RIMS) was the imaging solution used throughout the project. It was first proposed by Yang et al. (2014), it has similar properties to FocusClear but is a more affordable option.

4.3.5. Imaging

The cerebellar sections were imaged (Z-stack volume, 250 µm) using confocal laser microscopy (Nikon A1R, Nikon instruments) with the Galfano settings at excitation wavelengths of 488nm, 546nm and 647nm with an 20X objective (0.70 numerical aperture). Post image 3D projection was viewed using the NIS Elements viewer software (Nikon instruments) while 3D rendering was completed using Imaris software (Andor Technology plc)

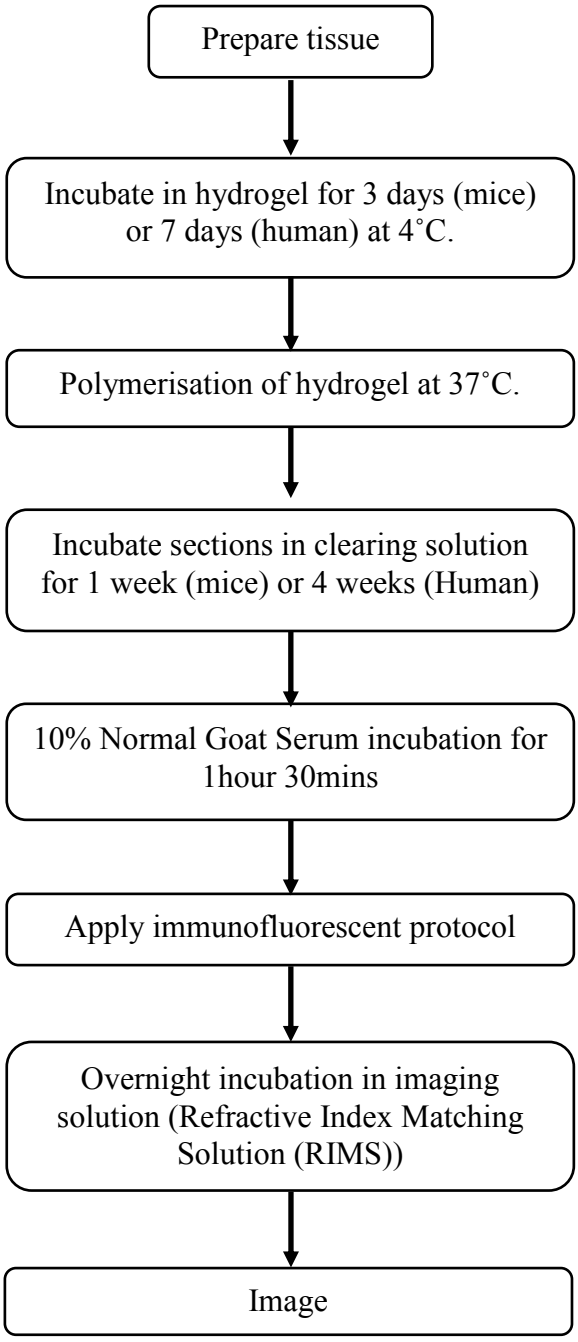

Figure 4.3: A flow diagram of the original CLARITY protocol.
The basic flow of steps that were applied to the sections of cerebellum tissue.

Antibody	Target	Host	Isotype	Dilution
Anti-neurofilament H 200kDa	neurofilament H (200 kDa)	Rabbit	IgG	1:200
Anti-NDUFA13	NDUFA13	Mouse	IgG2b	1:100
Anti-SMI-94	Myelin Basic Protein	Mouse	IgG1	1:500
Anti-Porin	porin	Mouse	IgG2b	1:100
Anti-MTCO1	Cytochrome C Oxidase subunit I (COX1)	Mouse	IgG2a	1:100
Anti-COX4 + COX4L2	cytochrome C oxidase subunit IV (COX4)	Mouse	IgG2a	1:100
Anti-SMI-31	Phosphorylated neurofilament H & M	Mouse	IgG1	1:1000
Anti-glut-1	Glut-1 (endothelial)	Rabbit	IgG	1:100
Anti-SDHA	Succinate Dehydrogenase Complex, Subunit A (SDHA)	Mouse	IgG1	1:100
Anti-myelin basic protein	Myelin Basic Protein	Chicken	IgY	1:100
Anti-GAD 65/67	Glutamic Acid Decarboxylase 65/67	Rabbit	IgG	1:100
Anti-neurofilament H 200kDa	Neurofilament H (200 kDa)	Chicken	IgY	1:100
Anti-α smooth muscle actin	α smooth muscle actin	Mouse	IgG2a	1:100
Anti-parvalbumin	Parvalbumin	Mouse	IgG1	1:100
Anti-calbindin D-28k	Calbindin D-28k	Mouse	IgG1	1:100

Table.4.2: Description of Primary antibodies used.

A summary of the different primary antibodies that have been used on passively cleared sections of both human mouse cerebellar tissue.

Antibody	Target
Alexa Fluor 633 anti-mouse IgG1	Mouse IgG1
Alexa Fluor 633 anti-mouse IgG2a	Mouse IgG2a
Alexa Fluor 647nm anti-mouse IgG1	Mouse IgG1
Alexa Fluor 405nm anti-rabbit IgG	Rabbit IgG
Alexa Fluor 488nm anti-mouse IgG1	Mouse IgG1
Alexa Fluor 488nm anti-mouse IgG2b	Mouse IgG2b
Alexa Fluor 488nm anti-mouse IgG2a	Mouse IgG2a
Fluorescein Goat Anti-Chicken IgY	Chicken IgY
Alexa Fluor 546nm anti-mouse IgG1	Mouse IgG1
Alexa Fluor 546nm anti-rabbit IgG	Rabbit IgG

Table.4.3: Description of secondary antibodies used in the optimisation of the CLARITY technique.
A summary of the different secondary antibodies that have been used on passively cleared sections of both human mouse cerebellar tissue. All secondary antibodies were raised in goat and the dilution used was 1:100µl

4.4. Results

Throughout this section I will describe the processes and results I achieved when optimising the different aspects of the CLARITY technique.

4.4.1. SeeDB

Before optimising the CLARITY protocol, I attempted the SeeDB method on the cerebellum taken from wild type 12 month old C57BL/6 mice. The SeeDB method uses increasing concentrations of fructose to match the RI of the sections (Ke et al., 2013) and is a simpler and faster method than the CLARITY technique. However, as the antibodies must be applied before the clearing process, there was no successful staining of targets and a substantial increase in the volume of tissue was observed (results not shown). Through these observations, it was decided to persist with the CLARITY technique.

4.4.2. Applying CLARITY to mouse sectioning

The mouse brains were processed and incubated with hydrogel solution that underwent polymerisation at 37˚C to provide a firm and defined hydrogel matrix around and within the section. Polymerised hydrogel forms a strong and durable structure so removing the whole cerebellum from the excess hydrogel was easy. However, the pre-sectioned tissues proved difficult to remove from the hydrogel and were more prone to damage following the physical removal. Therefore, the whole cerebellum was embedded in the hydrogel before sectioning to the required thickness (250µm) using a vibratome. Following sectioning on the vibratome, the sections were incubated in clearing buffer at 37˚C until the sections were visually determined as transparent. For mouse sections, it took 7 days for the sections to become fully clear (Figure 4.4).

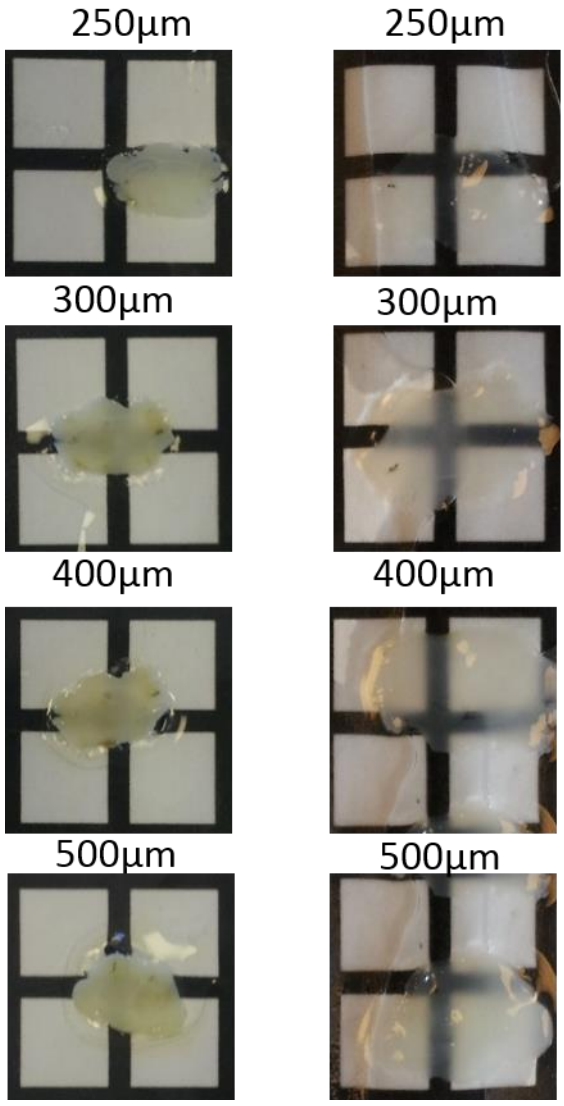

Figure 4.4: Before and after images of a passively cleared wild type mouse brain sections.

Wild type mouse cerebellar sections had undergone passive clearing in clearing solution at 37˚C for 7 days.

4.4.3. Immunofluorescent staining

Once the tissue was successfully cleared, the next step was to optimise the immunofluorescent protocol in order to label the different neuronal structure and mitochondrial proteins of interest. In order to determine the optimal conditions for immunofluorescent staining, the following reliable antibodies were used:

- Porin (to label mitochondria; 488nm),
- Neurofilament H (to label neurons and their neuritic processes; 546nm)
- Myelin basic protein (to label myelin; 633nm).

The first set of conditions to be tested for immunofluorescent staining was first described in the original study by Chung et al. (2013), where both the primary and secondary antibody solutions were diluted in a sodium borate buffer (SBB) and then incubated at 37˚C for 24hours for each (Figure 4.5A). The results with this condition were rather underwhelming, with only neurofilament H producing positive staining.

Despite increasing the temperature to 37˚C to improve antibody penetration and decrease the incubation time, the higher temperature reduced the specificity of the staining. Therefore, the staining was repeated using different experimental conditions: the temperature was decreased to 4˚C to increase the specificity of antibody binding while the length of the incubation was extended to 6 days for primary antibodies and 4 days for secondary antibodies (Figure 4.5B). The incubation length was increased to account for the decrease in diffusion rates of the antibodies due to the cold temperature. This resulted in specific staining of all three markers, including the mitochondrial marker porin (488nm). However, it was also observed that at 4˚C the SBB formed crystals both in the solution and on the sections, which most likely affected the quality of staining. Therefore the experiment was repeated using PBS instead of SBB, which produced strong positive staining of porin, neurofilament H and MBP, that was of higher quality than captured with SBB (Figure 4.5C). Due to the superior quality of staining, the dilution of antibodies in PBS at 4˚C with a prolonged incubation was used as the method of choice for immunostaining from here onwards. An un-cleared section underwent the most successful immunofluorescent protocol to show the benefits of using the CLARITY method (Figure 4.5D).

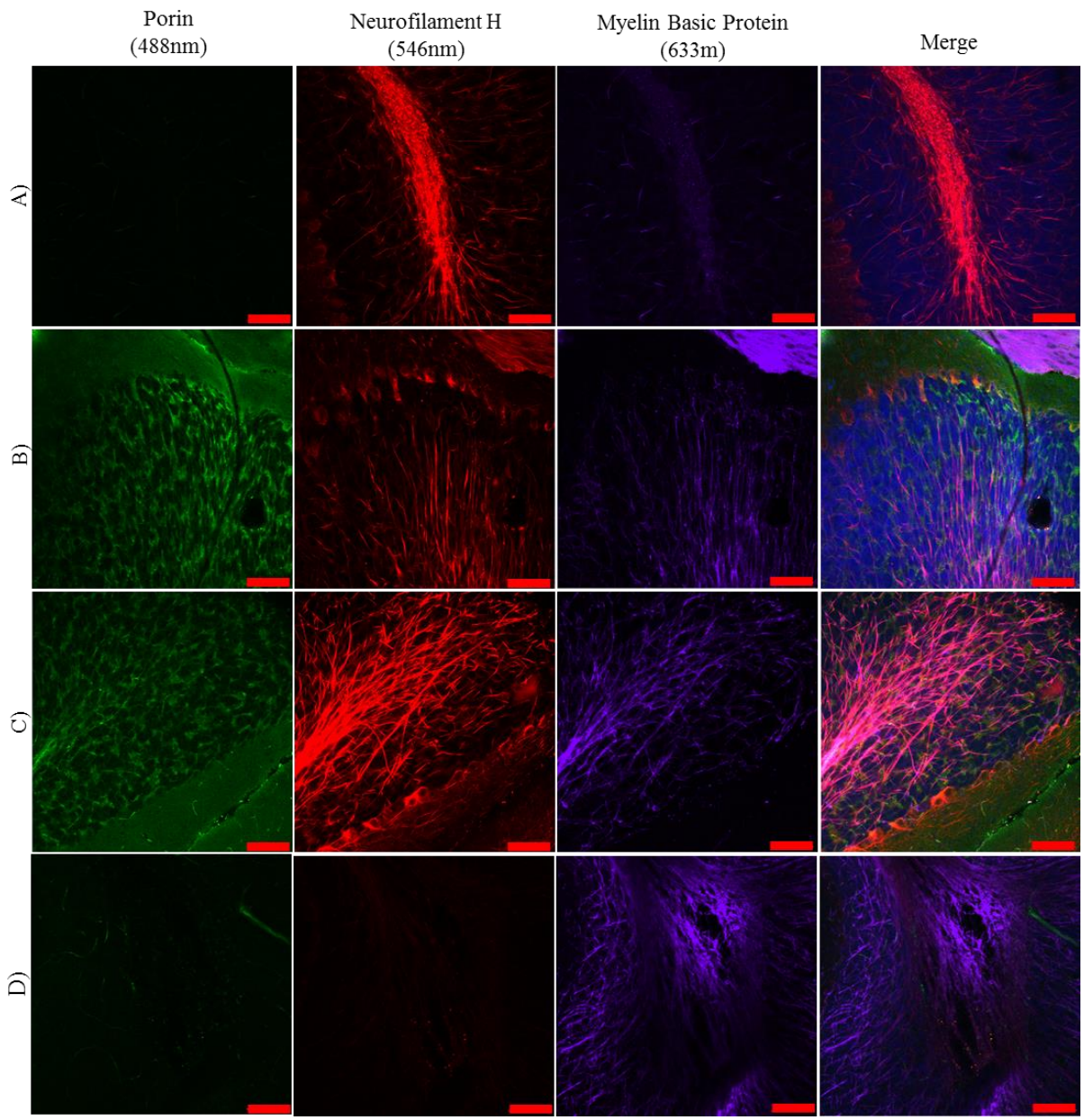

Figure 4.5: Optimisation of immunofluorescent protocol conditions on passively cleared 250µm thick wild type mouse cerebellar section.

Passively cleared wild type mouse cerebellum sections were stained with porin (488nm), neurofilament H 200kDa (546nm) and myelin basic protein (633nm) under various different conditions; A) sodium borate buffer at 37˚C for 24 hours B) sodium borate buffer at 4˚C for 6 days for the primary antibodies, then at 4˚C for 4 days for secondary antibodies. C) PBS at 4˚C for 6 days for the primary antibodies, then at 4˚C for 4 days for secondary antibodies. D) An uncleared cerebellar section was also stained for porin, neurofilament H 200kDa and myelin basic protein using protocol C. Scale=100µm

4.4.4. Antibody penetration

When completing the staining of serial sections with increasing thickness, it became apparent that there was a lack of antibody penetration into the thicker sections. It was observed that sections with a thickness greater than 300µm, there was strong positive staining at the edges of the section but reduced intensities towards the centre of the tissue. This is exemplified in figure 4.6, where a highly dense network of myelin can be seen in the extremities of the section and reduced intensities in the middle. 3D rendering of the section, however, shows that the myelin staining is present at the centre but the intensity is reduced compared to that of the section edges, suggesting lower penetration of antibodies.

In an attempt to increase the depth of antibody penetration by improving the permeability of the tissue, a proteinase K (10 mg/ml) incubation for 10 minutes following the hydrogel incubation was applied (Gleave et al., 2013). Following the application of proteinase K, the tissue lost structural integrity and slowly disintegrated, making it impossible to image.

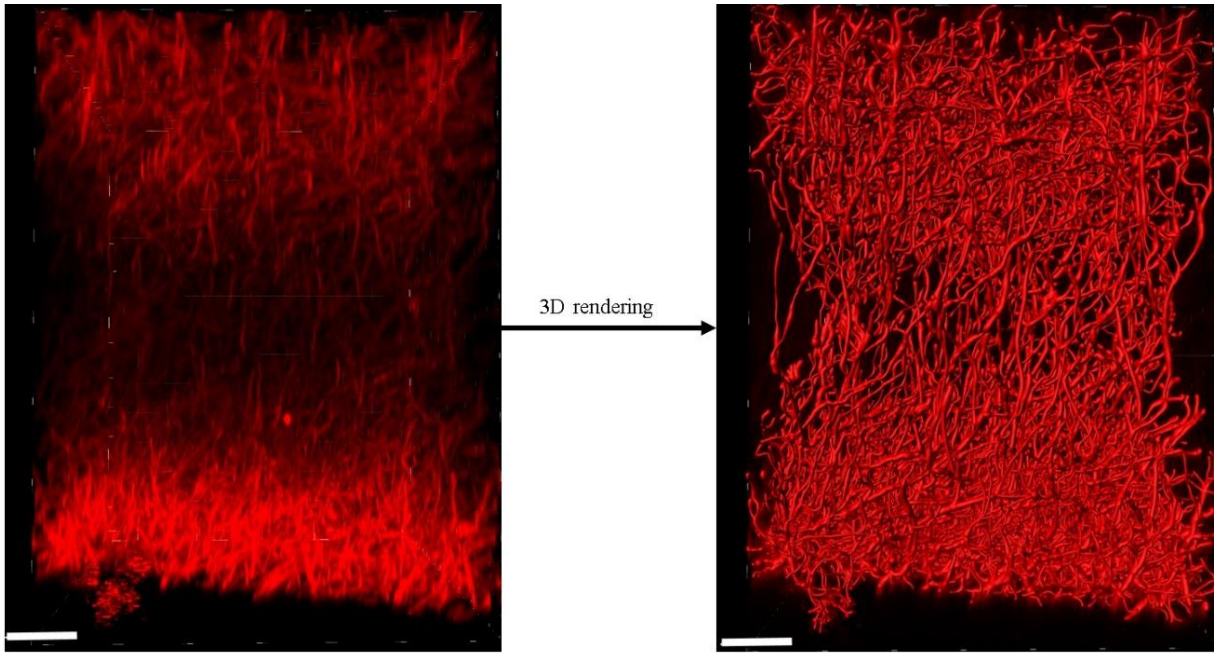

Figure 4.6: Poor antibody penetration in 500µm thick in mouse cerebellum section. Positive labelling of myelin basic protein can clearly be observed in the first and last 150µm of the section. However, in the middle of the section the intensity reduces. This is exemplified once the image has undergone 3D rendering using the Imaris software. The dense complex myelin structure can be observed at the surfaces/edges however in the middle there is still staining but nowhere as strong. Scale 100µm

4.4.5. Testing of various antibodies

In order to investigate axonal and circuitry pathology in the cerebellum of mitochondrial diseased patients, the next step was to trial a number of antibodies that would label Purkinje cells, either their cell bodies or projections, as well as labelling mitochondria to help determine the level of respiratory chain deficiency in the a single neuron.

Unfortunately there was no positive staining associated with the GAD65/67 antibody which labels glutamic decarboxylase 65/67, an enzyme only found in inhibitory neurons like Purkinje cells. However, the Purkinje cell bodies were clearly labelled with both parvalbumin (Figure 4.7A) and calbindin (Figure 4.7B). The axons were clearly labelled with the neurofilament H (Figure 4.7C) and SMI-31 antibody (Figure 4.7D) while the MBP (IgY) antibody produced non-specific staining and no specific staining of the myelin. There were mixed results with the mitochondrial antibodies, as there was no specific or positive labelling of mitochondria associated with the SDHA, NDUFA13 and COX4 antibodies, while there was partial positive staining with porin. The most success was observed with the COX1 antibody (Figure 4.7E).

Figure 4.7: Application of various mitochondrial and neuronal antibodies on cleared 250µm mouse cerebellum sections.
A number of mitochondrial and neuronal antibodies were tested to determine their success on cleared tissue. Positive staining of the Purkinje cell bodies was achieved with the calbindin (A) and parvalbumin (B) antibodies. While the axons were positively labelled with neurofilament H (C) and SMI-31 (phosphorylated neurofilament (D)) antibodies. There was mixed results with the mitochondrial antibodies with only COX1 (E) producing consistent positive staining across the section. Scale bar - 100µm

4.4.6. Microscopy

To begin with, imaging was completed using the Nikon A1R confocal microscope with the 10X objective as this had the greatest working distance of the objectives available (Figure 4.8A). Once it had become apparent that thinner sections were going to be used to overcome the lack of antibody penetration depth, it was possible to use the 20X objective (Figure 4.8B) which has a greater numerical aperture and improves the resolution of the images acquired compared to the 10X objective. This is shown by the increased detail of both neurofilament H and myelin basic protein, as well as observing punctate mitochondria in the Purkinje cell body.

Another useful tool for analysing axonal pathology is the ability to produce large field images of the section (Figure 4.9A). This image was achieved by taking 180 images at 20X magnification and then stitching together the individual tiles. The benefit of large field images at a higher magnification is that it is possible to zoom into any region and retain the high resolution (20X). This is exemplified in figure 4.9B where it is possible to see the intricate network of the axons in granular cell layer of a folia.

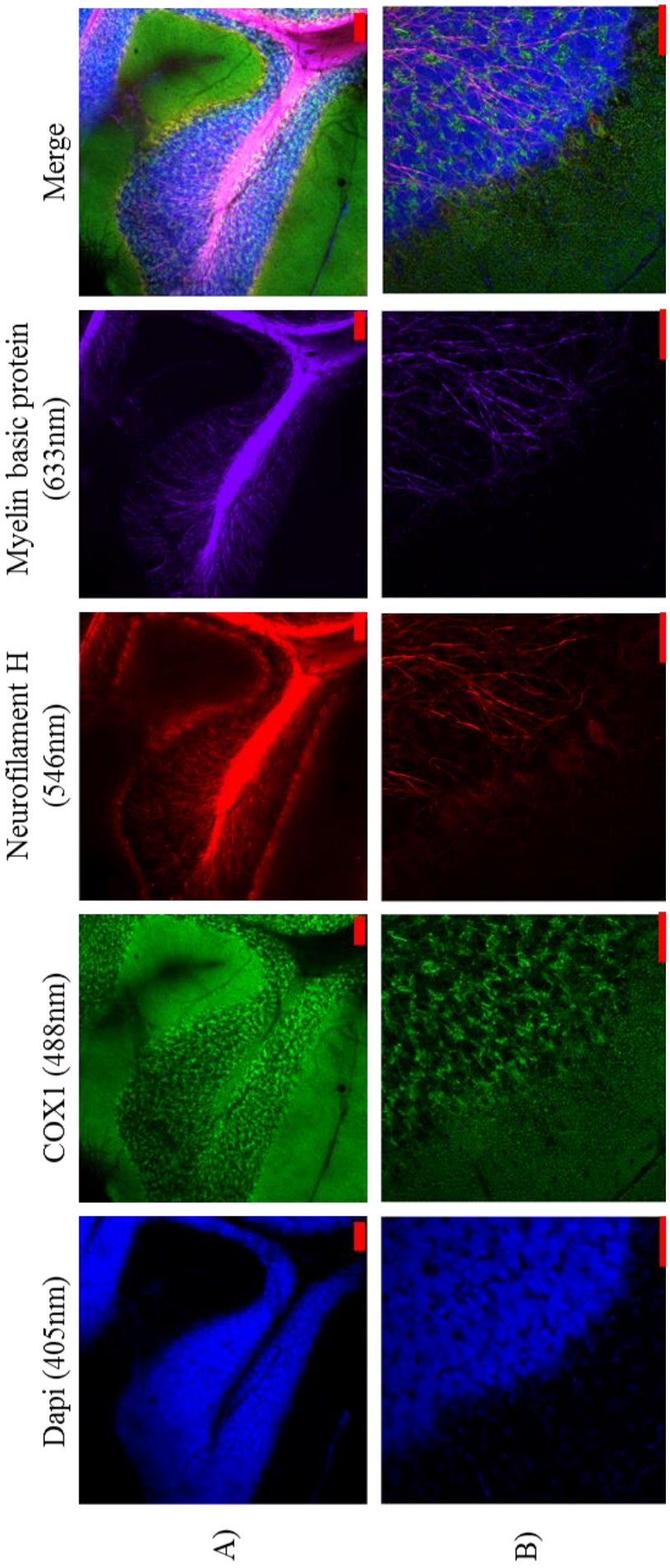

Figure 4.8: Optimisation of confocal microscopy for the imaging of cleared 250µm thick mouse cerebellum sections. A) Sections were initially imaged using a 10X objective due its greater working distance. B) As the section thickness was only 250µm, the magnification could be increased to 20X, making it is possible to produce images where punctate mitochondria (COX1 (488nm)) can be observed as well as the complex network of axons (neurofilament H (546nm), MBP (633nm)). scale bar = 100µm.

Figure 4.9: Tiled image acquisition of passively cleared 250µm thick mouse cerebellum sections. A) A large tiled image of the whole cerebellar section that was stained for mitochondria (COX1 (488nm)) and myelinated axons (neurofilament H (546nm), MBP (633nm)) was achieved by taking multiple images at 20X magnification in a grid and stitching the images together. B) A benefit of imaging at 20X is that it is possible to zoom into any section and view that region with a high level of resolution. Scale bar = 100µm

4.4.7. Human Tissue

After successfully clearing mouse tissue and devising a successful immunofluorescent protocol, the next step was to optimise the method for human tissue. I had started by completing the method on tissue obtained from control 15 and patient 6. As expected, the human tissue took longer to fully clear, with 250µm thick sections taking 4 weeks to clear (Figure 4.10).

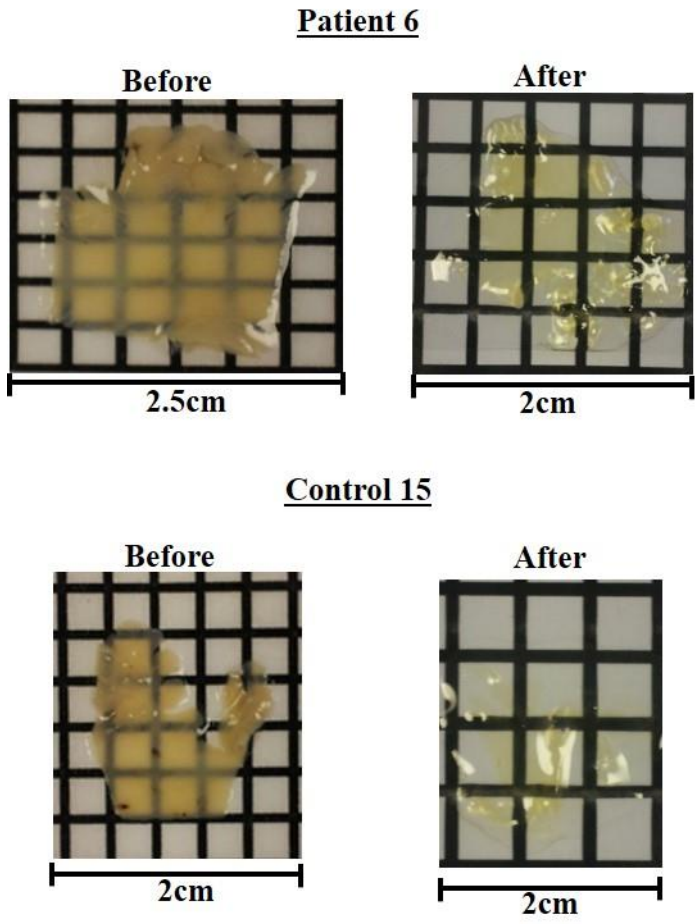

Figure 4.10: Before and after images of a passively cleared 250µm thick control human cerebellar section.
Human cerebellar sections had undergone passive clearing in clearing solution at 37˚C for 4 weeks.

4.4.8. Antibody staining conditions

Following the successful clearing of the human tissue, the conditions used on the mouse tissue were repeated on the human sections (Figure 4.11 and Figure 4.12). As before, the antibodies used to evaluate the efficacy of the subsequent conditions were: porin (488nm), neurofilament H (546nm) and myelin basic protein (633nm). The results observed were similar to those from the mouse tissue, with a lack of staining in both the control 15 and patient 6 sections when the antibodies were incubated in SBB (Figure 4.11A) or PBS (Figure 4.11B) at 37˚C for 24 hours. However, when using the previously successful protocol where the temperature was reduced to 4˚C with a prolonged incubation time, there was a lack of positive staining in the section from patient 6 but positive staining of all three antibodies in the 250µm cerebellar section from control 15 (Figure 4.12A). In the white matter, the neurofilament H and MBP co-localised confirming that the staining was specific. An uncleared 250µm cerebellar section from control 15 underwent the protocol of PBS at 4˚C, which produced minimal positive staining and confirmed the benefits of using cleared sections (Figure 4.12B).

A no primary antibody panel was completed and showed a high level of autofluorescence in the 405nm channel, where blood vessels (white arrows) can be observed, and slight autofluorescence in the 488nm channel (Figure 4.13).

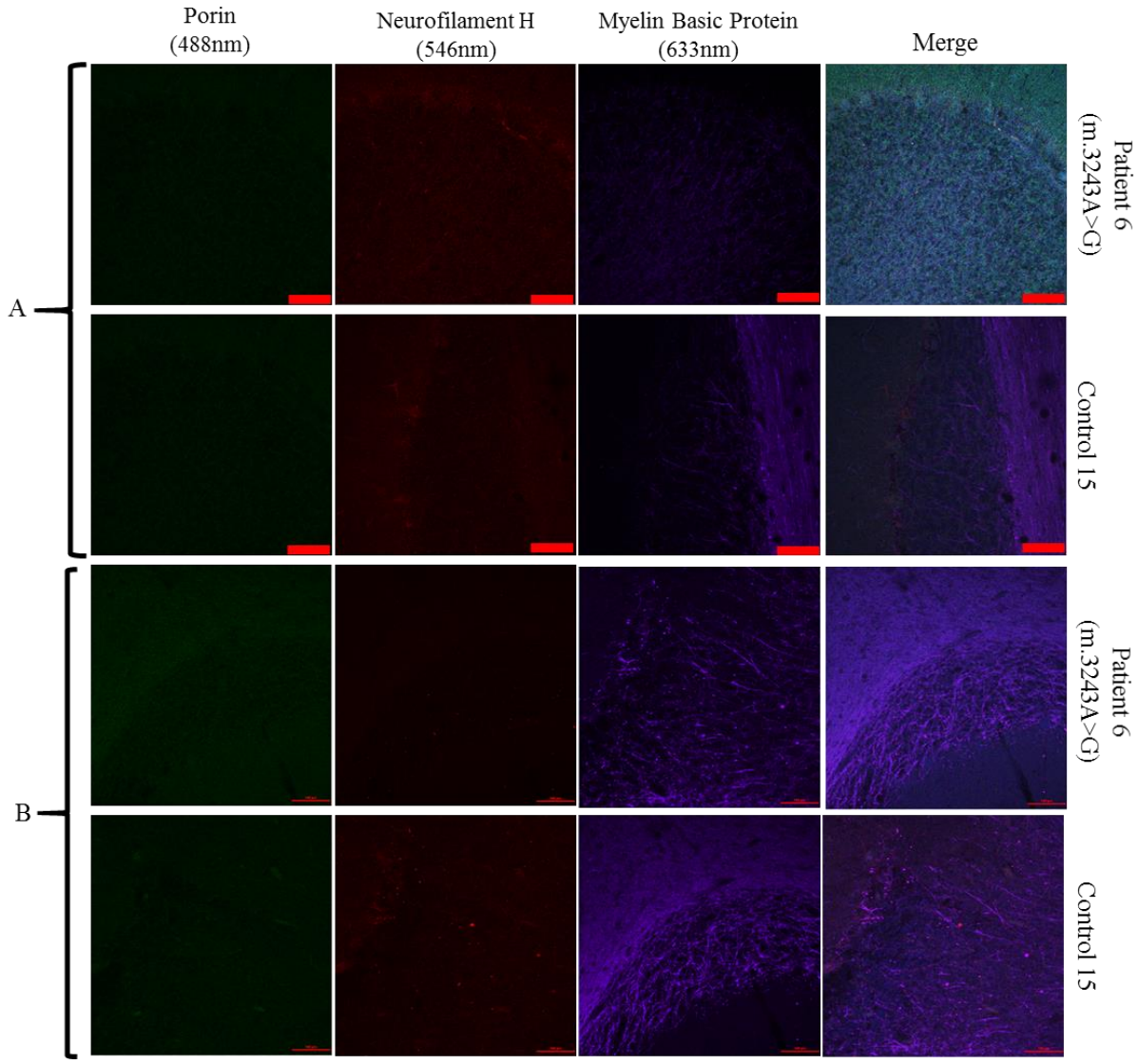

Figure 4.11: Optimisation of immunofluorescent protocol conditions on passively cleared 250µm human cerebellar sections.

Passively cleared cerebellum sections from control 15 and mitochondrial patient 6 were stained with porin (488nm), neurofilament H 200kDa (546nm) and myelin basic protein (633nm) under different conditions; A) sodium borate buffer at 37˚C for 24 hours B) PBS at 37˚C for 24 hours Scale bar=100µm

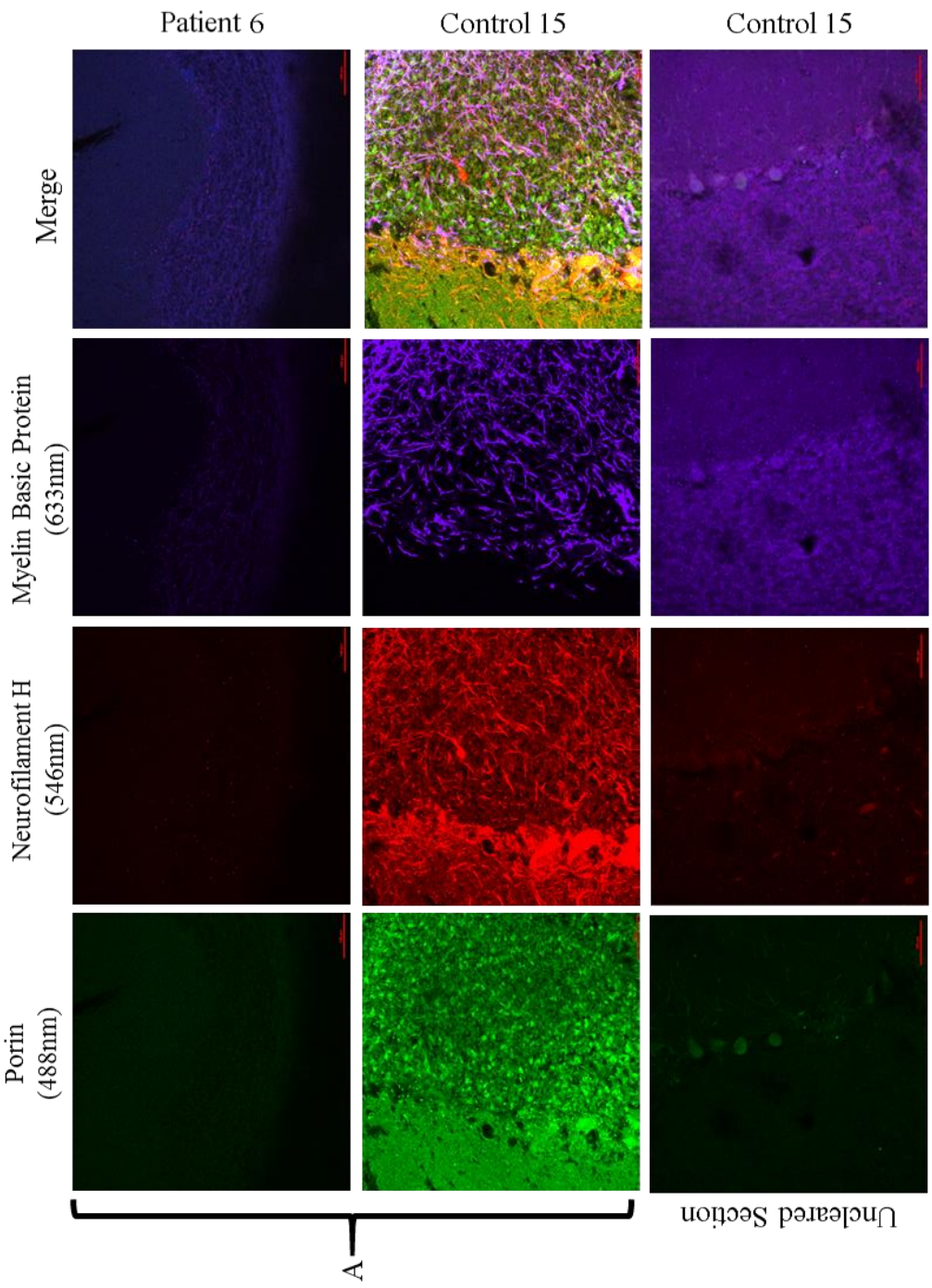

Figure 4.12: Optimisation of immunofluorescent protocol at 4°C on passively cleared and uncleared 250µm human cerebellar sections. Passively cleared cerebellum sections from control 15 and mitochondrial patient 6 and a uncleared section from control 15 were stained with porin (488nm), neurofilament H 200kDa (546nm) and myelin basic protein (633nm) PBS at 4˚C for 6 days for the primary antibodies, then at 4˚C for 4 days for secondary antibodies. A uncleared section is included to demonstrate the benefits of using the CLARITY technique. Scale bar=100µm

Figure 4.13: No-primary antibody staining in a passively cleared 250µm cerebellar control section. A no primary antibody section confirmed that there is non-specific staining or autofluorescence of the vascular system in the 405nm channel (white arrows) and is also detectable in the 488nm channel. Scale=100µm

4.4.9. Completion of CLARITY protocol on new sections

Now the clearing of human cerebellar sections and the immunofluorescent protocol to successfully label axons and myelin sheathes has been optimised, the next step was to complete the process on new cases. These were carefully chosen based on the criteria that they had been fixed in formalin for a maximum length of 6 years, which produced 6 new cases to trial (1 control and 5 patients with mitochondrial disease). As before, I used an antibody that labels a mitochondrial protein (COX1), neuronal marker (neurofilament H) and a myelin sheath maker (myelin basic protein) to determine the viability of the tissue to be used in the protocol.

The new cases were incubated in the hydrogel and following hydrogel polymerisation, sectioned to 250µm thickness. The sections were then passively cleared for 4 weeks before undergoing the immunofluorescent staining protocol and imaged on the Nikon A1 confocal microscope. It is clearly visible in control 16 and patient 13 that the staining has failed, with no positive labelling of either the axons or myelin sheath (Figure 4.14). In addition to the lack of staining, a large vascular vessel can be observed in the 488nm channel of control 16, indicating that there is a problem with auto fluorescence or non-specific staining of the antibodies, as a similar structure was observed in the no primary antibody control section (Figure 4.13).

Patients 9, 10, 11 and 12 had specific and positive labelling of both axons and myelin in cerebellum, making it possible to visualise the Purkinje cell axons running from the Purkinje cell layer into the white matter (Figure 4.15 and Figure 4.16). Along with the original control I successfully cleared and stained (figure 4.12), I can confirm that it is also possible to successfully clear and stain cerebellar human tissue from both control individuals and mitochondrial patients.

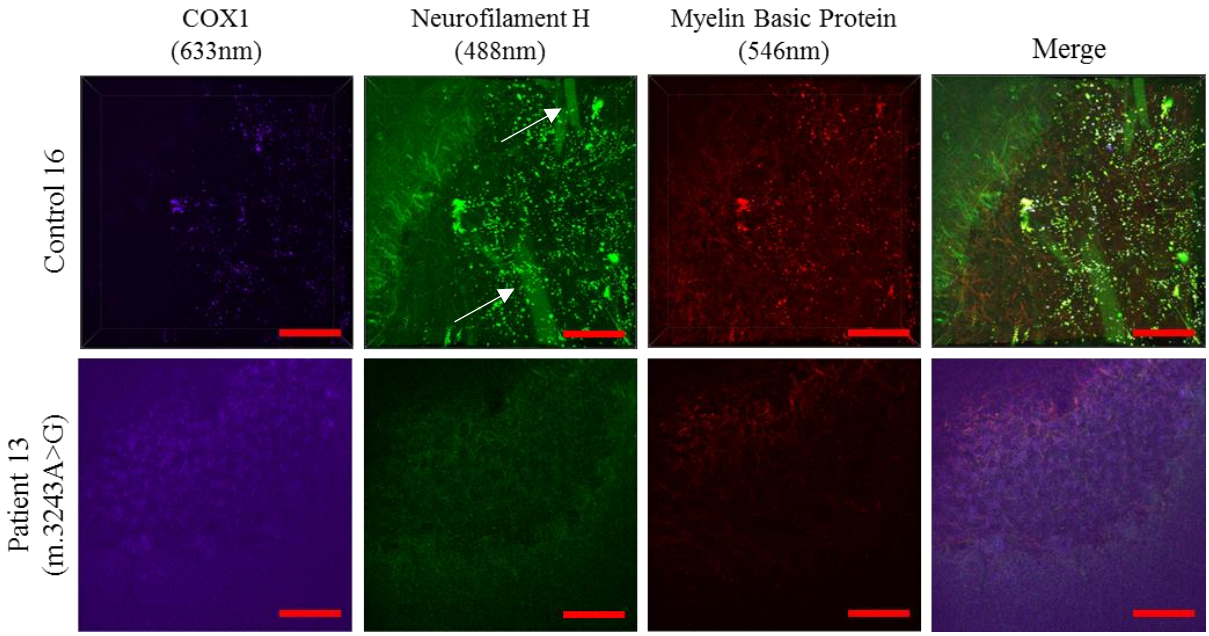

Figure 4.14: A lack of positive immunolabelling in newly cleared 250µm thick cerebellum sections from control 16 and patient 13 with mitochondrial disease.

There was a lack of positive immunolabelling in control 16 and patient 13 with no positive labelling of mitochondria, axons or myelin sheath. In control 13 there is aggregation of the secondary antibodies along with non-specific staining of the vascular network (white arrow) in the 488nm channel. Scale=100µm

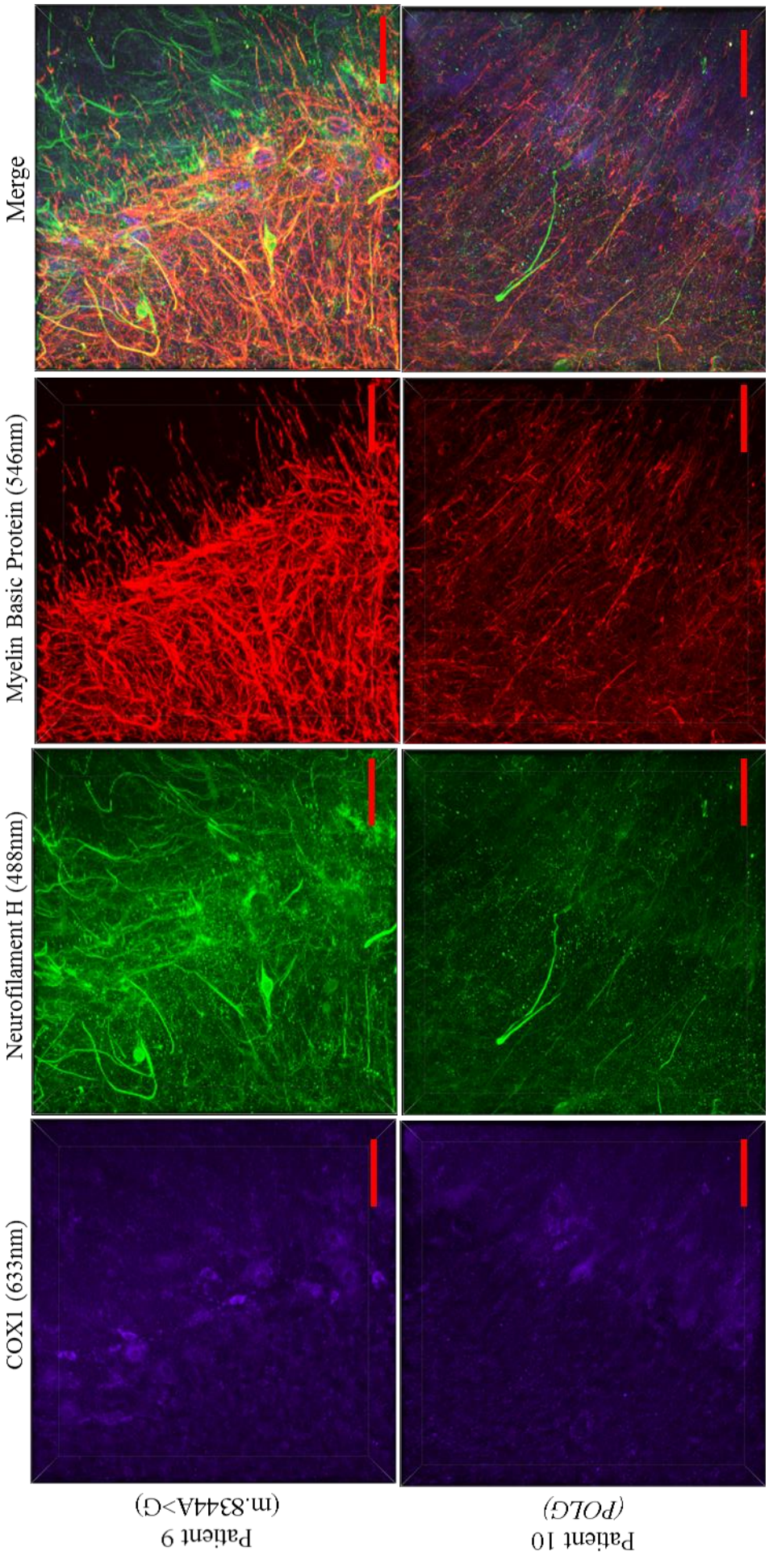

Figure 4.15: Immunolabelling of Purkinje cells and their axons in newly cleared 250µm thick cerebellum sections from patients with mitochondrial disease.
Passively cleared cerebellar sections from patient 9 (m.8344A>G) and patient 10 (*POLG*) were successfully stained for COX1 (633nm), neurofilament H (488nm) and myelin basic protein (546nm) allowing for the visualisation of Purkinje cell axons. Scale=100µm

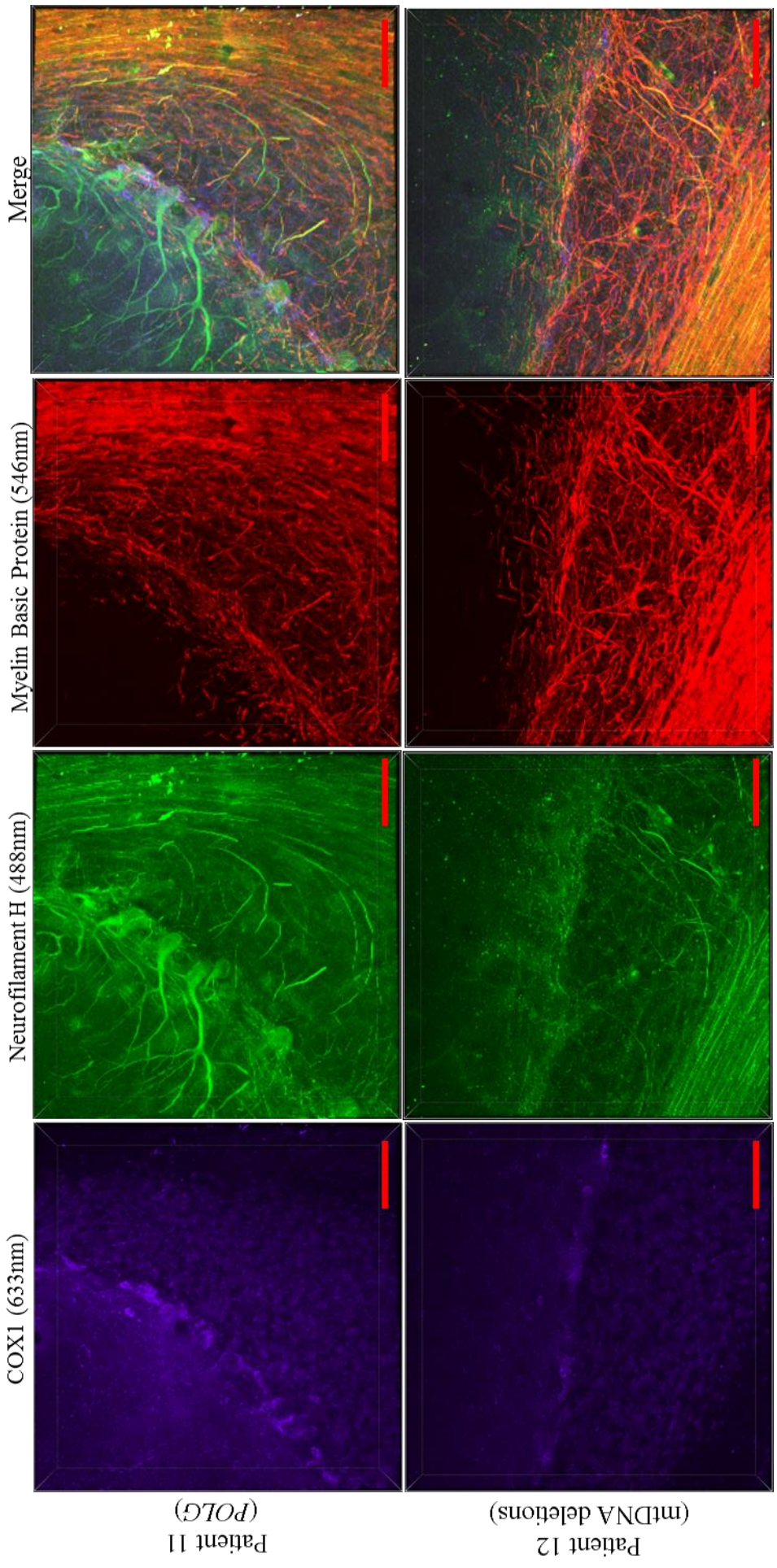

Figure 4.16: Immunolabelling of Purkinje cells and their axons in newly cleared 250µm thick cerebellum sections from patients with mitochondrial disease.
Passively cleared cerebellar sections from patient 11 (*POLG*) and patient 12 (mtDNA deletions) were successfully stained for COX1 (633nm), neurofilament H (488nm) and myelin basic protein (546nm) allowing for the visualisation of structural domains (axon, cell body and dendrites) of Purkinje cells. Scale=100µm

4.4.10. Quadruple Immunofluorescence

The end goal of this project is to determine respiratory chain deficiency in a single neuron from dendrites to synapse on a global scale and its effects on the connectivity of the neuron circuitry. To achieve this a quadruple immunofluorescent assay was attempted on cleared sections to visualise;

- NDUFA13 (to label complex I; 546nm)
- COX4 (to label mitochondria; 488nm),
- Neurofilament H (to label neurons and their neuritic processes; 405nm)
- Myelin basic protein (to label myelin; 633nm).

COX4 and MBP had strong positive staining in the cases shown (Figure 4.17). When comparing the staining of NDUFA13 between patients, there was variability in intensity which would be expected in patients with mitochondrial disease. However, as the quality of NDUFA13 staining in control 15 was variable, an increased number of controls will be needed to confirm the specificity of NDUF13 staining and to be able to confidently quantify respiratory chain deficiency.

In the 405nm channel, the observation of blood vessels reveals a high level of autofluorescence, which is similar to the observation in the no primary antibody control (Figure 4.13). This auto fluorescence in the 405nm channel currently prevents the use of the channel.

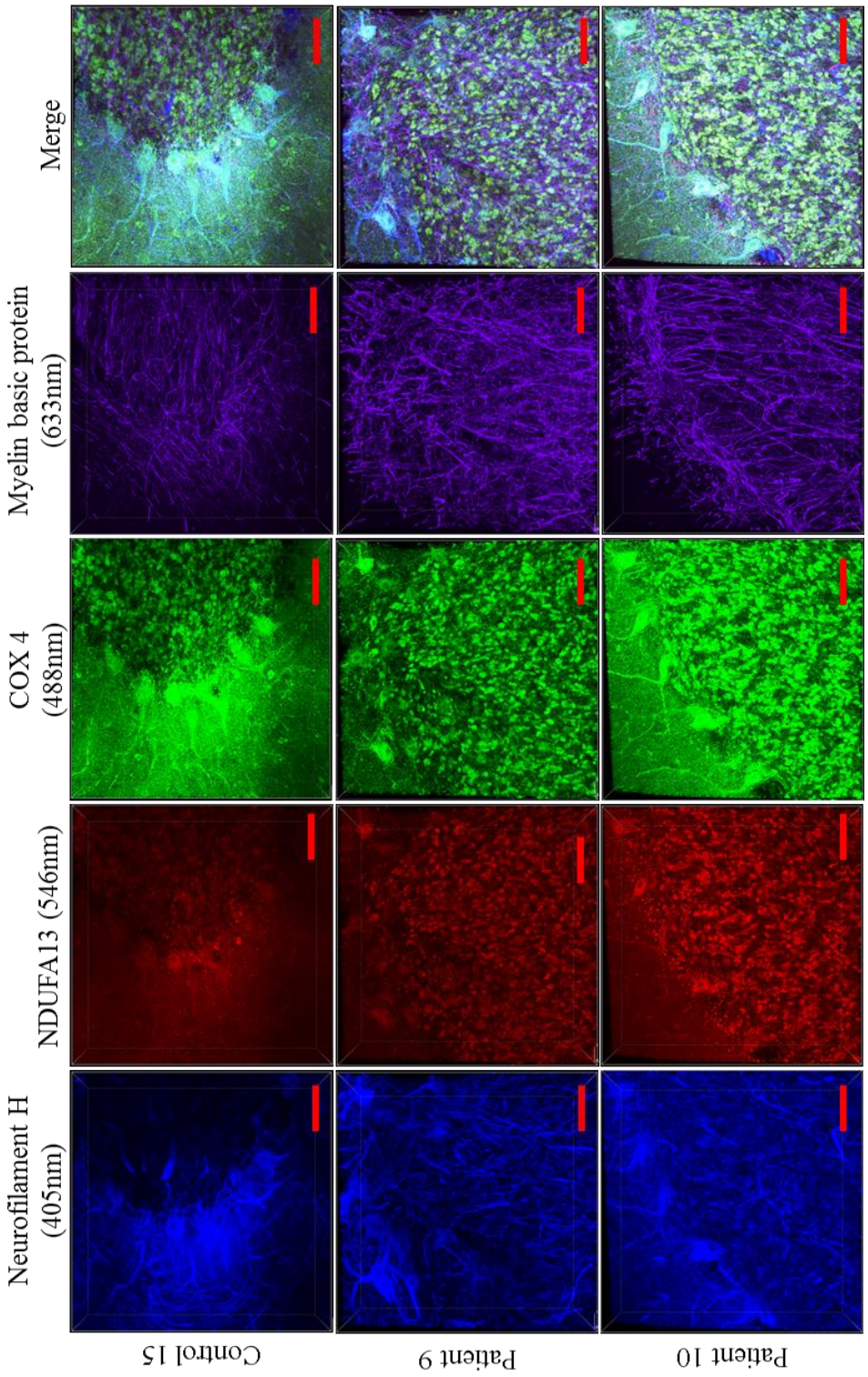

Figure 4.17: Quadruple immunofluorescent assay to identify respiratory chain deficiency. To investigate respiratory chain deficiency in Purkinje cell axons, quadruple immunofluorescence staining for neurofilament H (405nm), NDUFA13 (546nm), COX4 (488nm) and Myelin basic protein (633nm) was attempted. Variable staining of both mitochondrial antibodies (NDUFA13 (546nm) and COX4 (488nm)) can be observed through all the sections. While the myelin sheaths of the axons has been clearly labelled by the MBP antibody in all of the cases shown. At the current moment the auto fluorescence in the 405nm channel prevents the use of the quadruple assay.

4.4.11. Length of clearing on tissue

As expected, the duration of the clearing time is very important for the quality of the resulting staining procedure. Typically, the clearing method was kept to 4 weeks (Figure.18A) which produced strong and specific staining of both neurofilament H (488nm) and myelin basic protein (546nm). However, when the clearing incubation was only 2 weeks, there was minimal staining of neurofilament H, myelin basic protein or COX1 (Figure 4.18B).

4.4.12. Re-staining of the sections.

One of the main benefits of using the CLARITY technique is that hydrogel incorporates all macromolecules by forming covalent bonds between them. Therefore, it was proposed that the sections could be stained, imaged and then undergo another step of clearing before undergoing another round of staining and imaging. Here I originally stained a cerebellum section from control 15 with α-smooth muscle actin (633nm), a chicken anti-neurofilament H (488nm) and a GLUT-1 (546nm) antibody to look at the microvessels (Figure 4.19A). Both the α-smooth muscle actin and GLUT-1 produced specific staining of the vascular system in the cerebellar section, while the chicken anti-neurofilament H produced non-specific staining of vessels as well as a high level of background noise in the 488nm channel (Figure 4.18A). Once the sections had been imaged, they were incubated in the clearing solution for 1 week at 37˚C, with the solution changed every other day. The sections were then re-stained with COX1 (633nm), rabbit anti-Neurofilament H (488nm) and myelin basic protein (546nm) (Figure 4.18B). This round of staining produced specific and positive labelling of both axons (neurofilament H) and the myelin sheath (myelin basic protein), with both co-localising and showing the complex connectivity of the cerebellum. There was no visible labelling of the vascular system (Glut-1) in the 546nm channel, which would be expected if the original staining was still present, therefore confirming that the clearing process is sufficient to remove antibodies.

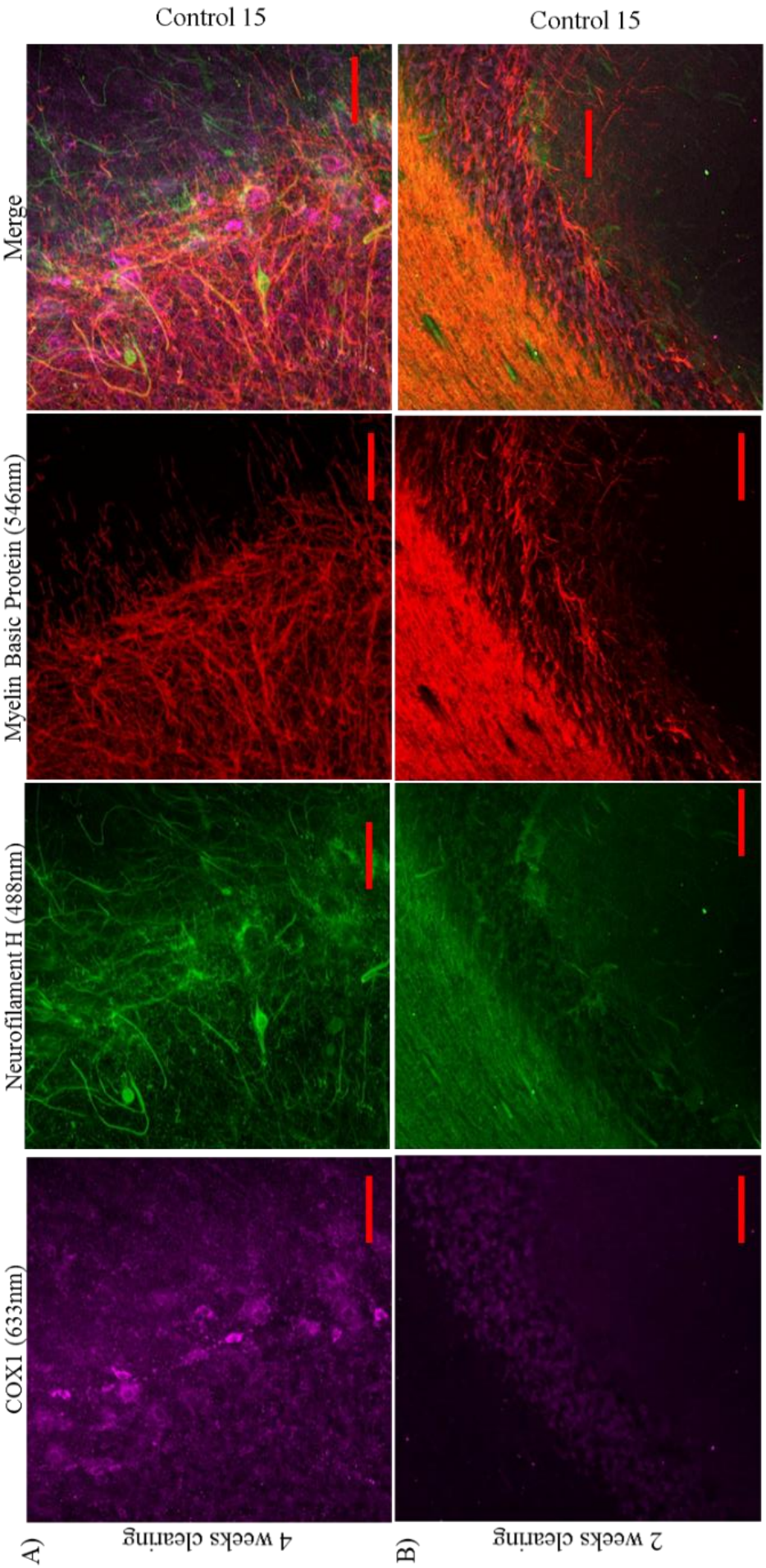

Figure 4.18: The effect of passive clearing time on the quality of immunofluorescent staining in 250µm control human cerebellum section. A) When the time of passive clearing was 4 weeks, the staining quality was vastly improved. Axons (neurofilament H) and their myelin sheaths (myelin basic protein) are clearly observable, while mitochondria (COX1) can be observed in the Purkinje cell bodies. B) When the length of passive clearing was restricted to two weeks, the quality of immunofluorescent staining is markedly reduced, with both neurofilament H (488nm) and myelin basic protein (546nm) showing minimal labelling of the white matter in the granular cell layer, and no positive staining of mitochondria (COX1 (633)). Scale=100µm

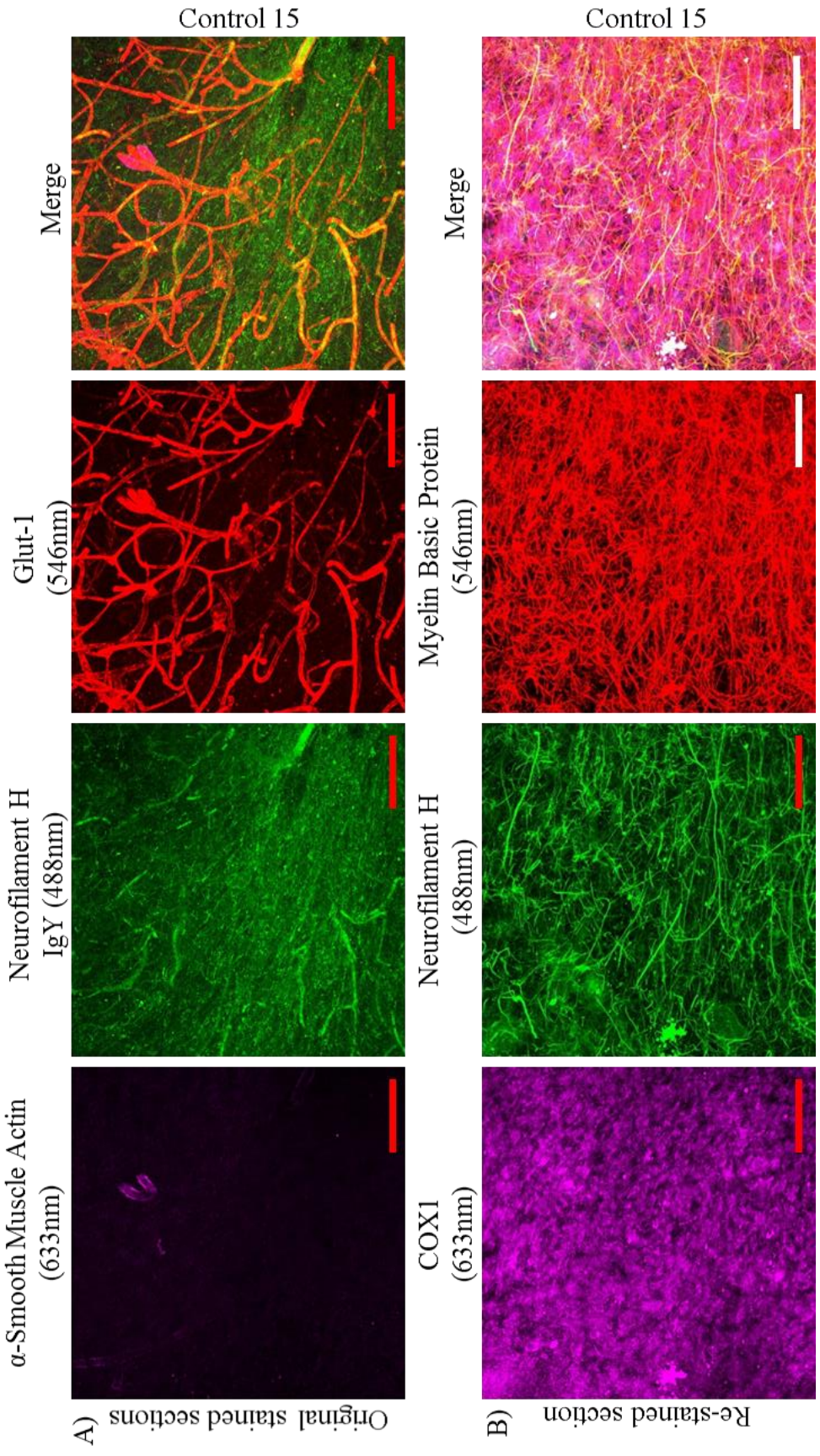

Figure 4.19: **Reusing passively cleared and stained 250µm thick control human cerebellum sections.**
A) Passively cleared sections were stained for α-smooth muscle actin, neurofilament H and Glut-1, producing a clear image of the vasculature network in the cerebellum (Glut-1 (546nm)). B) The sections were then immersed in the clearing solution for 1 week before being successfully re-stained with COX1, neurofilament H and myelin basic protein. Re-clearing was successful as there was no positive staining of Glut in the 546nm channel, as only the myelin sheaths were visible. Scale=100µm

4.4.13. Imaging of structures in the cerebellum of passively cleared sections

In addition to the visualisation of Purkinje cells soma and mitochondria in passively cleared human sections, I have also shown it is possible to visualise the dendrites, axons and the vascular network (Figure 4.20). The dendrites were labelled by neurofilament H (Figure 4.20A) while a combination of neurofilament H and myelin basic protein label myelinated axons (Figure 4.20B). Visualisation of the blood vessels was achieved through the use of antibodies targeting α smooth muscle actin and Glut-1 (Figure 4.20C). The lack of co-localisation between Glut-1 and α smooth muscle actin indicates that the labelling of α smooth muscle actin failed.

One of the main forms of axonal pathology are axonal torpedoes. By using this method and labelling neurofilament H and myelin basic protein, I have been able to observe the full structure of axonal torpedoes, and therefore I am aiming to provide more insights on the morphology of the axons entering and exiting the axonal torpedoes as well as determining if they are myelinated (Figure 4.20D).

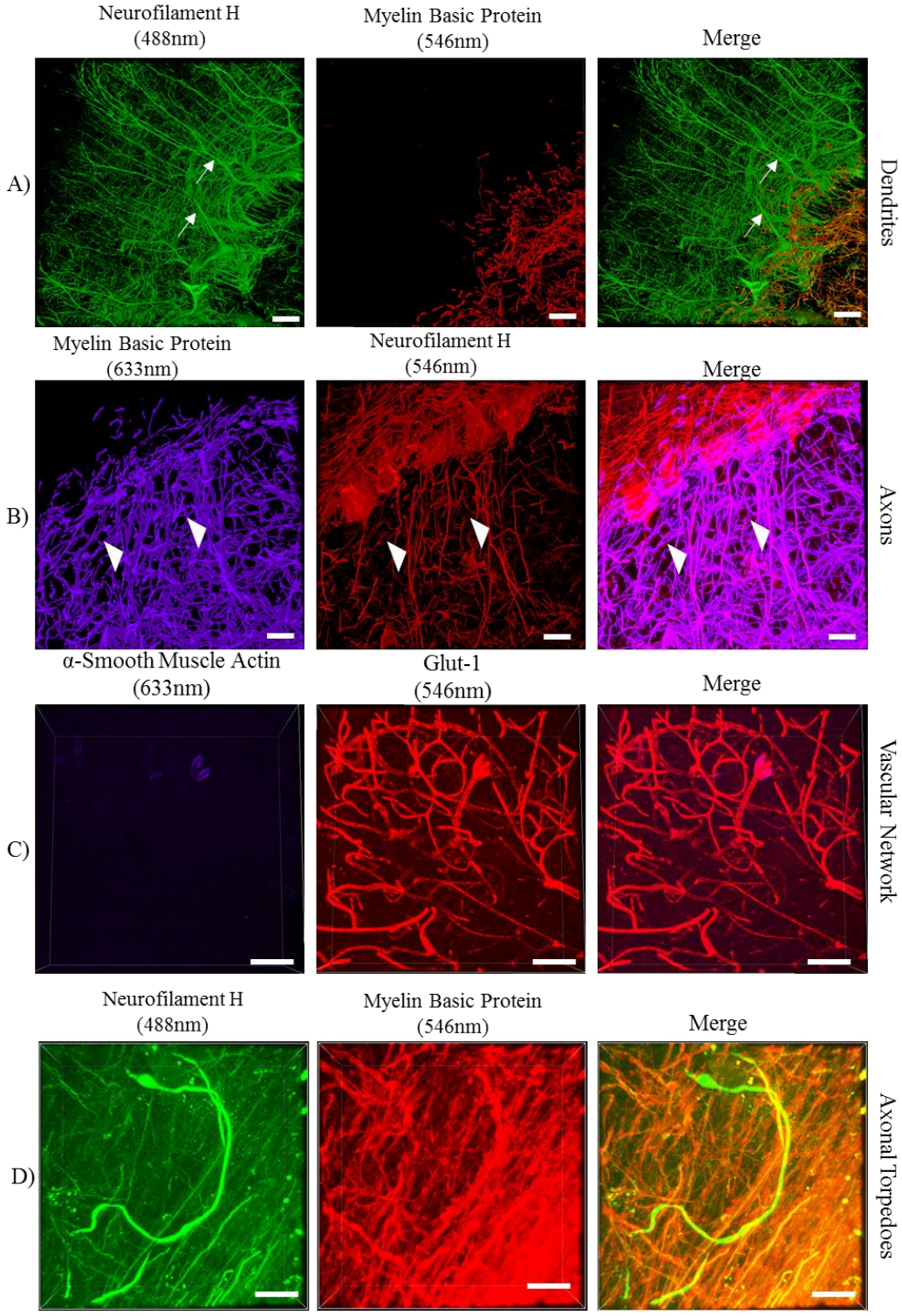

Figure 4.20: Visualising of structures in passively cleared control human cerebellum sections.

Visualisation of dendrites, axons, vascular network and axonal torpedoes was achieved in 250µm thick tissue passively cleared cerebellum of post-mortem human brain tissue. neurofilament H (488nm) clearly labels the dendritic tree (white arrow (A)) The combination of myelin basic protein (633nm) and neurofilament H (546nm) labels myelinated axons (white arrow head) projecting from the Purkinje cell layer to the deep cerebellar white matter (B). Positive staining of Glut-1 (546nm) has labelled the vascular network in the cerebellar sections (C). neurofilament H (488nm) and myelin basic protein (546nm) allow

for the visualisation of axonal torpedoes. While Axonal branching can be observed on the axons that are exiting the axonal torpedoes (D). Scale=100µm

4.5. Discussion

With the advent of confocal microscopy and the ability to scan a single focal plane in a section, the desire to use thicker sections to visualise the 3D structure of cells like neurons has increased. However, the light scattering properties of tissues was a major confounder for this, making this approach not possible for many years. To overcome this problem, a number of protocols have recently been developed to match the refractive indexes throughout the tissue and/or remove lipids, a main culprit for light scattering. One of those methods was Clear Lipid-exchanged Acrylamide-hybridized Rigid Imaging / Immunostaining / in situ-hybridization-compatible Tissue hYdrogel (CLARITY), which uses a combination of lipid removal and refractive index matching, to produce transparent tissue (Chung et al., 2013). Due to previous successful application of CLARITY to human tissue (Chung et al., 2013; Ando et al., 2014; Liu et al., 2016), this work aimed at applying the CLARITY protocol to both mouse and human cerebellar sections. Following this, optimising an immunofluorescent protocol in order to investigate the changes to Purkinje cell connectivity in the cerebellum of patients with mitochondrial disease.

CLARITY works by embedding sections in a hydrogel composed of acrylamide and PFA which forms covalent bonds with amine groups in the native molecules in the tissue, preventing the protein loss that is associated with lipid removal using solvents or detergents (Chung et al., 2013; Yang et al., 2014). Once the hydrogel has been polymerised, the sections can be either actively cleared using electrophoresis or passive clearing through immersion in a detergent at 37˚C. Since clearing via electrophoresis has problems with reproducibility and degradation of tissue (http://forum.CLARITYtechniques.org/), and passive clearing methods have been successfully validated (Tomer et al., 2014; Yang et al., 2014), the passive clearing step was used to create transparent cerebellar sections. Although the clearing length is extended, as the length of time to clear a section is dependent on both the rate of lipid solvation by the detergent and the diffusion rate of the detergent within the tissue (Hoffman, 2012), the preservation of tissue is increased. It was found that the time needed to clear mouse tissue (ranging from 250µm to 500µm thickness) was longer than active clearing, but only taking seven days. By contrast, clearance of human cerebellum sections (250µm thickness), took substantially longer requiring at least 4 weeks.

As expected, the appropriate/full clearing, which is dependent on the clearing length, is fundamental for producing quality immunofluorescent images. When sections were stained after 2 weeks of passive clearing, the staining was poor with very little labelling of the axons

or myelin sheath. However, when staining sections cleared for 4 weeks, both the axons and myelin sheath were positively labelled and co-localised, and mitochondria were labelled in the Purkinje cell bodies. The extended length of time needed to clear human sections, when compared to mouse sections, is likely to be caused by the longer formalin-fixation period for the human sections. Nevertheless, I show that it is possible to clear and stain formalin-fixed sections from both control individuals and patients with mitochondrial disease.

Once the sections had been cleared, the next step was to optimise an immunofluorescent protocol to produce the best quality images with the greatest depth of antibody penetration. A number of immunofluorescent protocols had been used on cleared CLARITY tissue. The original paper by Chung et al. (2013) incubated the cleared sections with the antibodies diluted in sodium borate buffer (pH8) at 37˚C with for 24hours followed by 12h washes. While this method was modified by Lee et al. (2014), who extended the length of incubation to 3 weeks for primary antibody incubation, 1 week washes and 2 weeks secondary antibodies, it produced variable staining of Purkinje cell bodies in the mouse cerebellum. The increased temperature aims at improving the rate of antibody diffusion and increasing binding affinity, therefore increasing the antibody penetration depth. However, the same increase in binding affinity leads to a decrease in specificity. These methods do diverge from the traditional immunofluorescent techniques that use PBS. Yang et al. (2014) tried for instance a more traditional method incubating passively cleared sections with a cocktail of antibodies diluted in PBS at room temperature for 2-5 days for each step. From these previously published protocols, I trialled the sodium borate buffer or PBS at 37˚C for 24 hour incubations or sodium borate buffer or PBS at 4˚C for 6 days of primary antibody incubation then a 4 day secondary antibody incubation with 12 hour washes in between. 4˚C was tested as the experience from previous immunofluorescent work I have completed showed that lowering the temperature to 4˚C increased the specificity of antibody binding. Indeed, I found that completing the immunolabelling at the higher temperature failed to produce any specific staining of either porin, neurofilament H or myelin basic protein. When the temperature was reduced to 4˚C with increased incubation lengths, positive labelling of porin, neurofilament H and myelin basic protein was achieved and myelinated axons from the Purkinje cell layer through the granular cell layer could be traced. One issue with reducing the temperature to 4˚C was the precipitation of sodium borate out of solution and formation of crystals on the sections. Therefore, the experimental conditions providing superior immunofluorescent images were: incubating sections with antibodies diluted in PBS, at 4˚C with longer incubation periods.

As the immunofluorescent technique used in this work utilises a combination of primary and secondary antibodies which are incubated at low temperatures (therefore low diffusion rates), the depth of antibody penetration needed to be checked. It was found that there was an initial penetration of ~150µm either side of the section before the staining started to lose its intensity. This loss of intensity through the sections was also observed by Ando et al. (2014) when they were investigating Aβ and tau plaques in cleared frontal cortex of patients with Alzheimer's disease. Following this observation, it was determined that only 250µm sections would be used for future usage of CLARITY, to ensure uniform labelling throughout the section and still maintain enough tissue volume to visualise large portions of Purkinje cell axons.

The sample size was then increased by applying the same methodology to cerebellar sections from five more patients with mitochondrial disease. Whereas 4 of these patients were successfully cleared and stained allowing the investigation of changes in axonal morphology, this was not observed in one of the patients (patient 6). It is unlikely that post mortem interval (PMI) influences the clearing and staining procedures, as patient 6 had a PMI of 21 hours and patient 11, which had a PMI of 112 hours, was successfully cleared and labelled. The same could be said for the length of fixation; patient 13, in which labelling failed, had a fixation of 2 years whereas successful labelling was achieved in control 15 with a fixation length of 7 years.

To expand the use of the technique, a quadruple immunofluorescent stain was attempted on successfully cleared tissue to be able to investigate respiratory chain deficiency in neuronal axons as well as the changes in both axonal projections and level of myelination. The quadruple assay contained two mitochondrial antibodies, one to determine the mitochondrial mass (COX4) and one to quantify the level of complex one deficiency (NDUFA13), while the axons were labelled by neurofilament H and the myelin sheath labelled by myelin basic protein. Out of the four markers, myelin basic protein produced the best stain, clearly labelling all the myelin sheath in the granular cell layer and appearing comparable across all the cases. With regards to the mitochondrial antibodies, the COX4 antibody positively labelled mitochondria in each of the cases, whilst the NDUFA13 antibody produced varying labelling among the cases, as exemplified by the lack of complex I staining in the section from control 15. Therefore, it is not be possible to confidently quantify the level of complex I deficiency at the current time. Regarding neurofilament H, there was a high level of autofluorescence and a lack of specific staining of the Purkinje cell axons. Indeed, the no

primary antibody section showed bright levels of autofluorescence in the 405nm channel, which is used to visualise the vascular network. It is known that brain tissue has a high level of autofluorescence and for that reason I have been using an incubation of 0.2M glycine for 15mins(Ando et al., 2014) to eliminate autofluorescence. However, it does not appear sufficient and therefore other alternative protocols such as 0.1M Ammonium chloride in PBS for 20 min prior to immunolabelling needs to be further attempted (http://forum.CLARITYtechniques.org/).

As the sections are embedded in a hydrogel that crosslinks to the native biological molecules, it effectively eliminates protein loss that is associated with lipid solvation steps (Chung et al., 2013; Yang et al., 2014). As a result, one of the main advantages of the CLARITY technique is that the sections can be reused post immunolabelling through a repeated incubation in the clearing solution (Chung et al., 2013). I was able to confirm that sections originally stained for a number of markers can undergo antibody removal via the clearing solution to then be stained with other of neuronal markers. The imaging of the re-stained sections showed no remnants of the original vasculature markers and there was positive staining of the axons and myelin sheath, validating this procedure. This is a highly attractive feature as it allows for sections to be used multiple times, therefore being able to image multiple cell types within the same section and location, as well as making a finite and rare resource such as brain tissue from individuals with rare disorders stretch further.

Through the work completed in this chapter, I have been able to confirm that it is possible to passively clear sections of both mouse and human cerebellum that have been embedded with an acrylamide based hydrogel. In addition, I have produced a protocol (Figure 4.21) that consistently labels the axons and myelin of Purkinje cells, as well as multitude of other mitochondrial components. Some antibodies require further optimisation as the lack of antigen retrieval and depth of penetration limit their use. However, at the current time, I have shown that it is possible to use thicker tissue sections to look at the changes in axonal pathology such as axonal torpedoes in patients with mitochondrial disease compared to controls, for which I will investigate further in the next chapter.

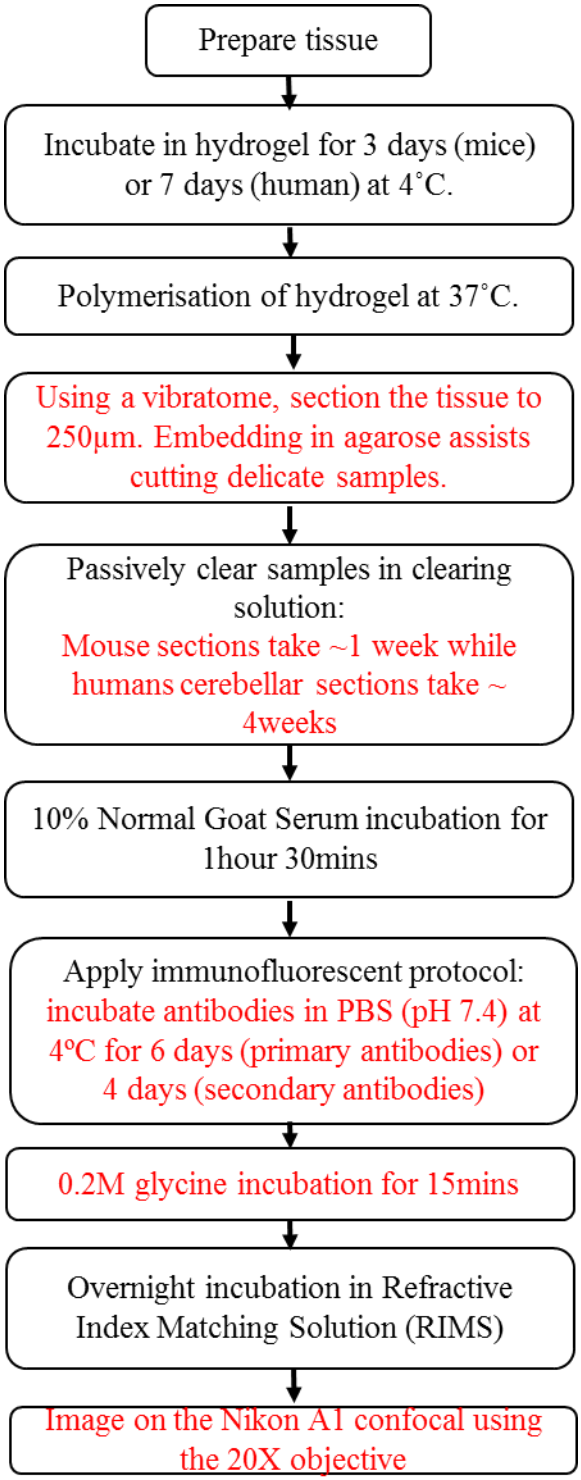

Figure 4.21: The final CLARITY protocol to consistently produce quality immunofluorescent images from passively cleared sections.
The steps in red are those that were optimised in this chapter and were added to the basic protocol to improve the quality and repeatability of the immunolabelling of the passively cleared sections.

Chapter 5. Quantifying Axonal Changes in the Cerebellum of Patients with Mitochondrial Disease

5.1. Introduction

The structure of the cerebellum is highly organised, whereby the Purkinje cell soma resides in the Purkinje cell layer with its dendrites projecting into the molecular layer. As described in section 1.11, the fully myelinated Purkinje cell axon is the final output from the cerebellar cortex. It projects from the Purkinje cell body on the parasagittal plane through the granular cell layer into deep cerebellar white matter before finally synapsing onto the deep cerebellar nuclei such as the dentate nucleus (Hamilton, 1973). In addition to projecting into the DCN, after the first node of Ranvier, the axons project a recurrent collateral at an acute angle that synapse on to neighbouring Purkinje cell soma and dendrites, basket cell projections, Golgi cells and Lugaro cells, forming the infranganglionic plexus in the upper granular cell and Purkinje cell layer (Babij et al., 2013). The vast distances that axons project and the complex connections they form are exemplified by the Purkinje cell projections. Perturbations to neuronal homeostasis within these structures, for instance, lack of ATP or morphological abnormalities of the axons, may be an early sign of neuronal degeneration following an insult.

5.1.1. Purkinje cells response to injury

The response of Purkinje cells following an insult, such as axotomy, has been well documented. Studies have shown that the Purkinje cell's response to axotomy is very different to the accepted neuronal response. The accepted neuronal response being that the cellular and molecular changes are normally reactive or compensatory to the insult. Eventually turning regressive and leading to atrophy or cell death (Lieberman, 1971). Purkinje cells are unique in that the axotomized axon undergoes a number of morphological changes that include: (i) the formation of axonal torpedoes on the transected axon in the granular cell layer; (ii) the initial neuritic segment and recurrent collaterals becomes hypertrophic; (iii) finally there is progressive atrophy of the corticofugal axons. Initially there is no sign of retraction or regeneration at the transected stump and these end bulbs can reside for up to 18 months (Dusart et al., 1999). Purkinje cells have been shown to lose their ability to regenerate by the end of the first post-natal week (Dusart et al., 1997; Ghoumari et al., 2000; Gianola and Rossi, 2001). Following a number of months, the transected stump is observed to begin spontaneous sprouting, in what is believed to be an attempt to maintain the individuals integrity by either creating new connections to maintain function or to access growth factors (Gianola and Rossi, 2002). One study investigated these morphological changes in the cerebellum of individuals with essential tremor in comparison to control individuals and found that changes in axonal shape, presence of axonal torpedoes and changes in axonal connectivity such as axonal recurrent collaterals, axonal branching and terminal axonal sprouting, were more prevalent in

the cerebellums of patients with essential tremor cases versus controls (Babij et al., 2013). In addition to morphologically changes, Purkinje cell soma are highly resistant to death, surviving multiple months after injury. This survivability has been contributed to a lack of cell body response to injury, whereby genes associated with injury or regeneration such as c-Jun, I-NOS ad GAP-43 are only minimally upregulated (Zagrebelsky et al., 1998). This results in the Purkinje cell remaining after injury but limits its ability to regenerate the axon, therefore resulting in the axonal sprouting to attempt to retain connectivity.

5.1.2. Molecular changes to axonal torpedoes

In addition to the changes in axonal morphology, it has been observed through electron microscopy that the myelin sheath around the axonal torpedo has been disrupted in a number of axonal torpedoes (Louis et al., 2009c). Additionally, immunohistochemical analysis of axonal torpedoes in Friedreich Ataxia (FRDA) cases has shown axonal torpedoes with varying degrees of myelin fragmentation (Kemp et al., 2016). In the CNS, it is the oligodendrocytes that ensheath the axons by wrapping their plasma membrane around the axons, forming a compact, multi-layered stack of membranes (Baumann and Pham-Dinh, 2001; Hartline, 2008). Each myelin segment is approximately 150μm in length, creating a defined structural boundary. A gap is present between each myelin segment, known as the nodes of Ranvier. Each node of Ranvier accommodates a high number of voltage gated sodium ion channels. The insulating properties of myelin increases the electrical resistance and decreases the capacitance across the axons membrane. This allows the action potential to jump from one node of Ranvier to the other, a process known as saltatory conduction, allowing for the fast and efficient transmission of action potential (Hille, 2001). The myelin sheath has a high lipid content with 73%-81% of the total dry weight of myelin being lipids (Chrast et al., 2011) with cholesterol accounting for 25% of that (Saher et al., 2005). In addition to the lipids, myelin is composed of about 19%-27% of membrane proteins which include proteolipid protein, myelin oligodendrocyte glycoprotein, myelin-associated glycoprotein and myelin basic protein (MBP). MBP is the most abundant protein in the myelin sheath, accounting for 30% of the total protein (Braun, 1984; de Ferra et al., 1985), and is essential for myelination. This is exemplified in mouse models, such as the shiverer mouse, where MBP has been disrupted, resulting in hypomyelination of the CNS, while in axons there is an increase in slow axonal transport, alterations to the cytoskeleton and a shortened life span (Rosenbluth, 1980; Brady et al., 1999). As mentioned, the importance of MBP, and its abundance in the myelin sheath, make it an ideal protein to target via an immunofluorescent assay in order to investigate the level of axonal torpedo myelination.

As mentioned, the gaps between the myelin segments leaves regions of exposed axonal membrane where nodes of Ranvier are formed. Nodes of Ranvier are characterised by the high density of voltage gated sodium channels, which are essential for the propagation of action potentials in saltatory conduction. Voltage gated sodium channels are large, multimeric complexes composed of a 260 kDa α subunit (Nav1.1-Nav1.9) and one or more auxiliary β subunits (β1, β2 and/or β3) of 33-36 kDa (Hartshorne and Catterall, 1981; Hartshorne et al., 1982) (Yu and Catterall, 2003). The α subunit contains the ion-conducting pore, as well as being responsible for channel opening, ion selectivity, and rapid inactivation (Yu and Catterall, 2003). In the mature CNS, the main sodium channel clustered at the node of Ranvier are the Nav1.6 channels, with a density of ~1000/μm2. However, they can also be found at a lower density of 25/μm2 along the myelinated portion of the axon (Ritchie and Rogart, 1977; Caldwell et al., 2000)). Nav1.2 and Nav1.8 channels are also found at the nodes of Ranvier, with Nav1.2 being highly expressed during development but is replaced by Nav1.6 as the CNS matures (Kaplan et al., 2001; Arroyo et al., 2002). Nav1.6 is not only restricted to axons, it is also located at dendrites, synapses, and the soma of Purkinje cells (Caldwell et al., 2000). Nav1.6 channels predominantly produce a persistent current, but can also generate rapidly activating and inactivating currents (Smith et al., 1998). Studies carried out within Experiment Autoimmune Encephalomyelitis (EAE) and Multiple Sclerosis (MS), where axonal demyelination within the CNS is observed, show that Nav1.6 is uncharacteristically expressed along the length of a demyelinated axon (Craner et al., 2003; Craner et al., 2004b). As axonal torpedoes appear to show a lack of myelination, it would be important to understand if they reacted like normal demyelinated axons by increasing the expression of Nav1.6 channels in an attempt to maintain electrical conductance.

5.2. Aims

As axonal torpedoes are much larger than normal axons, and there is a lack of myelin around them (Louis et al., 2009c). The aim of this work was to determine if the presence of axonal torpedoes within the mitochondrial disease patients was accompanied by the loss of myelin when compared to control patients. The loss of myelin would adversely affect the connectivity of the neurons. Furthermore, neurons that have already become demyelinated exhibit increased expression of Nav1.6, enabling the neuron to continue generating action potentials. Therefore, I further aim to determine whether Nav1.6 channels are present within axonal torpedoes, and if so, this would add weight to the hypothesis that there is a compensatory attempt to maintain electrical conductance within individual Purkinje cell.

Additionally, Babij et al. (2013) showed that there is an increase in axonal morphology changes, such as axonal branching and recurrent axons, associated with axonal torpedoes. The increase in axonal changes has been credited to a change in Purkinje cell connectivity. Using the CLARITY technique I developed in chapter 4, I aim to determine if there is an increase in axonal morphological changes as this may be indicative of Purkinje cells compensating for the loss of neighbouring Purkinje cells by increasing axonal branching, thereby maintaining neuronal connectivity. This work has the potential to delineate whether or not axonal torpedoes represent a compensatory mechanism to maintain connectivity rather than a detrimental pathological phenomenon.

In order to complete the aims of this chapter I will;

- Visualise and quantify the level of myelination around axonal torpedoes and compare to normal appearing axons.
- Utilise the recently developed CLARITY technique to quantify morphological changes to the Purkinje cell axons in mitochondrial patients versus controls.
- Determine if axonal torpedoes that have undergone demyelination have expression of Nav1.6 channels in an attempt to maintain electrical function.

5.3. Methods

The methods to be used in this chapter are immunofluorescence (chapter 2.2.2) and CLARITY (chapter 2.2.4). Immunofluorescent staining was completed on 5µm thick FFPE cerebellar sections while CLARITY was completed on 250µm thick cerebellar sections. Control and patients' details used in this chapter are summarised in table 5.1. The details about the specific antibodies used in this chapter are summarised in table 5.2.

5.3.1. Quantification of myelin volume around the axonal torpedoes and normal appearing axons.

5µm thick FFPE cerebellar sections from 10 patients with clinically defined mitochondrial disease and 12 control individuals were stained with Anti-SMI-94 (myelin basic protein) and Anti-neurofilament H 200kDa (neurofilament H). The quantification of myelin volume and axonal torpedo volume was completed using the Nikon A1R confocal microscope with the NIS Elements software. Axonal torpedoes and Purkinje cells axons in the granular cell layer were identified by neurofilaments H and were captured at 60x magnification with 4x electronic zoom under constant gain, offset and laser power. Using Volocity 3D Image Analysis Software (PerkinElmer, UK) a region of interest was drawn around either the axonal torpedoes or normal appearing axons using neurofilaments H. The volumes of axonal torpedoes and axons were calculated while only the volume of myelin that was touching the axonal torpedoes or normal appearing axons was calculated.

Using the statistical software SAS (SAS Institute Inc.), the myelin and axonal torpedo volume data underwent Box-Cox transformation to determine the appropriate method of transformation to normalise the data. The most appropriate transformation was for the data to undergo a Log10 transformation. To determine the difference between axonal torpedo myelination in controls and patients, either the unpaired t test or Mann Whitney tests were completed, the same was done for axonal myelination. To confirm that axonal torpedoes are demyelinated, Wilcoxon signed rank tests were completed to determine a difference between myelin volumes of axon and axonal torpedoes within an individual. Pearsons correlations was completed to determine a relationship between myelination volume and axonal torpedo volume or axon volume.

5.3.2. Quantification of axonal morphology in passively cleared 250µm thick human cerebellum sections

Passively cleared 250µm thick human cerebellum sections were labelled with Anti-neurofilament H 200kDa (neurofilament H) and Anti-SMI-94 (myelin basic protein). The sections were imaged on Nikon A1R confocal microscope, where through the NIS Elements software, large 3x3 field images of 10 randomly selected regions with a Z step of 10µm were captured for each case. Once the large image was captured, any axonal torpedoes (neurofilament H) that were present in the large field image were captured using an additional 1.5X of electronic magnification with a Z step of 5µm. Once all the images were captured, they were imported into ImageJ (National Institutes of Health) where a grid was place over the image and each form of axonal morphology was counted in each of the grid squares with the aid of the ImageJ counter add on.

5.3.3. Analysis of NaV1.6 Channels in Axonal Torpedoes and Normal Appearing Axons.

5µm thick FFPE cerebellar sections from 10 patients with clinically defined mitochondrial disease and 12 control individuals were stained with Anti-SMI-99 (myelin basic protein), Anti-NaV1.6 (Type VI Sodium Channels), and Anti-SMI-31R (Phosphorylated heavy subunit of neurofilaments). The visualisation of Type VI Sodium Channel in axonal torpedoes and normal appearing axons was completed using the Nikon A1R confocal microscope with the NIS Elements software. Axonal torpedoes and Purkinje cells axons in the granular cell layer were identified by smi-31R immunoreactivity and were captured at 60x magnification with 4x electronic zoom under constant gain, offset and laser power. Once the images had been captured, regions of interest were drawn around the axonal torpedoes or Purkinje cell axons using SMI-31R as a marker in Volocity 3D Image Analysis Software. Once the region of interest was drawn, counts of Type VI Sodium Channels were made and the volume of myelin touching the structures was calculated. As with the myelination data, SAS was used to complete a Box-Cox transformation to determine that Log10 was the most appropriate method to transform the data. Depending on the normality of the data, either unpaired t test or Mann Whitney tests were used to determine if there is was a difference between the NaV1.6 concentration in control axonal torpedoes and axons and patient's axonal torpedoes and axons. Spearman's ranks order correlations were used to determine a relationship between NaV1.6 concentration and myelin volume of axonal torpedoes or Purkinje cell axons in both controls and patients. Graphical representation of the data in all sections was completed using GraphPad prism (GraphPad prism, Inc.).

	Gender	Age (Years)	PMI (Hours)	Genetic defect
Individuals used in immunofluorescent analysis				
Patient 1	F	40	58	m.3243A>G
Patient 2	F	20	187	m.3243A>G
Patient 3	F	36	9	m.3243A>G
Patient 4	M	45	43	m.3243A>G
Patient 5	M	59	67	POLG (p.Gly848Ser and p.Ser1104Cys)
Patient 6	M	30	21	m.3243A>G
Patient 8	F	60	10	m.3243A>G
Patient 7	F	42	59	m.8344A>G
Patient 9	M	58	66	m.8344A>G
Patient 10	M	79	85	POLG (p.Thr251Ile/p.Pro587Leu; p.Ala467Thr)
Control 1	F	69	16	N/A
Control 2	F	74	53	
Control 3	M	55	51	
Control 4	F	74	67	
Control 5	M	70	72	
Control 6	F	77	83	
Control 7	M	48	46	
Control 8	M	44	83	
Control 9	M	45	44	
Control 11	M	61	61	
Control 13	M	72	17	
Control 14	F	78	34	
Individuals used in the CLARITY technique				
Control 15	F	72	27	N/A
Control 16	F	58	39	
Patient 9	M	58	66	m.8344A>G
Patient 11	M	55	112	POLG (p.Trp748Ser and p.Arg1096Cys)

Table 5.1: Patient and control details used in the quantification of axonal changes. Patient and control details include age, gender, Post Mortem Interval (PMI) and defined genetic defect. N/A – Not applicable

Antibody	Target	Host and isotype	Dilution
Primary antibodies			
Anti-SMI-31R	Phosphorylated heavy subunit of neurofilaments	Mouse IgG1	1:1000
Anti-SMI-94	Myelin Basic Protein	Mouse IgG1	1:1000
Anti-SMI-99	Myelin Basic Protein	Mouse IgG2b	1:500
Anti-neurofilament H 200kDa	neurofilament H (200 kDa)	Rabbit IgG	1:200
Anti-NaV1.6	Type VI Sodium Channel	Rabbit IgG	1:100
Secondary antibodies			
Alexa Fluor 488nm anti-Rabbit IgG	Rabbit IgG	Goat IgG	1:100
Alexa Fluor 546nm anti-Rabbit IgG	Rabbit IgG		
Alexa Fluor 488nm anti-mouse IgG1	Mouse IgG1		
Alexa Fluor 546nm anti-mouse IgG1	Mouse IgG1		
Alexa Fluor 633 anti-mouse IgG2b	Mouse IgG2b		

Table 5.2: Properties of antibodies used in the quantification of axonal changes.
Properties of the antibodies used to quantify the molecular and morphological changes in Purkinje cell axons.

5.4. Results

5.4.1. Myelination of Axonal Torpedoes

Immunofluorescent staining was carried out on sections from twelve controls and ten patients with mitochondrial disease to label axons, axonal torpedoes and the myelin sheath (Figure 5.1). In comparison to the normal appearing axon, which was fully myelinated (figure 5.1A), the axonal torpedoes were observed to be myelinated to varying degrees (Figure 5.1B-D). The level of axonal torpedo and axon myelination was quantified (Figure 5.2A-B). The level of myelination associated with axonal torpedoes was comparable in both controls and patients with mitochondrial disease (unpaired t-test, p=0.452 (Figure 5.2A)), with patient 3 (m.3243A>G) showing the only observable increase in axonal torpedo myelination. The level of axonal myelination was also comparable between controls and patients with mitochondrial disease (unpaired t-test, p=0.582 (Figure 5.2B)). There was no statistical difference in the volume of axonal torpedoes between controls and patients with mitochondrial disease (unpaired t test, p=0.617). However, the volume of control axons was significantly increased compared to the volume of patient axons (unpaired t test, p=0.018).

When comparing axonal torpedo myelination to axonal myelination in each patient, there was a signification reduction of axonal torpedo myelination in all cases (Wilcoxon signed rank test, (Control ($p<0.0001$), patients 2, 4, 5, 6, 7, 8 and 10 (Wilcoxon signed rank test, ($p=0.002$)), patient 3 and 9 (Wilcoxon signed rank test, ($p=0.004$)) and patient 1 (Wilcoxon signed rank test, ($p=0.016$)), confirming that axonal torpedoes are demyelinated in comparison to normal appearing axons.

The relationship between axonal torpedo volume and myelin volume was investigated (Figure 5.3A). A significant positive relationship was observed between myelin volume and axonal torpedo volume in the patients with mitochondrial disease (Pearsons correlation, $R2=0.618$, $p=0.007$). A similar relationship was observed in controls, however this was not significant (Pearsons correlation, $R2=0.340$ $p=0.0505$).

In the axons of controls, there was a significant positive relationship between axon volume and myelin volume whereby as the axonal volume increased so did the myelin volume (Pearsons correlation, $R2=0.400$, $p=0.027$). A positive relationship between axon volume and myelin volume was observed in the patient cohort, but this was not significant (Pearsons correlation, $R2=0.2216$, $p=0.170$)

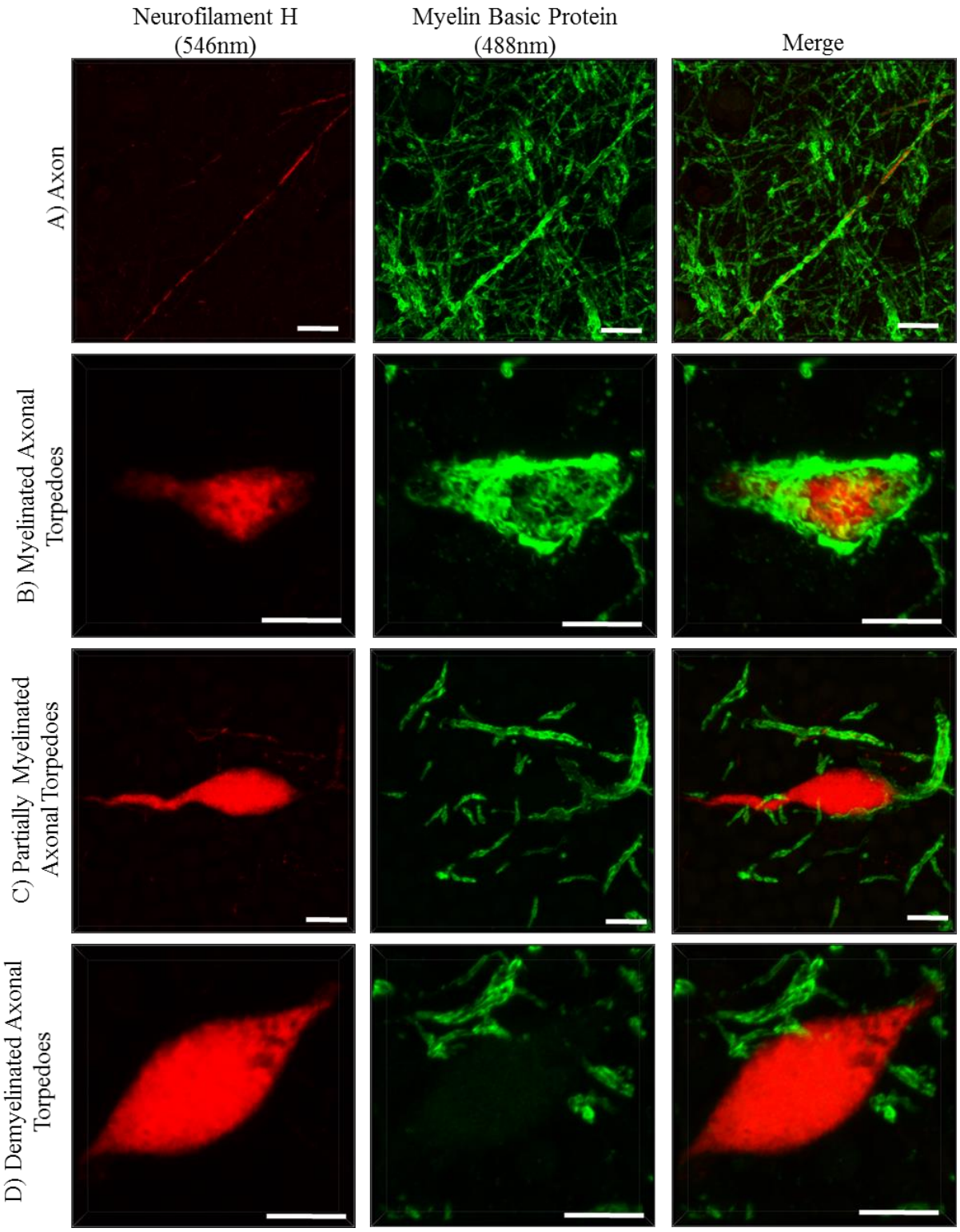

Figure 5.1: Myelination of axons and axonal torpedoes in the cerebellum.

Normal appearing axon (A) are fully myelinated (green) while axonal torpedoes display a varying level of myelination, with some being fully myelinated (B), partially myelinated (C) or completely devoid of a myelin sheath (D). Scale=10μm

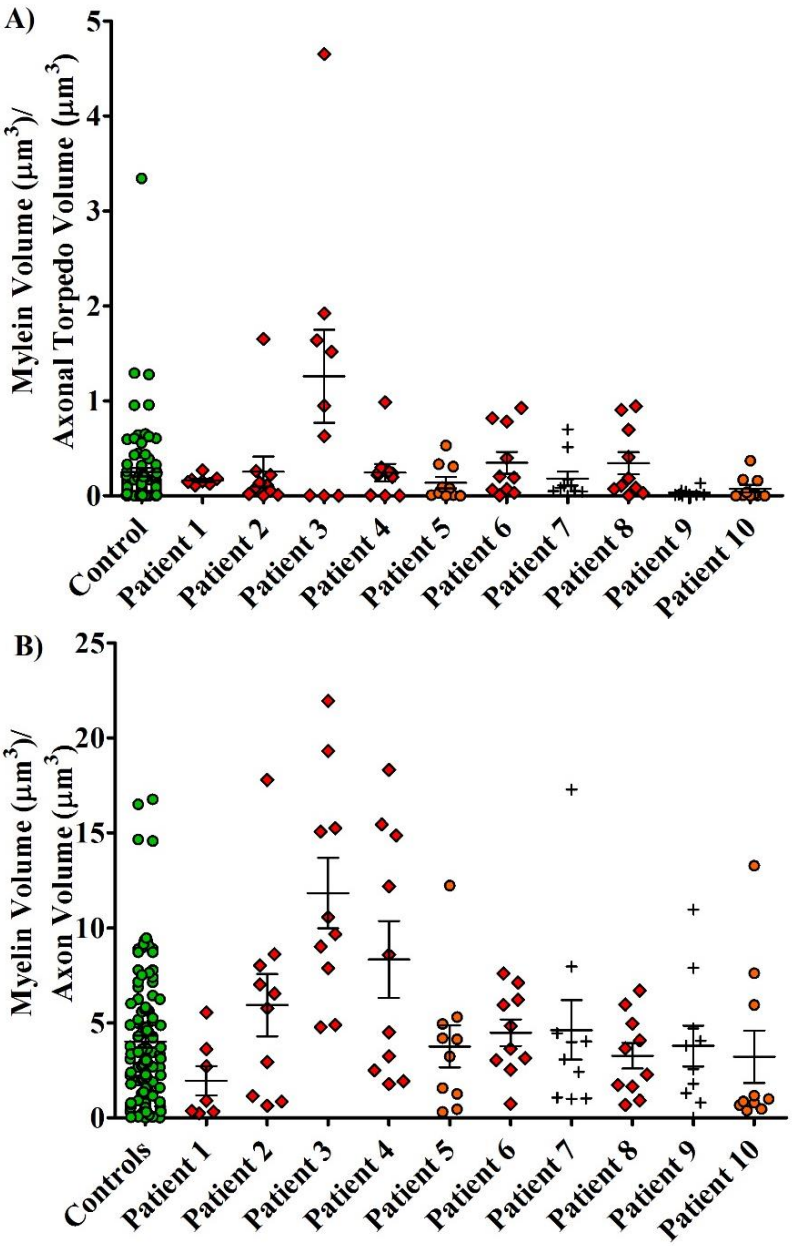

Figure 5.2: Quantification of myelin sheath around axonal torpedoes and normal appearing Purkinje cell axons in the cerebellum.

A) The level of axonal torpedo myelination in control was comparable to the level of axonal torpedo in patients with mitochondrial disease (unpaired t-test, p=0.452). B) As observed in axonal torpedoes, there was no statistical difference in the level of axonal myelination between controls and patients with mitochondrial disease (unpaired t-test, p=0.582). m.3243A>G- red diamonds, m.8344A>G-orange circles and POLG-crosses

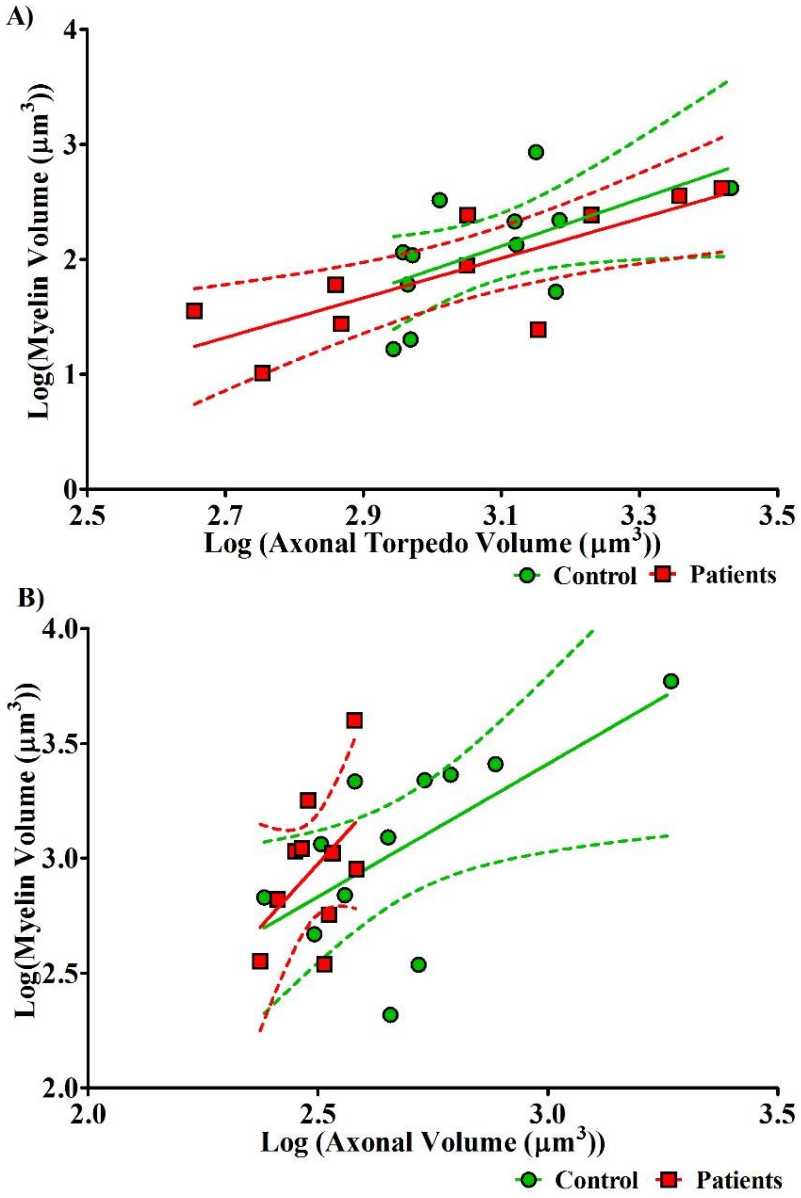

Figure 5.3: The relationship between myelin volume and the volume of axonal torpedoes or normal appearing Purkinje cell axons in the cerebellum.

A) In axonal torpedoes from patients with mitochondrial disease there was a significant positive relationship between myelin volume and axonal torpedo volume (Red line, Pearsons correlation, R2=0.618, p=0.007). The relationship in controls was comparable to patients but was not significant (Green line, Pearsons correlation, R2=0.340 p=0.0505). B) A significant positive relationship between control axon volume and control myelin volume was observed whereby as the axonal volume increased so did the myelin volume (Green line, Pearsons correlation, R2=0.400, p=0.027). In the patient cohort a positive relationship between axon volume and myelin volume was observed but this was not significant (Red line, Pearsons correlation, R2=0.2216, p=0.170). Each dot represents the mean data from each case. m.3243A>G- red diamonds, m.8344A>G-orange circles and POLG-crosses

5.4.2. Changes in axonal morphology

Following the development of the CLARITY protocol, two control and two patient cerebellums were rendered transparent using the CLARITY protocol and were stained for neurofilament H (488nm) and myelin basic protein (546nm). Using the Nikon A1 confocal microscope and NIS:elements software, ten large field images were captured from the controls (Figure 5.4) and patients with mitochondrial disease (Figure 5.5). The changes in axonal morphology to be quantified are axonal torpedoes (Figure 5.6A), thickened axons (Figure 5.6B), recurrent axonal collaterals (figure 5.6C) and axonal branching (Figure 5.6D). In addition to the morphological changes, the number of Purkinje cells were counted in each section (Figure 5.6E).

The quantification of changes to axonal morphology are shown in figure 5.7. Both patients were shown to have a reduction in Purkinje cell density compared to controls, with patient 9 (m.8344A>G) having the greatest reduction in Purkinje cell density. Axonal torpedo densities in patient 11 (POLG) and controls were comparable, whereas in patient 9 there was an increase in axonal torpedo densities compared to controls. The density of thickened axons was more prevalent in both patients compared to controls, with patient 11 having the greatest increase in density. There was no difference in the prevalence of recurrent axons in patients compared to controls. The largest difference was observed in the occurrence of axonal branching, with both patient 9 and patient 11 having a greater density of axonal branching compared to that observed in controls.

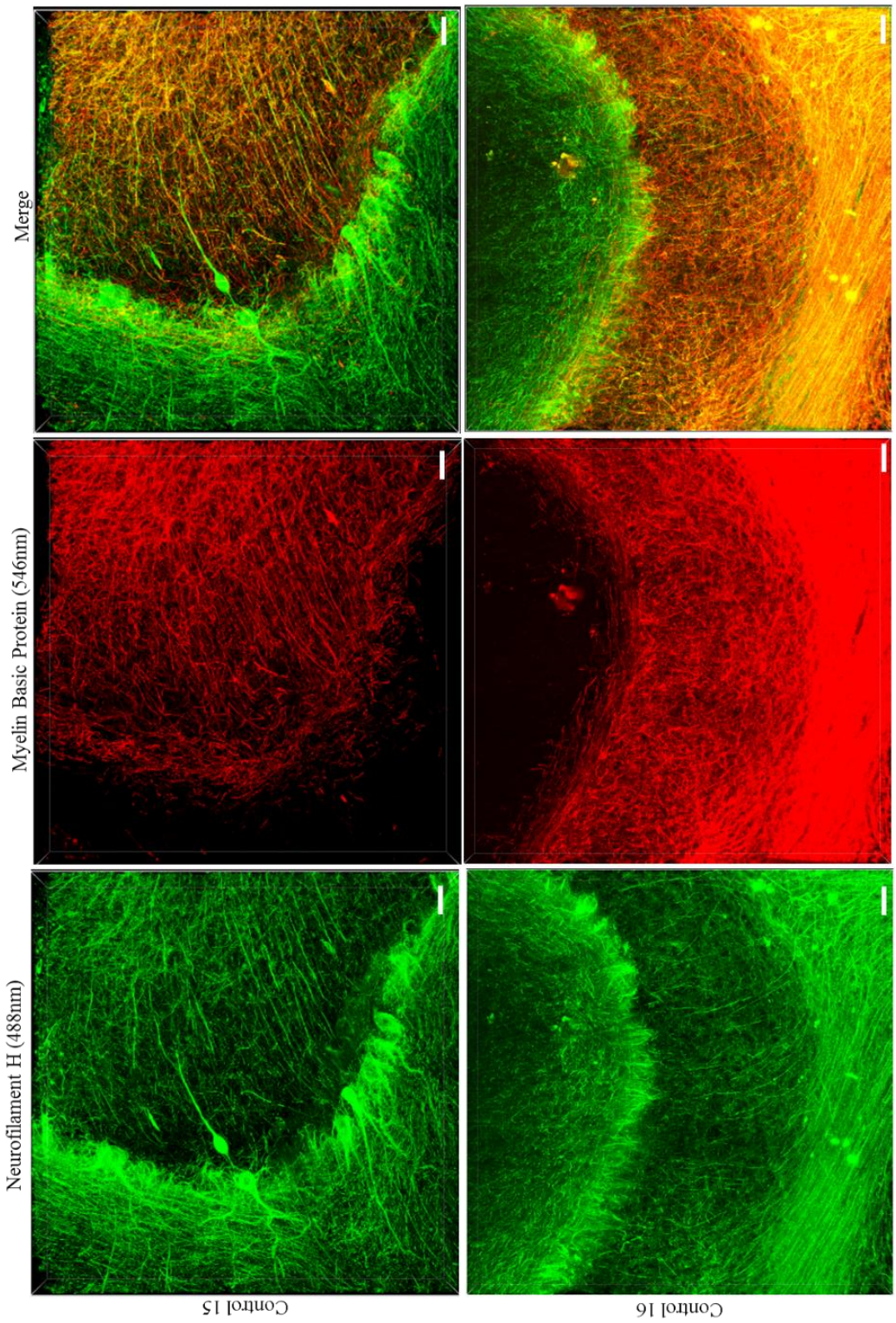

Figure 5.4: Large field imaging of 250µm passively cleared cerebellum from controls 15 and 16.
250µm thick passively cleared cerebellar sections were stained with neurofilament H (green) and myelin basic protein (red). Large images were achieved through the capturing of sequential 3x3 image fields that are stitched together through NIS:Elements software. Scale=100µm.

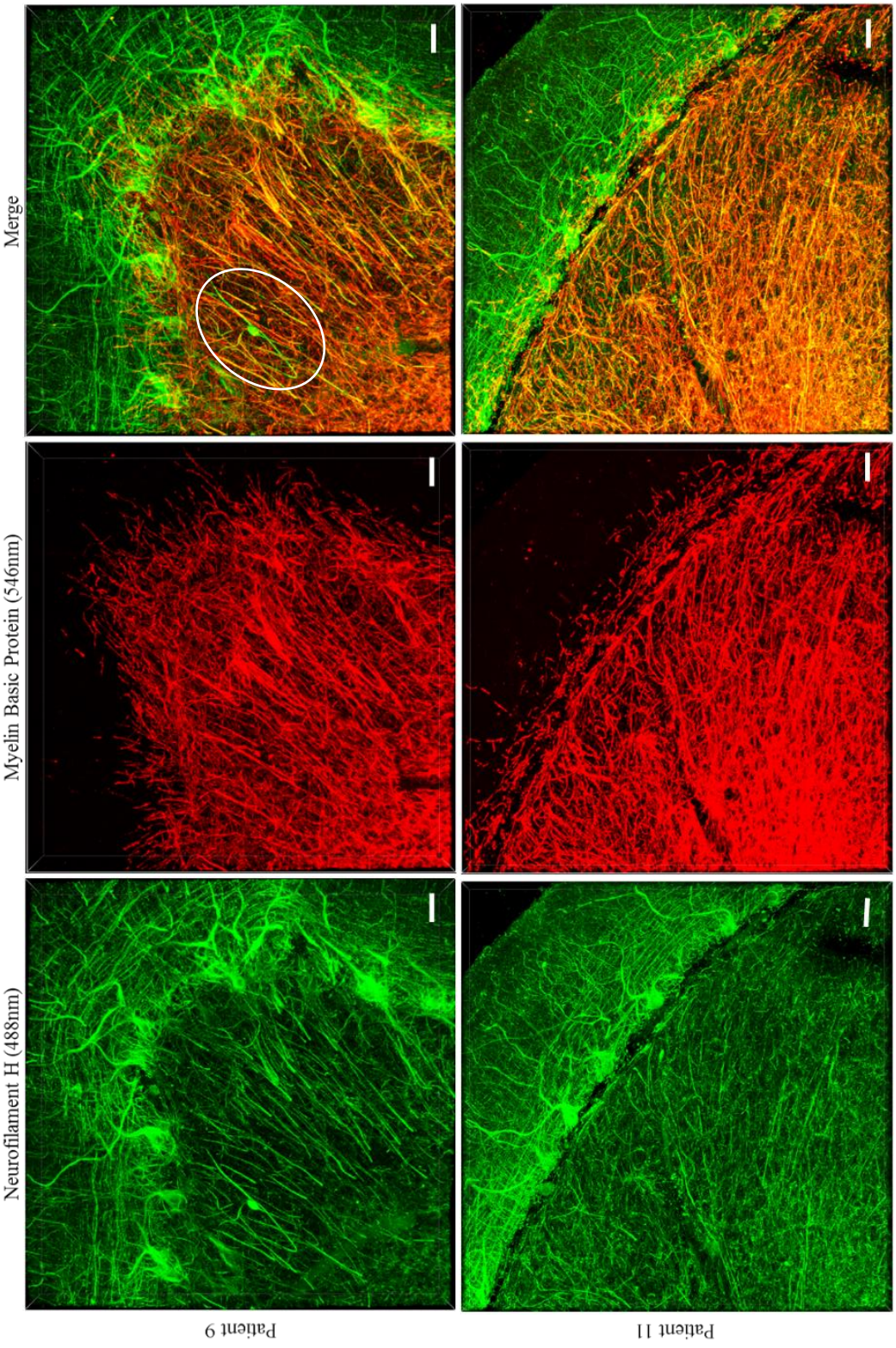

Figure 5.5: Large field imaging of 250µm passively cleared cerebellum from patients 9 and 11. Myelinated (myelin basic protein, red) Purkinje cell axons (neurofilament H, green) can be observed traversing from Purkinje cell bodies (white arrows) through the granular cell layer to the deep cerebellar white matter. An axonal torpedo (white circle) can be observed in the granular cell layer of patient 9. Scale=100µm.

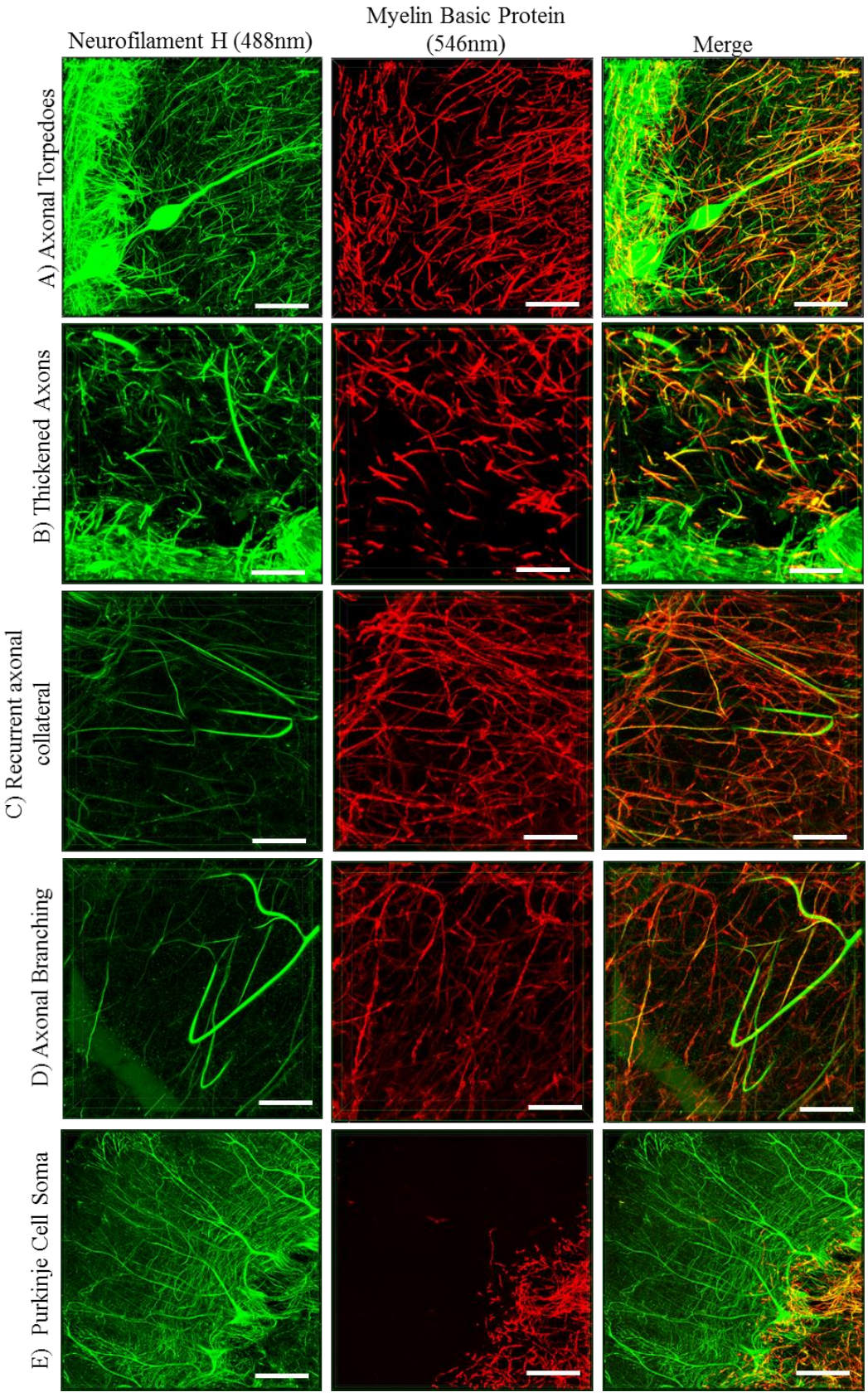

Figure 5.6: Visualisation of axonal morphology in 250µm passively cleared cerebellar sections.

Immunofluorescent staining of passively cleared cerebellum sections allows for the visualisation of morphological changes that include axonal torpedoes (A), thickened axons (B), recurrent axonal collaterals (C), axonal branching (D) and Purkinje cell soma (E). Scale=100µm

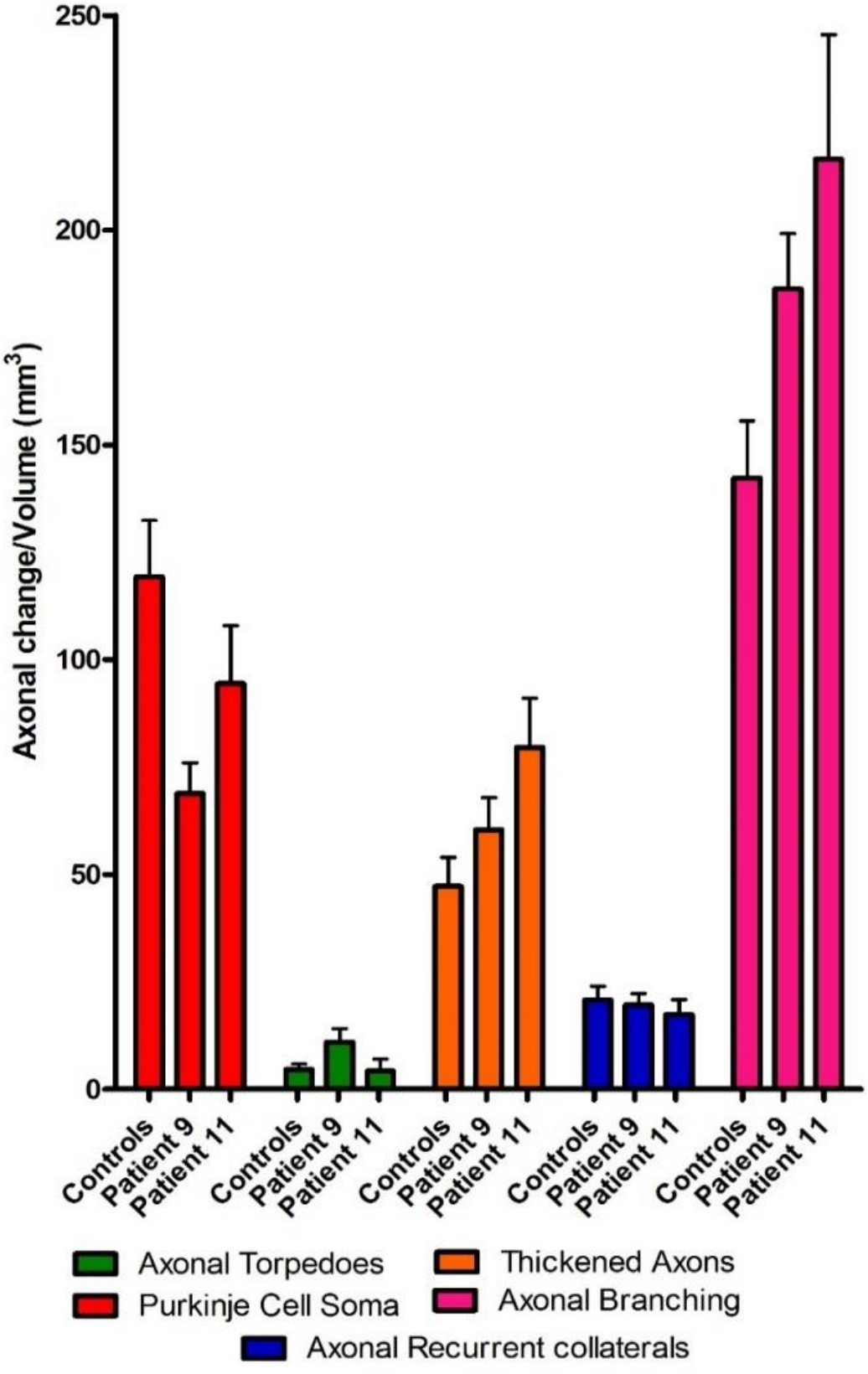

Figure 5.7: Quantification of morphological changes to Purkinje cell axons projecting through the granular cell layer.

The different types of Purkinje cell axon morphology were quantified in the granular cell layer of each large field scan and corrected to the volume (mm3) of the region quantified.

5.4.3. Morphology of axons relating to axonal torpedoes.

The benefit of using CLARITY has allowed for the full visualisation of axonal torpedoes and associated axons. Using neurofilament H (488nm) axonal torpedoes were imaged using 1.5X electronic magnification in conjunction with X20 objective on the Nikon A1R (Figure 5.8). The percentage of axons entering and exiting the axonal torpedoes was calculated (Figure 5.9A), and it was shown that in the controls 94.75% of the axonal torpedoes had an axon entering, while 81.25% of axonal torpedoes had an axon exiting distally. Patient 9 was shown to have 95% of axonal torpedoes with an entering axon, and 100% of torpedoes displaying an exiting axon. All of the axonal torpedoes of patient 11 displayed an axon entering, while 66.67% of the torpedoes had an axon exiting.

Following the confirmation that the majority of axonal torpedoes project an axon distally, the morphology of those axons were investigated (Figure 5.9B). A small number of proximal axonal torpedo axons were shown to display axonal branching, with 0% of proximal axons in patient 4, 5% in patient 2, and 7% in controls displaying axonal branching. Recurrent axon collaterals projecting distally from the axonal torpedoes were more prominent than axonal branching with 23% of controls, 35% of patient 2 and 50% of patient 4 having recurrent axons. A number of distal axonal torpedo axons were both recurrent and had axonal branches, and the quantification showed that 23% of control distal axons, 55% of patient 2 distal axons and 50% of patient 4 distal axons were both recurrent and had axonal branching. Only the control cohort had any proximal axonal projections that was not either recurrent or have axonal branching (47%).

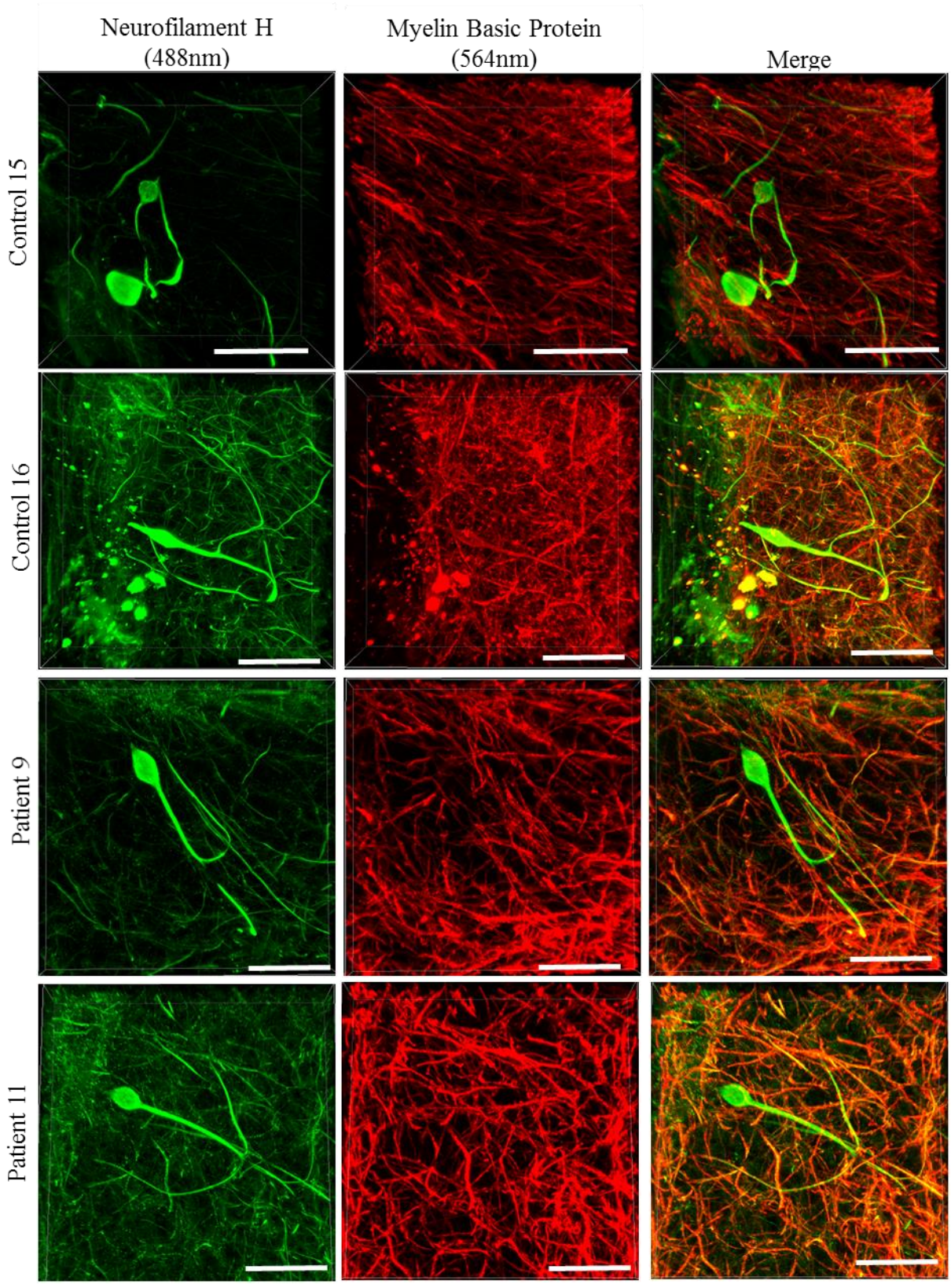

Figure 5.8: Visualisation of axonal torpedoes in 250µm passively cleared cerebellum sections.

Labelling of neurofilament H (green) and myelin basic protein (red) has allowed for the visualisation of axonal torpedoes and the axons projecting both to and from the structures. Scale=100µm

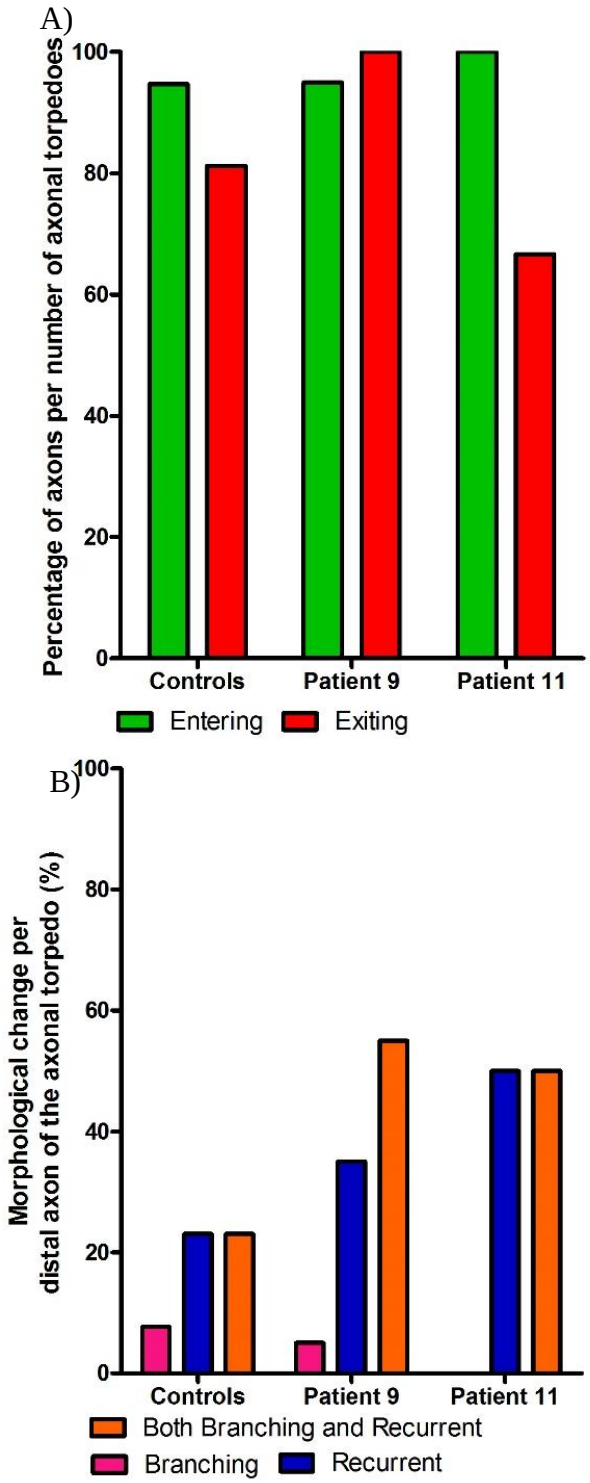

Figure 5.9: Quantification of the morphology of axonal torpedo projections.

A) The percentage of axons entering and exiting the axonal torpedoes was quantified, showing that the majority of axonal torpedoes had both an axon entering and exiting it. B) The morphology of the axons exiting distally from the axonal torpedoes was quantified. Both patients displayed a higher level of morphological change in the distal axon of the axonal torpedo compared to the controls.

5.4.4. Expression of sodium channels in axonal torpedoes

A triple immunofluorescent assay was utilised to investigate if the axonal torpedoes retained the potential to be functional by looking at the presence of sodium channels (Nav1.6) in both axons and axonal torpedoes. Punctate staining of sodium channels (NaV1.6, 488nm) can be observed in the axonal torpedoes (neurofilament H, 546nm) irrespective of the level of myelination ((myelin basic protein, 633nm) Figure 5.10). As with the axonal torpedoes, Nav1.6 can be observed in normal appearing axons that are traversing the granular cell layer (Figure 5.11).

The expression of Nav1.6 in both axonal torpedoes (Figure 5.12A) and normal appearing axons (Figure 5.12B) was quantified. In the axonal torpedoes, no statistically significant difference in the expression of Nav1.6 was observed between controls and patients with mitochondrial disease (Mann Whitney, $p=0.869$). As with axonal torpedoes, Nav1.6 density was comparable in patients and controls (unpaired t test, $p=0.213$).

The relationship between Nav1.6 density and volume of myelin associated with either axonal torpedoes (Figure 5.13A) or normal appearing axons (Figure5.13B) was investigated. In control axonal torpedoes there was no relationship observed between Nav1.6 density and myelin volume (Spearman's Rank-Order Correlation, $R2=0.1373$, $p=0.129$). However, in patients, a significant relationship was observed, with Nav1.6 density decreasing as myelin volume increased (Spearman's Rank-Order Correlation, $R2=0.465$, $p=0.03$). In the normal appearing axons, neither the patients (Pearsons correlation, $R2=0.442$, $p=0.574$) or controls (Pearsons Correlation, $R2=0.215$, $p=0.129$) displayed a significant relationship between sodium channel expression and myelin volume.

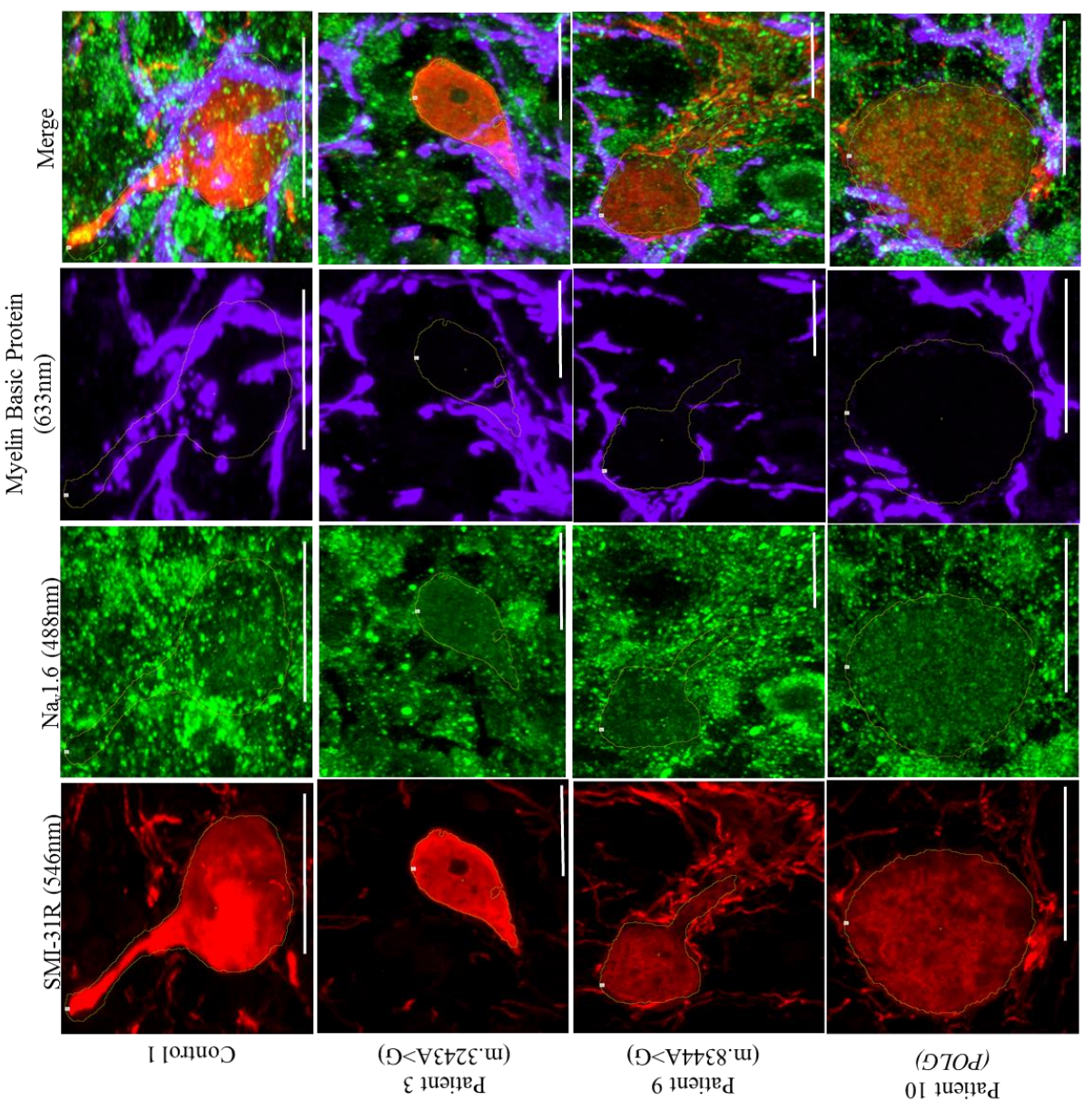

Figure 5.10: Visualisation of sodium channels in axonal torpedoes.
Sodium channels (Na$_v$1.6, green) are found throughout axonal torpedoes (yellow outline, SMI-31R (546nm)). The levels of Na$_v$1.6 expression appears to be comparable throughout the patients and controls. Varying levels of axonal torpedo myelination can be observed (633nm).
Scale Bar=10µm

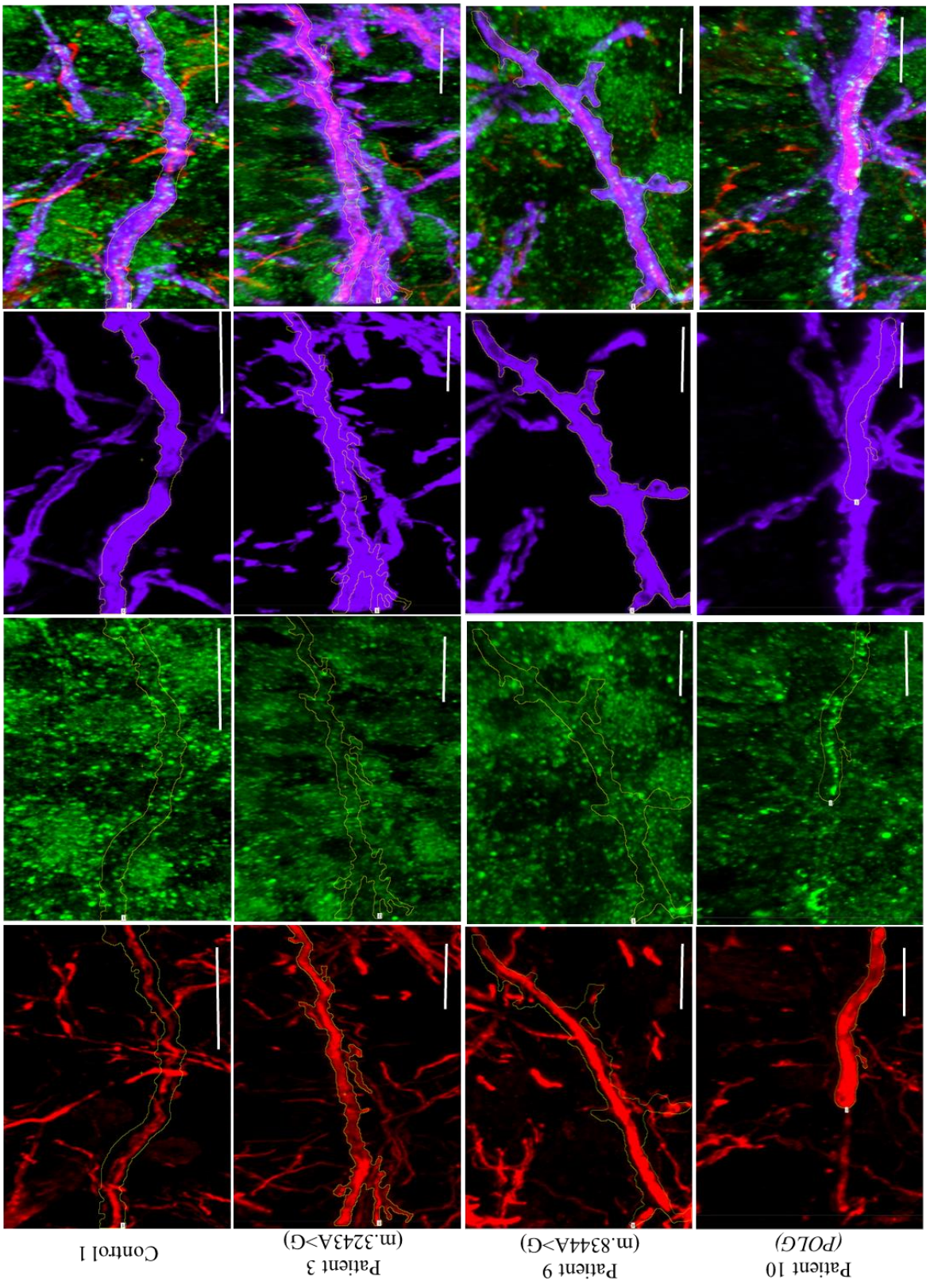

Figure 5.11: Visualisation of sodium channels (Nav1.6) in myelinated normal appearing axons. Sodium channels ($Na_v1.6$, 488nm) can clearly be seen within the myelinated (myelin basic protein, 633nm) axons (yellow outline, SMI-31R, 546nm). The level of $Na_v1.6$ expression is comparable in normal appearing axons from both controls and mitochondrial disease patients. Scale Bar=10µm

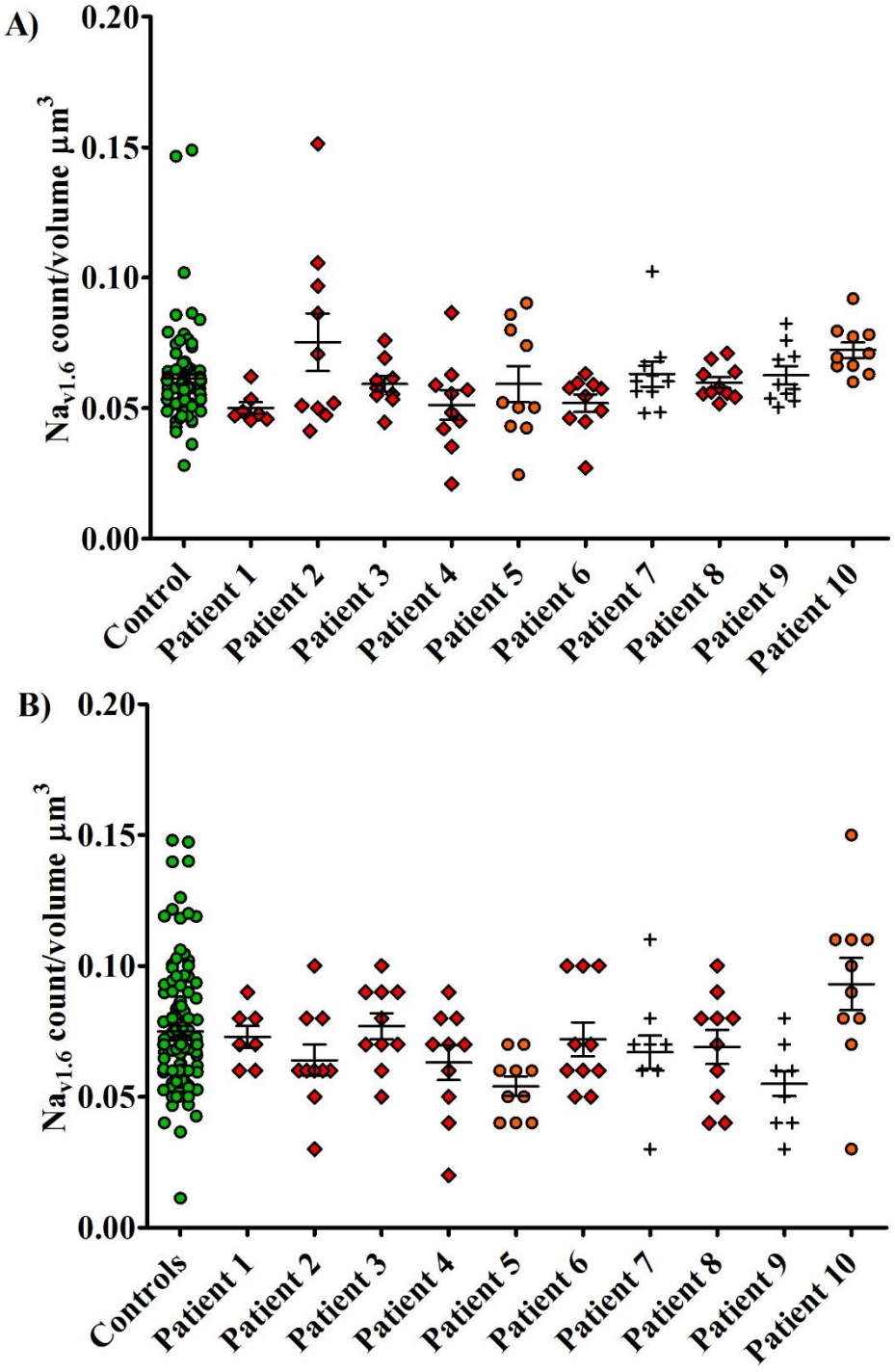

Figure 5.12: Quantification of sodium channels (Nav1.6) in axonal torpedoes and normal appearing Purkinje cell axons.

A) There was no statistical difference in Nav1.6 density between the axonal torpedoes from controls and patients with mitochondrial disease (Mann Whitney, p=0.869). B) Nav1.6 density was comparable in Purkinje cell axons from patients with mitochondrial disease and those from controls (unpaired t test, p=0.213). m.3243A>G- red diamonds, m.8344A>G-orange circles and POLG-crosses

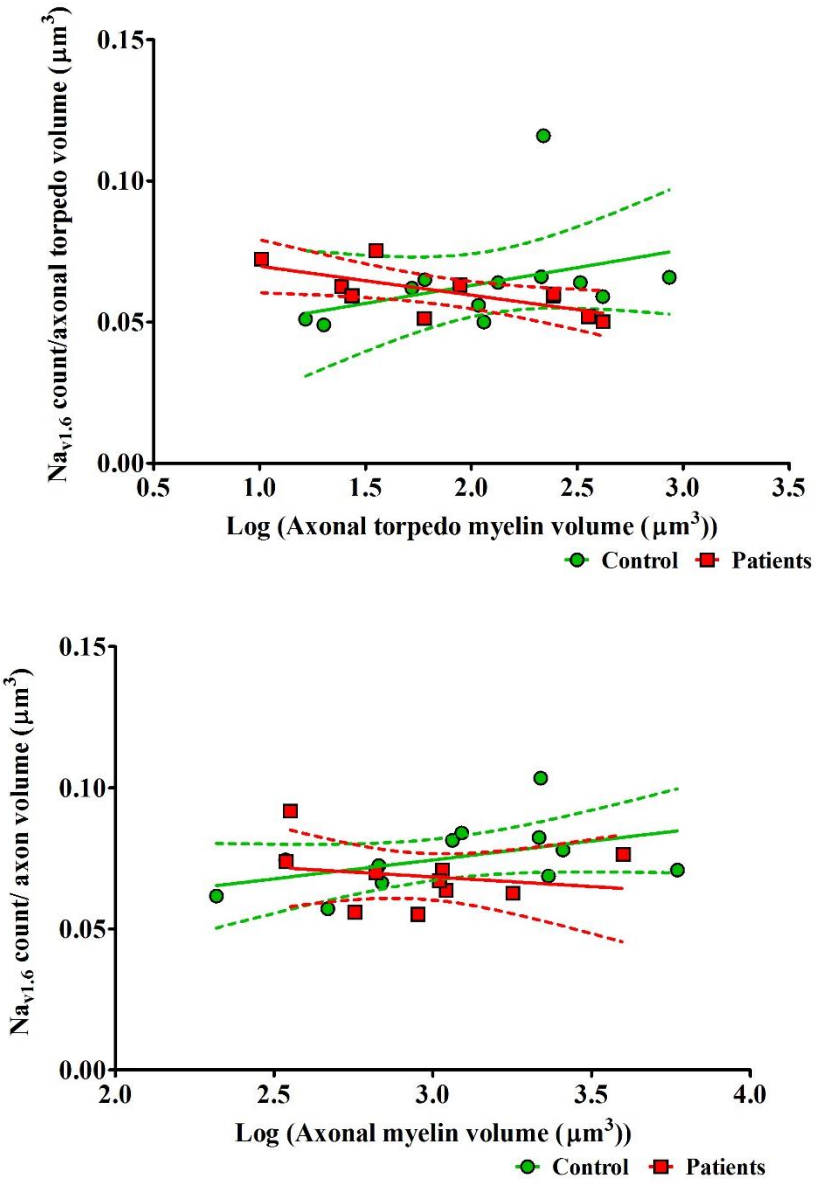

Figure 5.13: The relationship between Nav1.6 density and the myelin volume in either axonal torpedoes or normal appearing Purkinje cell axons in the cerebellum.

A) There was no relationship observed between Nav1.6 density and myelin volume in control axonal torpedoes (Spearman's Rank-Order Correlation, R2=0.1373, p=0.129). However, Nav1.6 density was observed to decrease as myelin volume increased in patient axonal torpedoes and this was a significant relationship (Spearman's Rank-Order Correlation, R2=0.465, p=0.03). No significant relationship between Nav1.6 density and myelin volume was observed in the normal appearing axons from either the patients (Pearsons Correlation, R2=0.442, p=0.574) or controls (Pearsons correlation R2=0.215, p=0.129). Each dot represents the mean data from each case.

5.5. Discussion

Purkinje cells are unique in that they react differently to stress or injury than any other neuronal populations. For instance, there is no sign of retraction or regeneration following transection with the end bulbs residing for up to 18 months (Dusart et al., 1999). Following an insult, the Purkinje cells reaction can be characterised by the structural remodelling of the axons and intracortical branches, with minimal cell body changes (Rossi et al., 2006). Even though Purkinje cells are highly resistant to axotomy, this property is made redundant by their inability to regenerate axons, even in permissive environments (Dusart et al., 1997). The structural remodelling of axons in an injured cerebellum include the formation of axonal torpedoes, hypertrophy of initial neurotic segment and recurrent collaterals and finally progressive atrophy of the corticofugal axons. The formation of recurrent collaterals from axons of Purkinje cells has been suggested to provide a feedback system, either through the inhibition of Golgi II cells resulting in the depression of their inhibitory activity on surrounding granule cells, or increasing the activity of Purkinje cells by inhibiting the basket cells (Chan-Palay, 1971).

Using the optimised CLARITY technique, it was possible to use passively cleared 250μm thick cerebellar sections from two controls and two patients with mitochondrial disease. This allowed the investigation into the axonal changes that can occur following a stress, such as respiratory chain deficiency. Quantification of the structural changes showed that the most significant changes in mitochondrial disease patients was the increased prevalence of thickened axons and axonal branching, with both patients exhibiting a significant increase in axonal branching. While an increase in thickened axons was observed in both patients, only patient four was found to be significant. The increase in structural changes in a diseased cerebellum is in agreement with a previous study where an increase in structural changes was observed in the cerebellum of patients with essential tremor (Babij et al., 2013). Babij and colleagues also observed that axons projecting from the axonal torpedoes were more likely to display a structural change. When I investigated the axonal morphology associated with axonal torpedoes, I was firstly able to confirm, through the use of CLARITY, that the majority of axonal torpedoes had both an axon entering and exiting the axonal torpedoes. When focusing on the morphology of the axons leaving distally from the axonal torpedo, it was observed that the axons were more likely to be recurrent or exhibit both axonal branching and be recurrent, indicating that the presence of axonal torpedoes was associated with an increase in axonal remodelling. This observation is in agreement with that observed in the study conducted by Babij et al. (2013).

In addition to the remodelling of the axons, it has been observed via electron microscopy and immunohistochemistry that there is myelin fragmentation and loss to axonal torpedoes (Louis et al., 2009c; Kemp et al., 2016). Myelination of an axon enables the neuron to transmit information extremely quickly and efficiently by increasing the resistance and decreasing the capacitance of the axons as well as creating structural boundaries which enables saltatory conduction through nodes of Ranvier. Using an immunofluorescent assay, it was shown that the level of axonal torpedo myelination was variable, with some axonal torpedoes fully demyelinated while others were partially or fully myelinated. The quantification of axonal torpedo myelination showed that there was no difference between controls and patients. There was also no significant difference in the volume of axonal torpedoes between controls and patients. As with axonal torpedoes, there was no significant difference between the myelination of normal axons in controls and patients, confirming that mitochondrial disease does not cause demyelination of Purkinje cell axons. Unlike the axonal torpedoes, there was a significant difference in volume of Purkinje cell axons from patients and controls, with the Purkinje cell axons in patients being smaller in volume than those in controls. The reduction in axonal volume would likely reduce the conduction velocities in the cerebellum, as the axonal calibre is a large factor in determining the conduction velocity of a neuron (Boyd and Kalu, 1979; Waxman, 1980).

When comparing the level of myelination between axonal torpedoes and normal axons, there was a significant difference in the level of myelination, confirming that axonal torpedo formation results in the loss of myelin sheath around the axonal torpedo. As the axonal torpedoes are proximal to the Purkinje cell body, they may form in the axon initial segment (AIS). The AIS is a region of the axon that is not myelinated, if the axonal torpedoes were formed in the AIS, then I would not expect myelin to be present around the axonal torpedoes. It is unlikely that that the axonal torpedoes form in the AIS as I observed axonal torpedoes with myelin fragmentation, as has Kemp et al. (2016) when they were investigating axonal torpedoes in the cerebellum of FRDA patients. To fully conclude that axonal torpedoes do not form in the AIS, I would complete a immunofluorescent assay that would label the AIS (ankyrinG or neurofascin-186) in conjunction with markers of axonal torpedoes (neurofilament H). If the AIS marker was found to co-localise with axonal torpedo marker then this would indicate axonal torpedoes do form in the AIS and would explain the lack of myelination around the axonal torpedoes.

The increase in axonal calibre associated with axonal torpedo formation could disrupt the myelin/axon interaction which initiates axonal sprouting and remodelling as it has been

observed that the myelin-neurite interaction is inhibitory to axonal growth. Myelin is known to contain inhibitory growth factors, and the inhibition of these growth factors through experimental application of antibodies increased the expression of several axotomy-associated genes in Purkinje cells that are needed for axonal regrowth as well as neurite sprouting along the intracortical segment of Purkinje cell axons (Zagrebelsky et al., 1998; Foscarin et al., 2009). Therefore, the removal of myelin by the formation of an axonal torpedo may remove this interaction and promote axonal plasticity.

Following demyelination of the axonal torpedoes, I have shown that there is expression of sodium channels in the axonal torpedoes. The expression of sodium channels in axonal torpedoes was comparable to normal appearing axons. The relationship between Nav1.6 density and myelin volume in both axons and axonal torpedoes from patients with mitochondrial disease differed from the one observed in controls. This may indicate that the function of axonal torpedoes differs in patients and controls. In demyelinated axons there is an increase in the expression of NaV1.6 channels in an attempt to maintain normal function (Craner et al., 2003; Craner et al., 2004b). However, in the acute plaques in MS patients, the increase in expression of NaV1.6 and its co-localisation with the sodium calcium exchanger (NCX) has been proposed as a method for degeneration (Craner et al., 2004a). As the NaV1.6 channel can produce substantial persistent current (Rush et al., 2005), it can result in the reversal of NCX, causing an influx of calcium ions and activating calcium dependent caspases (Craner et al., 2004a). Typically, the co-localisation between NaV1.6 and NCX was observed in axons immunopositive for APP, a marker for axonal damage, indicating that this process may only occur in damaged axons. Regarding axonal torpedoes, I have shown in chapter 3.4.1 that axonal torpedoes are not immunoreactive for APP, inferring that they are not involved in a degenerating process in the axonal torpedoes. Additionally, the change in Nav1.6 density in the patients may be associated with an attempt to modulate the firing ability of the Purkinje cell.

In summary, I have provided evidence of increased Purkinje cell axon remodelling in patients with mitochondrial disease than in the cerebellum of control individual. I have also shown that there is myelin fragmentation and loss due to axonal torpedoes in both patients and controls. Whereas, the density of NaV1.6 channels in axonal torpedoes was observed to be at a comparable level to normal appearing axons following the loss of myelin. The combination of these findings suggest that axonal torpedoes are not part of a pathological and degenerative process as previously suggested, but are part of a process that attempts to remodel and reorganise the connections and circuitry in order to prevent cell death and maintain normal neuronal function.

Chapter 6. Final Discussion

Primary mtDNA mutations, or mutations in nuclear DNA affecting mtDNA maintenance and expression, intra-organelle protein synthesis or mitochondrial dynamics lead to respiratory chain dysfunction and a group of disorders known as mitochondrial diseases. Mitochondrial diseases are a very heterogeneous group of disorders as demonstrated by the variability in their age of onset, severity and disease progression. One of the main characteristics of mitochondrial disease is the involvement of the central nervous system resulting in progressive and severe neurological deficits. These are varied and typically dependent on the brain region affected but symptoms can include ataxia, dementia, migraine, neural deafness, central and peripheral neuropathy and stroke-like episodes (DiMauro et al., 2013).

Affecting 70% of adult patients recruited to the UK MRC Mitochondrial Disease Patient Cohort, cerebellar ataxia is one of the most frequently observed neurological deficits in patients with mitochondrial disease (Lax et al., 2012b; Nesbitt et al., 2013). Cerebellar ataxia causes progressive disability through an inability to coordinate balance, gait, extremity and eye movements (Ferrarin et al., 2005). As cerebellar ataxia is such a common feature, the cerebellum has been heavily investigated to help understand its susceptibility to perturbed OXPHOS function. Neuroradiological imaging of patients with mitochondrial defects showed that abnormalities in the cerebellum were a primary feature (Scaglia et al., 2004; Bindu et al., 2015), while neuropathological studies have shown cerebellar atrophy, Purkinje cell loss and a reduction in complex I expression in surviving cells in post mortem tissue (Tanji et al., 2001; Lax et al., 2012b; Chrysostomou et al., 2016).

A frequently observed phenomenon in the neuropathological studies is the presence of axonal torpedoes in the granular cell layer of the cerebellum (Mori et al., 2000a; Lax et al., 2012b). Axonal torpedoes are fusiform swellings of the Purkinje cell axon and previous studies have shown that the main constituents of the axonal torpedoes are phosphorylated neurofilaments (Louis et al., 2009c). Originally it had been hypothesised that the formation of axonal torpedoes was part of a degenerative process that "strangled" the neuron and resulted in neuronal death (Figure 6.1). It was speculated that a stress stimuli would initiate a pathway resulting in the accumulation of phosphorylated neurofilaments which would eventually block fast axonal transport (FAT). The block in FAT would prevent vital proteins, organelles and metabolites from reaching the distal end of the neuron subsequently "starving" and "strangling" the neuron, eventually causing the neuron to die back and form an end bulb or in the case of Purkinje cells, an axonal torpedo.

Studies in patients with mitochondrial disease have only described axonal torpedoes superficially, therefore the original aim of this project was to investigate the role axonal torpedoes play in the loss of Purkinje cells in patients with mitochondrial disease and how this relates to respiratory chain deficiency. The project involved the quantification and characterisation of axonal torpedoes in both patients with mitochondrial disease, and age matched controls, leading to the optimisation of a clearing technique CLARITY in order to further characterise axonal morphology changes in the cerebellum of patients with mitochondrial disease.

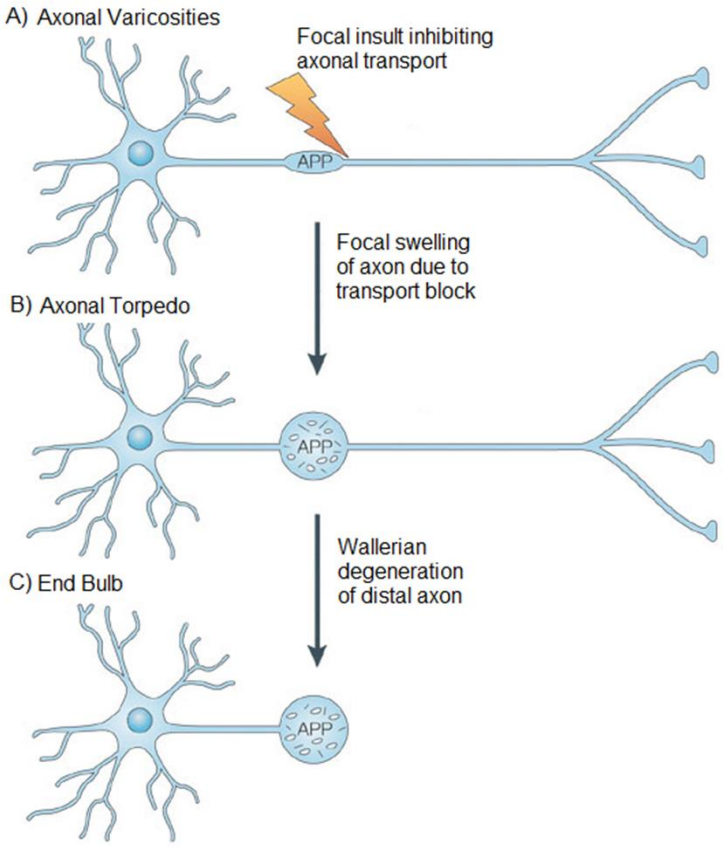

Figure 6.1: Proposed mechanism of axonal torpedo formation.
A) The axon receives a focal insult resulting in the cessation of fast axonal transport (A). B) The inhibition of fast axonal transport results in the accumulation of proteins like amyloid precursor protein and causes a focal swelling of the axon and ultimately forms a axonal torpedo. C) Eventually the block in transport becomes too severe and initiates Wallerian degeneration of the distal axon creating an end bulb. Image modified from Coleman (2005).

6.1. Characterisation of axonal torpedoes in patients with mitochondrial disease.

As axonal torpedoes were viewed as a pathological phenomenon, the first aim was to confirm that they were more prevalent in patients with mitochondrial disease compared to age matched controls. To complete this, immunohistochemical techniques were applied that enabled a quantitative comparative analysis of axonal torpedo and Purkinje cell density in patients with mitochondrial disease and age-matched controls. This work confirmed that Purkinje cell density is lower in patients with mitochondrial disease which is in agreement with previous studies (Lax et al., 2012b), while there is a higher density of axonal torpedoes in patients, especially those harbouring the m.3243A>G mutation relative to controls cases. The observation that there is a high axonal torpedo density in other neurodegenerative disorders like Alzheimer's disease and Parkinson's disease (Louis et al., 2009a) along with the increased density of axonal torpedoes in patients with mitochondrial disease indicates that the formation of axonal torpedoes is a response to a toxic stimuli causing neurodegeneration, with different factors causing their formation. Thus, it is unlikely that respiratory chain deficiency is the sole cause but it may be the primary cause for torpedo formation in patients with mitochondrial disease

As axonal torpedoes were observed in control individuals, the relationship between age and axonal torpedo density was investigated. It was shown that there was no relationship in the patients but in the controls, axonal torpedo density increased with age. The observation of a correlation in the control individuals but not the patients, indicates that in control individuals, age is the primary factor in axonal torpedo formation where as in the patients it is a different factor, most likely respiratory chain deficiency as a result of the mitochondrial disease that causes the formation of axonal torpedoes. The correlation between age and axonal torpedo density does contradict previous evidence (Louis et al., 2009a), however the quantification methods employed in this study are different to those that were used by Louis et al. (2009a). Louis and colleagues only counted axonal torpedoes from a 3 × 20 × 25 mm parasagittal section, whereas my data was corrected to the Purkinje cell density. Additionally, the correlation between age and axonal torpedo density I saw was in a disease free control cohort whereas the control group used by Louis et al. (2009a) contained both disease free controls and individuals with essential tremor, AD, and PD, potentially distorting the relationship with age

It is difficult to conclude definitive relationships between axonal torpedoes and other observations such as Purkinje cell densities since the cerebellum is dynamic and is likely to be undergoing torpedo formation and loss, Purkinje cell remodelling and Purkinje cell loss simultaneously, making it difficult to conclude relationships in thin post-mortem cerebellar sections which are only representative of changes at the end-stage of disease.

Originally, as mentioned above, it was postulated that the mis-accumulation of neurofilaments in the axonal torpedoes would lead to the "strangulation" of the neuron by inhibiting both anterograde and retrograde transport in the axon, ultimately leading to degeneration (Louis et al., 2009c). Components of FAT were investigated to determine if they were present or if there is was abnormal accumulation of FAT proteins in the axonal torpedoes. Microtubules are essential for FAT, as they provide the tracks for the motor proteins, dynein and kinesin to move along. Using an immunofluorescent assay I confirmed that the monomers of microtubules were present in the axonal torpedoes. As the microtubule network was still intact, Synaptophysin, a protein that undergoes fast axonal transport to the synapse which would accumulate in the axon or axonal torpedo if there was a block in FAT, was investigated. Using immunohistochemistry there was no accumulation of synpatophysin in the axonal torpedoes. A similar observation was made of APP, which is an indicator of axonal degeneration when it is found accumulated in axons. The absence of synaptophysin and APP immunoreactivity in the axonal torpedoes suggests that axonal transport is not blocked and that there is no axonal degeneration happening. These findings do not support the proposed theory of axonal torpedo formation through a block in FAT and indicates that axonal torpedoes may not be involved in a degenerative process.

Axonal torpedoes were originally viewed as a pathological phenomenon involved in the degeneration of a Purkinje cell, initiated by a toxic or stress stimuli, which in the case of patients with mitochondrial disease, would be respiratory chain deficiency. Therefore, it would be expected that the axonal torpedoes would form in Purkinje cell axons which displayed the greatest level of respiratory chain deficiency. To confirm this, a triple immunofluorescent assay was used to investigate the presence of mitochondria in the axonal torpedoes and determine the level of respiratory chain deficiency in those mitochondria as well as mitochondria in adjacent Purkinje cell bodies and normal appearing axons. To quantify respiratory chain deficiency, complex I subunit NDUFA13 was used a marker as a decrease in the protein expression of NDUFA13 protein has been previously observed in patients with mitochondrial disease (Lax et al., 2012b). The protein expression of NDUFA13 was corrected to a mitochondrial mass marker (COX4). Even though COX is a multi-subunit

enzyme complex that has 3 subunits encoded by the mtDNA, it has been shown that there is no loss of COX expression in the cerebellum of patients with mitochondrial disease (Lax et al., 2012b; Chrysostomou et al., 2016), making COX4 an adequate mitochondrial mass marker. Mitochondria were shown to be localised throughout the axonal torpedoes in both controls and patients with mitochondrial disease. Quantification of NDUFA13 expression in axonal torpedoes, Purkinje cell soma and normal appearing axons, revealed that respiratory chain deficiency exists in all three neuronal compartments and that Purkinje cell soma had the greatest loss of NDUFA13 expression compared to other neuronal compartments. If axonal torpedoes were to be involved in a degenerative process it would be expected that the mitochondria in the axonal torpedoes would have the greatest level of complex I deficiency as that Purkinje cell would be the most affected and most vulnerable to degeneration. However, this data indicates that the axonal torpedoes are forming in the ”healthier” neurons and, rather than being a part of a degenerative process, are involved in the remodelling process of a surviving neuron to compensate for loss of neighbouring neurons due to respiratory chain deficiency. Unfortunately, 5µm thick sections are too thin to be able to comprehensively investigate changes to Purkinje cell morphology. Therefore, the next step was to optimise a recently published tissue clearing technique (Chung et al., 2013) that would allow for the morphology of Purkinje cell axons to be investigate changes in the cerebellum by permitting the use of thicker tissue sections (~250µm).

6.2. Optimisation of CLARITY

As mentioned before a main limitation of the standard immunofluorescent technique is that only extremely thin (5µm) sections can be used. This is extremely problematic when looking at structures that have expansive processes like axons as only small region can be visualised. The use of thicker sections is limited due to the heterogeneous nature of tissue, as there are different cell types each with a differing refractive index and the high lipid content of the brain which further scatters and blocks light during imaging. Therefore, the light emitted from fluorophores is severely scattered, a process which increases with increasing section thickness. A recent novel technique known as Clear Lipid-exchanged Acrylamide-hybridized Rigid Imaging compatible Tissue hYdrogel (CLARITY) was devised by Chung et al. (2013) that allowed for thicker sections to be used. This protocol involved the incorporation of the biological molecules within the sample into a matrix and then removed the lipids through a clearing process while the important biological material is retained. Once the lipids are removed, the samples are incubated in an imaging solution that matches the refractive indexes throughout the section, further reducing the level of light scattering.

One of the aims of my project was to optimise the CLARITY technique and a subsequent immunofluorescent protocol to use on post mortem tissue from patients with mitochondrial disease. The development of a consistent and reliable clearing and staining method would allow for the use of thicker sections and provide the opportunity to further investigate changes to the morphology of Purkinje cell axons. I decided to develop passive clearing process rather than an active clearing process as the experience of others had indicated that the tissue is more likely to survive this process (http://forum.CLARITYtechniques.org/), thus preserving a finite resource of patient tissue. I have shown that it is possible to passively clear both mouse and human cerebellum sections. As expected, due to the length of fixation that the human sections had undergone, human sections took considerably longer to clear (four weeks) compared to the mouse sections (seven days). Once the sections had been cleared, the next step was to determine the best immunofluorescent staining protocol. I used the original method described by Chung et al. (2013) and one that I devised which included a prolonged incubation at 4˚C (Phillips et al., 2016). The protocol I developed produced significantly better results than other previously reported methods (Chung et al., 2013; Lee et al., 2014; Poguzhelskaya et al., 2014). The staining protocol I developed was more successful than those previously published is due to the lower temperatures used, 4ºC compared to is 37ºC. The higher temperature results in less antibody specificity as there is more kinetic energy in the system meaning that less energy is required for the antibody to bind to an antigen increasing the probability of the antibody binding to the incorrect antigen, resulting in non-specific binding and an increase in background fluorescence. Although the decrease in temperature does reduce the diffusion rates of the antibodies I addressed this issue by increasing the incubation length from hours to days. Following the staining, it was found that the antibody penetration at best was 150µm, this had also been observed by (Ando et al., 2014). Therefore, the section thickness used was limited to 250µm, however there was a benefit to this as it decreased the length of time needed to clear the sections. The development of the immunofluorescent protocol allowed for the reliable visualisation of Purkinje cell axons in the cerebellum of both control individuals and patients with mitochondrial disease providing the opportunity to investigate changes to the morphology of Purkinje cell axons.

6.3. Axonal morphology changes in mitochondrial disease

Due to the issue of antibody penetration, the section thickness was limited to 250µm but this still allowed for the complete visualisation of axonal torpedoes and the investigation of morphology changes to Purkinje cell axons in the cerebellum of patients with mitochondrial disease compared to control individuals. A previous study used immunohistochemistry on

100μm thick sections from patients with essential tremor to investigate both axonal torpedoes and axonal morphology (Babij et al., 2013). In comparison to the study byBabij et al. (2013), the benefit of using passively cleared sections is that thicker sections are able to be used (250μm > 100μm) and secondly where they only used a single antibody (calbindin 28kDa), I was able to use two antibodies (Neurofilament H and Myelin basic protein). I have also shown it is possible to complete triple immunofluorescence on tissue that has undergone CLARITY, further expanding the possible applications that can be utilised. For example, it would allow for the investigation of respiratory chain deficiency in the cleared sections as well. Unfortunately, quadruple immunofluorescent labelling of cleared sections was unsuccessful as there was a significant level of autofluorescence in the 405nm channel. Even though I applied a 0.2M glycine incubation step at the end of the immunolabelling protocol to reduce the level of autofluorescence this was not adequate in reducing the level of autofluorescence in the 405nm channel. There are some alternative methods that are used to quench autofluorescence and I can attempt these in the future, in an attempt to reduce the 405nm channel autofluorescence and make quadruple immunofluorescence achievable.

The development of CLARITY and a reliable immunofluorescent labelling protocol allowed for the investigation into morphology changes to the Purkinje cell axon. Even though, there was a small sample size (2 controls vs 2 patients with mitochondrial disease), it was shown that there was a difference in Purkinje cell morphology, especially the observation of an increase in thickened axons and axonal branching in the cerebellum of patients with mitochondrial disease compared to control individuals, however a significance could not be applied to this.. The changes observed in Purkinje cell morphology is in line with previous observations by Babij and colleagues in patients with essential tremor.

In combination with the observation of axonal morphology changes in the GCL, a significant reduction in the volume of Purkinje cell axons was also observed in patient with mitochondrial disease. As the axonal caliber is known to be a determining factor in conduction velocity (Boyd and Kalu, 1979; Waxman, 1980), this reduction in volume along with the general loss of Purkinje cells could severely affect the signal output of the cerebellar circuitry and could be a potential mechanism behind cerebellar ataxia.

With the use of CLARITY it was possible to visualise entire axonal torpedoes as well as the projecting axons. It was shown that the majority of axonal torpedoes studied had both an entering and exiting axon. The axons exiting the torpedo were observed to be more complex than normal axons, as recurrent axons in axonal torpedoes were very common and the observation of axonal branching on a recurrent axon was not uncommon. 47% of axons

exiting axonal torpedoes from the controls were observed to have no morphological changes. The observation that axons with axonal torpedoes have more morphological features indicates that the formation of axonal torpedoes is more likely to be involved in a remodelling process than a degenerative process.

Recurrent Purkinje cell axons have been shown to synapse on to other Purkinje cells, Lugaro cells and molecular layer interneurons (MLI) within a narrow (<100µm) parasagittal plane (Witter et al., 2016). It has been hypothesised that the recurrent Purkinje cell axons allow for the cerebellar output to modulate and control the gain of the cerebellar cortex. As the Purkinje cells are inhibitory and are the main output neurons of the cerebellum, it is possible for the gain to be controlled by the output neurons (Brown et al., 2014). The formation of recurrent axons could have a number of consequences depending on where they synapse. If the connection is between a Purkinje cell and a MLI, then there would be a positive feedback on the circuit as the MLI inhibition of Purkinje cells would be decreased. However, negative feedback would be initiated if the connection was between two Purkinje cells as there would there would be an increase in output inhibition. Additionally, through modelling, Purkinje cell to Purkinje cell connections have been proposed to cause fire-rate changes (Maex and Steuber, 2013). The observation of recurrent axons and axonal branching in the axons projecting from the axonal torpedo indicates that the formation of axonal torpedoes may be involved in a compensatory process that increases the number of recurrent axons following the loss of neighbouring Purkinje cells to enhance the feedback loop in the cerebellum to regulate the cerebellar output in an attempt to maintain a normal cerebellar output.

As axonal torpedoes reach a considerable size and evidence suggests that there is no myelin sheath around the axonal torpedoes (Mann et al., 1980; Louis et al., 2009c), I aimed to confirm that there is a lack of axonal torpedo myelination. With the use of immunofluorescence I was able to confirm that axonal torpedoes become demyelinated compared to normal axons. There was no difference in the level of myelination of axonal torpedoes between controls and patients with mitochondrial disease, the same was true for normal appearing axons.

As I have shown that axonal torpedoes loose myelination compared to normal axons, I then looked at the distribution of sodium channels in axonal torpedoes. It has been shown in axons that have become demyelinated that there is an increase in the expression of sodium channels, Nav1.6 and Nav1.2, in an attempt to main electrical conductivity (Craner et al., 2004b). Through immunofluorescent staining, I have shown that the sodium channel Nav1.6 is present in the axonal torpedoes and that the level of expression is comparable to that observed in

axons. It has been proposed that the presence of Nav1.6 and its persistent current in demyelinated axons causes degeneration through the reversal of the sodium calcium exchanger (Craner et al., 2004a). In the case of axonal torpedoes it is unlikely that the presence of Nav1.6 channels is indicative of degeneration since the expression of Nav1.6 is comparable in both axonal torpedoes and axons. My data indicates that the presence of Nav1.6 maintains electrical conductivity, however this would need further work to confirm, such as determining if there is a difference in the co-localisation of Nav1.6 channels and NCX in axonal torpedoes compared to normal appearing axons.

6.4. Conclusion

Through the work I have completed in the characterisation of axonal torpedoes and the optimisation of the CLARITY technique for use in humans, I have shown that; A) torpedoes are more prevalent in patients with mitochondrial disease, B) there appears to be no disruption or inhibition to axonal transport, C) respiratory chain deficient mitochondria are found in axonal torpedoes but a higher degree of deficiency is observed in the Purkinje cell soma, D) axonal torpedoes are demyelinated, E) a comparable expression of Nav1.6 channels are found in axons and axonal torpedoes and finally F) there is an increase in complex axonal morphology observed in the cerebellum of patients with mitochondrial disease compared to controls, especially the axons exiting axonal torpedoes.

The prevailing theory about axonal torpedoes is that the accumulation of phosphorylated neurofilaments results in a blockade of axonal transport resulting in the “strangulation” of the neuron leading to distal degeneration of the Purkinje cell (Louis et al., 2009c). However, following the results obtained in this project I do not agree with this theory. Specifically, if there was a block in transport and “strangulation” of the neuron, I would expect to observe an accumulation of proteins that undergo fast axonal transport and I did not observe an accumulation of either APP or synaptophysin in the axonal torpedoes. In addition microtubules were observed in the axonal torpedoes and therefore were not displaced by the accumulated neurofilament. Furthermore, the use of CLARITY has shown that the axonal torpedoes are not merely just axonal end bulbs as they have axons projecting distally and those axons are complex structures with recurrent collaterals and multiple branching points that project back towards the Purkinje cell layer.

Therefore, I propose that axonal torpedoes are likely a phenomenon that forms during a period of stress in a process of remodelling to maintain functionality rather than as a part of a degenerative process (Figure 6.2). For example, in patients with mitochondrial disease, respiratory chain deficiency results in an inadequate supply of ATP and consequently the

Purkinje cells degenerate and are lost. As the Purkinje cell, is the main output neuron in the cerebellum, any significant loss in Purkinje cell numbers will affect the pattern of activity exiting the cerebellum. This work suggests that the formation of axonal torpedoes in surviving Purkinje cell axons is involved in the remodelling of the axons, resulting in an increase in recurrent axons to form plexuses in the molecular and granular layers to provide a feed-back mechanism. This feedback or inhibition results in the modulation of Purkinje cell activity in an attempt to maintain homeostatic balance. The exact role of axonal torpedoes in this process is not known and would be difficult to determine in post-mortem tissue as it only provides an insight at the end-stage point.

Returning to the larger picture of respiratory chain deficiency in the cerebellum and what is the primary site of degeneration, I have shown that axonal changes are present in the cerebellum of individuals with mitochondrial disease but these are probably secondary changes. Additionally, Chrysostomou et al. (2016) have shown changes to the Purkinje cell synapse in patients with mitochondrial disease but evidence suggest these are not primary either. My data shows that the Purkinje cell soma had the highest level of respiratory chain deficiency. Hence, the main respiratory deficiency hit is to the Purkinje cell soma but it's not sufficient to cause neuronal loss. However, the effects of respiratory chain deficiency is also sensed throughout the neuron resulting in alterations to the axons and synapses in an attempt to maintain normal function. The neuron may be able to survive one change or stress at a time but the cumulative effect of multiple stresses results in Purkinje cell death. As each Purkinje cell is lost, neighbouring neurons are put under more stress since they increase their function in order to compensate for the loss exacerbating the problem. Even though Purkinje cells are the main output neurons from the cerebellar cortex and their loss has been quantified, I do believe the generation of cerebellar ataxia is multifactorial, and investigating other neurons in the cerebellar circuitry and the effects of respiratory chain deficiency on them would be most beneficial, in determining the mechanisms behind cerebellar ataxia.

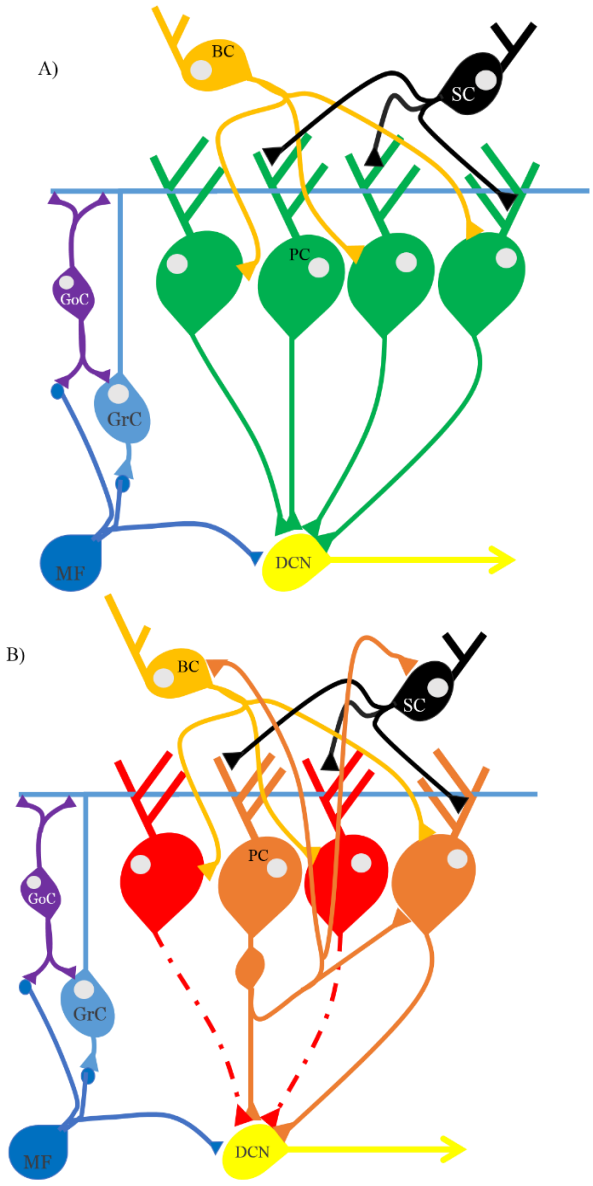

Figure 6.2: Proposed purpose of axonal torpedo formation.

A) In the healthy cerebellum the Purkinje cells (PC) receive indirect input from mossy fibres (MF) via granule cells (GrC) and Golgi cells (GoC) or directly through climbing fibres that originate in the inferior olive (Not shown). The main target of the PC's are neurons in the deep cerebellar nuclei (DCN). B) When there is a loss of Purkinje cells (red) due to an insult such as respiratory chain deficiency as seen in patients with mitochondrial disease, the inhibitory output from the PC's is reduced and the excitability of the DCN is increased. In the surviving PC's, an axonal torpedo will form as a part of the PC axon remodelling process that involves the increase in recurrent collaterals projecting towards either neighbouring PC's or interneurons (stellate (SC) and basket cells (BC)). These collaterals will create a feedback or inhibition of interneurons resulting in the modulation of Purkinje cells activity in an attempt to return in it to a normal signal by decreasing the DCNs excitability.

6.5. Limitations

As the human samples that can qualify for use in the optimised CLARITY method need to have been in formalin for less than 6 years, it restricts the number of possible cases available to be used. Additionally, I was constrained by time to include more individuals in the study as it takes roughly 7 weeks from collection of wet tissue to visualisation of passively cleared tissue. This limitation is apparent in the study investigating the axonal morphology in axons and axonal torpedoes where there was a limited sample size with only two controls and two patients with mitochondrial disease. At the moment, the study shows the differences between patients with mitochondrial disease and controls however, the sample size is not large enough to make statistically robust conclusions.

One of the major limitations of the project is that the tissue used in the project is post-mortem. Post-mortem tissue does allow for the investigation of both structural and molecular changes happening in individuals with disease compared to control individuals but this is at the terminal stage of disease. Therefore, making it difficult to delineate what are the primary drivers of degeneration and which signs are secondary. This limitation is exemplified by the neuropathological studies in the cerebellum of patients with mitochondrial disease where changes are seen in the axons, synapses (Chrysostomou et al., 2016) and Purkinje cell soma (Lax et al., 2012b) but as post-mortem tissue is not dynamic and is fixed at the end-point of the disease it makes it difficult to determine what is the primary cause.

6.6. Future work

6.6.1. Axonal torpedoes

As axonal torpedoes are found in numerous neurological disorders including essential tremor, Alzheimer's disease, Parkinson's disease (Louis et al., 2007) and multiple sclerosis (Redondo et al., 2015), it would be interesting to characterise those axonal torpedoes to determine if they have a similar composition and to understand the mechanism of their formation.

Using confocal microscopy, it was shown that the monomers of microtubules were present in the axonal torpedoes. However, light microscopy does not provide the resolution and detail to determine if the microtubules are correctly arranged to facilitate FAT. There have not been any extensive studies of axonal torpedoes using electron microscopy, therefore, completing said study would both allow for the confirmation of whether microtubules are properly arranged, and also allow for investigation into the mitochondria present in the axonal torpedoes. This would be particularly pertinent to axonal torpedoes found in patients with mitochondrial disease, as results here have shown that mitochondria are present in the axonal

torpedoes but election micrographs would provide insight into the quality of mitochondria and determine if there were any structural abnormalities to those mitochondria.

It was shown that the expression of Nav1.6 was comparable in the axonal torpedoes when compared to the normal appearing axons in both the controls and patients with mitochondrial disease. However in the patients with mitochondrial disease, the trend between Nav1.6 and myelin volume was reversed in comparison to controls and may allude to a role of Nav1.6 in degeneration in the patients. As previously stated, co-localisation of Nav1.6 with the sodium calcium ion exchanger (NCX) is indicative of axonal degeneration. Investigating if Nav1.6 co-localises with NCX in the axonal torpedoes in patients with mitochondrial will help determine if the axonal torpedoes are undergoing axonal degeneration. Additionally, if Nav1.6 and NCX co-localisation differs between patient and control axonal torpedoes, it would suggest that the outcome of their formation in patients would differ to the mechanisms in controls.

The data obtained in this work was achieved through work completed on post mortem human cerebellar sections. This is a limitation as it only allows for an investigation into the end point of the disease and does provide any insight into time course and progression of axonal changes in the cerebellum of patients with mitochondrial disease. As axonal torpedoes have been identified in normal aging mice (Baurle and Grusser-Cornehls, 1994), a mouse model would be sufficient to further research axonal torpedoes formation by taking cerebellar sections at different time points which would hopefully allow for the visualisation of axonal torpedoes forming. Additionally, if there was a model of mitochondrial disease caused by a mitochondrial defect specifically to the Purkinje cell, it would also allow for the investigation into how mitochondrial dysfunction alters the Purkinje cell axon morphology and determine if Purkinje cell loss due to mitochondrial dysfunction causes a remodelling of the Purkinje cell circuitry. CLARITY could be used on 250µm cerebellar sections from different time points, for example P28, P84, P126 and P168, in both the wild type mice and mice with dysfunctional mitochondria in the Purkinje cells. Using Purkinje cell markers such as parvalbumin and calretinin, large areas of Purkinje cells could be imaged using a confocal microscope. The recurrent axons and axonal torpedoes would then be reconstructed and analysed using software such as Matlab and a neurite tracer module on ImageJ (Longair et al., 2011) . A similar method was used by Witter et al. (2016) which showed that the recurrent axons are confined to a parasagittal plane and the recurrent axons make contact with contact Purkinje cells, Lugaro cells, and MLI. If this experiment was carried out in conjunction with ex vivo electrophysiological recordings of the same cerebellar sections, then the electrical

activity of the cerebellum in could be recorded. This would show the effects of mitochondrial dysfunction on the electrical activity of the cerebellum and in combination with the immunofluorescent study mentioned above, it would be possible to determine how the physical changes and remodelling relate to changes in electrical activity.

6.6.2. CLARITY

As mentioned in section 6.5, the sample size in the study investigating axonal morphology was too small. To address that issue, I would look at including more controls and patients in that study and I have already acquired samples from two patients with mitochondrial disease. Additionally, I have started the CLARITY protocol on a control sample that had been fixed in PFA and frozen in order to determine if sections fixed and stored in this manner would be a viable source of tissue for further experiments using CLARITY.

An issue that arose with the use of CLARITY was the lack of antibody penetration which restricted the thickness of the tissue to 250μm. This issue has been experienced by other authors and they have tried to address the issue. One paper utilised the polarity of antibodies and applied an electrical current to increase the penetration into the antibodies (Li et al., 2015). Whereas, Lee et al. (2016) used centrifugal force both spinning the sections at 600 x g for 3 hours for each antibody incubation. This was shown to successfully increase the depth of specific labelling and also reduced the length of incubation. Both methods utilise a simple set up which could be applied to the cleared tissue used in this project. To determine if the methods were an improvement, I would simultaneously stain sections with the protocol I developed while staining different sections with the methods described above to allow for a direct comparison. Alternatively, Fragment antigen-binding F(ab) antibodies conjugated with a fluorophore could be used instead of a whole IgG antibody. F(ab) antibodies are produced when whole IgG antibodies undergo pepsin digestion which removes the majority of the Fc region while leaving the antigen binding intact some of the hinge region. F(ab) antibodies have a molecular weight of 110kDa, compared to 160kDa of a whole IgG antibody. The smaller and lighter F(ab) antibodies would diffuse into the tissue far easier as there would be less steric hindrance increasing the depth and rate at which they will diffuse into the tissue.

In addition to improving the penetration of antibodies, a final important step of optimisation in the CLARITY method is to optimise the use of mitochondrial antibodies in the passively cleared human sections so that I can confidently quantify the level of respiratory chain deficiency in those sections. Once that has been completed, it would allow for the investigation into the distribution of dysfunctional mitochondria in the different neuronal compartments of the same neuron.

The observation of reduced Purkinje cell axon volume was made in 5µm sections, therefore I would like to complete a more comprehensive study of individual Purkinje cell axon volume in the CLARITY sections. Using CLARITY would allow for a larger portion of the complete axon to be measured making the observation of a reduction in axonal volume more robust. As Purkinje cell axon volume was found to be significantly reduced in the granular cell layer of patients with mitochondrial disease compared to controls, it would be worthwhile looking at axons in other regions of the brain where there is a reduction in conduction velocities or white matter abnormalities to determine if a reduction in axon is present there.

In mitochondrial disease, the grey matter has typically gained the most attention when understanding the role of respiratory chain deficiency in neurodegeneration. The development of the CLARITY techniques provides an important tool for understanding changes in the connectivity and white matter in other brain region. MRI studies have observed deep white matter changes in the frontal and occipital lobe in patients with MELAS (Fujii et al., 1990) hence, using CLARITY in those regions can determine what those changes are microscopically and will provide further insights into how respiratory chain deficiency affects the neuronal connectivity.

An additional application of the CLARITY technique would be to compare the vascular network between areas with stroke-like cortical lesions and neighbouring non-lesioned regions. Using markers such as Glut-1 and α-smooth muscle actin will help determine the density and morphology of arterioles and capillaries in these regions. This work would help determine if dysfunction and degeneration of small arteries, arterioles and capillaries is the primary cause of stroke-like lesions as proposed by the mitochondrial angiopathy theory (Koga et al., 2010).

Bibliography

Ackerley, S., Thornhill, P., Grierson, A.J., Brownlees, J., Anderton, B.H., Leigh, P.N., Shaw, C.E. and Miller, C.C. (2003) 'Neurofilament heavy chain side arm phosphorylation regulates axonal transport of neurofilaments', J Cell Biol, 161(3), pp. 489-95.

Aerts, L., Craessaerts, K., De Strooper, B. and Morais, V.A. (2015) 'PINK1 kinase catalytic activity is regulated by phosphorylation on serines 228 and 402', J Biol Chem, 290(5), pp. 2798-811.

Allard, J.C., Tilak, S. and Carter, A.P. (1988) 'CT and MR of MELAS syndrome', AJNR Am J Neuroradiol, 9(6), pp. 1234-8.

Anderson, S., Bankier, A.T., Barrell, B.G., Debruijn, M.H.L., Coulson, A.R., Drouin, J., Eperon, I.C., Nierlich, D.P., Roe, B.A., Sanger, F., Schreier, P.H., Smith, A.J.H., Staden, R. and Young, I.G. (1981) 'Sequence and Organization of the Human Mitochondrial Genome', Nature, 290(5806), pp. 457-465.

Ando, K., Laborde, Q., Lazar, A., Godefroy, D., Youssef, I., Amar, M., Pooler, A., Potier, M.C., Delatour, B. and Duyckaerts, C. (2014) 'Inside Alzheimer brain with CLARITY: senile plaques, neurofibrillary tangles and axons in 3-D', Acta Neuropathol, 128(3), pp. 457-9.

Aoyagi, Y., Kawakami, R., Osanai, H., Hibi, T. and Nemoto, T. (2015) 'A rapid optical clearing protocol using 2,2'-thiodiethanol for microscopic observation of fixed mouse brain', PLoS One, 10(1), p. e0116280.

Apostolova, L.G., White, M., Moore, S.A. and Davis, P.H. (2005) 'Deep white matter pathologic features in watershed regions: a novel pattern of central nervous system involvement in MELAS', Arch Neurol, 62(7), pp. 1154-6.

Apps, R. and Hawkes, R. (2009) 'Cerebellar cortical organization: a one-map hypothesis', Nat Rev Neurosci, 10(9), pp. 670-81.

Arnberg, A., Van Bruggen, E.F.J., Ter Schegget, J. and Borst, P. (1971) 'The presence of DNA molecules with a displacement loop in standard mitochondrial DNA preparations', Biochimica et Biophysica Acta (BBA)-Nucleic Acids and Protein Synthesis, 246(2), pp. 353-357.

Arroyo, E.J., Xu, T., Grinspan, J., Lambert, S., Levinson, S.R., Brophy, P.J., Peles, E. and Scherer, S.S. (2002) 'Genetic dysmyelination alters the molecular architecture of the nodal region', The Journal of neuroscience : the official journal of the Society for Neuroscience, 22(5), pp. 1726-1737.

Ashrafi, G., Schlehe, J.S., LaVoie, M.J. and Schwarz, T.L. (2014) 'Mitophagy of damaged mitochondria occurs locally in distal neuronal axons and requires PINK1 and Parkin', J Cell Biol, 206(5), pp. 655-70.

Attwell, D. and Laughlin, S.B. (2001) 'An energy budget for signaling in the grey matter of the brain', Journal of Cerebral Blood Flow & Metabolism, 21(10), pp. 1133-1145.

Babij, R., Lee, M., Cortes, E., Vonsattel, J.P., Faust, P.L. and Louis, E.D. (2013) 'Purkinje cell axonal anatomy: quantifying morphometric changes in essential tremor versus control brains', Brain, 136(Pt 10), pp. 3051-61.

Barkovich, A.J., Good, W.V., Koch, T.K. and Berg, B.O. (1993) 'Mitochondrial Disorders - Analysis of Their Clinical and Imaging Characteristics', American Journal of Neuroradiology, 14(5), pp. 1119-1137.

Barrell, B.G., Anderson, S., Bankier, A.T., de Bruijn, M.H., Chen, E., Coulson, A.R., Drouin, J., Eperon, I.C., Nierlich, D.P. and Roe, B.A. (1980) 'Different pattern of codon recognition by mammalian mitochondrial tRNAs', Proceedings of the National Academy of Sciences, 77(6), pp. 3164-3166.

Baughman, J.M., Perocchi, F., Girgis, H.S., Plovanich, M., Belcher-Timme, C.A., Sancak, Y., Bao, X.R., Strittmatter, L., Goldberger, O., Bogorad, R.L., Koteliansky, V. and Mootha, V.K. (2011) 'Integrative genomics identifies MCU as an essential component of the mitochondrial calcium uniporter', Nature, 476(7360), pp. 341-U111.

Baumann, N. and Pham-Dinh, D. (2001) 'Biology of oligodendrocyte and myelin in the mammalian central nervous system', Physiological reviews.

Baurle, J. and Grusser-Cornehls, U. (1994) 'Axonal torpedoes in cerebellar Purkinje cells of two normal mouse strains during aging', Acta Neuropathol, 88(3), pp. 237-45.

Becker, K., Jahrling, N., Saghafi, S., Weiler, R. and Dodt, H.U. (2012) 'Chemical clearing and dehydration of GFP expressing mouse brains', PLoS One, 7(3), p. e33916.

Bernardi, P. (1999) 'Mitochondrial transport of cations: channels, exchangers, and permeability transition', Physiol Rev, 79(4), pp. 1127-55.

Bestwick, M.L. and Shadel, G.S. (2013) 'Accessorizing the human mitochondrial transcription machinery', Trends Biochem Sci, 38(6), pp. 283-91.

Betts-Henderson, J., Jaros, E., Krishnan, K.J., Perry, R.H., Reeve, A.K., Schaefer, A.M., Taylor, R.W. and Turnbull, D.M. (2009) 'Alpha-synuclein pathology and Parkinsonism associated with POLG1 mutations and multiple mitochondrial DNA deletions', Neuropathology and Applied Neurobiology, 35(1), pp. 120-124.

Bindu, P.S., Arvinda, H., Taly, A.B., Govindaraju, C., Sonam, K., Chiplunkar, S., Kumar, R., Gayathri, N., Bharath Mm, S., Nagappa, M., Sinha, S., Khan, N.A., Govindaraj, P., Nunia, V., Paramasivam, A. and Thangaraj, K. (2015) 'Magnetic resonance imaging correlates of genetically characterized patients with mitochondrial disorders: A study from south India', Mitochondrion, 25, pp. 6-16.

Bjartmar, C., Kidd, G., Mork, S., Rudick, R. and Trapp, B.D. (2000) 'Neurological disability correlates with spinal cord axonal loss and reduced N-acetyl aspartate in chronic multiple sclerosis patients', Ann Neurol, 48(6), pp. 893-901.

Bocquet, A., Berges, R., Frank, R., Robert, P., Peterson, A.C. and Eyer, J. (2009) 'Neurofilaments bind tubulin and modulate its polymerization', J Neurosci, 29(35), pp. 11043-54.

Bogenhagen, D.F., Pinz, K.G. and Perez-Jannotti, R.M. (2001) 'Enzymology of mitochondrial base excision repair', Prog Nucleic Acid Res Mol Biol, 68, pp. 257-71.

Bonawitz, N.D., Clayton, D.A. and Shadel, G.S. (2006) 'Initiation and beyond: multiple functions of the human mitochondrial transcription machinery', Mol Cell, 24(6), pp. 813-25.

Boyd, I.A. and Kalu, K.U. (1979) 'Scaling factor relating conduction velocity and diameter for myelinated afferent nerve fibres in the cat hind limb', J Physiol, 289, pp. 277-97.

Brady, S.T., Witt, A.S., Kirkpatrick, L.L., de Waegh, S.M., Readhead, C., Tu, P.H. and Lee, V.M.Y. (1999) 'Formation of compact myelin is required for maturation of the axonal cytoskeleton', Journal of Neuroscience, 19(17), pp. 7278-7288.

Brannan, T.S., Burger, A.A. and Chaudhary, M.Y. (1980) 'Bilateral basal ganglia calcifications visualised on CT scan', J Neurol Neurosurg Psychiatry, 43(5), pp. 403-6.

Braun, P.E. (1984) Molecular organization of myelin. Springer.

Brini, M., Pinton, P., King, M.P., Davidson, M., Schon, E.A. and Rizzuto, R. (1999) 'A calcium signaling defect in the pathogenesis of a mitochondrial DNA inherited oxidative phosphorylation deficiency', Nat Med, 5(8), pp. 951-4.

Brion, J.P., Couck, A.M., Bruce, M., Anderton, B. and Flament-Durand, J. (1991) 'Synaptophysin and chromogranin A immunoreactivities in senile plaques of Alzheimer's disease', Brain Res, 539(1), pp. 143-50.

Brochu, G., Maler, L. and Hawkes, R. (1990) 'Zebrin II: a polypeptide antigen expressed selectively by Purkinje cells reveals compartments in rat and fish cerebellum', J Comp Neurol, 291(4), pp. 538-52.

Bron, S., Holsappel, S., Venema, G. and Peeters, B.P.H. (1991) 'Plasmid Deletion Formation between Short Direct Repeats in Bacillus-Subtilis Is Stimulated by Single-Stranded Rolling-Circle Replication Intermediates', Molecular & General Genetics, 226(1-2), pp. 88-96.

Brown, G.C. and Borutaite, V. (2012) 'There is no evidence that mitochondria are the main source of reactive oxygen species in mammalian cells', Mitochondrion, 12(1), pp. 1-4.

Brown, J., Pan, W.-X. and Dudman, J.T. (2014) 'The inhibitory microcircuit of the substantia nigra provides feedback gain control of the basal ganglia output', eLife, 3, p. e02397.

Brown, T.A., Cecconi, C., Tkachuk, A.N., Bustamante, C. and Clayton, D.A. (2005) 'Replication of mitochondrial DNA occurs by strand displacement with alternative light-strand origins, not via a strand-coupled mechanism', Genes Dev, 19(20), pp. 2466-76.

Brown, W.M., George, M. and Wilson, A.C. (1979) 'Rapid evolution of animal mitochondrial DNA', Proceedings of the National Academy of Sciences, 76(4), pp. 1967-1971.

Bua, E., Johnson, J., Herbst, A., Delong, B., McKenzie, D., Salamat, S. and Aiken, J.M. (2006) 'Mitochondrial DNA-deletion mutations accumulate intracellularly to detrimental levels in aged human skeletal muscle fibers', Am J Hum Genet, 79(3), pp. 469-80.

Buckner, R.L. (2013) 'The cerebellum and cognitive function: 25 years of insight from anatomy and neuroimaging', Neuron, 80(3), pp. 807-15.

Burke, R.E. and O'Malley, K. (2013) 'Axon degeneration in Parkinson's disease', Exp Neurol, 246, pp. 72-83.

Butts, T., Green, M.J. and Wingate, R.J.T. (2014) 'Development of the cerebellum: simple steps to make a ‘little brain’', Development, 141(21), pp. 4031-4041.

Cai, Q. and Sheng, Z.-H. (2009) 'Moving or Stopping Mitochondria: Miro as a Traffic Cop by Sensing Calcium', Neuron, 61(4), pp. 493-496.

Cai, Q., Zakaria, H.M., Simone, A. and Sheng, Z.H. (2012) 'Spatial parkin translocation and degradation of damaged mitochondria via mitophagy in live cortical neurons', Curr Biol, 22(6), pp. 545-52.

Caldwell, J.H., Schaller, K.L., Lasher, R.S., Peles, E. and Levinson, S.R. (2000) 'Sodium channel Nav1. 6 is localized at nodes of Ranvier, dendrites, and synapses', Proceedings of the National Academy of Sciences, 97(10), pp. 5616-5620.

Campello, S. and Scorrano, L. (2010) 'Mitochondrial shape changes: orchestrating cell pathophysiology', EMBO Rep, 11(9), pp. 678-84.

Carelli, V., Ghelli, A., Bucchi, L., Montagna, P., De Negri, A., Leuzzi, V., Carducci, C., Lenaz, G., Lugaresi, E. and Degli Esposti, M. (1999) 'Biochemical features of mtDNA 14484 (ND6/M64V) point mutation associated with Leber's hereditary optic neuropathy', Ann Neurol, 45(3), pp. 320-8.

Carpenter, S. (1968) 'Proximal axonal enlargement in motor neuron disease', Neurology, 18(9), pp. 841-51.

Castillo, M., Kwock, L. and Green, C. (1995) 'MELAS syndrome: imaging and proton MR spectroscopic findings', AJNR Am J Neuroradiol, 16(2), pp. 233-9.

Cecchini, G. (2003) 'Function and structure of complex II of the respiratory chain', Annu Rev Biochem, 72, pp. 77-109.

Chan-Palay, V. (1971) 'The recurrent collaterals of Purkinje cell axons: a correlated study of the rat's cerebellar cortex with electron microscopy and the Golgi method', Zeitschrift für Anatomie und Entwicklungsgeschichte.

Chen, H., Chomyn, A. and Chan, D.C. (2005) 'Disruption of fusion results in mitochondrial heterogeneity and dysfunction', J Biol Chem, 280(28), pp. 26185-92.

Chen, H., Detmer, S.A., Ewald, A.J., Griffin, E.E., Fraser, S.E. and Chan, D.C. (2003) 'Mitofusins Mfn1 and Mfn2 coordinately regulate mitochondrial fusion and are essential for embryonic development', J Cell Biol, 160(2), pp. 189-200.

Chinnery, P.F., DiMauro, S., Shanske, S., Schon, E.A., Zeviani, M., Mariotti, C., Carrara, F., Lombes, A., Laforet, P., Ogier, H., Jaksch, M., Lochmuller, H., Horvath, R., Deschauer, M., Thorburn, D.R., Bindoff, L.A., Poulton, J., Taylor, R.W., Matthews, J.N. and Turnbull, D.M. (2004) 'Risk of developing a mitochondrial DNA deletion disorder', Lancet, 364(9434), pp. 592-6.

Chinnery, P.F., Johnson, M.A., Wardell, T.M., Singh-Kler, R., Hayes, C., Brown, D.T., Taylor, R.W., Bindoff, L.A. and Turnbull, D.M. (2000) 'The epidemiology of pathogenic mitochondrial DNA mutations', Ann Neurol, 48(2), pp. 188-93.

Choi, C., Sunwoo, I.N., Kim, H.S. and Kim, D.I. (2000) 'Transient improvement of pyruvate metabolism after coenzyme Q therapy in Kearns-Sayre syndrome: MRS study', Yonsei Med J, 41(5), pp. 676-9.

Chrast, R., Saher, G., Nave, K.-A. and Verheijen, M.H.G. (2011) 'Lipid metabolism in myelinating glial cells: lessons from human inherited disorders and mouse models', Journal of lipid research, 52(3), pp. 419-434.

Chrysostomou, A., Grady, J.P., Laude, A., Taylor, R.W., Turnbull, D.M. and Lax, N.Z. (2016) 'Investigating complex I deficiency in Purkinje cells and synapses in patients with mitochondrial disease', Neuropathol Appl Neurobiol, 42(5), pp. 477-92.

Chu, B.C., Terae, S., Takahashi, C., Kikuchi, Y., Miyasaka, K., Abe, S., Minowa, K. and Sawamura, T. (1999) 'MRI of the brain in the Kearns-Sayre syndrome: report of four cases and a review', Neuroradiology, 41(10), pp. 759-64.

Chung, K., Wallace, J., Kim, S.Y., Kalyanasundaram, S., Andalman, A.S., Davidson, T.J., Mirzabekov, J.J., Zalocusky, K.A., Mattis, J., Denisin, A.K., Pak, S., Bernstein, H., Ramakrishnan, C., Grosenick, L., Gradinaru, V. and Deisseroth, K. (2013) 'Structural and molecular interrogation of intact biological systems', Nature, 497(7449), pp. 332-7.

Cipolat, S., Martins de Brito, O., Dal Zilio, B. and Scorrano, L. (2004) 'OPA1 requires mitofusin 1 to promote mitochondrial fusion', Proc Natl Acad Sci U S A, 101(45), pp. 15927-32.

Clayton, D.A. (1982) 'Replication of animal mitochondrial DNA', Cell, 28(4), pp. 693-705.

Clayton, D.A., Doda, J.N. and Friedberg, E.C. (1974) 'The absence of a pyrimidine dimer repair mechanism in mammalian mitochondria', Proc Natl Acad Sci U S A, 71(7), pp. 2777-81.

Coleman, M. (2005) 'Axon degeneration mechanisms: commonality amid diversity', Nat Rev Neurosci, 6(11), pp. 889-98.

Corral-Debrinski, M., Horton, T., Lott, M.T., Shoffner, J.M., Beal, M.F. and Wallace, D.C. (1992) 'Mitochondrial DNA deletions in human brain: regional variability and increase with advanced age', Nat Genet, 2(4), pp. 324-9.

Cote, F., Collard, J.F. and Julien, J.P. (1993) 'Progressive neuronopathy in transgenic mice expressing the human neurofilament heavy gene: a mouse model of amyotrophic lateral sclerosis', Cell, 73(1), pp. 35-46.

Craner, M.J., Hains, B.C., Lo, A.C., Black, J.A. and Waxman, S.G. (2004a) 'Co-localization of sodium channel Nav1.6 and the sodium-calcium exchanger at sites of axonal injury in the spinal cord in EAE', Brain, 127(Pt 2), pp. 294-303.

Craner, M.J., Lo, A.C., Black, J.A. and Waxman, S.G. (2003) 'Abnormal sodium channel distribution in optic nerve axons in a model of inflammatory demyelination', Brain : a journal of neurology, 126(Pt 7), pp. 1552-1561.

Craner, M.J., Newcombe, J., Black, J.A., Hartle, C., Cuzner, M.L. and Waxman, S.G. (2004b) 'Molecular changes in neurons in multiple sclerosis: altered axonal expression of Nav1.2 and Nav1.6 sodium channels and Na+/Ca2+ exchanger', Proc Natl Acad Sci U S A, 101(21), pp. 8168-73.

Crick, F.H.C. (1965) 'Codon-anticodon pairing: the wobble hypothesis'.

Davidzon, G., Greene, P., Mancuso, M., Klos, K.J., Ahlskog, J.E., Hirano, M. and DiMauro, S. (2006) 'Early-onset familial parkinsonism due to POLG mutations', Annals of neurology, 59(5), pp. 859-862.

de Ferra, F., Engh, H., Hudson, L., Kamholz, J., Puckett, C., Molineaux, S. and Lazzarini, R.A. (1985) 'Alternative splicing accounts for the four forms of myelin basic protein', Cell, 43(3 Pt 2), pp. 721-7.

Deas, E., Plun-Favreau, H., Gandhi, S., Desmond, H., Kjaer, S., Loh, S.H., Renton, A.E., Harvey, R.J., Whitworth, A.J., Martins, L.M., Abramov, A.Y. and Wood, N.W. (2011) 'PINK1 cleavage at position A103 by the mitochondrial protease PARL', Hum Mol Genet, 20(5), pp. 867-79.

Deglincerti, A. and Jaffrey, S.R. (2012) 'Insights into the roles of local translation from the axonal transcriptome', Open Biol, 2(6), p. 120079.

Delettre, C., Lenaers, G., Griffoin, J.M., Gigarel, N., Lorenzo, C., Belenguer, P., Pelloquin, L., Grosgeorge, J., Turc-Carel, C., Perret, E., Astarie-Dequeker, C., Lasquellec, L., Arnaud, B., Ducommun, B., Kaplan, J. and Hamel, C.P. (2000) 'Nuclear gene OPA1, encoding a mitochondrial dynamin-related protein, is mutated in dominant optic atrophy', Nat Genet, 26(2), pp. 207-10.

DiMauro, S., Schon, E.A., Carelli, V. and Hirano, M. (2013) 'The clinical maze of mitochondrial neurology', Nat Rev Neurol, 9(8), pp. 429-44.

Doda, J.N., Wright, C.T. and Clayton, D.A. (1981) 'Elongation of Displacement-Loop Strands in Human and Mouse Mitochondrial-DNA Is Arrested near Specific Template Sequences', Proceedings of the National Academy of Sciences of the United States of America-Biological Sciences, 78(10), pp. 6116-6120.

Driggers, W.J., Ledoux, S.P. and Wilson, G.L. (1993) 'Repair of Oxidative Damage within the Mitochondrial-DNA of Rinr-38 Cells', Journal of Biological Chemistry, 268(29), pp. 22042-22045.

Dunbar, D.R., Moonie, P.A., Swingler, R.J., Davidson, D., Roberts, R. and Holt, I.J. (1993) 'Maternally transmitted partial direct tandem duplication of mitochondrial DNA associated with diabetes mellitus', Hum Mol Genet, 2(10), pp. 1619-24.

Durham, S.E., Samuels, D.C., Cree, L.M. and Chinnery, P.F. (2007) 'Normal levels of wild-type mitochondrial DNA maintain cytochrome c oxidase activity for two pathogenic mitochondrial DNA mutations but not for m.3243A-->G', Am J Hum Genet, 81(1), pp. 189-95.

Dusart, I., Airaksinen, M.S. and Sotelo, C. (1997) 'Purkinje Cell Survival and Axonal Regeneration Are Age Dependent: An In Vitro Study', The Journal of Neuroscience, 17(10), pp. 3710-3726.

Dusart, I., Morel, M.P., Wehrlé, R. and Sotelo, C. (1999) 'Late axonal sprouting of injured Purkinje cells and its temporal correlation with permissive changes in the glial scar', The Journal of comparative neurology, 408(3), pp. 399-418.

Dutta, R., McDonough, J., Yin, X., Peterson, J., Chang, A., Torres, T., Gudz, T., Macklin, W.B., Lewis, D.A., Fox, R.J., Rudick, R., Mirnics, K. and Trapp, B.D. (2006) 'Mitochondrial

dysfunction as a cause of axonal degeneration in multiple sclerosis patients', Ann Neurol, 59(3), pp. 478-89.

Eccles, J.C., Llinas, R. and Sasaki, K. (1966) 'The excitatory synaptic action of climbing fibres on the Purkinje cells of the cerebellum', J Physiol, 182(2), pp. 268-96.

Eiyama, A. and Okamoto, K. (2015) 'PINK1/Parkin-mediated mitophagy in mammalian cells', Current Opinion in Cell Biology, 33, pp. 95-101.

Elgass, K.D., Smith, E.A., LeGros, M.A., Larabell, C.A. and Ryan, M.T. (2015) 'Analysis of ER-mitochondria contacts using correlative fluorescence microscopy and soft X-ray tomography of mammalian cells', J Cell Sci, 128(15), pp. 2795-804.

Erol, I., Alehan, F., Horvath, R., Schneiderat, P. and Talim, B. (2009) 'Demyelinating disease of central and peripheral nervous systems associated with a A8344G mutation in tRNALys', Neuromuscul Disord, 19(4), pp. 275-8.

Escobar-Khondiker, M., Hollerhage, M., Muriel, M.P., Champy, P., Bach, A., Depienne, C., Respondek, G., Yamada, E.S., Lannuzel, A., Yagi, T., Hirsch, E.C., Oertel, W.H., Jacob, R., Michel, P.P., Ruberg, M. and Hoglinger, G.U. (2007) 'Annonacin, a natural mitochondrial complex I inhibitor, causes tau pathology in cultured neurons', J Neurosci, 27(29), pp. 7827-37.

Evans, M.J. and Scarpulla, R.C. (1989) 'Interaction of Nuclear Factors with Multiple Sites in the Somatic Cytochrome-C Promoter - Characterization of Upstream Nrf-1, Atf, and Intron Sp1 Recognition Sequences', Journal of Biological Chemistry, 264(24), pp. 14361-14368.

Faxen, K., Gilderson, G., Adelroth, P. and Brzezinski, P. (2005) 'A mechanistic principle for proton pumping by cytochrome c oxidase', Nature, 437(7056), pp. 286-9.

Ferguson, B., Matyszak, M.K., Esiri, M.M. and Perry, V.H. (1997) 'Axonal damage in acute multiple sclerosis lesions', Brain, 120 (Pt 3)(3), pp. 393-9.

Ferrarin, M., Gironi, M., Mendozzi, L., Nemni, R., Mazzoleni, P. and Rabuffetti, M. (2005) 'Procedure for the quantitative evaluation of motor disturbances in cerebellar ataxic patients', Med Biol Eng Comput, 43(3), pp. 349-56.

Ferrer, I. (2002) 'Synaptic pathology and cell death in the cerebellum in Creutzfeldt-Jakob disease', Cerebellum, 1(3), pp. 213-22.

Floreani, M., Napoli, E., Martinuzzi, A., Pantano, G., De Riva, V., Trevisan, R., Bisetto, E., Valente, L., Carelli, V. and Dabbeni-Sala, F. (2005) 'Antioxidant defences in cybrids harboring mtDNA mutations associated with Leber's hereditary optic neuropathy', FEBS J, 272(5), pp. 1124-35.

Foscarin, S., Gianola, S., Carulli, D., Fazzari, P., Mi, S., Tamagnone, L. and Rossi, F. (2009) 'Overexpression of GAP-43 modifies the distribution of the receptors for myelin-associated growth-inhibitory proteins in injured Purkinje axons', The European journal of neuroscience, 30(10), pp. 1837-1848.

Fransson, A., Ruusala, A. and Aspenstrom, P. (2003) 'Atypical Rho GTPases have roles in mitochondrial homeostasis and apoptosis', J Biol Chem, 278(8), pp. 6495-502.

Frey, T.G. and Mannella, C.A. (2000) 'The internal structure of mitochondria', Trends Biochem Sci, 25(7), pp. 319-24.

Frezza, C., Cipolat, S., Martins de Brito, O., Micaroni, M., Beznoussenko, G.V., Rudka, T., Bartoli, D., Polishuck, R.S., Danial, N.N., De Strooper, B. and Scorrano, L. (2006) 'OPA1 controls apoptotic cristae remodeling independently from mitochondrial fusion', Cell, 126(1), pp. 177-89.

Friedman, J.R., Lackner, L.L., West, M., DiBenedetto, J.R., Nunnari, J. and Voeltz, G.K. (2011) 'ER tubules mark sites of mitochondrial division', Science, 334(6054), pp. 358-62.

Fujii, T., Okuno, T., Ito, M., Motoh, K., Hamazaki, S., Okada, S., Kusaka, H. and Mikawa, H. (1990) 'CT, MRI, and autopsy findings in brain of a patient with MELAS', Pediatr Neurol, 6(4), pp. 253-6.

Fukuhara, N. (1991) 'Merrf - a Clinicopathological Study - Relationships between Myoclonus Epilepsies and Mitochondrial Myopathies', Revue Neurologique, 147(6-7), pp. 476-479.

Fuste, J.M., Wanrooij, S., Jemt, E., Granycome, C.E., Cluett, T.J., Shi, Y., Atanassova, N., Holt, I.J., Gustafsson, C.M. and Falkenberg, M. (2010) 'Mitochondrial RNA polymerase is needed for activation of the origin of light-strand DNA replication', Mol Cell, 37(1), pp. 67-78.

Gandre-Babbe, S. and van der Bliek, A.M. (2008) 'The novel tail-anchored membrane protein Mff controls mitochondrial and peroxisomal fission in mammalian cells', Mol Biol Cell, 19(6), pp. 2402-12.

Gennerich, A. and Vale, R.D. (2009) 'Walking the walk: how kinesin and dynein coordinate their steps', Curr Opin Cell Biol, 21(1), pp. 59-67.

Gentleman, S.M., Nash, M.J., Sweeting, C.J., Graham, D.I. and Roberts, G.W. (1993) 'Beta-amyloid precursor protein (beta APP) as a marker for axonal injury after head injury', Neurosci Lett, 160(2), pp. 139-44.

Ghelli, A., Zanna, C., Porcelli, A.M., Schapira, A.H., Martinuzzi, A., Carelli, V. and Rugolo, M. (2003) 'Leber's hereditary optic neuropathy (LHON) pathogenic mutations induce mitochondrial-dependent apoptotic death in transmitochondrial cells incubated with galactose medium', J Biol Chem, 278(6), pp. 4145-50.

Ghoumari, A.M., Wehrle, R., Bernard, O., Sotelo, C. and Dusart, I. (2000) 'Implication of Bcl-2 and Caspase-3 in age-related Purkinje cell death in murine organotypic culture: an in vitro model to study apoptosis', Eur J Neurosci, 12(8), pp. 2935-49.

Gianola, S. and Rossi, F. (2001) 'Evolution of the Purkinje cell response to injury and regenerative potential during postnatal development of the rat cerebellum', Journal of Comparative Neurology, 430(1), pp. 101-117.

Gianola, S. and Rossi, F. (2002) 'Long-term injured purkinje cells are competent for terminal arbor growth, but remain unable to sustain stem axon regeneration', Experimental neurology, 176(1), pp. 25-40.

Gilkerson, R.W., Schon, E.A., Hernandez, E. and Davidson, M.M. (2008) 'Mitochondrial nucleoids maintain genetic autonomy but allow for functional complementation', Journal of Cell Biology, 181(7), pp. 1117-1128.

Gioio, A.E., Eyman, M., Zhang, H., Lavina, Z.S., Giuditta, A. and Kaplan, B.B. (2001) 'Local synthesis of nuclear-encoded mitochondrial proteins in the presynaptic nerve terminal', J Neurosci Res, 64(5), pp. 447-53.

Glauser, L., Sonnay, S., Stafa, K. and Moore, D.J. (2011) 'Parkin promotes the ubiquitination and degradation of the mitochondrial fusion factor mitofusin 1', J Neurochem, 118(4), pp. 636-45.

Gleave, J.A., Lerch, J.P., Henkelman, R.M. and Nieman, B.J. (2013) 'A method for 3D immunostaining and optical imaging of the mouse brain demonstrated in neural progenitor cells', PLoS One, 8(8), p. e72039.

Gleyzer, N., Vercauteren, K. and Scarpulla, R.C. (2005) 'Control of mitochondrial transcription specificity factors (TFB1M and TFB2M) by nuclear respiratory factors (NRF-1 and NRF-2) and PGC-1 family coactivators', Mol Cell Biol, 25(4), pp. 1354-66.

Goldstein, M.E., Sternberger, N.H. and Sternberger, L.A. (1987) 'Phosphorylation protects neurofilaments against proteolysis', J Neuroimmunol, 14(2), pp. 149-60.

Gorman, G.S., Schaefer, A.M., Ng, Y., Gomez, N., Blakely, E.L., Alston, C.L., Feeney, C., Horvath, R., Yu-Wai-Man, P., Chinnery, P.F., Taylor, R.W., Turnbull, D.M. and McFarland, R. (2015) 'Prevalence of nuclear and mitochondrial DNA mutations related to adult mitochondrial disease', Ann Neurol, 77(5), pp. 753-9.

Goto, Y.-i., Nonaka, I. and Horai, S. (1990) 'A mutation in the tRNALeu(UUR) gene associated with the MELAS subgroup of mitochondrial encephalomyopathies', Nature, 348(6302), pp. 651-653.

Goto, Y., Horai, S., Matsuoka, T., Koga, Y., Nihei, K., Kobayashi, M. and Nonaka, I. (1992) 'Mitochondrial myopathy, encephalopathy, lactic acidosis, and stroke-like episodes (MELAS): a correlative study of the clinical features and mitochondrial DNA mutation', Neurology, 42(3 Pt 1), pp. 545-50.

Grafstein, B. and Forman, D.S. (1980) 'Intracellular transport in neurons', Physiol Rev, 60(4), pp. 1167-283.

Grandis, M. and Shy, M.E. (2005) 'Current Therapy for Charcot-Marie-Tooth Disease', Curr Treat Options Neurol, 7(1), pp. 23-31.

Greene, A.W., Grenier, K., Aguileta, M.A., Muise, S., Farazifard, R., Haque, M.E., McBride, H.M., Park, D.S. and Fon, E.A. (2012) 'Mitochondrial processing peptidase regulates PINK1 processing, import and Parkin recruitment', EMBO Rep, 13(4), pp. 378-85.

Grenier, K., McLelland, G.L. and Fon, E.A. (2013) 'Parkin- and PINK1-Dependent Mitophagy in Neurons: Will the Real Pathway Please Stand Up?', Front Neurol, 4, p. 100.

Grohmann, K., Amairic, F., Crews, S. and Attardi, G. (1978) 'Failure to detect "cap" structures in mitochondrial DNA-coded poly(A)-containing RNA from HeLa cells', Nucleic Acids Res, 5(3), pp. 637-51.

Grossman, L.I. (1990) 'Mitochondrial DNA in sickness and in health', Am J Hum Genet, 46(3), pp. 415-7.

Grunewald, A., Lax, N.Z., Rocha, M.C., Reeve, A.K., Hepplewhite, P.D., Rygiel, K.A., Taylor, R.W. and Turnbull, D.M. (2014) 'Quantitative quadruple-label immunofluorescence of mitochondrial and cytoplasmic proteins in single neurons from human midbrain tissue', J Neurosci Methods, 232(0), pp. 143-9.

Gumy, L.F., Yeo, G.S., Tung, Y.C., Zivraj, K.H., Willis, D., Coppola, G., Lam, B.Y., Twiss, J.L., Holt, C.E. and Fawcett, J.W. (2011) 'Transcriptome analysis of embryonic and adult sensory axons reveals changes in mRNA repertoire localization', RNA, 17(1), pp. 85-98.

Haas, R. and Dietrich, R. (2004) 'Neuroimaging of mitochondrial disorders', Mitochondrion, 4(5-6), pp. 471-90.

Haass, C., Kaether, C., Thinakaran, G. and Sisodia, S. (2012) 'Trafficking and Proteolytic Processing of APP', Cold Spring Harbor Perspectives in Medicine, 2(5).

Hafezparast, M., Klocke, R., Ruhrberg, C., Marquardt, A., Ahmad-Annuar, A., Bowen, S., Lalli, G., Witherden, A.S., Hummerich, H., Nicholson, S., Morgan, P.J., Oozageer, R., Priestley, J.V., Averill, S., King, V.R., Ball, S., Peters, J., Toda, T., Yamamoto, A., Hiraoka, Y., Augustin, M., Korthaus, D., Wattler, S., Wabnitz, P., Dickneite, C., Lampel, S., Boehme, F., Peraus, G., Popp, A., Rudelius, M., Schlegel, J., Fuchs, H., Hrabe de Angelis, M., Schiavo, G., Shima, D.T., Russ, A.P., Stumm, G., Martin, J.E. and Fisher, E.M. (2003) 'Mutations in dynein link motor neuron degeneration to defects in retrograde transport', Science, 300(5620), pp. 808-12.

Hagerhall, C. (1997) 'Succinate: quinone oxidoreductases. Variations on a conserved theme', Biochim Biophys Acta, 1320(2), pp. 107-41.

Hakonen, A.H., Goffart, S., Marjavaara, S., Paetau, A., Cooper, H., Mattila, K., Lampinen, M., Sajantila, A., Lönnqvist, T. and Spelbrink, J.N. (2008) 'Infantile-onset spinocerebellar ataxia and mitochondrial recessive ataxia syndrome are associated with neuronal complex I defect and mtDNA depletion', Human molecular genetics, 17(23), pp. 3822-3835.

Hama, H., Kurokawa, H., Kawano, H., Ando, R., Shimogori, T., Noda, H., Fukami, K., Sakaue-Sawano, A. and Miyawaki, A. (2011) 'Scale: a chemical approach for fluorescence imaging and reconstruction of transparent mouse brain', Nat Neurosci, 14(11), pp. 1481-8.

Hamilton, G.F. (1973) 'The Comparative Anatomy and Histology of the Cerebellum. Vol. 3. The Human Cerebellum, Cerebellar Connections, and Cerebellar Cortex', Journal of Anatomy, 115(Pt 3), pp. 467-467.

Harding, B.N. (1990) 'Progressive neuronal degeneration of childhood with liver disease (Alpers-Huttenlocher syndrome): a personal review', J Child Neurol, 5(4), pp. 273-87.

Hartline, D.K. (2008) 'What is myelin?', Neuron glia biology.

Hartshorne, R.P. and Catterall, W.A. (1981) 'Purification of the saxitoxin receptor of the sodium channel from rat brain', Proc Natl Acad Sci U S A, 78(7), pp. 4620-4.

Hartshorne, R.P., Messner, D.J., Coppersmith, J.C. and Catterall, W.A. (1982) 'The saxitoxin receptor of the sodium channel from rat brain. Evidence for two nonidentical beta subunits', Journal of Biological Chemistry, 257(23), pp. 13888-13891.

Hawkes, R. and Herrup, K. (1995) 'Aldolase C/zebrin II and the regionalization of the cerebellum', J Mol Neurosci, 6(3), pp. 147-58.

Hess, J.F., Parisi, M.A., Bennett, J.L. and Clayton, D.A. (1991) 'Impairment of mitochondrial transcription termination by a point mutation associated with the MELAS subgroup of mitochondrial encephalomyopathies', Nature, 351(6323), pp. 236-9.

Hille, B. (2001) 'Ion channels of excitable membranes', Ion channels of excitable membranes.

Hillefors, M., Gioio, A.E., Mameza, M.G. and Kaplan, B.B. (2007) 'Axon viability and mitochondrial function are dependent on local protein synthesis in sympathetic neurons', Cellular and molecular neurobiology, 27(6), pp. 701-716.

Hirano, M., Silvestri, G., Blake, D.M., Lombes, A., Minetti, C., Bonilla, E., Hays, A.P., Lovelace, R.E., Butler, I., Bertorini, T.E. and et al. (1994) 'Mitochondrial neurogastrointestinal encephalomyopathy (MNGIE): clinical, biochemical, and genetic features of an autosomal recessive mitochondrial disorder', Neurology, 44(4), pp. 721-7.

Hirokawa, N. (1993) 'Axonal transport and the cytoskeleton', Curr Opin Neurobiol, 3(5), pp. 724-31.

Hirokawa, N., Niwa, S. and Tanaka, Y. (2010) 'Molecular motors in neurons: transport mechanisms and roles in brain function, development, and disease', Neuron, 68(4), pp. 610-38.

Hisanaga, S., Gonda, Y., Inagaki, M., Ikai, A. and Hirokawa, N. (1990) 'Effects of phosphorylation of the neurofilament L protein on filamentous structures', Cell Regul, 1(2), pp. 237-48.

Hisanaga, S. and Hirokawa, N. (1989) 'The effects of dephosphorylation on the structure of the projections of neurofilament', J Neurosci, 9(3), pp. 959-66.

Hisanaga, S., Kusubata, M., Okumura, E. and Kishimoto, T. (1991) 'Phosphorylation of Neurofilament H Subunit at the Tail Domain by Cdc2 Kinase Dissociates the Association to Microtubules', Journal of Biological Chemistry, 266(32), pp. 21798-21803.

Hoffman, A.S. (2012) 'Hydrogels for biomedical applications', Advanced Drug Delivery Reviews, 64, pp. 18-23.

Holt, I.J. (2009) 'Mitochondrial DNA replication and repair: all a flap', Trends in Biochemical Sciences, 34(7), pp. 358-365.

Holt, I.J., Harding, A.E., Petty, R.K. and Morgan-Hughes, J.A. (1990) 'A new mitochondrial disease associated with mitochondrial DNA heteroplasmy', Am J Hum Genet, 46(3), pp. 428-33.

Holt, I.J., Lorimer, H.E. and Jacobs, H.T. (2000) 'Coupled leading- and lagging-strand synthesis of mammalian mitochondrial DNA', Cell, 100(5), pp. 515-24.

Howarth, C., Peppiatt-Wildman, C.M. and Attwell, D. (2010) 'The Energy Use Associated with Neural Computation in the Cerebellum', Journal of Cerebral Blood Flow & Metabolism, 30(2), pp. 403-414.

Hua, L., Zhou, R., Thirumalai, D. and Berne, B.J. (2008) 'Urea denaturation by stronger dispersion interactions with proteins than water implies a 2-stage unfolding', Proc Natl Acad Sci U S A, 105(44), pp. 16928-33.

Hudson, G. and Chinnery, P.F. (2006) 'Mitochondrial DNA polymerase-gamma and human disease', Hum Mol Genet, 15 Spec No 2, pp. R244-52.

Ingerman, E., Perkins, E.M., Marino, M., Mears, J.A., McCaffery, J.M., Hinshaw, J.E. and Nunnari, J. (2005) 'Dnm1 forms spirals that are structurally tailored to fit mitochondria', J Cell Biol, 170(7), pp. 1021-7.

Ito, H., Mori, K., Harada, M., Minato, M., Naito, E., Takeuchi, M., Kuroda, Y. and Kagami, S. (2008a) 'Serial brain imaging analysis of stroke-like episodes in MELAS', Brain Dev, 30(7), pp. 483-8.

Ito, M. (2008) 'Control of mental activities by internal models in the cerebellum', Nat Rev Neurosci, 9(4), pp. 304-13.

Ito, S., Shirai, W., Asahina, M. and Hattori, T. (2008b) 'Clinical and brain MR imaging features focusing on the brain stem and cerebellum in patients with myoclonic epilepsy with ragged-red fibers due to mitochondrial A8344G mutation', American Journal of Neuroradiology, 29(2), pp. 392-395.

Jaffe, H., Veeranna, Shetty, K.T. and Pant, H.C. (1998) 'Characterization of the phosphorylation sites of human high molecular weight neurofilament protein by electrospray ionization tandem mass spectrometry and database searching', Biochemistry, 37(11), pp. 3931-40.

James, D.I., Parone, P.A., Mattenberger, Y. and Martinou, J.C. (2003) 'hFis1, a novel component of the mammalian mitochondrial fission machinery', Journal of Biological Chemistry, 278(38), pp. 36373-36379.

Jaros, E., Mahad, D.J., Hudson, G., Birchall, D., Sawcer, S.J., Griffiths, P.G., Sunter, J., Compston, D.A., Perry, R.H. and Chinnery, P.F. (2007) 'Primary spinal cord neurodegeneration in Leber hereditary optic neuropathy', Neurology, 69(2), pp. 214-6.

Jemt, E., Persson, O., Shi, Y., Mehmedovic, M., Uhler, J.P., Davila Lopez, M., Freyer, C., Gustafsson, C.M., Samuelsson, T. and Falkenberg, M. (2015) 'Regulation of DNA replication at the end of the mitochondrial D-loop involves the helicase TWINKLE and a conserved sequence element', Nucleic Acids Res, 43(19), pp. 9262-75.

Jin, S.M., Lazarou, M., Wang, C., Kane, L.A., Narendra, D.P. and Youle, R.J. (2010) 'Mitochondrial membrane potential regulates PINK1 import and proteolytic destabilization by PARL', J Cell Biol, 191(5), pp. 933-42.

Jitpimolmard, S., Small, J., King, R.H., Geddes, J., Misra, P., McLaughlin, J., Muddle, J.R., Cole, M., Harding, A.E. and Thomas, P.K. (1993) 'The sensory neuropathy of Friedreich's ataxia: an autopsy study of a case with prolonged survival', Acta Neuropathol, 86(1), pp. 29-35.

Johnson, A.A., Tsai, Y., Graves, S.W. and Johnson, K.A. (2000) 'Human mitochondrial DNA polymerase holoenzyme: reconstitution and characterization', Biochemistry, 39(7), pp. 1702-8.

Kaether, C., Skehel, P. and Dotti, C.G. (2000) 'Axonal membrane proteins are transported in distinct carriers: a two-color video microscopy study in cultured hippocampal neurons', Mol Biol Cell, 11(4), pp. 1213-24.

Kageyama, Y., Zhang, Z., Roda, R., Fukaya, M., Wakabayashi, J., Wakabayashi, N., Kensler, T.W., Reddy, P.H., Iijima, M. and Sesaki, H. (2012) 'Mitochondrial division ensures the survival of postmitotic neurons by suppressing oxidative damage', J Cell Biol, 197(4), pp. 535-51.

Kaplan, M.R., Cho, M.H., Ullian, E.M., Isom, L.L., Levinson, S.R. and Barres, B.A. (2001) 'Differential control of clustering of the sodium channels Na(v)1.2 and Na(v)1.6 at developing CNS nodes of ranvier', Neuron, 30(1), pp. 105-119.

Kasamatsu, H., Robberson, D.L. and Vinograd, J. (1971) 'A novel closed-circular mitochondrial DNA with properties of a replicating intermediate', Proceedings of the National Academy of Sciences, 68(9), pp. 2252-2257.

Ke, M.T., Fujimoto, S. and Imai, T. (2013) 'SeeDB: a simple and morphology-preserving optical clearing agent for neuronal circuit reconstruction', Nat Neurosci, 16(8), pp. 1154-61.

Kearns, T.P. and Sayre, G.P. (1958) 'Retinitis pigmentosa, external ophthalmoplegia, and complete heart block: unusual syndrome with histologic study in one of two cases', AMA archives of ophthalmology, 60(2), pp. 280-289.

Kelly, D.P. and Scarpulla, R.C. (2004) 'Transcriptional regulatory circuits controlling mitochondrial biogenesis and function', Genes Dev, 18(4), pp. 357-68.

Kemp, K.C., Cook, A.J., Redondo, J., Kurian, K.M., Scolding, N.J. and Wilkins, A. (2016) 'Purkinje cell injury, structural plasticity and fusion in patients with Friedreich's ataxia', Acta Neuropathol Commun, 4(1), p. 53.

Kerrison, J.B., Howell, N., Miller, N.R., Hirst, L. and Green, W.R. (1995) 'Leber Hereditary Optic Neuropathy', Ophthalmology, 102(10), pp. 1509-1516.

Khan, A., Trevenen, C., Wei, X.C., Sarnat, H.B., Payne, E. and Kirton, A. (2012) 'Alpers syndrome: the natural history of a case highlighting neuroimaging, neuropathology, and fat metabolism', J Child Neurol, 27(5), pp. 636-40.

Kinghorn, K.J., Kaliakatsos, M., Blakely, E.L., Taylor, R.W., Rich, P., Clarke, A. and Omer, S. (2013) 'Hypertrophic olivary degeneration on magnetic resonance imaging in mitochondrial syndromes associated with POLG and SURF1 mutations', J Neurol, 260(1), pp. 3-9.

Kirino, Y., Yasukawa, T., Ohta, S., Akira, S., Ishihara, K., Watanabe, K. and Suzuki, T. (2004) 'Codon-specific translational defect caused by a wobble modification deficiency in mutant tRNA from a human mitochondrial disease', Proc Natl Acad Sci U S A, 101(42), pp. 15070-5.

Knierim, J. (1997) 'Cerebellum'.

Koc, E.C. and Spremulli, L.L. (2002) 'Identification of mammalian mitochondrial translational initiation factor 3 and examination of its role in initiation complex formation with natural mRNAs', J Biol Chem, 277(38), pp. 35541-9.

Koga, Y., Povalko, N., Nishioka, J., Katayama, K., Kakimoto, N. and Matsuishi, T. (2010) 'MELAS and L-arginine therapy: pathophysiology of stroke-like episodes', Ann N Y Acad Sci, 1201, pp. 104-10.

Koshiba, T., Detmer, S.A., Kaiser, J.T., Chen, H., McCaffery, J.M. and Chan, D.C. (2004) 'Structural basis of mitochondrial tethering by mitofusin complexes', Science, 305(5685), pp. 858-62.

Kowald, A. and Kirkwood, T.B. (2011) 'Evolution of the mitochondrial fusion-fission cycle and its role in aging', Proc Natl Acad Sci U S A, 108(25), pp. 10237-42.

Koyano, F., Okatsu, K., Kosako, H., Tamura, Y., Go, E., Kimura, M., Kimura, Y., Tsuchiya, H., Yoshihara, H., Hirokawa, T., Endo, T., Fon, E.A., Trempe, J.F., Saeki, Y., Tanaka, K. and Matsuda, N. (2014) 'Ubiquitin is phosphorylated by PINK1 to activate parkin', Nature, 510(7503), pp. 162-6.

Krishnan, K.J., Reeve, A.K., Samuels, D.C., Chinnery, P.F., Blackwood, J.K., Taylor, R.W., Wanrooij, S., Spelbrink, J.N., Lightowlers, R.N. and Turnbull, D.M. (2008) 'What causes mitochondrial DNA deletions in human cells?', Nature genetics, 40(3), pp. 275-279.

Kriz, J., Zhu, Q.Z., Julien, J.P. and Padjen, A.L. (2000) 'Electrophysiological properties of axons in mice lacking neurofilament subunit genes: disparity between conduction velocity and axon diameter in absence of NF-H', Brain Research, 885(1), pp. 32-44.

Kukat, C., Wurm, C.A., Spahr, H., Falkenberg, M., Larsson, N.G. and Jakobs, S. (2011) 'Super-resolution microscopy reveals that mammalian mitochondrial nucleoids have a uniform size and frequently contain a single copy of mtDNA', Proc Natl Acad Sci U S A, 108(33), pp. 13534-9.

Kuwabara, T., Watanabe, H., Tanaka, K., Tsuji, S., Ohkubo, M., Ito, T., Sakai, K. and Yuasa, T. (1994) 'Mitochondrial encephalomyopathy: elevated visual cortex lactate unresponsive to photic stimulation--a localized 1H-MRS study', Neurology, 44(3 Pt 1), pp. 557-9.

Labauge, P., Durant, R., Castelnovo, G. and Dubois, A. (2002) 'MNGIE: Diarrhea and leukoencephalopathy', Neurology, 58(12), p. 1862.

Lax, N. and Jaros, E. (2012) 'Neurodegeneration in primary mitochondrial disorders', in Mitochondrial Dysfunction in Neurodegenerative Disorders. Springer, pp. 21-41.

Lax, N.Z., Campbell, G.R., Reeve, A.K., Ohno, N., Zambonin, J., Blakely, E.L., Taylor, R.W., Bonilla, E., Tanji, K., DiMauro, S., Jaros, E., Lassmann, H., Turnbull, D.M. and Mahad, D.J. (2012a) 'Loss of myelin-associated glycoprotein in kearns-sayre syndrome', Arch Neurol, 69(4), pp. 490-9.

Lax, N.Z., Grady, J., Laude, A., Chan, F., Hepplewhite, P.D., Gorman, G., Whittaker, R.G., Ng, Y., Cunningham, M.O. and Turnbull, D.M. (2016) 'Extensive respiratory chain defects in inhibitory interneurones in patients with mitochondrial disease', Neuropathol Appl Neurobiol, 42(2), pp. 180-93.

Lax, N.Z., Hepplewhite, P.D., Reeve, A.K., Nesbitt, V., McFarland, R., Jaros, E., Taylor, R.W. and Turnbull, D.M. (2012b) 'Cerebellar ataxia in patients with mitochondrial DNA disease: a molecular clinicopathological study', J Neuropathol Exp Neurol, 71(2), pp. 148-61.

Lax, N.Z., Pienaar, I.S., Reeve, A.K., Hepplewhite, P.D., Jaros, E., Taylor, R.W., Kalaria, R.N. and Turnbull, D.M. (2012c) 'Microangiopathy in the cerebellum of patients with mitochondrial DNA disease', Brain, 135(Pt 6), pp. 1736-50.

Lax, N.Z., Whittaker, R.G., Hepplewhite, P.D., Reeve, A.K., Blakely, E.L., Jaros, E., Ince, P.G., Taylor, R.W., Fawcett, P.R. and Turnbull, D.M. (2012d) 'Sensory neuronopathy in patients harbouring recessive polymerase gamma mutations', Brain, 135(Pt 1), pp. 62-71.

Leber, T. (1871) 'Über hereditäre und congenital-angelegte Sehnervenleiden', Albrecht von Graefes Archiv für Ophthalmologie, 17(2), pp. 249-291.

Lebre, A.S., Rio, M., Faivre d'Arcier, L., Vernerey, D., Landrieu, P., Slama, A., Jardel, C., Laforet, P., Rodriguez, D., Dorison, N., Galanaud, D., Chabrol, B., Paquis-Flucklinger, V., Grevent, D., Edvardson, S., Steffann, J., Funalot, B., Villeneuve, N., Valayannopoulos, V., de Lonlay, P., Desguerre, I., Brunelle, F., Bonnefont, J.P., Rotig, A., Munnich, A. and Boddaert, N. (2011) 'A common pattern of brain MRI imaging in mitochondrial diseases with complex I deficiency', J Med Genet, 48(1), pp. 16-23.

Lee, E., Choi, J., Jo, Y., Kim, J.Y., Jang, Y.J., Lee, H.M., Kim, S.Y., Lee, H.-J., Cho, K., Jung, N., Hur, E.M., Jeong, S.J., Moon, C., Choe, Y., Rhyu, I.J., Kim, H. and Sun, W. (2016) 'ACT-PRESTO: Rapid and consistent tissue clearing and labeling method for 3-dimensional (3D) imaging', Scientific Reports, 6, p. 18631.

Lee, H., Park, J.H., Seo, I., Park, S.H. and Kim, S. (2014) 'Improved application of the electrophoretic tissue clearing technology, CLARITY, to intact solid organs including brain, pancreas, liver, kidney, lung, and intestine', BMC Dev Biol, 14(1), p. 48.

Lee, J.Y., Koga, H., Kawaguchi, Y., Tang, W., Wong, E., Gao, Y.S., Pandey, U.B., Kaushik, S., Tresse, E., Lu, J., Taylor, J.P., Cuervo, A.M. and Yao, T.P. (2010a) 'HDAC6 controls autophagosome maturation essential for ubiquitin-selective quality-control autophagy', EMBO J, 29(5), pp. 969-80.

Lee, J.Y., Nagano, Y., Taylor, J.P., Lim, K.L. and Yao, T.P. (2010b) 'Disease-causing mutations in parkin impair mitochondrial ubiquitination, aggregation, and HDAC6-dependent mitophagy', J Cell Biol, 189(4), pp. 671-9.

Lee, M.K., Xu, Z., Wong, P.C. and Cleveland, D.W. (1993) 'Neurofilaments are obligate heteropolymers in vivo', J Cell Biol, 122(6), pp. 1337-50.

Lee, Y.J., Jeong, S.Y., Karbowski, M., Smith, C.L. and Youle, R.J. (2004) 'Roles of the mammalian mitochondrial fission and fusion mediators Fis1, Drp1, Opa1 in apoptosis', Molecular Biology of the Cell, 15(11), pp. 5001-5011.

Lee, Y.S., Kennedy, W.D. and Yin, Y.W. (2009) 'Structural insight into processive human mitochondrial DNA synthesis and disease-related polymerase mutations', Cell, 139(2), pp. 312-24.

Li, J., Czajkowsky, D.M., Li, X. and Shao, Z. (2015) 'Fast immuno-labeling by electrophoretically driven infiltration for intact tissue imaging', Sci Rep, 5, p. 10640.

Li, J.Y. and Dahlstrom, A. (1997) 'Axonal transport of synaptic vesicle proteins in the rat optic nerve', J Neurobiol, 32(2), pp. 237-50.

Lieberman, A.R. (1971) 'The axon reaction: a review of the principal features of perikaryal responses to axon injury', Int Rev Neurobiol, 14(1), pp. 49-124.

Ligon, L.A. and Steward, O. (2000) 'Movement of mitochondria in the axons and dendrites of cultured hippocampal neurons', The Journal of Comparative Neurology, 427(3), pp. 340-350.

Lill, R., Diekert, K., Kaut, A., Lange, H., Pelzer, W., Prohl, C. and Kispal, G. (1999) 'The essential role of mitochondria in the biogenesis of cellular iron-sulfur proteins', Biol Chem, 380(10), pp. 1157-66.

Ling, M., Merante, F., Chen, H.S., Duff, C., Duncan, A.M. and Robinson, B.H. (1997) 'The human mitochondrial elongation factor tu (EF-Tu) gene: cDNA sequence, genomic localization, genomic structure, and identification of a pseudogene', Gene, 197(1-2), pp. 325-36.

Liu, A.K., Hurry, M.E., Ng, O.T., DeFelice, J., Lai, H.M., Pearce, R.K., Wong, G.T., Chang, R.C. and Gentleman, S.M. (2016) 'Bringing CLARITY to the human brain: visualization of Lewy pathology in three dimensions', Neuropathol Appl Neurobiol, 42(6), pp. 573-87.

Liu, Q., Xie, F., Alvarado-Diaz, A., Smith, M.A., Moreira, P.I., Zhu, X. and Perry, G. (2011) 'Neurofilamentopathy in neurodegenerative diseases', Open Neurol J, 5(1), pp. 58-62.

Liu, R. and Chan, D.C. (2015) 'The mitochondrial fission receptor Mff selectively recruits oligomerized Drp1', Mol Biol Cell, 26(24), pp. 4466-77.

Lo, K.Y., Kuzmin, A., Unger, S.M., Petersen, J.D. and Silverman, M.A. (2011) 'KIF1A is the primary anterograde motor protein required for the axonal transport of dense-core vesicles in cultured hippocampal neurons', Neurosci Lett, 491(3), pp. 168-73.

Longair, M.H., Baker, D.A. and Armstrong, J.D. (2011) 'Simple Neurite Tracer: open source software for reconstruction, visualization and analysis of neuronal processes', Bioinformatics, 27(17), pp. 2453-2454.

Loson, O.C., Song, Z., Chen, H. and Chan, D.C. (2013) 'Fis1, Mff, MiD49, and MiD51 mediate Drp1 recruitment in mitochondrial fission', Mol Biol Cell, 24(5), pp. 659-67.

Louis, E.D., Faust, P.L., Vonsattel, J.P., Honig, L.S., Rajput, A., Rajput, A., Pahwa, R., Lyons, K.E., Ross, W.G., Elble, R.J., Erickson-Davis, C., Moskowitz, C.B. and Lawton, A. (2009a) 'Torpedoes in Parkinson's disease, Alzheimer's disease, essential tremor, and control brains', Mov Disord, 24(11), pp. 1600-5.

Louis, E.D., Faust, P.L., Vonsattel, J.P., Honig, L.S., Rajput, A., Robinson, C.A., Rajput, A., Pahwa, R., Lyons, K.E., Ross, G.W., Borden, S., Moskowitz, C.B., Lawton, A. and Hernandez, N. (2007) 'Neuropathological changes in essential tremor: 33 cases compared with 21 controls', Brain, 130(Pt 12), pp. 3297-307.

Louis, E.D., Kuo, S.H., Vonsattel, J.P.G. and Faust, P.L. (2014) 'Torpedo Formation and Purkinje Cell Loss: Modeling their Relationship in Cerebellar Disease', Cerebellum, 13(4), pp. 433-439.

Louis, E.D., Vonsattel, J.P., Honig, L.S., Ross, G.W., Lyons, K.E. and Pahwa, R. (2006) 'Neuropathologic findings in essential tremor', Neurology, 66(11), pp. 1756-9.

Louis, E.D., Yi, H., Erickson-Davis, C., Vonsattel, J.P. and Faust, P.L. (2009b) 'Structural study of Purkinje cell axonal torpedoes in essential tremor', Neurosci Lett, 450.

Louis, E.D., Yi, H., Erickson-Davis, C., Vonsattel, J.P. and Faust, P.L. (2009c) 'Structural study of Purkinje cell axonal torpedoes in essential tremor', Neurosci Lett, 450(3), pp. 287-91.

Lucking, C.B., Durr, A., Bonifati, V., Vaughan, J., De Michele, G., Gasser, T., Harhangi, B.S., Meco, G., Denefle, P., Wood, N.W., Agid, Y. and Brice, A. (2000) 'Association between early-onset Parkinson's disease and mutations in the parkin gene', N Engl J Med, 342(21), pp. 1560-7.

MacAskill, A.F., Rinholm, J.E., Twelvetrees, A.E., Arancibia-Carcamo, I.L., Muir, J., Fransson, A., Aspenstrom, P., Attwell, D. and Kittler, J.T. (2009) 'Miro1 Is a Calcium Sensor for Glutamate Receptor-Dependent Localization of Mitochondria at Synapses', Neuron, 61(4), pp. 541-555.

Mackey, D.A., Oostra, R.J., Rosenberg, T., Nikoskelainen, E., Bronte-Stewart, J., Poulton, J., Harding, A.E., Govan, G., Bolhuis, P.A. and Norby, S. (1996) 'Primary pathogenic mtDNA mutations in multigeneration pedigrees with Leber hereditary optic neuropathy', Am J Hum Genet, 59(2), pp. 481-5.

Maday, S., Twelvetrees, A.E., Moughamian, A.J. and Holzbaur, E.L. (2014) 'Axonal transport: cargo-specific mechanisms of motility and regulation', Neuron, 84(2), pp. 292-309.

Maday, S., Wallace, K.E. and Holzbaur, E.L. (2012) 'Autophagosomes initiate distally and mature during transport toward the cell soma in primary neurons', J Cell Biol, 196(4), pp. 407-17.

Maex, R. and Steuber, V. (2013) 'An integrator circuit in cerebellar cortex', European Journal of Neuroscience, 38(6), pp. 2917-2932.

Mahad, D.J., Ziabreva, I., Campbell, G., Lax, N., White, K., Hanson, P.S., Lassmann, H. and Turnbull, D.M. (2009) 'Mitochondrial changes within axons in multiple sclerosis', Brain, 132(Pt 5), pp. 1161-74.

Mallilankaraman, K., Cardenas, C., Doonan, P.J., Chandramoorthy, H.C., Irrinki, K.M., Golenar, T., Csordas, G., Madireddi, P., Yang, J., Muller, M., Miller, R., Kolesar, J.E., Molgo, J., Kaufman, B., Hajnoczky, G., Foskett, J.K. and Madesh, M. (2012) 'MCUR1 is an essential component of mitochondrial Ca2+ uptake that regulates cellular metabolism', Nat Cell Biol, 14(12), pp. 1336-43.

Man, P.Y.W. (2002) 'Leber hereditary optic neuropathy', Journal of Medical Genetics, 39(3), pp. 162-169.

Mancuso, M., Orsucci, D., Angelini, C., Bertini, E., Carelli, V., Comi, G.P., Donati, A., Minetti, C., Moggio, M., Mongini, T., Servidei, S., Tonin, P., Toscano, A., Uziel, G., Bruno, C., Ienco, E.C., Filosto, M., Lamperti, C., Catteruccia, M., Moroni, I., Musumeci, O., Pegoraro, E., Ronchi, D., Santorelli, F.M., Sauchelli, D., Scarpelli, M., Sciacco, M., Valentino, M.L., Vercelli, L., Zeviani, M. and Siciliano, G. (2014) 'The m.3243A>G mitochondrial DNA mutation and related phenotypes. A matter of gender?', J Neurol, 261(3), pp. 504-10.

Mancuso, M., Orsucci, D., Angelini, C., Bertini, E., Carelli, V., Comi, G.P., Minetti, C., Moggio, M., Mongini, T., Servidei, S., Tonin, P., Toscano, A., Uziel, G., Bruno, C., Caldarazzo Ienco, E., Filosto, M., Lamperti, C., Martinelli, D., Moroni, I., Musumeci, O., Pegoraro, E., Ronchi, D., Santorelli, F.M., Sauchelli, D., Scarpelli, M., Sciacco, M., Spinazzi, M., Valentino, M.L., Vercelli, L., Zeviani, M. and Siciliano, G. (2013) 'Phenotypic heterogeneity of the 8344A>G mtDNA "MERRF" mutation', Neurology, 80(22), pp. 2049-54.

Mandavilli, B.S., Santos, J.H. and Van Houten, B. (2002) 'Mitochondrial DNA repair and aging', Mutation Research/Fundamental and Molecular Mechanisms of Mutagenesis, 509(1–2), pp. 127-151.

Manfredi, G., Schon, E.A., Moraes, C.T., Bonilla, E., Berry, G.T., Sladky, J.T. and Dimauro, S. (1995) 'A New Mutation Associated with Melas Is Located in a Mitochondrial-DNA Polypeptide-Coding Gene', Neuromuscular Disorders, 5(5), pp. 391-398.

Manfredi, G., Vu, T., Bonilla, E., Schon, E.A., DiMauro, S., Arnaudo, E., Zhang, L., Rowland, L.P. and Hirano, M. (1997) 'Association of myopathy with large-scale mitochondrial DNA duplications and deletions: which is pathogenic?', Ann Neurol, 42(2), pp. 180-8.

Mann, D.M., Stamp, J.E., Yates, P.O. and Bannister, C.M. (1980) 'The fine structure of the axonal torpedo in Purkinje cells of the human cerebellum', Neurol Res, 1(4), pp. 369-78.

Manni, E. and Petrosini, L. (2004) 'A century of cerebellar somatotopy: a debated representation', Nat Rev Neurosci, 5(3), pp. 241-249.

Margulies, M.M., Bücher, J.W.T., Neupert, W., Sebald, W. and Werner, S. (1976) 'Genetics and Biogenesis of Chloroplasts and Mitochondria'. North-Holland, Amsterdam.

Martin, A.J. (2002) 'The Cerebellum', Neuroanatomy: text and atlas.

Mathews, F.S. (1985) 'The structure, function and evolution of cytochromes', Prog Biophys Mol Biol, 45(1), pp. 1-56.

McCombe, P.A., Pfluger, C., Singh, P., Lim, C.Y., Airey, C. and Henderson, R.D. (2015) 'Serial measurements of phosphorylated neurofilament-heavy in the serum of subjects with amyotrophic lateral sclerosis', J Neurol Sci, 353(1-2), pp. 122-9.

McCormack, J.G. and Denton, R.M. (1989) 'The role of Ca2+ ions in the regulation of intramitochondrial metabolism and energy production in rat heart', Mol Cell Biochem, 89(2), pp. 121-5.

McFarland, R., Taylor, R.W. and Turnbull, D.M. (2010) 'A neurological perspective on mitochondrial disease', Lancet Neurol, 9(8), pp. 829-40.

Meglinski, I.V., Churmakov, D.Y., Bashkatov, A.N., Genina, E.A. and Tuchin, V.V. (2004) 'The enhancement of confocal images of tissues at bulk optical immersion', Laser Physics 13, pp. 65-69.

Milesi, J., Rocca, M.A., Bianchi-Marzoli, S., Petrolini, M., Pagani, E., Falini, A., Comi, G. and Filippi, M. (2012) 'Patterns of white matter diffusivity abnormalities in Leber's hereditary optic neuropathy: a tract-based spatial statistics study', J Neurol, 259(9), pp. 1801-7.

Millecamps, S., Gowing, G., Corti, O., Mallet, J. and Julien, J.P. (2007) 'Conditional NF-L transgene expression in mice for in vivo analysis of turnover and transport rate of neurofilaments', J Neurosci, 27(18), pp. 4947-56.

Millecamps, S. and Julien, J.-P. (2013) 'Axonal transport deficits and neurodegenerative diseases', Nat Rev Neurosci, 14(3), pp. 161-176.

Miller, H., Fernandes, A.S., Zaika, E., McTigue, M.M., Torres, M.C., Wente, M., Iden, C.R. and Grollman, A.P. (2004) 'Stereoselective excision of thymine glycol from oxidatively damaged DNA', Nucleic Acids Res, 32(1), pp. 338-45.

Miller, K.E. and Sheetz, M.P. (2004) 'Axonal mitochondrial transport and potential are correlated', J Cell Sci, 117(Pt 13), pp. 2791-804.

Mink, J.W., Blumenschine, R.J. and Adams, D.B. (1981) 'Ratio of central nervous system to body metabolism in vertebrates: its constancy and functional basis', Am J Physiol, 241(3), pp. R203-12.

Mitchell, P. (1961) 'Coupling of phosphorylation to electron and hydrogen transfer by a chemi-osmotic type of mechanism', Nature, 191(4784), pp. 144-8.

Mizukami, K., Sasaki, M., Suzuki, T., Shiraishi, H., Koizumi, J., Ohkoshi, N., Ogata, T., Mori, N., Ban, S. and Kosaka, K. (1992) 'Central nervous system changes in mitochondrial encephalomyopathy: light and electron microscopic study', Acta Neuropathol, 83(4), pp. 449-52.

Montoya, J., Ojala, D. and Attardi, G. (1981) 'Distinctive features of the 5'-terminal sequences of the human mitochondrial mRNAs', Nature, 290(5806), pp. 465-70.

Mori, O., Yamazaki, M., Ohaki, Y., Arai, Y., Oguro, T., Shimizu, H. and Asano, G. (2000a) 'Mitochondrial encephalomyopathy with lactic acidosis and stroke like episodes (MELAS) with prominent degeneration of the intestinal wall and cactus-like cerebellar pathology', Acta Neuropathologica, 100(6), pp. 712-717.

Mori, O., Yamazaki, M., Ohaki, Y., Arai, Y., Oguro, T., Shimizu, H. and Asano, G. (2000b) 'Mitochondrial encephalomyopathy with lactic acidosis and stroke like episodes (MELAS) with prominent degeneration of the intestinal wall and cactus-like cerebellar pathology', Acta Neuropathol, 100(6), pp. 712-7.

Morten, K.J., Cooper, J.M., Brown, G.K., Lake, B.D., Pike, D. and Poulton, J. (1993) 'A new point mutation associated with mitochondrial encephalomyopathy', Hum Mol Genet, 2(12), pp. 2081-7.

Muller, F.L., Liu, Y. and Van Remmen, H. (2004) 'Complex III releases superoxide to both sides of the inner mitochondrial membrane', J Biol Chem, 279(47), pp. 49064-73.

Murgia, M., Pizzo, P., Sandoná, D., Zanovello, P., Rizzuto, R. and Di Virgilio, F. (1992) 'Mitochondrial DNA is not fragmented during apoptosis', Journal of Biological Chemistry, 267(16), pp. 10939-10941.

Nakada, K., Inoue, K., Ono, T., Isobe, K., Ogura, A., Goto, Y.I., Nonaka, I. and Hayashi, J.I. (2001) 'Inter-mitochondrial complementation: Mitochondria-specific system preventing mice from expression of disease phenotypes by mutant mtDNA', Nat Med, 7(8), pp. 934-40.

Napper, R.M. and Harvey, R.J. (1988) 'Number of parallel fiber synapses on an individual Purkinje cell in the cerebellum of the rat', J Comp Neurol, 274(2), pp. 168-77.

Narendra, D., Tanaka, A., Suen, D.F. and Youle, R.J. (2008) 'Parkin is recruited selectively to impaired mitochondria and promotes their autophagy', J Cell Biol, 183(5), pp. 795-803.

Nass, M.M.K., Nass, S. and Afzelius, B.A. (1965) 'The general occurrence of mitochondrial DNA', Experimental cell research, 37(3), pp. 516-539.

Naviaux, R.K. and Nguyen, K.V. (2004) 'POLG mutations associated with Alpers' syndrome and mitochondrial DNA depletion', Annals of neurology, 55(5), pp. 706-12.

Naviaux, R.K., Nyhan, W.L., Barshop, B.A., Poulton, J., Markusic, D., Karpinski, N.C. and Haas, R.H. (1999) 'Mitochondrial DNA polymerase gamma deficiency and mtDNA depletion in a child with Alpers' syndrome', Ann Neurol, 45(1), pp. 54-8.

Nelson, M.R. and Chazin, W.J. (1998) 'Structures of EF-hand Ca(2+)-binding proteins: diversity in the organization, packing and response to Ca2+ binding', Biometals, 11(4), pp. 297-318.

Nesbitt, V., Pitceathly, R.D., Turnbull, D.M., Taylor, R.W., Sweeney, M.G., Mudanohwo, E.E., Rahman, S., Hanna, M.G. and McFarland, R. (2013) 'The UK MRC Mitochondrial Disease Patient Cohort Study: clinical phenotypes associated with the m.3243A>G mutation--implications for diagnosis and management', J Neurol Neurosurg Psychiatry, 84(8), pp. 936-8.

Ngo, H.B., Kaiser, J.T. and Chan, D.C. (2011) 'The mitochondrial transcription and packaging factor Tfam imposes a U-turn on mitochondrial DNA', Nat Struct Mol Biol, 18(11), pp. 1290-6.

Nishino, I., Spinazzola, A. and Hirano, M. (1999) 'Thymidine phosphorylase gene mutations in MNGIE, a human mitochondrial disorder', Science, 283(5402), pp. 689-92.

Nishioka, K., Ohtsubo, T., Oda, H., Fujiwara, T., Kang, D., Sugimachi, K. and Nakabeppu, Y. (1999) 'Expression and differential intracellular localization of two major forms of human 8-oxoguanine DNA glycosylase encoded by alternatively spliced OGG1 mRNAs', Mol Biol Cell, 10(5), pp. 1637-52.

O'Brien, T.W. (2003) 'Properties of human mitochondrial ribosomes', IUBMB life, 55(9), pp. 505-513.

Oettinghaus, B., Schulz, J.M., Restelli, L.M., Licci, M., Savoia, C., Schmidt, A., Schmitt, K., Grimm, A., More, L., Hench, J., Tolnay, M., Eckert, A., D'Adamo, P., Franken, P., Ishihara, N., Mihara, K., Bischofberger, J., Scorrano, L. and Frank, S. (2016) 'Synaptic dysfunction, memory deficits and hippocampal atrophy due to ablation of mitochondrial fission in adult forebrain neurons', Cell Death Differ, 23(1), pp. 18-28.

Ohama, E., Ikuta, F. and Nakamura, N. (1988) 'Mitochondrial abnormalities in choroid plexus of Leigh disease', Brain Dev, 10(1), pp. 30-5.

Ojala, D., Montoya, J. and Attardi, G. (1981) 'tRNA punctuation model of RNA processing in human mitochondria', Nature, 290(5806), pp. 470-4.

Okatsu, K., Koyano, F., Kimura, M., Kosako, H., Saeki, Y., Tanaka, K. and Matsuda, N. (2015) 'Phosphorylated ubiquitin chain is the genuine Parkin receptor', J Cell Biol, 209(1), pp. 111-28.

Okatsu, K., Uno, M., Koyano, F., Go, E., Kimura, M., Oka, T., Tanaka, K. and Matsuda, N. (2013) 'A dimeric PINK1-containing complex on depolarized mitochondria stimulates Parkin recruitment', J Biol Chem, 288(51), pp. 36372-84.

Oldfors, A., Fyhr, I.M., Holme, E., Larsson, N.G. and Tulinius, M. (1990) 'Neuropathology in Kearns-Sayre syndrome', Acta Neuropathol, 80(5), pp. 541-6.

Olichon, A., Baricault, L., Gas, N., Guillou, E., Valette, A., Belenguer, P. and Lenaers, G. (2003) 'Loss of OPA1 perturbates the mitochondrial inner membrane structure and integrity, leading to cytochrome c release and apoptosis', J Biol Chem, 278(10), pp. 7743-6.

Otera, H., Wang, C.X., Cleland, M.M., Setoguchi, K., Yokota, S., Youle, R.J. and Mihara, K. (2010) 'Mff is an essential factor for mitochondrial recruitment of Drp1 during mitochondrial fission in mammalian cells', Journal of Cell Biology, 191(6), pp. 1141-1158.

Palade, G.E. (1953) 'An electron microscope study of the mitochondrial structure', J Histochem Cytochem, 1(4), pp. 188-211.

Palmer, C.S., Elgass, K.D., Parton, R.G., Osellame, L.D., Stojanovski, D. and Ryan, M.T. (2013) 'Adaptor proteins MiD49 and MiD51 can act independently of Mff and Fis1 in Drp1 recruitment and are specific for mitochondrial fission', J Biol Chem, 288(38), pp. 27584-93.

Palmer, C.S., Osellame, L.D., Laine, D., Koutsopoulos, O.S., Frazier, A.E. and Ryan, M.T. (2011) 'MiD49 and MiD51, new components of the mitochondrial fission machinery', EMBO Rep, 12(6), pp. 565-73.

Pant, H.C. (1988) 'Dephosphorylation of Neurofilament Proteins Enhances Their Susceptibility to Degradation by Calpain', Biochemical Journal, 256(2), pp. 665-668.

Parone, P.A., Da Cruz, S., Tondera, D., Mattenberger, Y., James, D.I., Maechler, P., Barja, F. and Martinou, J.C. (2008) 'Preventing mitochondrial fission impairs mitochondrial function and leads to loss of mitochondrial DNA', PLoS One, 3(9), p. e3257.

Pham, A.H., Meng, S., Chu, Q.N. and Chan, D.C. (2012) 'Loss of Mfn2 results in progressive, retrograde degeneration of dopaminergic neurons in the nigrostriatal circuit', Hum Mol Genet, 21(22), pp. 4817-26.

Phillips, J., Laude, A., Lightowlers, R., Morris, C.M., Turnbull, D.M. and Lax, N.Z. (2016) 'Development of passive CLARITY and immunofluorescent labelling of multiple proteins in human cerebellum: understanding mechanisms of neurodegeneration in mitochondrial disease', Sci Rep, 6, p. 26013.

Poguzhelskaya, E., Artamonov, D., Bolshakova, A., Vlasova, O. and Bezprozvanny, I. (2014) 'Simplified method to perform CLARITY imaging', Mol Neurodegener, 9(1), p. 19.

Poulton, J. (1992) 'Duplications of mitochondrial DNA: implications for pathogenesis', J Inherit Metab Dis, 15(4), pp. 487-98.

Poulton, J., Deadman, M.E. and Gardiner, R.M. (1989) 'Tandem direct duplications of mitochondrial DNA in mitochondrial myopathy: analysis of nucleotide sequence and tissue distribution', Nucleic Acids Res, 17(24), pp. 10223-9.

Puigserver, P. and Spiegelman, B.M. (2003) 'Peroxisome proliferator-activated receptor-gamma coactivator 1 alpha (PGC-1 alpha): transcriptional coactivator and metabolic regulator', Endocr Rev, 24(1), pp. 78-90.

Rajput, A.H., Adler, C.H., Shill, H.A. and Rajput, A. (2012) 'Essential tremor is not a neurodegenerative disease', Neurodegenerative disease management, 2(3), pp. 259-268.

Rao, M.V., Campbell, J., Yuan, A., Kumar, A., Gotow, T., Uchiyama, Y. and Nixon, R.A. (2003) 'The neurofilament middle molecular mass subunit carboxyl-terminal tail domains is essential for the radial growth and cytoskeletal architecture of axons but not for regulating neurofilament transport rate', J Cell Biol, 163(5), pp. 1021-31.

Rao, M.V., Mohan, P.S., Kumar, A., Yuan, A., Montagna, L., Campbell, J., Veeranna, Espreafico, E.M., Julien, J.P. and Nixon, R.A. (2011) 'The myosin Va head domain binds to the neurofilament-L rod and modulates endoplasmic reticulum (ER) content and distribution within axons', PLoS One, 6(2), p. e17087.

Rebelo, A.P., Dillon, L.M. and Moraes, C.T. (2011) 'Mitochondrial DNA transcription regulation and nucleoid organization', J Inherit Metab Dis, 34(4), pp. 941-51.

Redondo, J., Kemp, K., Hares, K., Rice, C., Scolding, N. and Wilkins, A. (2015) 'Purkinje Cell Pathology and Loss in Multiple Sclerosis Cerebellum', Brain Pathol, 25(6), pp. 692-700.

Reeve, A., Meagher, M., Lax, N., Simcox, E., Hepplewhite, P., Jaros, E. and Turnbull, D. (2013) 'The impact of pathogenic mitochondrial DNA mutations on substantia nigra neurons', J Neurosci, 33(26), pp. 10790-801.

Rehm, H., Wiedenmann, B. and Betz, H. (1986) 'Molecular characterization of synaptophysin, a major calcium-binding protein of the synaptic vesicle membrane', EMBO J, 5(3), pp. 535-41.

Renault, T.T., Floros, K.V. and Chipuk, J.E. (2013) 'BAK/BAX activation and cytochrome c release assays using isolated mitochondria', Methods, 61(2), pp. 146-155.

Rhee, S.G., Bae, Y.S., Lee, S.-R. and Kwon, J. (2000) 'Hydrogen peroxide: a key messenger that modulates protein phosphorylation through cysteine oxidation.', Science Signaling, 2000(53), pp. pe1-pe1.

Richardson, D.S. and Lichtman, J.W. (2015a) 'Clarifying Tissue Clearing', Cell, 162(2), pp. 246-257.

Richardson, D.S. and Lichtman, J.W. (2015b) 'Clarifying Tissue Clearing', Cell, 162(2), pp. 246-57.

Ritchie, J.M. and Rogart, R.B. (1977) 'Density of sodium channels in mammalian myelinated nerve fibers and nature of the axonal membrane under the myelin sheath', Proceedings of the National Academy of Sciences of the United States of America, 74(1), pp. 211-215.

Rojo, M., Legros, F., Chateau, D. and Lombes, A. (2002) 'Membrane topology and mitochondrial targeting of mitofusins, ubiquitous mammalian homologs of the transmembrane GTPase Fzo', J Cell Sci, 115(Pt 8), pp. 1663-74.

Rosenbluth, J. (1980) 'Central myelin in the mouse mutant shiverer', The Journal of comparative neurology, 194(3), pp. 639-648.

Rossi, F., Gianola, S. and Corvetti, L. (2006) 'The strange case of Purkinje axon regeneration and plasticity', Cerebellum (London, England), 5(2), pp. 174-182.

Rossignol, R., Malgat, M., Mazat, J.-P. and Letellier, T. (1999) 'Threshold Effect and Tissue Specificity: IMPLICATION FOR MITOCHONDRIAL CYTOPATHIES', Journal of Biological Chemistry, 274(47), pp. 33426-33432.

Rub, U., Hoche, F., Brunt, E.R., Heinsen, H., Seidel, K., Del Turco, D., Paulson, H.L., Bohl, J., von Gall, C., Vonsattel, J.P., Korf, H.W. and den Dunnen, W.F. (2013) 'Degeneration of the cerebellum in Huntington's disease (HD): possible relevance for the clinical picture and potential gateway to pathological mechanisms of the disease process', Brain Pathol, 23(2), pp. 165-77.

Rudrabhatla, P., Jaffe, H. and Pant, H.C. (2011) 'Direct evidence of phosphorylated neuronal intermediate filament proteins in neurofibrillary tangles (NFTs): phosphoproteomics of Alzheimer's NFTs', FASEB J, 25(11), pp. 3896-905.

Rush, A.M., Dib-Hajj, S.D. and Waxman, S.G. (2005) 'Electrophysiological properties of two axonal sodium channels, Nav1.2 and Nav1.6, expressed in mouse spinal sensory neurones', The Journal of Physiology, 564(3), pp. 803-815.

Sadun, A.A., Kashima, Y., Wurdeman, A.E., Dao, J., Heller, K. and Sherman, J. (1994) 'Morphological Findings in the Visual-System in a Case of Lebers Hereditary Optic Neuropathy', Clinical Neuroscience, 2(2), pp. 165-172.

Sadun, A.A., Win, P.H., Ross-Cisneros, F.N., Walker, S.O. and Carelli, V. (2000) 'Leber's hereditary optic neuropathy differentially affects smaller axons in the optic nerve', Trans Am Ophthalmol Soc, 98, pp. 223-32; discussion 232-5.

Saher, G., Brügger, B., Lappe-Siefke, C., Möbius, W., Tozawa, R.-i., Wehr, M.C., Wieland, F., Ishibashi, S. and Nave, K.-A. (2005) 'High cholesterol level is essential for myelin membrane growth', Nature neuroscience, 8(4), pp. 468-475.

Salinas, S., Bilsland, L.G. and Schiavo, G. (2008) 'Molecular landmarks along the axonal route: axonal transport in health and disease', Curr Opin Cell Biol, 20(4), pp. 445-53.

Samuels, D.C., Schon, E.A. and Chinnery, P.F. (2004) 'Two direct repeats cause most human mtDNA deletions', Trends Genet, 20(9), pp. 393-8.

Scaglia, F., Towbin, J.A., Craigen, W.J., Belmont, J.W., Smith, E.O., Neish, S.R., Ware, S.M., Hunter, J.V., Fernbach, S.D., Vladutiu, G.D., Wong, L.J. and Vogel, H. (2004) 'Clinical spectrum, morbidity, and mortality in 113 pediatric patients with mitochondrial disease', Pediatrics, 114(4), pp. 925-31.

Scarpulla, R.C. (2002) 'Transcriptional activators and coactivators in the nuclear control of mitochondrial function in mammalian cells', Gene, 286(1), pp. 81-9.

Schwartz, M. and Vissing, J. (2002) 'Paternal inheritance of mitochondrial DNA', N Engl J Med, 347(8), pp. 576-80.

Sciacco, M., Bonilla, E., Schon, E.A., DiMauro, S. and Moraes, C.T. (1994) 'Distribution of wild-type and common deletion forms of mtDNA in normal and respiration-deficient muscle fibers from patients with mitochondrial myopathy', Hum Mol Genet, 3(1), pp. 13-9.

Sena, L.A. and Chandel, N.S. (2012) 'Physiological roles of mitochondrial reactive oxygen species', Mol Cell, 48(2), pp. 158-67.

Sgarbi, G., Baracca, A., Lenaz, G., Valentino, L.M., Carelli, V. and Solaini, G. (2006) 'Inefficient coupling between proton transport and ATP synthesis may be the pathogenic mechanism for NARP and Leigh syndrome resulting from the T8993G mutation in mtDNA', Biochem J, 395(3), pp. 493-500.

Shaw, G., Yang, C., Ellis, R., Anderson, K., Parker Mickle, J., Scheff, S., Pike, B., Anderson, D.K. and Howland, D.R. (2005) 'Hyperphosphorylated neurofilament NF-H is a serum biomarker of axonal injury', Biochem Biophys Res Commun, 336(4), pp. 1268-77.

Shea, T.B., Chan, W.K., Kushkuley, J. and Lee, S. (2009) 'Organizational dynamics, functions, and pathobiological dysfunctions of neurofilaments', Results Probl Cell Differ, 48, pp. 29-45.

Shen, Q., Yamano, K., Head, B.P., Kawajiri, S., Cheung, J.T., Wang, C., Cho, J.H., Hattori, N., Youle, R.J. and van der Bliek, A.M. (2014) 'Mutations in Fis1 disrupt orderly disposal of defective mitochondria', Mol Biol Cell, 25(1), pp. 145-59.

Shiba-Fukushima, K., Arano, T., Matsumoto, G., Inoshita, T., Yoshida, S., Ishihama, Y., Ryu, K.Y., Nukina, N., Hattori, N. and Imai, Y. (2014) 'Phosphorylation of mitochondrial polyubiquitin by PINK1 promotes Parkin mitochondrial tethering', PLoS Genet, 10(12), p. e1004861.

Shiba-Fukushima, K., Imai, Y., Yoshida, S., Ishihama, Y., Kanao, T., Sato, S. and Hattori, N. (2012) 'PINK1-mediated phosphorylation of the Parkin ubiquitin-like domain primes mitochondrial translocation of Parkin and regulates mitophagy', Sci Rep, 2, p. 1002.

Shoshan-Barmatz, V., De Pinto, V., Zweckstetter, M., Raviv, Z., Keinan, N. and Arbel, N. (2010) 'VDAC, a multi-functional mitochondrial protein regulating cell life and death', Molecular Aspects of Medicine, 31(3), pp. 227-285.

Silvestri, G., Moraes, C.T., Shanske, S., Oh, S.J. and DiMauro, S. (1992) 'A new mtDNA mutation in the tRNA(Lys) gene associated with myoclonic epilepsy and ragged-red fibers (MERRF)', Am J Hum Genet, 51(6), pp. 1213-7.

Slupphaug, G., Mol, C.D., Kavli, B., Arvai, A.S., Krokan, H.E. and Tainer, J.A. (1996) 'A nucleotide-flipping mechanism from the structure of human uracil-DNA glycosylase bound to DNA', Nature, 384(6604), pp. 87-92.

Smirnova, E., Griparic, L., Shurland, D.L. and van der Bliek, A.M. (2001) 'Dynamin-related protein Drp1 is required for mitochondrial division in mammalian cells', Molecular Biology of the Cell, 12(8), pp. 2245-2256.

Smith, M.R., Smith, R.D., Plummer, N.W., Meisler, M.H. and Goldin, A.L. (1998) 'Functional analysis of the mouse Scn8a sodium channel', The Journal of neuroscience, 18(16), pp. 6093-6102.

Soleimanpour-Lichaei, H.R., Kuhl, I., Gaisne, M., Passos, J.F., Wydro, M., Rorbach, J., Temperley, R., Bonnefoy, N., Tate, W., Lightowlers, R. and Chrzanowska-Lightowlers, Z. (2007) 'mtRF1a is a human mitochondrial translation release factor decoding the major termination codons UAA and UAG', Mol Cell, 27(5), pp. 745-57.

Spalteholz, W. (1914) 'Uber das Durchsichtigmachen von menschlichen und tierischen Praparaten', S.Hierzel.

Sparaco, M., Bonilla, E., Dimauro, S. and Powers, J.M. (1993) 'Neuropathology of Mitochondrial Encephalomyopathies Due to Mitochondrial-DNA Defects', Journal of Neuropathology and Experimental Neurology, 52(1), pp. 1-10.

Spelbrink, J.N., Li, F.Y., Tiranti, V., Nikali, K., Yuan, Q.P., Tariq, M., Wanrooij, S., Garrido, N., Comi, G., Morandi, L., Santoro, L., Toscano, A., Fabrizi, G.M., Somer, H., Croxen, R., Beeson, D., Poulton, J., Suomalainen, A., Jacobs, H.T., Zeviani, M. and Larsson, C. (2001) 'Human mitochondrial DNA deletions associated with mutations in the gene encoding Twinkle, a phage T7 gene 4-like protein localized in mitochondria', Nat Genet, 28(3), pp. 223-31.

Spence, R.D., Kurth, F., Itoh, N., Mongerson, C.R.L., Wailes, S.H., Peng, M.S. and MacKenzie-Graham, A.J. (2014) 'Bringing CLARITY to gray matter atrophy', NeuroImage, 101, pp. 625-632.

Steinke, H. and Wolff, W. (2001) 'A modified Spalteholz technique with preservation of the histology', Ann Anat, 183(1), pp. 91-5.

Stepanova, T., Slemmer, J., Hoogenraad, C.C., Lansbergen, G., Dortland, B., De Zeeuw, C.I., Grosveld, F., van Cappellen, G., Akhmanova, A. and Galjart, N. (2003) 'Visualization of microtubule growth in cultured neurons via the use of EB3-GFP (end-binding protein 3-green fluorescent protein)', Journal of Neuroscience, 23(7), pp. 2655-2664.

Sternberger, L.A. and Sternberger, N.H. (1983) 'Monoclonal antibodies distinguish phosphorylated and nonphosphorylated forms of neurofilaments in situ', Proc Natl Acad Sci U S A, 80(19), pp. 6126-30.

Stewart, J.B. and Chinnery, P.F. (2015) 'The dynamics of mitochondrial DNA heteroplasmy: implications for human health and disease', Nat Rev Genet, 16(9), pp. 530-42.

Stokin, G.B., Lillo, C., Falzone, T.L., Brusch, R.G., Rockenstein, E., Mount, S.L., Raman, R., Davies, P., Masliah, E., Williams, D.S. and Goldstein, L.S. (2005) 'Axonopathy and transport deficits early in the pathogenesis of Alzheimer's disease', Science, 307(5713), pp. 1282-8.

Stoodley, C.J. (2012) 'The cerebellum and cognition: evidence from functional imaging studies', Cerebellum, 11(2), pp. 352-65.

Sue, C.M., Crimmins, D.S., Soo, Y.S., Pamphlett, R., Presgrave, C.M., Kotsimbos, N., Jean-Francois, M.J.B., Byrne, E. and Morris, J.G.L. (1998) 'Neuroradiological features of six kindreds with MELAS tRNALeu A3243G point mutation: implications for pathogenesis', Journal of Neurology, Neurosurgery & Psychiatry, 65(2), pp. 233-240.

Sung, J.S. and Demple, B. (2006) 'Roles of base excision repair subpathways in correcting oxidized abasic sites in DNA', FEBS J, 273(8), pp. 1620-9.

Sutovsky, P. and Schatten, G. (2000) 'Paternal contributions to the mammalian zygote: fertilization after sperm-egg fusion', Int Rev Cytol, 195, pp. 1-65.

Synofzik, M., Srulijes, K., Godau, J., Berg, D. and Schols, L. (2012) 'Characterizing POLG ataxia: clinics, electrophysiology and imaging', Cerebellum, 11(4), pp. 1002-11.

Taffe, B.G., Larminat, F., Laval, J., Croteau, D.L., Anson, R.M. and Bohr, V.A. (1996) 'Gene-specific nuclear and mitochondrial repair of formamidopyrimidine DNA glycosylase-sensitive sites in Chinese hamster ovary cells', Mutat Res, 364(3), pp. 183-92.

Takahashi, T., Yagishita, S., Amano, N., Yamaoka, K. and Kamei, T. (1997) 'Amyotrophic lateral sclerosis with numerous axonal spheroids in the corticospinal tract and massive degeneration of the cortex', Acta Neuropathol, 94(3), pp. 294-9.

Takamori, S., Holt, M., Stenius, K., Lemke, E.A., Gronborg, M., Riedel, D., Urlaub, H., Schenck, S., Brugger, B., Ringler, P., Muller, S.A., Rammner, B., Grater, F., Hub, J.S., De Groot, B.L., Mieskes, G., Moriyama, Y., Klingauf, J., Grubmuller, H., Heuser, J., Wieland, F. and Jahn, R. (2006) 'Molecular anatomy of a trafficking organelle', Cell, 127(4), pp. 831-46.

Takeda, S., Wakabayashi, K., Ohama, E. and Ikuta, F. (1988) 'Neuropathology of myoclonus epilepsy associated with ragged-red fibers (Fukuhara's disease)', Acta Neuropathol, 75(5), pp. 433-40.

Tanahashi, C., Nakayama, A., Yoshida, M., Ito, M., Mori, N. and Hashizume, Y. (2000) 'MELAS with the mitochondrial DNA 3243 point mutation: a neuropathological study', Acta Neuropathol, 99(1), pp. 31-8.

Tanaka, Y., Kanai, Y., Okada, Y., Nonaka, S., Takeda, S., Harada, A. and Hirokawa, N. (1998) 'Targeted disruption of mouse conventional kinesin heavy chain, kif5B, results in abnormal perinuclear clustering of mitochondria', Cell, 93(7), pp. 1147-58.

Tanji, K., DiMauro, S. and Bonilla, E. (1999) 'Disconnection of cerebellar Purkinje cells in Kearns-Sayre syndrome', J Neurol Sci, 166(1), pp. 64-70.

Tanji, K., Kunimatsu, T., Vu, T.H. and Bonilla, E. (2001) 'Neuropathological features of mitochondrial disorders', Semin Cell Dev Biol, 12(6), pp. 429-39.

Tatuch, Y., Christodoulou, J., Feigenbaum, A., Clarke, J.T., Wherret, J., Smith, C., Rudd, N., Petrova-Benedict, R. and Robinson, B.H. (1992) 'Heteroplasmic mtDNA mutation (T----G) at 8993 can cause Leigh disease when the percentage of abnormal mtDNA is high.', American Journal of Human Genetics, 50(4), pp. 852-858.

Taylor, A.M., Berchtold, N.C., Perreau, V.M., Tu, C.H., Li Jeon, N. and Cotman, C.W. (2009) 'Axonal mRNA in uninjured and regenerating cortical mammalian axons', The Journal of neuroscience : the official journal of the Society for Neuroscience, 29(15), pp. 4697-4707.

Taylor, R.W., Chinnery, P.F., Haldane, F., Morris, A.A., Bindoff, L.A., Wilson, J. and Turnbull, D.M. (1996) 'MELAS associated with a mutation in the valine transfer RNA gene of mitochondrial DNA', Ann Neurol, 40(3), pp. 459-62.

Taylor, R.W. and Turnbull, D.M. (2005) 'Mitochondrial DNA mutations in human disease', Nat Rev Genet, 6(5), pp. 389-402.

Temperley, R., Richter, R., Dennerlein, S., Lightowlers, R.N. and Chrzanowska-Lightowlers, Z.M. (2010) 'Hungry codons promote frameshifting in human mitochondrial ribosomes', Science, 327(5963), p. 301.

Terauchi, A., Tamagawa, K., Morimatsu, Y., Kobayashi, M., Sano, T. and Yoda, S. (1996) 'An autopsy case of mitochondrial encephalomyopathy, lactic acidosis and stroke-like episodes (MELAS) with a point mutation of mitochondrial DNA', Brain Dev, 18(3), pp. 224-9.

Tomer, R., Ye, L., Hsueh, B. and Deisseroth, K. (2014) 'Advanced CLARITY for rapid and high-resolution imaging of intact tissues', Nat Protoc, 9(7), pp. 1682-97.

Toyoshima, I., Sugawara, M., Kato, K., Wada, C., Hirota, K., Hasegawa, K., Kowa, H., Sheetz, M.P. and Masamune, O. (1998) 'Kinesin and cytoplasmic dynein in spinal spheroids with motor neuron disease', J Neurol Sci, 159(1), pp. 38-44.

Trapp, B.D., Peterson, J., Ransohoff, R.M., Rudick, R., Mork, S. and Bo, L. (1998) 'Axonal transection in the lesions of multiple sclerosis', N Engl J Med, 338(5), pp. 278-85.

Trapp, B.D. and Stys, P.K. (2009) 'Virtual hypoxia and chronic necrosis of demyelinated axons in multiple sclerosis', Lancet Neurol, 8(3), pp. 280-91.

Trevelyan, A.J., Kirby, D.M., Smulders-Srinivasan, T.K., Nooteboom, M., Acin-Perez, R., Enriquez, J.A., Whittington, M.A., Lightowlers, R.N. and Turnbull, D.M. (2010) 'Mitochondrial DNA mutations affect calcium handling in differentiated neurons', Brain, 133(Pt 3), pp. 787-96.

Trumpower, B.L. (1990) 'The protonmotive Q cycle. Energy transduction by coupling of proton translocation to electron transfer by the cytochrome bc1 complex', J Biol Chem, 265(20), pp. 11409-12.

Tsai, P.S., Kaufhold, J.P., Blinder, P., Friedman, B., Drew, P.J., Karten, H.J., Lyden, P.D. and Kleinfeld, D. (2009) 'Correlations of neuronal and microvascular densities in murine cortex revealed by direct counting and colocalization of nuclei and vessels', The Journal of Neuroscience, 29(46), pp. 14553-14570.

Turnbull, H.E., Lax, N.Z., Diodato, D., Ansorge, O. and Turnbull, D.M. (2010) 'The mitochondrial brain: From mitochondrial genome to neurodegeneration', Biochimica et Biophysica Acta (BBA) - Molecular Basis of Disease, 1802(1), pp. 111-121.

Tzoulis, C., Engelsen, B.A., Telstad, W., Aasly, J., Zeviani, M., Winterthun, S., Ferrari, G., Aarseth, J.H. and Bindoff, L.A. (2006) 'The spectrum of clinical disease caused by the A467T and W748S POLG mutations: a study of 26 cases', Brain, 129(Pt 7), pp. 1685-92.

Tzoulis, C., Neckelmann, G., Mork, S.J., Engelsen, B.E., Viscomi, C., Moen, G., Ersland, L., Zeviani, M. and Bindoff, L.A. (2010) 'Localized cerebral energy failure in DNA polymerase gamma-associated encephalopathy syndromes', Brain, 133(Pt 5), pp. 1428-37.

Tzoulis, C., Tran, G.T., Coxhead, J., Bertelsen, B., Lilleng, P.K., Balafkan, N., Payne, B., Miletic, H., Chinnery, P.F. and Bindoff, L.A. (2014) 'Molecular pathogenesis of polymerase gamma-related neurodegeneration', Ann Neurol, 76(1), pp. 66-81.

Tzoulis, C., Tran, G.T., Schwarzlmuller, T., Specht, K., Haugarvoll, K., Balafkan, N., Lilleng, P.K., Miletic, H., Biermann, M. and Bindoff, L.A. (2013) 'Severe nigrostriatal degeneration without clinical parkinsonism in patients with polymerase gamma mutations', Brain, 136(Pt 8), pp. 2393-404.

Ugalde, C., Vogel, R., van den Heuvel, B., Smeitink, J. and Nijtmans, L. (2004) 'Human mitochondrial complex I assembles through the combination of evolutionary conserved modules: a framework to interpret complex I deficiencies', Human Molecular Genetics, 13(20), pp. 2461-2472.

Vale, R.D. (2003) 'The molecular motor toolbox for intracellular transport', Cell, 112(4), pp. 467-80.

Valente, E.M., Abou-Sleiman, P.M., Caputo, V., Muqit, M.M., Harvey, K., Gispert, S., Ali, Z., Del Turco, D., Bentivoglio, A.R., Healy, D.G., Albanese, A., Nussbaum, R., Gonzalez-Maldonado, R., Deller, T., Salvi, S., Cortelli, P., Gilks, W.P., Latchman, D.S., Harvey, R.J., Dallapiccola, B., Auburger, G. and Wood, N.W. (2004) 'Hereditary early-onset Parkinson's disease caused by mutations in PINK1', Science, 304(5674), pp. 1158-60.

Valtorta, F., Pennuto, M., Bonanomi, D. and Benfenati, F. (2004) 'Synaptophysin: leading actor or walk-on role in synaptic vesicle exocytosis?', Bioessays, 26(4), pp. 445-53.

Van Goethem, G., Martin, J.J., Dermaut, B., Lofgren, A., Wibail, A., Ververken, D., Tack, P., Dehaene, I., Van Zandijcke, M., Moonen, M., Ceuterick, C., De Jonghe, P. and Van Broeckhoven, C. (2003) 'Recessive POLG mutations presenting with sensory and ataxic neuropathy in compound heterozygote patients with progressive external ophthalmoplegia', Neuromuscul Disord, 13(2), pp. 133-42.

Veeranna, Yang, D.S., Lee, J.H., Vinod, K.Y., Stavrides, P., Amin, N.D., Pant, H.C. and Nixon, R.A. (2011) 'Declining phosphatases underlie aging-related hyperphosphorylation of neurofilaments', Neurobiol Aging, 32(11), pp. 2016-29.

Vergani, L., Martinuzzi, A., Carelli, V., Cortelli, P., Montagna, P., Schievano, G., Carrozzo, R., Angelini, C. and Lugaresi, E. (1995) 'MtDNA mutations associated with Leber's hereditary optic neuropathy: studies on cytoplasmic hybrid (cybrid) cells', Biochem Biophys Res Commun, 210(3), pp. 880-8.

Vogel, F., Bornhovd, C., Neupert, W. and Reichert, A.S. (2006) 'Dynamic subcompartmentalization of the mitochondrial inner membrane', J Cell Biol, 175(2), pp. 237-47.

von Ahsen, O., Renken, C., Perkins, G., Kluck, R.M., Bossy-Wetzel, E. and Newmeyer, D.D. (2000) 'Preservation of mitochondrial structure and function after Bid-or Bax-mediated cytochrome c release', The Journal of cell biology, 150(5), pp. 1027-1036.

Voogd, J. and Glickstein, M. (1998) 'The anatomy of the cerebellum', Trends in cognitive sciences.

Wagner, K., Mick, D.U. and Rehling, P. (2009) 'Protein transport machineries for precursor translocation across the inner mitochondrial membrane', Biochim Biophys Acta, 1793(1), pp. 52-9.

Wagner, O.I., Rammensee, S., Korde, N., Wen, Q., Leterrier, J.F. and Janmey, P.A. (2007) 'Softness, strength and self-repair in intermediate filament networks', Exp Cell Res, 313(10), pp. 2228-35.

Wakabayashi, J., Zhang, Z., Wakabayashi, N., Tamura, Y., Fukaya, M., Kensler, T.W., Iijima, M. and Sesaki, H. (2009) 'The dynamin-related GTPase Drp1 is required for embryonic and brain development in mice', J Cell Biol, 186(6), pp. 805-16.

Walker, R.L., Anziano, P. and Meltzer, P.S. (1997) 'A PAC containing the human mitochondrial DNA polymerase gamma gene (POLG) maps to chromosome 15q25', Genomics, 40(2), pp. 376-8.

Wallace, D.C., Shoffner, J.M., Trounce, I., Brown, M.D., Ballinger, S.W., Corral-Debrinski, M., Horton, T., Jun, A.S. and Lott, M.T. (1995) 'Mitochondrial DNA mutations in human degenerative diseases and aging', Biochim Biophys Acta, 1271(1), pp. 141-51.

Wang, J., Yang, M., Yang, L., Zhang, Y., Yuan, J., Liu, Q., Hou, X. and Fu, L. (2015a) 'A Confocal Endoscope for Cellular Imaging', Engineering, 1(3), pp. 351-360.

Wang, K., Yin, X.M., Chao, D.T., Milliman, C.L. and Korsmeyer, S.J. (1996) 'BID: a novel BH3 domain-only death agonist', Genes Dev, 10(22), pp. 2859-69.

Wang, W., Cao, L., Wang, C., Gigant, B. and Knossow, M. (2015b) 'Kinesin, 30 years later: Recent insights from structural studies', Protein Sci, 24(7), pp. 1047-56.

Wang, X. and Schwarz, T.L. (2009) 'The mechanism of Ca2+ -dependent regulation of kinesin-mediated mitochondrial motility', Cell, 136(1), pp. 163-74.

Wang, X., Winter, D., Ashrafi, G., Schlehe, J., Wong, Y.L., Selkoe, D., Rice, S., Steen, J., LaVoie, M.J. and Schwarz, T.L. (2011) 'PINK1 and Parkin target Miro for phosphorylation and degradation to arrest mitochondrial motility', Cell, 147(4), pp. 893-906.

Wang, Y.S. and Bogenhagen, D.F. (2006) 'Human mitochondrial DNA nucleoids are linked to protein folding machinery and metabolic enzymes at the mitochondrial inner membrane', Journal of Biological Chemistry, 281(35), pp. 25791-25802.

Waterham, H.R., Koster, J., van Roermund, C.W., Mooyer, P.A., Wanders, R.J. and Leonard, J.V. (2007) 'A lethal defect of mitochondrial and peroxisomal fission', N Engl J Med, 356(17), pp. 1736-41.

Waxman, S.G. (1980) 'Determinants of conduction velocity in myelinated nerve fibers', Muscle Nerve, 3(2), pp. 141-50.

Werner, P., Pitt, D. and Raine, C.S. (2001) 'Multiple sclerosis: altered glutamate homeostasis in lesions correlates with oligodendrocyte and axonal damage', Ann Neurol, 50(2), pp. 169-80.

Whittaker, R.G., Devine, H.E., Gorman, G.S., Schaefer, A.M., Horvath, R., Ng, Y., Nesbitt, V., Lax, N.Z., McFarland, R., Cunningham, M.O., Taylor, R.W. and Turnbull, D.M. (2015) 'Epilepsy in adults with mitochondrial disease: A cohort study', Ann Neurol, 78(6), pp. 949-57.

Wider, C., Dickson, D.W., Schweitzer, K.J., Broderick, D.F. and Wszolek, Z.K. (2009) 'Familial idiopathic basal ganglia calcification: a challenging clinical-pathological correlation', J Neurol, 256(5), pp. 839-42.

Willis, S.N., Fletcher, J.I., Kaufmann, T., van Delft, M.F., Chen, L., Czabotar, P.E., Ierino, H., Lee, E.F., Fairlie, W.D., Bouillet, P., Strasser, A., Kluck, R.M., Adams, J.M. and Huang, D.C.S. (2007) 'Apoptosis initiated when BH3 ligands engage multiple Bcl-2 homologs, not Bax or Bak', Science, 315(5813), pp. 856-859.

Wiltshire, E., Davidzon, G., DiMauro, S., Akman, H.O., Sadleir, L., Haas, L., Zuccollo, J., McEwen, A. and Thorburn, D.R. (2008) 'Juvenile Alpers disease', Arch Neurol, 65(1), pp. 121-4.

Witter, L., Rudolph, S., Pressler, R.T., Lahlaf, Safiya I. and Regehr, Wade G. (2016) 'Purkinje Cell Collaterals Enable Output Signals from the Cerebellar Cortex to Feed Back to Purkinje Cells and Interneurons', Neuron, 91(2), pp. 312-319.

Wittig, I. and Schagger, H. (2008) 'Structural organization of mitochondrial ATP synthase', Biochim Biophys Acta, 1777(7-8), pp. 592-8.

Wong, L.J., Naviaux, R.K., Brunetti-Pierri, N., Zhang, Q., Schmitt, E.S., Truong, C., Milone, M., Cohen, B.H., Wical, B., Ganesh, J., Basinger, A.A., Burton, B.K., Swoboda, K., Gilbert, D.L., Vanderver, A., Saneto, R.P., Maranda, B., Arnold, G., Abdenur, J.E., Waters, P.J. and

Copeland, W.C. (2008) 'Molecular and clinical genetics of mitochondrial diseases due to POLG mutations', Hum Mutat, 29(9), pp. E150-72.

Wong, T.W. and Clayton, D.A. (1985) 'In vitro replication of human mitochondrial DNA: accurate initiation at the origin of light-strand synthesis', Cell, 42(3), pp. 951-958.

Wu, Z.D., Puigserver, P., Andersson, U., Zhang, C.Y., Adelmant, G., Mootha, V., Troy, A., Cinti, S., Lowell, B., Scarpulla, R.C. and Spiegelman, B.M. (1999) 'Mechanisms controlling mitochondrial biogenesis and respiration through the thermogenic coactivator PGC-1', Cell, 98(1), pp. 115-124.

Yabe, J.T., Jung, C., Chan, W.K. and Shea, T.B. (2000) 'Phospho-dependent association of neurofilament proteins with kinesin in situ', Cell Motil Cytoskeleton, 45(4), pp. 249-62.

Yakubovskaya, E., Mejia, E., Byrnes, J., Hambardjieva, E. and Garcia-Diaz, M. (2010) 'Helix unwinding and base flipping enable human MTERF1 to terminate mitochondrial transcription', Cell, 141(6), pp. 982-93.

Yang, B., Treweek, J.B., Kulkarni, R.P., Deverman, B.E., Chen, C.K., Lubeck, E., Shah, S., Cai, L. and Gradinaru, V. (2014) 'Single-Cell Phenotyping within Transparent Intact Tissue through Whole-Body Clearing', Cell, 158(4), pp. 945-958.

Yasukawa, T., Reyes, A., Cluett, T.J., Yang, M.Y., Bowmaker, M., Jacobs, H.T. and Holt, I.J. (2006) 'Replication of vertebrate mitochondrial DNA entails transient ribonucleotide incorporation throughout the lagging strand', EMBO J, 25(22), pp. 5358-71.

Yasukawa, T., Suzuki, T., Ishii, N., Ueda, T., Ohta, S. and Watanabe, K. (2000) 'Defect in modification at the anticodon wobble nucleotide of mitochondrial tRNA(Lys) with the MERRF encephalomyopathy pathogenic mutation', Febs Letters, 467(2-3), pp. 175-178.

Yi, M., Weaver, D. and Hajnoczky, G. (2004) 'Control of mitochondrial motility and distribution by the calcium signal: a homeostatic circuit', J Cell Biol, 167(4), pp. 661-72.

Yokoyama, T., Hasegawa, K., Obama, R., Ishihara, T. and Yagishita, S. (2010) 'MELAS with diffuse degeneration of the cerebral white matter: report of an autopsy case', Neuropathology, 30(1), pp. 56-60.

Yoneda, M., Maeda, M., Kimura, H., Fujii, A., Katayama, K. and Kuriyama, M. (1999) 'Vasogenic edema on MELAS: a serial study with diffusion-weighted MR imaging', Neurology, 53(9), pp. 2182-4.

Yoneda, M., Miyatake, T. and Attardi, G. (1995) 'Heteroplasmic mitochondrial tRNALys mutation and its complementation in MERRF patient-derived mitochondrial transformants', Muscle & nerve, 18(S14), pp. S95-S101.

Yoon, Y., Krueger, E.W., Oswald, B.J. and McNiven, M.A. (2003) 'The mitochondrial protein hFis1 regulates mitochondrial fission in mammalian cells through an interaction with the dynamin-like protein DLP1', Molecular and Cellular Biology, 23(15), pp. 5409-5420.

Yoshida, M., Muneyuki, E. and Hisabori, T. (2001) 'ATP synthase--a marvellous rotary engine of the cell', Nat Rev Mol Cell Biol, 2(9), pp. 669-77.

Yoshikawa, S., Muramoto, K., Shinzawa-Itoh, K., Aoyama, H., Tsukihara, T., Shimokata, K., Katayama, Y. and Shimada, H. (2006) 'Proton pumping mechanism of bovine heart cytochrome c oxidase', Biochim Biophys Acta, 1757(9-10), pp. 1110-6.

Yu, F.H. and Catterall, W.A. (2003) 'Overview of the voltage-gated sodium channel family', Genome biology, 4(3), p. 207.

Yuan, A., Rao, M.V., Veeranna and Nixon, R.A. (2012) 'Neurofilaments at a glance', J Cell Sci, 125(Pt 14), pp. 3257-63.

Zagrebelsky, M., Buffo, A., Skerra, A., Schwab, M.E., Strata, P. and Rossi, F. (1998) 'Retrograde regulation of growth-associated gene expression in adult rat Purkinje cells by myelin-associated neurite growth inhibitory proteins', The Journal of neuroscience : the official journal of the Society for Neuroscience, 18(19), pp. 7912-7929.

Zeviani, M., Moraes, C.T., DiMauro, S., Nakase, H., Bonilla, E., Schon, E.A. and Rowland, L.P. (1988) 'Deletions of mitochondrial DNA in Kearns-Sayre syndrome. 1988', Neurology, 51(6), pp. 1525-1533.

Zhao, J., Liu, T., Jin, S., Wang, X., Qu, M. and Uhlen, P. (2011) 'Human MIEF1 recruits Drp1 to mitochondrial outer membranes and promotes mitochondrial fusion rather than fission', The EMBO ….

Zhou, C., Huang, Y., Shao, Y., May, J., Prou, D., Perier, C., Dauer, W., Schon, E.A. and Przedborski, S. (2008) 'The kinase domain of mitochondrial PINK1 faces the cytoplasm', Proc Natl Acad Sci U S A, 105(33), pp. 12022-7.

Zuchner, S., Mersiyanova, I.V., Muglia, M., Bissar-Tadmouri, N., Rochelle, J., Dadali, E.L., Zappia, M., Nelis, E., Patitucci, A., Senderek, J., Parman, Y., Evgrafov, O., Jonghe, P.D., Takahashi, Y., Tsuji, S., Pericak-Vance, M.A., Quattrone, A., Battaloglu, E., Polyakov, A.V., Timmerman, V., Schroder, J.M. and Vance, J.M. (2004) 'Mutations in the mitochondrial GTPase mitofusin 2 cause Charcot-Marie-Tooth neuropathy type 2A', Nat Genet, 36(5), pp. 449-51.